Ricardo Tucceri

Poly(o-aminophenol) Film Electrodes

Synthesis, Transport Properties and Practical Applications

Springer

Engineering Materials

Ricardo Tucceri

Poly(o-aminophenol) Film Electrodes

Synthesis, Transport Properties and Practical Applications

🌓 Springer

Ricardo Tucceri
Department of Chemistry
Institute of Theoretical and Applied
  Physicochemical Research (INIFTA)
La Plata
Argentina

Preface

During three decades, poly(*o*-aminophenol) (POAP) has been investigated with electrochemical, spectroelectrochemical, ellipsometry, EQCM (Electrochemical Quartz Crystal Microbalance), ESR (Electron Spin Resonance), surface resistance and impedance measurements and applied in sensors, biosensors and corrosion protection. In the present book, I have attempted to identify and document the most significant advances that have been reported in electrochemistry about synthesis, conduction properties and practical applications of Poly(*o*-aminophenol) Film Electrodes. This book is organized as follows. In Chap. 1, synthesis methods of POAP films and their characterization by using different electrochemical and spectroscopic techniques are described. Also, some relevant mechanisms of electropolymerization of *ortho*-aminophenol (OAP) that lead to POAP, and the different structures proposed for this polymer, are presented. In Chap. 2, the nature of the charging process of POAP is discussed. In this sense, special attention is paid to electron and ion transport processes inside the polymer film and interfacial charge transfer processes across metal-polymer and polymer-solution interfaces. Also, in this Chap. 2, the transport process across POAP films in contact with media containing redox active couples (redox mediation), is extensively discussed. In Chap. 3, specific practical applications of POAP, such as, electron-transfer catalyst (or mediator), electrochemical sensor, amperometric biosensor, and others, are treated. There are at least two major reasons for this intense interest in POAP: first, is the wide range of practical applications of the polymer and the second is the intellectual curiosity of scientists to understand the electrochemical behaviour of this polymer. It is expected that the present book will be helpful to the colleagues who pretend to achieve a more complete knowledge about the particular properties of poly(*o*-aminophenol).

Contents

Chapter 1
Electropolymerization of *o*-aminophenol on Different Electrode Materials and in Different Electrolyte Media: Formation of Poly(*o*-aminophenol) Film Electrodes

1.1 Introduction

Oxidation of *o*-aminophenol on different electrode materials (gold, platinum, carbon, indium-tin oxide, etc.) in aqueous medium was shown to form poly-*o*-aminophenol (POAP). Like aniline, *o*-AP can be polymerized electrochemically in acidic, neutral and alkaline solutions. However, while a conducting film is only formed in acidic media, POAP synthesized in neutral and alkaline media leads to a nonconducting film.

Electropolymerization of *o*-AP in acid medium yields an electroactive polymer that exhibits its maximal electroactivity within the potential range -0.2 V $< E < 0.5$ V (vs. SCE) at *pH* values lower than 3. The electroactivity of POAP was explained by a redox mechanism that involves an addition/elimination of protons coupled with a reversible electron transfer. The charge-transport process at POAP films was studied by employing different electrochemical techniques. It was demonstrated that external variables, such as film thickness, solution *pH* and redox couple concentration in solution, affect both the permeation process of electroactive species and the electron motion through a POAP film.

The properties of POAP synthesized in basic medium are favourable to its applications in the field of bioelectrochemistry and electrocatalysis. In this regard, a nonconducting material is obtained that exhibits several advantages with respect to other polymers. POAP can be synthesized on different electrode surfaces, and the polymer thickness can be controlled within 10–100 nm due to a self-limiting growth. Employed as material to build amperometric biosensors, POAP has shown to be permselective. In this regard, the interference from electroactive species, such as ascorbic acid and uric acid, which are generally encountered in the determination of physiological sample, was significantly reduced by the use of a POAP film. Also, POAP is able to immobilize biological macromolecules. It was proved that large amounts of glucose oxidase could be immobilized at POAP films, which is essential to the good performance of an amperometric glucose sensor. In the field of electrocatalysis, an interesting characteristic of POAP is the presence of an electron-donating OH group next to the imine nitrogen that

increases the electron density at the imine sites. In addition, OH by itself is also a potential coordinating site. These factors combine to provide a strong acceptor binding of POAP with several metal cations. In this regard, POAP was employed to develop stable electrocatalysts for oxygen reduction.

1.2 Electropolymerization of *o*-aminophenol in Acidic Media

Barbero et al. [1] reported a study about the oxidation of *ortho*aminophenol (*o*-AP) and closely related compounds employing electrochemical, chemical, and spectroscopic measurements. The electro-oxidation of *o*-AP was studied on different electrode materials (Pt, Au, and glassy carbon (GC)) and different electrolyte media ($1 < pH < 7$). A typical voltammogram of a Pt electrode in contact with a 0.1 mol/L HClO$_4$ + 0.4 mol/L NaClO$_4$ + 1×10^{-3} mol/L *o*-AP aqueous solution (*pH* 1) is shown in Fig. 1.1. On the first positive sweep two peaks are defined (**a**) at 0.60 V (SCE) attributed to the oxidation of *o*-AP to the monocation radical (*o*-AP•+) and another peak (**b**) at 0.85 V, which was assigned to the oxidation of (*o*-AP•+) to dication. On the negative sweep none of these peaks show complementary peaks, indicating chemical follow-up reactions giving products detected as peaks **c–c′** and **d–d′** on the subsequent sweeps. It was observed that the system **c–c′** diminishes after continuous cycling in the same way as **a**, but the peak system **d–d′** increases, also showing the characteristic behaviour of a deposited electroactive substance. This was verified by stirring the solution while cycling, because the system **d–d′** remained unchanged, as expected for an irreversible adsorbed electroactive substance. Analysis of the products employing IR and UV–vis spectroscopy showed that the **d–d′** couple corresponds to a polymer of 3-aminophenoxazone (3APZ).

A mechanism for the *o*-AP electro-oxidation was proposed in Ref. [1] where the *o*-AP•+, formed in the first charge-transfer step, may follow different reaction paths. Thus, the formation of a composite of two different films, one of linear chain structure similar to polyaniline (PANI) and the other, with a phenoxazine-like chain structure, was proposed in Ref. [1]. The latter was considered to be the predominant product. To reinforce the conclusion about the proposed structure for the electroactive substance, the electrochemical properties of several compounds (*o*-anisidine, *p*- and *m*-aminophenol, *o*-phenylenediamine, etc.) with similar structures to *o*-AP were also analyzed in Ref. [1]. The presence of phenoxazine units in the structure of the polymer formed by the oxidation of *o*-AP was also confirmed by Barbero et al. in another work [2] by employing FT-IR spectroscopy. The electroactive substance formed by oxidation of *o*-AP was denominated poly(*o*-aminophenol) (POAP). An analysis of the voltammetric peak current (i_{pa}) as a function of the sweep rate (v) and the initial concentration of *o*-AP was also carried out in Ref. [1]. It was observed that high concentrations of monomer favour

higher rates of polymerization, with the consequent partial blocking of the electrode surface. This effect was more noticeable at high temperatures. However, the blocking effect was negligible at low monomer concentrations, and then the normal behaviour for the cation radical dimerization reactions was observed. Barbero et al. [1] also prepared the electroactive polymer by chemical oxidation of *o*-AP, and its properties were compared with those of the electrochemically produced POAP. The chemical synthesis of POAP confirmed that the actual monomer in the formation of the polymer is the cyclic dimer of *o*-AP, 3APZ. A calculation of a global value of the rate constant for the dimerization reaction was carried out in Ref. [1]. With regard to the solution *pH*, a similar voltammetric response to the one shown in Fig. 1.1 was observed for *pH* values lower than 3. At *pH* values between 3 and 7, a diminished current of the peak system **d**–**d′**, assigned to the film formation, was observed. Barbero et al. [1] remark that if extreme care is not taken in the preparation of a POAP film, not only in the concentration but also in the potential ranges, the possibility of side reactions and consequently "side" polymers, increases, and the real structures of the films obtained could be quite complex. Then, the best conditions proposed in Ref. [1] for obtaining a reproducible POAP film are the repetitive cycling between −0.25 and 0.70 V (SCE) of an *o*-AP aqueous acid solution (*pH* 1) and an *o*-AP concentration less than 20 mmol/L. Figure 1.2 shows the voltammetric response of POAP in a monomer-free solution. The voltammogram is highly asymmetric, suggesting a complex redox behavior that does not follow the simple Nernstian model. The phenoxazine-like chain structure proposed by Barbero et al. [1] is shown in Fig. 1.3, which demonstrates the redox switching of POAP in acidic media.

   The electrochemical formation of POAP was also described by Ortega [3]. Ortega [3] focused his attention on the monomer purification before electropolymerization. *O*-AP (purum 90 %) was purified by recrystallizing it three times in ethyl acetate. The very pale white plates were dried in a warm water bath under vacuum to eliminate residual solvent. The monomer was stored in a desiccator under vacuum until required. MNR, IR, and C13 spectra were recorded to ensure the absence of contaminant oxidation species in the monomer.

Fig. 1.1 Cyclic voltammogram of a Pt electrode contacting a 0.1 mol/L $HClO_4$ + 0.4 mol/L $NaClO_4$ + 1 × 10^{-3} mol/L *o*-aminophenol (*o*-AP) solution, *pH* 1. Scan rate, $v = 0.1$ V s^{-1}; electrode area, $A = 0.126$ cm^2 [1]
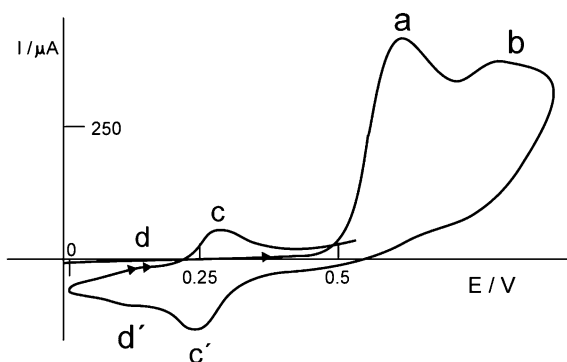
Fig. 1.2 Cyclic voltammogram of poly-*o*-aminophenol (POAP) at *pH* 1. Scan rate, $v = 0.1$ V s^{-1}; Pt electrode, electrode area $A = 0.126$ cm^2; supporting electrolyte, 0.4 mol/L NaClO$_4$ + 0.1 mol/L HClO$_4$ [1]
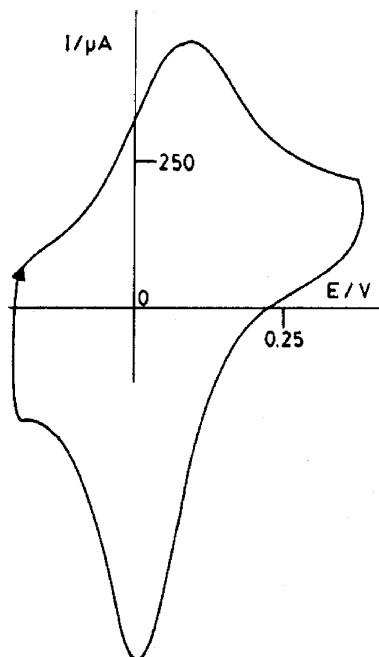
A typical cyclic multisweep voltammogram of the Pt electrode in contact with 0.4 mol cm^{-3} of NaClO$_4$ and 10^{-2} mol dm^{-3} of monomer solution is shown in Fig. 1.4.

The electrode potential was continuously swept at 100 mV s^{-1} between -0.25 and 0.75 V (SCE). On the first positive sweep, only one irreversible peak is defined at 0.65 V (peak **a**, only visible at lower sensibility), which was attributed to the oxidation of the monomer to the monocation radical. No complementary peak to **a,** was observed on the negative scan, whereas a large peak appeared at 0.23 V (peak **b**). This peak has a complementary one (peak **e**) at 0.29 V in the next positive scan and it was assigned to the redox reaction of a dimer formed prior to cyclization to produce 3APZ. It was also observed that, while peak **a** rapidly and continuously decreases up to a minimum, peaks **b** and **e** fall correspondingly. Also, after 8 or 10 min of cycling, the current response in the potential range from 0.0 to 0.2 V begins to increase continuously with successive potential scans, giving rise
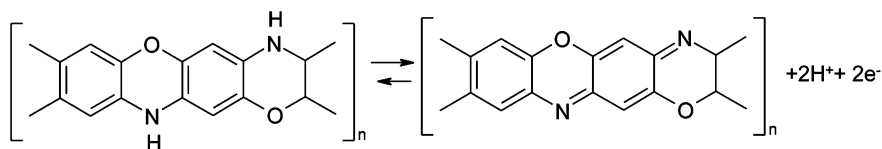
Fig. 1.3 Reaction scheme of poly-*o*-aminophenol (POAP) redox switching including oxidized and reduced forms [1]

Fig. 1.4 Cyclic
voltammograms of *o*-
aminophenol (*o*-AP) at *pH*
0.9 in a solution containing
0.4 mol dm^{-3} NaClO$_4$
($v = 100$ mV s^{-1}). Area of
the working electrode,
1.9×10^{-3} cm^2. *Arrows*
indicate the change in the
peak height as the
electropolymerization is
taking place [3]
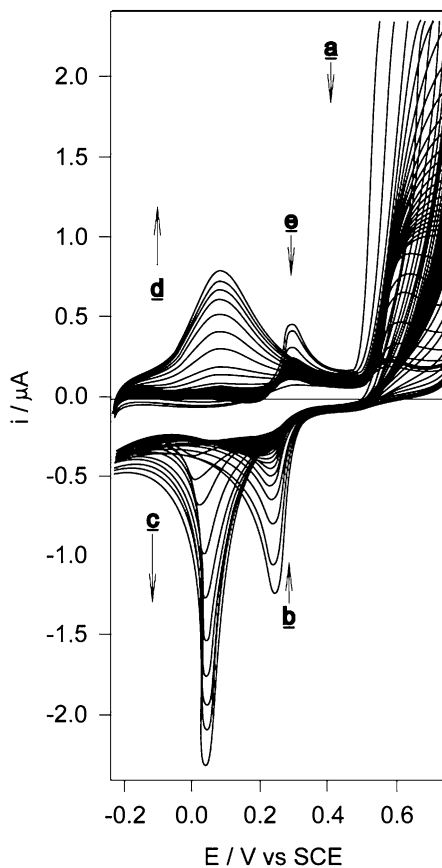
to peaks **c** and **d**, which were assigned to the build-up of an electroactive poly-
meric product on the electrode. Neither polymer nor couple **b** and **e,** were formed
if the potential scan did not reach 0.65 V. On the other hand, peaks from **b** to
d were not observed when potential cycling took place under continuous nitrogen
bubbling. Thus, Ortega [3] indicates that a slow chemical reaction is associated
with the peaks **b** and **e** and, under stirred conditions, the intermediate corre-
sponding to **b** and **e** peaks is moved away from the electrode, so that its further
transformation into polymer is prevented. The comparison of voltammograms
presented in Fig. 1.4 with those shown by Barbero et al. [1] for 3APZ, allowed
Ortega to conclude that the coupling of 3APZ units to form the polymer is the
process that occurs during the propagation of the polymeric chains, therefore,
peaks **c** and **d** in Fig. 1.4 should be assigned to the redox reaction of 3APZ and
POAP. Ortega [3] remarked that the charge propagation proceeds slowly during
the formation of POAP. The slow diffusion of *o*-AP species through the film to
reach the electrode and produce more monocation radical was considered to be the
cause by which peaks **a**, **b**, and **e** decrease with time, and then the produced film

does not oxidize monomer because it is nonconducting at positive potentials. Also, that fact that the growth of the polymer starts after an induction time long after the peaks corresponding to *o*-AP radical cation and dimer become small was considered by Ortega as a confirmation that the propagation process involves further oxidation and coupling of 3APZ.

The electrochemical synthesis of POAP on the surface of a carbon paste electrode (CPE) in the presence of sodium dodecyl sulphate (SDS) is described by Ojani et al. [4] These authors showed (as did Barbero et al. [1] and Ortega [3]) that, in the absence of SDS, *o*-AP is irreversibly oxidized at positive potential values (0.7 V vs. Ag/AgCl/KCl 3 mol/L) without corresponding cathodic processes in the reverse scan. As in other works, after consecutive cycles one redox process was observed on the voltammetric response, which was assigned to 3APZ. The peaks corresponding to this process did not increase considerably with potential cycling. This effect was attributed by Ojani et al. [4] to soluble products produced on the electrode surface that do not allow the monomer to reach the electrode surface and produce the monocation radical. Therefore, prolonged potential cycling was needed for transformation of the soluble 3APZ to POAP, which was observed within a potential range (0.2 V $< E <$ 0.3 V) less positive than that of 3APZ. When SDS is added to the monomer solution, the monomer oxidation potential was shifted to less positive potentials (almost 0.075 V) and the oxidation current increased, as compared with the process in the absence of SDS. The rate of polymerization also increased considerably in the presence of SDS, and the peaks attributed to POAP grew simultaneously with that corresponding to 3APZ growth. Ojani et al. [4] remark that, in the presence of SDS, the monomer *o*-AP can easily reach the electrode surface and produce more monocation radical than in the absence of SDS. The rate of polymerization depends on the SDS concentration. Up to 0.1 mmol/L of SDS the rate of polymerization was not much larger than that observed without SDS. However, for SDS concentration values higher than 0.1 mmol/L, the rate of polymerization increased rapidly and, finally, it saturated at around 4 mmol/L. The redox behaviour of the polymers synthesized in the absence and in the presence of SDS was also investigated in the supporting electrolyte solution. The comparison of the electrochemical response of the immediately prepared SDS/POAP/CPE electrode with that obtained after immersing the electrode for 1 h in 0.5 mol/L HClO$_4$ demonstrated that the immediately prepared electrode shows two redox couples at about 0.2 and 0.3 V, which were assigned to the phenoxazine units of POAP and 3APZ, respectively.

The electrochemical oxidation of *o*-AP from a 0.2 mol/L NaClO$_4$ + 0.1 mol/L HClO$_4$ solution on platinum Pt and GC electrodes employing cyclic voltammetry (CV), was studied by Bulhoes et al. [5]. Cyclic voltammograms of Pt and GC electrodes in the electrolyte solution containing 5 mmol^{-1} of *o*-AP are compared in Fig. 1.5.

O-AP oxidizes irreversibly on both electrodes, and two anodic peaks (I and II) are observed without corresponding cathodic processes in the reverse scan. Peaks I and II appear for the GC electrode as well separated waves and at more negative potentials than for Pt, which was attributed to a more favourable process of
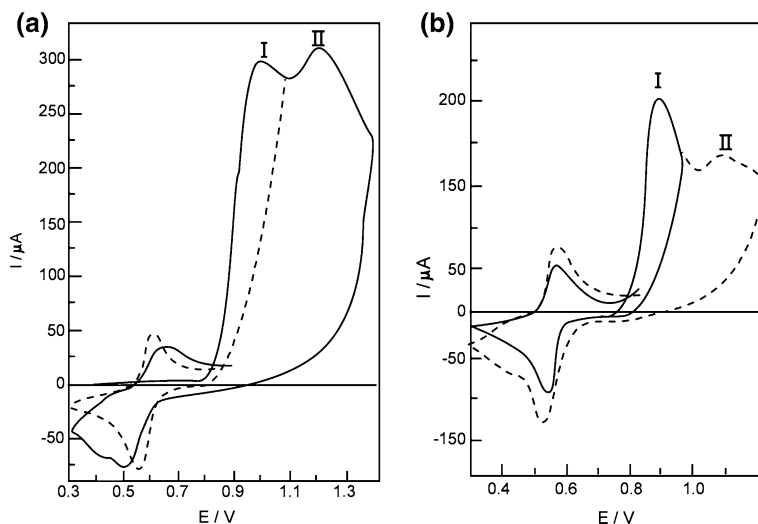
Fig. 1.5 Cyclic voltammograms of (**a**) Pt and (**b**) glassy carbon (GC) electrodes in a 0.2 mol/L NaClO$_4$ + 0.1 mol/L HClO$_4$ + 5 mmol L^{-1} *o*-aminophenol (*o*-AP) solution. Scan rate, $v = 100$ mV s^{-1} [5]

oxidation on the former electrode material. Peak II was related to follow-up oxidation reactions after peak I. Besides the nature of the electrode surface, the characteristics of the films synthesized by Bulhoes et al. [5] depended on variables such as the final potential and the value of the potential scan rate. It was observed that the current of peak I increased linearly with the square root of the scan rate ($v^{0.5}$), indicating a process controlled by ion diffusion. The current function ($Ip \, v^{0.5} c$) versus $v^{0.5}$ plot showed the existence of successive electrochemical–chemical–electrochemical steps ($E(CE)n$) during the *o*-AP oxidation, and two electrons were estimated to be involved in the process. Bulhoes et al. postulated that, besides a film with a ladder structure, the oxidation of *o*-AP can produce intermediate benzoquinone monoamine after successive cycling. They [5] also remarked that, although APZ is formed in solution after successive cycling, it does not polymerize as proposed by Barbero et al. [1] and Ortega [3]. The electrode material seems to affect the *o*-AP electropolymerization process. In this regard, the redox processes of the POAP films deposited on Pt and GC electrodes in the supporting electrolyte were found to be different. A less electroactive film was obtained on Pt electrodes as compared with GC electrodes.

The effect of the electrode surface on the electropolymerization process of *o*-AP was studied in detail by Yong and Zugeng [6]. GC electrodes were chemically and electrochemically pretreated before electropolymerization of *o*-AP. The electrode surfaces were polished carefully to a mirror finish and then cleaned ultrasonically with triply distilled water for 3 min. This kind of electrode was denoted [6] as an "untreated" electrode. In addition, electrochemical treatment of the electrodes was

achieved by placing the polished electrodes in 0.1 mol/L H_2SO_4 at 1.85 V (SCE) for 5 min, and then they were cycled between -0.2 and 0.7 V for 15 min. Chemical pretreatment of the electrodes was achieved by immersing the electrodes in concentrated nitric acid (67 % w/w) and sulphuric acid (98 % w/w) for 10 min, respectively. In most of the experiments described in Ref. [6]. CV was employed to synthesize POAP films, using a potential sweep rate of 100 mV s^{-1}. Electropolymerizations were carried out on these different surfaces by cycling the electrode potential between -0.2 and 0.7 V and the net charge passed in each kind of electrode was assessed. As was proposed by Barbero et al. [1] a composite of two different (ladderlike and linear chain) structures was considered to be formed on the electrode surfaces under the polymerization conditions employed in Ref. [6]. Figure 1.6a–c compare three stable cyclic voltammograms of POAP films on untreated, chemically pretreated, and electrochemically pretreated GC electrode surfaces, respectively. The net charge during the electropolymerization process of each polymer film was 46 mC cm^{-2}. The oxidation current peak **1** and the reduction current peak **1′** were attributed to the redox reaction of the polymer film.

The highest peak current was obtained for the electrochemically treated GC electrode (Fig. 1.6c). The peak current value for the film formed on the
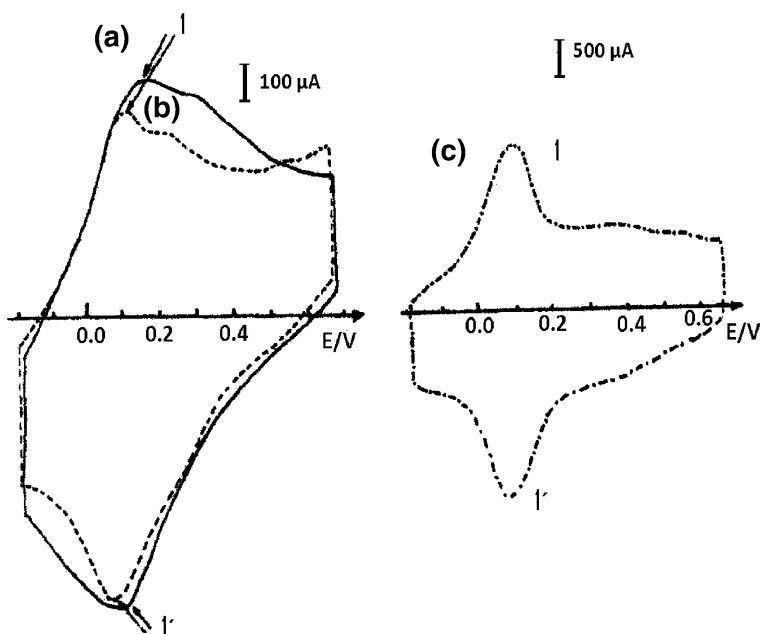
Fig. 1.6 Cyclic voltammograms of poly-*o*-aminophenol (POAP) films (46 mC cm^{-2}) on different carbon electrode substrates in 0.1 mol/L H_2SO_4. **a** Original glassy carbon (GC) electrode. **b** Chemically pretreated electrode using 98 % sulfuric acid for 10 min. **c** Electrochemically pretreated GC electrode at 1.85 V for 5 min, then cycled between -0.2 and 0.7 V for another 15 min in 0.1 mol/L H_2SO_4 [6]

electrochemically pretreated electrode was about four times that of the untreated electrode. The reversibility of the redox reaction was also improved and the ratio Ipa/Ipc was nearer to unity in the electrochemically pretreated electrode. These differences were attributed, in part at least, to the formation of thicker POAP films on the pretreated electrode owing to chemical oxidation of *o*-AP by some oxide species present on the surface electrode after pretreatment. The C_n $^+HSO_4^-$ species on the GC surface was considered as a possible oxidant and (or) newly formed oxide species after electrochemical pretreatment. On the other hand, Yong and Zugeng [6] also verified that the electron-transfer rate from the polymer film to the electrode substrate on electrochemically pretreated GC electrodes was at least twice that of the electron-transfer rate for the untreated electrode. It was proposed that some functional group, such as quinone-like species, may serve as an "electron mediator" at the polymer–solution interface. The effect of the pretreatment potential on the electropolymerization rate of *o*-AP was also analyzed by Yong and Zugeng [6]. The electropolymerization rate for the pretreated electrode was not very different from that for the untreated electrodes when the pretreatment potential was 1.55 V. However, it was observed that for pretreatment potentials of 1.85 and 2.05 V, the electropolymerization rate of the monomer increased with the increase of the pretreatment potential. The faster polymerization rate at higher pretreatment potentials was attributed to the higher amounts of surface oxide species formed on the electrode surface. This study [6] on different GC surfaces seems to indicate that oxide species formed on the electrode surface can play the role of oxidants within the electropolymerization process of *o*-AP and these species oxidize *o*-AP•+ to the oligomer of *o*-AP. With regard to chemical pretreatment of the electrodes, Yong and Zugeng [6] remarked that external reflection FT-IR spectra and attenuated total reflection (ATR) FT-IR spectra showed evidence that nitro groups are formed on carbon after chemical treatment with nitric acid. The effect of nitro and sulphate groups present at the surfaces of chemically pretreated GC electrodes on the electropolymerization of *o*-AP was also analyzed by Yong and Zugeng [6]. It was observed that the electropolymerization rate for the electrodes that were treated with nitric acid was quite slow, even slower than the rate for untreated electrodes. In this regard, a polymer film whose charge was 46 mC cm^{-2} was obtained in about 40 s on electrochemically pretreated GC electrodes. On both untreated and sulfuric acid-treated electrodes, the formation of a similar thickness of film took about 5 min. However, only a 23 mC cm^{-2} thickness film was obtained on nitric acid-treated electrodes after 30 min of polymerization. All these findings allowed Yong and Zugeng [6] to conclude that the different surface species present on different chemically pretreated GC electrodes may have different effects on the electropolymerization process of *o*-AP and different electropolymerization mechanisms may also be involved in the formation of POAP.

Oyama et al. [7] prepared POAP on basal-plane pyrolytic graphite (BPG) and In–Sn oxide conducting glass (indium thin oxide, ITO) by electro-oxidative polymerization of *o*-AP. The electrode potential was cycled between −0.4 and 1.0 V (vs. a sodium chloride saturated calomel electrode) at 50 mV s^{-1} in a

0.5 mol/L Na_2SO_4 solution (*pH* 1) containing 50 mmol/L *o*-AP. As reported in other works [1–3, 5], *o*-AP electro-oxidizes irreversibly at high positive potentials and, after the first reverse scans, anodic and cathodic currents are developed within the potential region between −0.2 and 0.2 V. The current response within this last potential region increased continuously with successive potential scans, indicating the build-up of the electroactive polymeric product POAP. As the potential scan was continued, both electrode (BPG and ITO) surfaces were covered with a brownish orange thin film. A reversible redox response of the POAP film was observed only in the presence of the supporting electrolyte solution (0.2 mol/L $NaClO_4$, *pH* 1). The amount of charge involved in both oxidation and reduction processes was found to be almost equal. POAP films obtained by Oyama et al. [7] were characterized by IR spectroscopy, and the spectra of POAP were compared with those of *o*-AP and phenoxazine. From this comparison two structures of POAP were proposed: a partially ring-opened structure (Fig. 1.7) and another partially hydrolyzed structure (Fig. 1.8).

Zhang et al. [8] studied the electrochemical synthesis of POAP on GC in a 1 mol/L SO_4H_2 + 0.5 mol/L Na_2SO_4 solution by CV and Raman spectroscopy. The evolution of the cyclic voltammograms during polymerization of *o*-AP within the potential range comprised between −0.2 and 1.0 V (SCE) was analyzed by Zhang et al. [8]. Three redox pairs were observed. The most negative redox pair was observed at around 0–0.15 V and it was the only noticeable feature in the cyclic voltammogram of POAP in an acid medium without the monomer. While this redox pair was attributed to the redox reactions of *o*-AP polymers and (or) oligomers, the other two more positive peak systems were associated with the oxidation of *o*-AP to the radical cation (OAP•+) and its further oxidation to the dication, respectively. While the peaks of the redox pair at 0–0.15 V increased steadily with increasing the number of scans, showing the gradual but continual formation of electroactive POAP, the peaks of the other two redox pairs decreased. The flattening of the two more positive peak systems was attributed to a limitation on *o*-AP diffusion during the polymerization process. The scarce formation of the radical cation (polaron) and dication (bipolaron) during the polymerization was associated with restricted charge-transport processes and electron delocalization effects along a partly cross-linked polymer chain.

Zhang et al. [8] proposed that POAP is formed predominantly by the attack of oxidized monomers on the polymer growing chain. Their in situ Raman spectroscopy measurements suggest that the POAP matrix contains alternating oxidized (quinonoid) and reduced the (*N*-phenyl-*p*-phenylenediamine) repeating units (Fig. 1.9) [8].

Fig. 1.7 Partially ring-opened structure of poly-*o*-aminophenol (POAP) [7]
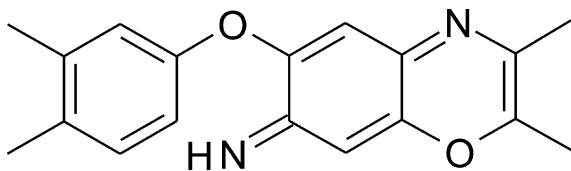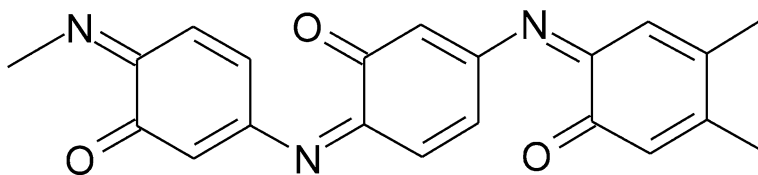
Fig. 1.8 Partially hydrolyzed structure of poly-*o*-aminophenol (POAP) [7]

Zhang et al. in another work [9] synthesized POAP on GC and Pt electrodes from a solution containing 0.05 mol/L *o*-AP in a mixture of 1 mol/L H_2SO_4 and 0.5 mol/L Na_2SO_4 to study the oxidation process of POAP deposits of different thicknesses. Potential was scanned from -0.2 to 0.8 V (SCE) at 100 mV s^{-1} for different numbers of cycles (*N*). The extent of the oxidation of the polymer films was investigated at the open-circuit potential of POAP. The synthesis conditions employed by Zhang et al. [9] allowed them to propose the same POAP structure formulated in Ref. [8] (Fig. 1.9). The relative proportions of alternating oxidized (quinonediimine) and reduced (phenylenediamine) repeating units were found to be dependent on the oxidation state of the polymer. Although the polymer synthesized in Ref. [8] corresponds to the reduced state ($E = -0.2$ V) of POAP, it was observed in Ref. [9] that it is readily oxidized by dissolved oxygen in the electrolyte and the extension of the oxidation depends on the film thickness. Thick films were more difficult to oxidize and often resulted in a mixture of reduced and oxidized forms. With the diffusion of oxygen impeded by the increase of the film thickness, oxidation of thick POAP films was confined mostly to the polymer exterior. The structure of POAP proposed by Zhang et al. [9] also allowed them to explain the interaction of the polymer with metal cations. In this regard, it was observed that when POAP films deposited from 150 voltammetric cycles are equilibrated in a 0.1 mol/L $AgNO_3$ solution for 30 min, the films capture silver cations. The cation capturing process was attributed to the simultaneous presence of hydroxyl and amino groups of the polymeric backbone of POAP, in which the lone pair electrons are available to coordinate with metal cations (Fig. 1.9). The interaction of POAP with silver ions ranged from redox reactions, in which cations
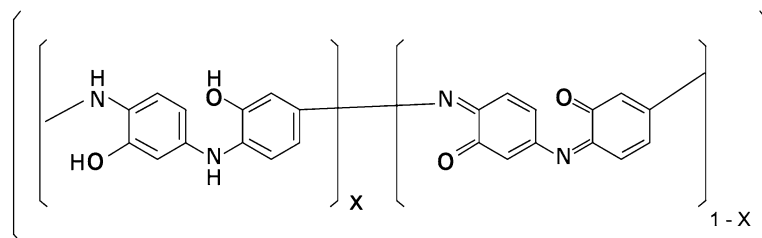
Fig. 1.9 Structure of poly-*o*-aminophenol (POAP) as an alternating series of oxidized (quinonoid) and reduced (*N*-phenyl-*p*-phenylenediamine) repeating units [8]

were reduced to the metallic form, to a partial charge transfer between the metal and the polymer resulting in the formation of a metal–polymer complex. These two types of interactions predominate in thick films ($N = 120$) and thin films ($N = 1$). Films of moderate thickness ($N = 20$) exhibited intermediate behaviour. The Ag^+–POAP complex synthesized in Ref. [9] was also compared with that of Ag^+–PANI [10]. It was indicated that the Ag^+–POAP complex presents an improved stability over that of Ag^+–PANI because of the cooperative action of the oxygen atom in the POAP chemical structure. Since the redox reaction of silver is within the range of the POAP redox reaction, changes of POAP conductivity were not significant during the redox reactions of the POAP–Ag^+ complex. This was very different from the situation of the Ag^+–PANI complex, where the redox switching of PANI between the insulating state of leucoemeraldine and the conducting state of emeraldine has substantial influence on the voltammetric response of silver redox behaviour. Also, it was demonstrated by Zhang et al. [9] that POAP is more resistant than PANI to electrochemical degradation and can capture four times more silver than PANI. The POAP–Ag(I) complex also exhibits electrocatalytic activity in dissolved oxygen reduction. However, it was observed that silver can be released from the complex upon acidification of the nitrogen and oxygen atoms or upon application of a sufficient positive potential.

The 1,4-substituted molecular structure of POAP proposed by Zhang et al. [8, 9] (Fig. 1.9) also seems to be consistent with the electrochemical response of POAP films to ferric cation in solution [11, 12]. It was reported by Yano et al. [11] that POAP films obtained on ITO electrodes by electropolymerization of *o*-AP (0.1 mol/L) in a 0.1 mol/L H_2SO_4 aqueous solution, after being soaked in a ferric cation solution, can act as potentiometric Fe(III) ion sensors. In this regard, the POAP films immediately synthesized [11] showed IR spectra that correspond to a 1,4-substituted structure. When these POAP films were soaked for 24 h in a 0.1 mol/L H_2SO_4 aqueous solution containing 50 mmol/L $Fe_2(SO4)_3$, their XPS spectra showed iron ion capture. The ferric cation capturing process was attributed to the simultaneous presence of hydroxyl and amino groups of the polymeric backbone of POAP. After this cation capture process, the electrode potential of the POAP film was measured in various aqueous solutions containing Zn(II), Ni(II), Cu(II), Fe(II), and Fe(III) ions at different concentrations. The relationship between the electrode potential (E) and the logarithm of the concentration (C) of the different cations in solutions was recorded. The electrode showed no potential response to ion concentration for Zn(II), Ni(II), Cu(II), and Fe(II) ions. However, it showed a Nernstian potential response to Fe(III) ions with a slope -57 mV/log[Fe(III)]. The response time was less than 10 s, and the response was observed until [Fe(III)] = 10^{-4} mol/L. The response to Fe(III) ions in solution was considered indicative of the presence of Fe(II) in the POAP film. The presence of Fe(II) into the film was explained by considering that the captured Fe(III) are, at least in part, reduced to Fe(II) by the film. The potentiometric response was attributed to the electron transfer between Fe(II) ions into the film and Fe(III) ions in solution.

Despite the extensive electrochemical studies of potentiodynamically synthesized POAP, Holze et al. [13] investigated the potentiostatic electrochemical polymerization of *o*-AP at different electrode potentials ($E = 0.7$, 0.8, and 0.9 V vs. SCE) with the aim of comparing the redox behaviours of the synthesized polymer by CV and potentiostatically. POAP films potentiostatically synthesized at 0.7 V showed two redox processes. The first redox process was centred at $E = 0.16/0.15$ V (SCE) and the second one was observed at $E = 0.35/0.29$ V. The contribution of the second redox process decreases as the potential applied during the electrosynthesis is increased. Voltammograms of POAP obtained at the higher potential (i.e., 0.90 V) showed a sharp cathodic peak with two distinct anodic peaks on the forward scan. Furthermore, the voltammogram of POAP obtained at $E = 0.90$ V presented a somewhat intermediate behaviour between that of films obtained potentiostatically at $E = 0.7$ V and that of film potentiodynamically synthesized. To interpret the second redox process at potentiostatically synthesized POAP films, the dependence of the cyclic voltammogram upon potential scan rate and solution *pH* was analyzed by Holze et al. [13]. With regard to potential scan rate, both the anodic and cathodic peak currents of the first redox process were found to scale linearly with the potential sweep rate in the range 10 mV s^{-1} < v < 100 mV s^{-1}, indicating that the electrochemical process of POAP is a surface process and kinetically controlled. The second redox process was not well-defined enough to apply the same analysis. With regard to the *pH* effect, by increasing the solution *pH* from 0 to 1.0, the first redox couple remained almost unaffected, whereas the peak currents of the second redox pair were decreased. Whereas the first redox pair showed a little change up to *pH* 2.0, the second redox pair was affected to a great extent as the anodic peak was replaced by a shoulder and the cathodic peak by a current plateau. By increasing the solution *pH* to 3.0, the first redox pair was further shifted towards negative potentials, but the second pair was almost completely replaced by anodic and cathodic current plateaus. Beyond *pH* 3, the first redox couple was also affected very much. Raman and UV–vis spectra were also recorded by Holze et al. [13] to differentiate potentiostatically and potentiodynamically synthesized POAP films. Although Raman and UV–vis spectra of potentiostatically and potentiodynamically synthesized POAP films were found to be similar, some differences were observed in the dependence of the band intensities on the applied potential. These differences were assigned to the ladder-type polymer structure. Raman and UV–vis spectroscopic measurements reveal that the redox transition of potentiostatically synthesized POAP from the completely reduced state to the completely oxidized one proceeds through two consecutive reactions in which a charged intermediate species takes part. Then, in the light of these electrochemical and spectroscopic analyses [13], a mechanism for the redox transformation of potentiostatically prepared POAP films was proposed, in which phenoxazine units take part.

The development of a NO sensor based on hybrid films of POAP and the metal complex sulfonated nickel phtalocyanine (NiSuPh) was reported by Barbero et al. [14]. POAP films were produced by cycling the base electrode (Pt or GC) between -0.25 and 0.7 V (SCE) at 50 mV s^{-1} in a 0.05 mol/L *o*-AP solution in 0.5 mol/L

$HClO_4$. To incorporate the metal complex, NiSuPh was added to the solution at a 10 mmol/L concentration. The polymerization in the presence of the metal complex was faster than with *o*-AP alone. This fact was attributed to a template effect of the sulfonic groups. After several cycles (>50) a film of POAP/NiSuPh was deposited on the electrode. The incorporation of the metal complex into the polymer film was tested by ex situ reflection–absorption FT-IR spectroscopy. The hybrid film, produced with the metal complex, revealed new bands at 1063 and 1030 cm^{-1}, with respect to those corresponding to POAP. These bands were assigned to stretching of the sulfonate group. The bands were retained in a solution after cycling without the complex, even at *pH* 7. The modified electrodes were tested for NO electrochemical oxidation. A peak at 0.95 V was observed on the cyclic voltammogram that corresponds to NO oxidation, and it increases with NO concentration. It was observed that both POAP and POAP/NiSuPh films present higher electrocatalytic activity for NO oxidation than the base substrate (GC). The oxidation current, in the electrode modified with the complex, is higher and the oxidation overpotential is lower, indicating that the Ni complex incorporated into the hybrid film could electrocatalyze NO oxidation. The peak current was measured to determine the concentration of NO in the solution. The peak current was linear up to a concentration of 200 mol/L.

The electro-oxidation of methanol in aqueous acid solutions using GC electrodes modified by a thin film of POAP containing dispersed Pt and Pt alloy microparticles was studied by Golabi and Nozad [15]. Pt, Pt–Ru, and Pt–Sn particles were incorporated into the polymer film by electrochemical deposition and the following electrodes were synthesized: GC/POAP/Pt, GC/POAP/Pt–Ru, and GC/POAP/Pt–Sn. A mean value of 0.52 $\pm$ 0.02 μm was employed for the polymer film thicknesses in the different electrodes. Electropolymerization of *o*-AP was performed either by potentiodynamic or potentiostatic methods. In the potentiodynamic procedure the electrode potential was swept between −0.10 and 1.00 V (SCE) at a scan rate of 20 mV s^{-1}. In the potentiostatic method, the electrode potential was fixed at 1.0 V for a given time. In both cases, an aqueous solution containing 0.10 mol/L $HClO_4$ and 0.10 mol/L *o*-AP was used as electrolyte. In all experiments the working electrode was submerged in open-circuit position into the methanol solutions. Voltammograms were recorded by sweeping the potential from 0.0 to 1.00 V (vs. SCE). Although the Pt loading for both electrodes (GC/Pt and GC/POAP/Pt) was similar, it was observed that the peak current for the oxidation of methanol (0.63 V vs. SCE) increased from 0.48 mA (GC/Pt electrode) to 1.73 mA (GC/POAP/Pt) (area of the GC electrodes, 0.07 cm^2). This result was explained in terms of an enhancement of Pt microparticle efficiency towards the catalytic oxidation of methanol in the presence of POAP. Similar results were also obtained when Pt was replaced by Pt–Sn or Pt–Ru alloys. Chronoamperometric experiments indicated the existence of an increase in the real surface area of a GC/POAP/Pt electrode with respect to that of a GC/Pt electrode (the area of the GC/POAP/Pt electrode was 2.85 times larger than that of the GC/Pt electrode). An augmentation of the real surface was invoked then [15] to explain the increase in reactivity of the electrocatalyst deposited in the presence of POAP.

Thus, the role of the polymeric matrix is not directly connected with an increase of the intrinsic specific activity of the electrocatalyst, but the polymer film only acts as a good and proper bed for deposition of electrocatalyst particles and increases the catalytic activity of active sites.

1.3 Electropolymerization of *o*-aminophenol in Alkaline and Neutral Media

The electropolymerization of *o*-AP from a 0.3 mol/L NaOH hydroalcoholic solution (70 vol % H_2O, 30 vol % CH_3OH) containing 0.1 mol/L *o*-AP to produce a protective polymer layer on different substrates (vitreous carbon, platinum, and copper) was described by Guenbour et al. [16]. Figure 1.10a–c show the CV curves obtained, respectively, for vitreous carbon (VC), Pt, and copper in the 0.3 mol/L NaOH hydroalcoholic solution free of monomer (broken line). The

Fig. 1.10 Voltammograms obtained in 0.3 mol/L NaOH hydroalcoholic solutions (*pH* 12.7) for **a** vitreous carbon, **b** platinum, and (**c**) copper. (—) with 0.1 mol/L *o*-aminophenol (*o*-AP) and (- · · -) without *o*-AP. Scan rate, 30 mV s^{-1} [16]
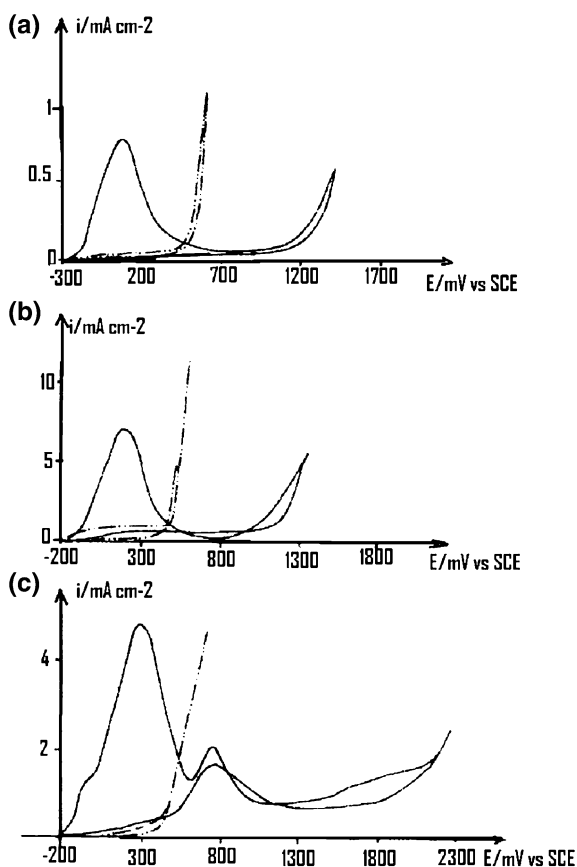
oxidation leads to an increase of the current near 0.3 V (SCE). The addition of 0.1 mol/L of *o*-AP to the hydroalcoholic solution (continuous line) induced a current peak with a maximum at 0.09 V(VC), 0.16 V(Pt), and 0.2 V (copper). This peak was attributed to the oxidation of *o*-AP that began at −0.2 V and *pH* 12. In the case of VC and Pt substrates (Fig. 1.10a, b, respectively) the peak of current was followed by a wide passivity domain, characterized by a very weak current, showing the formation of a very protective film. After the forward part, the reverse curve with negligible current confirmed the insulating character of the film and showed the irreversibility of the system.

Figure 1.10c illustrates the behaviour of the copper substrate. The forward part of the curve for copper presents a second peak at a high potential (0.765 V vs. SCE), attributed to the substrate oxidation through the holes of the growing film. To confirm this assertion, the polarization curve was stopped before the apparition of the second peak; the reverse curve shows the presence of the protective film. However, as the voltammetric scan was extended towards the second peak domain, the voltammetric response did not show the formation of a protective layer. Then, the films synthesized [16] by using the cyclic potential sweep method in the first potential domain, between −0.2 and 0.65 V, were washed with ethanol and water and then heated in an oven at 120 °C for 30 min. The films obtained were yellowish and very adherent. The films in acidic solution became brownish orange. However, films obtained on copper in the second potential domain were not adherents, which was attributed to the oxidation products of the substrate mixed with the organic film. To avoid strong corrosion of the copper substrate the potential was kept below 0.65 V [16]. Chronoamperometric studies were also carried out [26]. For constant potential values within the first peak domain, below 0.65 V, a progressive decrease of current densities for the three substrates was observed. Stationary currents were achieved after 20 min. This behaviour confirmed the insulating character of the film. For copper polarized at 0.51 V (near the maximum potential peak or slightly higher), very uniform yellowish layers were obtained. After washing and heating at 120 °C for 30 min, the resultant films were very adherent. For the copper substrate, the electrochemical treatment at high potentials corresponding to the second peak of the polarization curve led to a very different behaviour. It was observed that, during a treatment at 0.76 V, current densities have high values, which were attributed to the corrosion phenomenon. The analysis of the electrolyte by atomic absorption revealed the presence of copper ions in the solution, which confirmed the dissolution of the substrate. The physical characteristics of the film deposited on copper were dependent on the concentration ratio $R = [NaOH/o\text{-}AP]$. Results reported by Guenbour et al. [16] refer to hydroalcoholic solutions containing 0.3 mol/L NaOH and 0.1 mol/L *o*-AP ($R = 3$), and the films obtained were homogeneous and very adherent. However, the authors remark that with $R = 1$ the films were not adherent and presented cracks and large pores. POAP layers deposited on the copper substrate (four cycles between −0.23 and 1.2 V) were also analyzed by Guenbour et al. [16] by employing IR and XPS spectrometry techniques.

Thin nonconducting POAP films synthesized in neutral media were also employed as protective layers for biosensor applications. In general, POAP films are simultaneously synthesized with different electroactive materials such as hemoglobin, quinhydrone, carbon nanotubes, Prussian Blue (PB), and other polymers such as poly(*o*-phenylenediamine) and polypyrrole (PPy), which act as electron mediators [17–27] for the building of different biosensors. POAP is also widely used as an enzyme matrix in the construction of hydrogen peroxide biosensors because of its catalytic properties towards hydrogen peroxide reduction and limited permeability to small organic molecules [18–21, 26, 27]. The construction and characteristics of some biosensors based on POAP are described in Chap. 3 of this book.

1.4 The Structure of Electrochemically Synthesized Poly (*o*-aminophenol) Films Studied by Spectroscopic Methods: The Oxidation Products of *o*-aminophenol —The Redox Process of Poly(*o*-aminophenol)

As well as electrochemical methods, knowledge about the structure of POAP in both acidic and basic media was obtained by the application of different spectroscopic techniques. The study of the redox conversion of POAP employing spectroscopic analysis has also greatly contributed to the elucidation of the structure of the polymer.

1.4.1 Spectroscopic Characterization of Poly(o-aminophenol) Films Synthesized in an Acid Medium

Characterization of electrochemically synthesized POAP films in an acid medium employing IR and UV–vis spectroscopy was carried out by Barbero et al. [1] These authors compared the IR spectrum of an electrochemically prepared POAP film with that of 3-aminophenoxazone (Fig. 1.11).

The broad band centred at 3400 cm^{-1} was assigned to the stretching of the N–H bonds and the bands at 1350 and 1240 cm^{-1} were ascribed to the –C–N–C– stretching of the secondary amines (Fig. 11a). Although stretching of the C=N bond was observed at 1633, 1462, and 1384 cm^{-1}, some of these bands were also assigned to the C–C bond. The characteristic =C–C=O stretching in 3APZ at 1573 cm^{-1} (Fig. 1.11b) only appears as a weak absorption in the POAP. This band in POAP was assigned to a terminal group. The C–O (1201 cm^{-1}) and the –C–O–C– symmetric stretching are very well defined in POAP. The peak at 800 cm^{-1} was assigned to the –C–H– bending vibration of aromatic orthosubstituted aromatic rings. The peak at 1092 cm^{-1} was ascribed to the ClO_4^- band. However, this
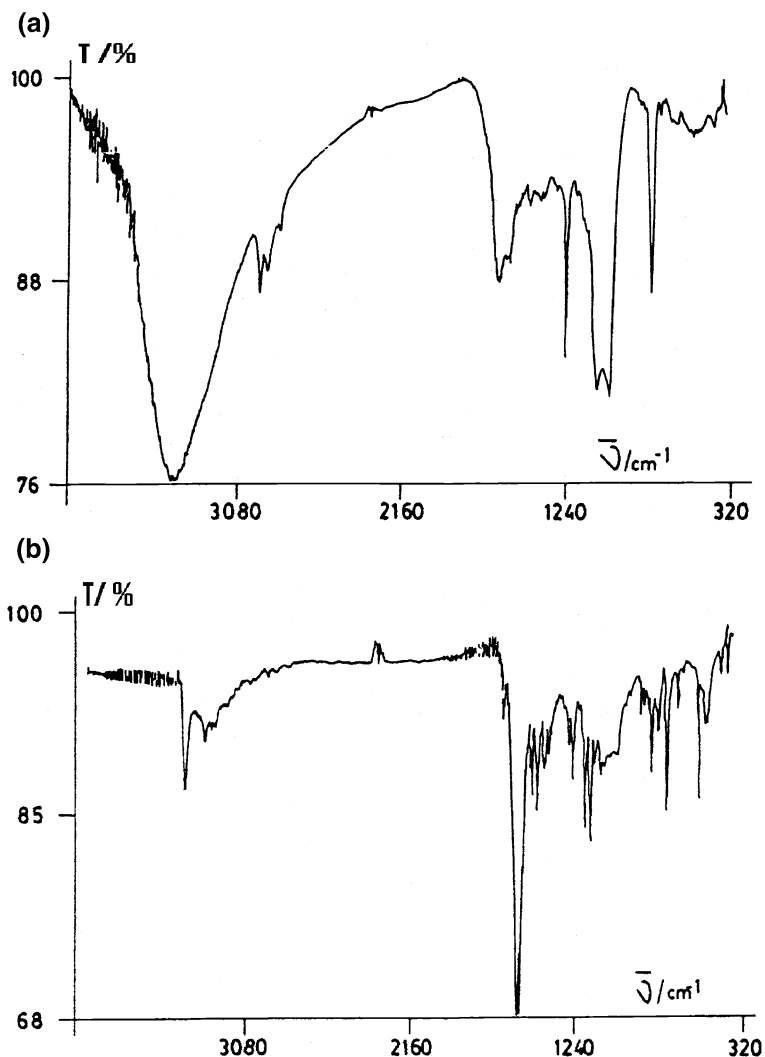
Fig. 1.11 IR spectra of (**a**) electrochemically prepared poly-*o*-aminophenol (POAP) and (**b**) 3-aminophenoxazone [1]

last peak was associated with an impurity because it disappeared after exhaustive washing of the film. Barbero et al. [1] noted the absence of the characteristic strong absorption of the carbonyl group ($1680\ cm^{-1}$) and the phenol group ($2600\ cm^{-1}$) in the POAP spectrum. The absence of the carbonyl band was considered to be an indication of an insignificant quantity of *o*-quinone in the film. In the same way, the absence of an important hydroxyl group absorption band was attributed to a low proportion of a linear chain polymer structure. The POAP structure was also studied by in situ UV–vis spectroscopy by Barbero et al. [1] A broad maximum

Fig. 1.12 IR absorption spectra of **a** a poly-*o*-aminophenol (POAP) film (oxidized form), **b** *o*-aminophenol (*o*-AP), and (**c**) phenoxazine. The POAP film was prepared on pyrolytic graphite (BPG) [7]
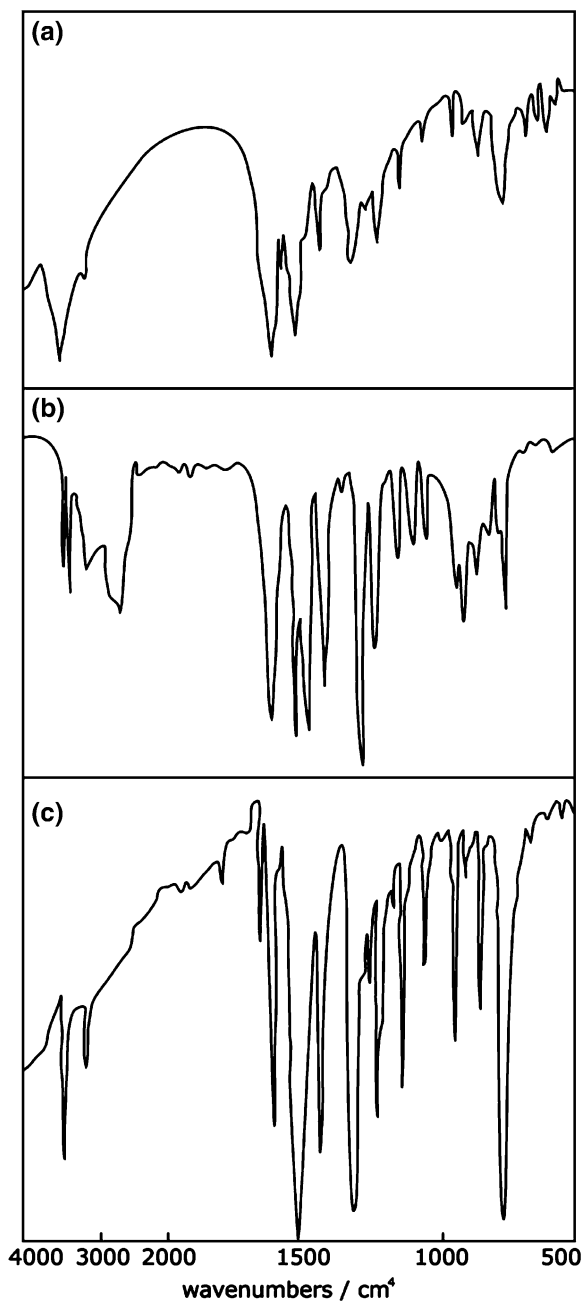
around 480 nm was observed in the oxidized state of POAP. As the UV–vis spectrum has the same characteristics of that reported for 3APZ, it was considered as a confirmation that the film consists of phenoxazine-like units. Then, on the

basis of the IR and UV–vis spectroscopic analysis, the structures shown in Fig. 1.3 were proposed for POAP in the reduced state and in the oxidized one, respectively.

The IR absorption spectrum of the oxidized form of POAP was compared with those of *o*-AP and phenoxazine by Kunimura et al. [7] (Fig. 1.12a–c). Some common absorption peaks were observed for the three compounds, but other peaks were not common. The absorption peaks due to the N–H stretching vibrations of the imino group of the POAP film and phenoxazine were observed at 3420 cm^{-1}, whereas two absorption peaks corresponding to the N–H stretching vibrations of the amino groups of *o*-AP were, as expected, observed at 3340 and 3420 cm^{-1}. The presence of a relatively strong absorption peak around 3420 cm^{-1} was considered as an indication that POAP does not possess a completely ring-closed structure (Fig. 1.3), as proposed by Barbero et al. [1]. In this regard, a partially ring-opened structure as the one shown in Fig. 1.7 and (or) a relatively low degree of polymerization of *o*-AP was proposed by Kunimura et al. [7]. The absorption peaks ascribable to the stretching vibrations of C–N bonds were observed for POAP at 1250 and 1310 cm^{-1}. Similar peaks were observed for *o*-AP and phenoxazine.

The peak at 1645 cm^{-1} in the POAP spectrum was assigned to the stretching of the C=N bonds present in a ladder polymer with phenoxazine rings. The absorption peaks at 1050 and 1235 cm^{-1}, which are characteristic of the C–O–C stretching vibration, were observed for POAP and phenoxazine, but not for *o*-AP. Peaks at 760, 850, and 935 cm^{-1} for POAP were assigned to 1,2-disubstituted, 1,2,4-trisubstituted, and (or) 1,2,4,5-tetrasubstituted benzene structures, respectively. All of these structures were considered to be possible for POAP. Furthermore, from the fact that the absorption peak assigned to the stretching vibration of the C=O bonds of the aromatic keto groups was observed at 1670 cm^{-1}, the partially hydrolyzed structure shown in Fig. 1.7 was proposed for POAP by Kunimura et al. [7], and the structure shown in Fig. 1.8, which was assumed to proceed from a polymerization via C–N=C bonds, was also proposed as a possible structure of POAP.

The role of laccase on the electrochemical synthesis of POAP from 0.1 mol/L phosphate buffer (*pH* 5.5) solutions was described by Palys et al. [24]. They demonstrated that laccase can be utilized as a polymerization initiator with no need of electrochemical monomer oxidation [24]. Raman spectra of POAP electrode-posited at *pH* 5.5 with and without the presence of laccase in the polymerization bath and the spectrum of the POAP obtained by the enzyme polymerization of *o*-AP were compared in Ref. [24]. Raman bands of 2,2′-dihydroxyazobenzene (DHAB) and 3APZ were observed in the spectra obtained at *pH* 5.5. Raman spectra of DHAB are characterized by the strong band at 1390–1400 cm^{-1} owing to the N=N stretching mode. The electrochemically synthesized POAP film shows a strong band at 1397 cm^{-1}, which was attributed to the N=N stretching mode of DHBA. This band is weaker in the spectrum of the POAP film electrodeposited in the presence of laccase and it disappears completely in the spectrum of POAP obtained by enzymatic polymerization of *o*-AP. This effect was attributed to the fact that N–N coupling only occurs during the electrochemical oxidation of *o*-AP.

Several 3APZ modes were also observed in the spectra of the three POAP samples (578, 1150, 1278, 1475, 1505, 1605, and 1660 cm^{-1}). Slight shifts in band positions were attributed to further oxidative polymerization of 3APZ to POAP. Since the POAP structure contains conjugated double bonds, shifts of aromatic ring modes were considered probable. Despite the presence of laccase in the electrodeposited POAP films being confirmed by a test using syringaldazine, its contribution to the Raman spectra seems to be very weak. Only weak features at 468 and 1264 cm^{-1} were assigned to the enzyme. The enzymatically synthesized spectrum of POAP shows a very strong band at 1504 cm^{-1}, with a frequency that is identical to the aromatic ring mode of 3APZ. As this frequency also coincides with the primary amine deformation mode of *o*-AP, it was suggested that it is related to either the monomer that did not react, to 3APZ, or to short oligomers. Typical UV–vis spectra of POAP electrodeposited in the presence and in the absence of laccase were also obtained by Palys et al. [24]. Both spectra are characterized by a broad absorption band with a maximum at 445 and 430 nm for the film obtained in the presence and absence of laccase, respectively. As a similar band was observed for potentiostatic (410 nm) [13] and potentiodynamically (440 nm) [28, 29] electrodeposited POAP films, the bands at 445 and 430 nm in Ref. [24] were attributed to the conjugated π bonds of POAP. The small difference in the position of the bands was related to possible differences in the chain lengths of POAP prepared in the presence and the absence of laccase.

With the aim of discerning between the possibility that 2-aminophenoxazin-3-one (APZ) is the repetitive unit of POAP films and the possibility that it is incorporated onto the film structure during its synthesis, a spectroscopic characterization of soluble products in an electrolyzed *o*-AP solution was carried out by Bulhoes et al. [5]. Drastic optical changes were noted after applying a constant potential of 0.85 V (vs. reversible hydrogen electrode (RHE)) on a Pt wire immersed into a spectrophotometer cell containing an *o*-AP solution. Each deconvoluted UV–vis spectrum of this solution led to two or three main absorption bands, depending on the time at which the measurement was taken. For the purpose of comparison, the spectra of the electrolyzed solution were compared with that of APZ. Whereas the electrolyzed solution presented an absorption band at 400 nm, a well-defined band at 460–470 nm characterized APZ. The absorption band at 400 nm was assigned to quinone intermediates continuously formed during electrolysis (benzoquinone, benzoquinone–monoimine, and benzoquinone–diimine). Although the isolation of intermediates failed [5], APZ was identified as the final product after extraction from the electrolyzed *o*-AP solution. This assignment was supported by not only UV–vis spectroscopy but also IR and 1H NMR spectroscopy and elemental analysis. To establish if APZ undergoes any polymerization processes, Pt and GC electrodes were cycled in a medium containing chemically synthesized APZ. While no process of charge transfer was obtained for Pt electrodes cycled in the APZ medium, GC electrodes present one well-resolved redox process. However, the electroactive response of GC was only associated with an activation process of the electrode surface after prolonged cycling [5]. Therefore, the voltammetric results obtained by Bulhoes et al. [5] seem to indicate that APZ does not undergo any

polymerization processes. In another experiment carried out by Bulhoes et al. [5], chemically prepared APZ was dissolved in acetone and dropped on Pt and GC electrodes to prepare APZ films. In this case, a single well-defined redox process was observed on the voltammograms on both Pt and GC electrodes. Owing to the similarities between redox responses of POAP-modified Pt and GC electrodes and APZ-modified Pt and GC electrodes, an IR study was also performed [5] to establish whether APZ is the repetitive unit of POAP films, if it is incorporated into the film structure, or if POAP films and modified electrodes cycled in an APZ medium may present similar redox responses. The IR spectra of the chemically synthesized APZ, the soluble product extracted after electrolysis of *o*-AP solution, a POAP film and phenoxazine were then compared by Bulhoes et al. [5] (Fig. 1.13a–d, respectively). Similar IR signals for the extracted product and APZ

Fig. 1.13 IR spectra of (**a**) the extracted product from electrolyzed *o*-aminophenol (*o*-AP) solution, **b** chemically synthesized 2-aminophenoxazin-3-one (APZ), **c** poly-*o*-aminophenol (POAP) film (prepared on Pt by cyclic voltammetry, 400 cycles), and (**d**) model compound (phenoxazine) [5]
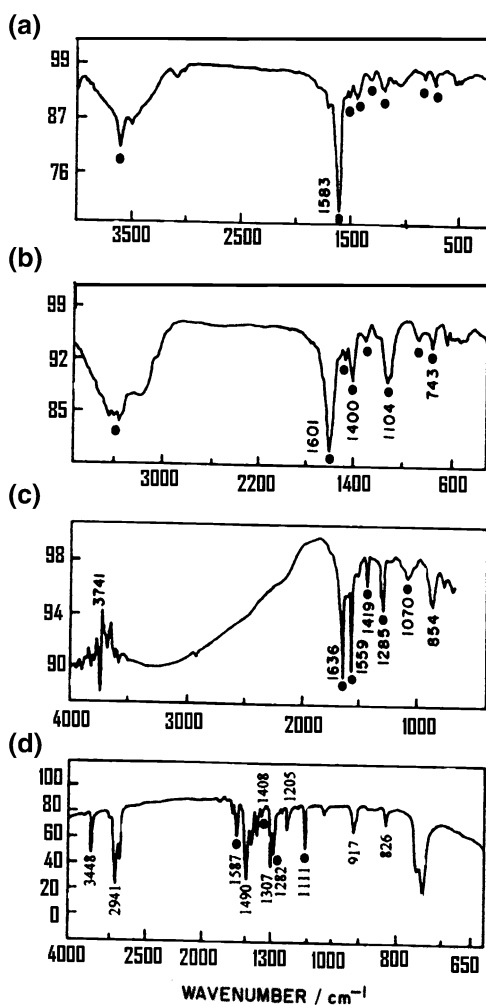
indicated that they are the same materials. In this regard, Fig. 1.13a, b present similar signals (the main coincident peaks are indicated with points) at 3300–3500 cm^{-1} owing to the presence of NH_2 groups and at about 1600 cm^{-1} owing to the axial stretching of the C=O groups in the APZ structure. However, POAP presents a different spectrum (Fig. 1.13c) and, therefore, different structures were proposed by Bulhoes et al. [5] for POAP films and APZ. Common peaks are observed in Fig. 1.13c, d at 1070 and 1111 cm^{-1}, respectively, which were assigned to the stretching of the C–O–C linkages. Also, the peaks in the 1400–1600 cm^{-1} region, were attributed to the stretching of C–H and C–C groups. Similarities were found between the POAP film spectrum and that of phenoxazine. It was concluded by Bulhoes et al. [5] that, although POAP films may be present as phenoxazine units and similar redox responses can be expected for POAP films and APZ-modified electrodes, APZ does not polymerize.

Salvagione et al. [2] studied the oxidation of *o*-AP, and the polymer formed, by in situ FT-IR spectroscopy. The aim of this work was to prove that the most probable structure of the polymer formed in the oxidation of *o*-AP contains the phenoxazine unit. Figure 1.14 shows the spectra of a 1 mol/L $HClO_4$ + 5 × 10^{-3} mol/L *o*-AP solution with a polycrystalline Pt electrode immersed in it being polarized at different potential values.

The electrode was immersed at 0.1 V (RHE) into the spectroelectrochemical cell and then the potential was stepped up to 0.4 V and the reference spectrum was collected. The potential was then polarized to higher values to oxidize the *o*-AP, and the sample spectra were acquired at 0.8 and 1.0 V. In the spectrum at 0.8 V (RHE) (Fig. 1.14a) two positive bands at 1510 and 1471 cm^{-1} were observed. These two bands were assigned to the aromatic C=C stretching vibration and the ring C=C vibration of meta-disubstituted benzenes. The positive character of these

Fig. 1.14 FT-IR spectra for a Pt electrode in a 1 mol/L $HClO_4$ + 5 × 10^{-3} mol/L *o*-aminophenol (*o*-AP) solution. **a** Sample potential, 0.8 V; **b** sample potential, 1.0 V; and (**c**) spectrum obtained at 0.9 V in deuterated water. P-polarized light, 100 interferograms. Reference potential, 0.4 V [2]
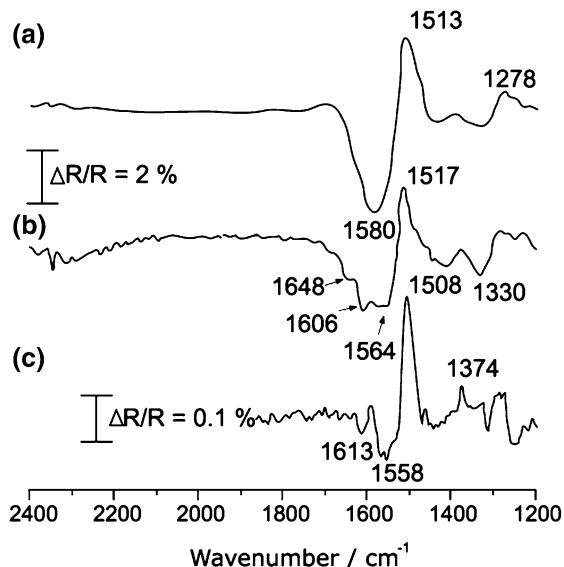
bands was attributed to consumption of the species related to these features at the sample potential. At 1.0 V (Fig. 1.14b), these two bands were observed together with a strong band at 2345 cm^{-1} corresponding to the formation of CO$_2$ in the solution. No clear bands were observed at lower sample potentials. When the same spectrum is collected in deuterated water (Fig. 1.14c), two negative bands at 1683 and 1645 cm^{-1} were observed. These bands were associated with the C=O and C=N stretching vibrations, respectively.

Figure 1.15a, b show the spectra of POAP in 1 mol/L HClO$_4$ solution in the absence of *o*-AP in water and in deuterated water, respectively. The reference spectrum was obtained at 0.1 V, so it contains the vibrational information corresponding to the reduced form of the film. The electrode was then polarized to 0.7 V (RHE), and the sample spectrum was collected. Similar bands were observed in both spectra. Figure 1.15a displays two clear positive bands at 1513 and 1278 cm^{-1} and a broad negative band at 1580 cm^{-1}. The band at 1513 cm^{-1} is also present in the spectra in D$_2$O (Fig. 1.15b), but, in this case it was observed at 1517 cm^{-1} and was assigned to the C=C stretching of the aromatic ring. This band was not observed after polymer oxidation. The broad negative band at 1580 cm^{-1} was also present in deuterated water, but, in this case, the band has contributions from several bands at 1564, 1606, and 1648 cm^{-1}, and it was assigned to either a quinoid ring or a C=N stretching vibration in the phenoxazine units produced upon complete polymer oxidation (Fig. 1.3). The 1648 cm^{-1} band was attributed to C=N stretching where conjugation with a phenyl group shifts its frequency to higher values, and it was more clearly observed in deuterated water owing to the reduced interference of water absorptions. Another negative band was observed at 1330 cm^{-1} in both spectra, which was also clearly seen at low

potentials. This band was assigned to the C=N stretching of quinoid rings containing C=N and C–N groups. To check these assignations the spectra for phenoxazine in the same range of potentials was also obtained by Salvagione et al. [2]. Figure 1.15c shows the spectrum obtained from a 1 mol/L $HClO_4$ + 5×10^{-4} -mol/L phenoxazine solution in deuterated water, where the polycrystalline platinum electrode immersed in it was polarized at different potential values. A series of reference and sample spectra were collected at 0.2 and 0.7 V and then co-added. The spectrum obtained showed a sharp and negative band at 1508 cm^{-1} corresponding to the disappearance of the aromatic ring at the sample potential. A positive band at 1374 cm^{-1} was also observed that was assigned to the C–N stretching of the secondary aromatic amine that also disappeared at 0.7 V. Two negative bands were observed at 1558 cm^{-1} that were associated with the C=N stretching vibration of the imine group that is produced at higher potentials in the oxidation of phenoxazine. Salvagione et al. [2] concluded that the most probable structure of the polymer formed in the oxidation of *o*-AP contains the phenoxazine unit as the main constituent of its structure. Theoretical calculations carried out by Salvagione et al. [2] seemed to confirm that the polymer obtained by electro-oxidation of *o*-AP has a ladder structure built by phenoxazine units. In this regard, they [2] calculated the electronic density of *o*-AP by employing the semiempirical selfconsistent field method (AMI). They determined that *o*-AP has a high electron density in the *para* position with respect to the $-NH_2$ group. Therefore, dimers could be formed through the attack of the cation radical at that position. The dimer of *o*-AP has a higher electron density in the para position with respect to the $-OH$ group, allowing the closing of the phenoxazine ring.

1.4.2 The Redox Process of POAP in Acid Medium Studied by Spectroscopic Methods: Intermediate Species During the Redox Switching of POAP

Raman spectroscopy and voltammetry were coupled to identify structural changes during the redox process of POAP. Voltammetric measurements at different perchloric acid concentrations carried out by Salvagione et al. [30] revealed the existence of two redox processes for POAP films. Raman spectra of a POAP film deposited on an Au electrode at different electrode potentials were obtained. The different bands of POAP extracted from a in situ Raman spectrum acquired at 0.1 V are listed in Table 1.1. Bands at 1593, 1474, 1390, and 1160 cm^{-1} were associated with quinoid groups and bands at 1520 and 576 cm^{-1} were assigned to aromatic rings. The band at 1638 cm^{-1} was attributed to the –C=N– in quinonimine units. The intensity of some of these bands was found to be dependent on the applied potential. The behaviour of the bands with the applied potential shows that when the potential increases, the band at 1474 cm^{-1} increases and the band at 1638 cm^{-1} also increases until a potential of about 0.2 V and, thereafter, it

Table 1.1 Vibrational bands in Raman spectra (λ_o = 647.1 nm) for a poly(*o*-aminophenol) (POAP) film in a 0.5 mol/L H_2SO_4 solution [30]

Wavenumber/ cm^{-1}	Vibration modes
1638	—C=N— stretching of quinonimine units
1593	>C=C< stretching of quinoid units or N–H$^+$ deformation vibration on secondary amines
1520	—C=C— stretching in the aromatic ring
1474	—C=N—stretching of quinoid units
1390	C—C stretching of quinoid units
1328	>C—N$^{\bullet+}$— stretching
1160	C—H bending in plane
925	Perchlorate vibration band
576	Ring deformation of benzeniod units

diminishes. The fitting of both bands by Lorentz curves allowed for the quantification of the evolution with the potential of the corresponding species associated to these bands. The integrated intensity was related to the concentrations of species responsible for these bands. The behaviour of the band at 1638 cm^{-1} was attributed to a typical intermediate species. Since POAP has a conductivity maximum at about 0.04 V (SCE), the intermediate species was related to the polymer conductivity and, therefore, it was assigned to a charged species.

The existence of intermediate species was associated to an oxidation process that occurs by two consecutive reactions from the totally reduced phenoxazine form to the completely oxidized one, through a charged species, which was considered to be a cation radical. The behaviour of the integrated Raman intensity of the band at 1638 cm^{-1} was considered to be similar to that of the band at 750 nm observed in the absorbance vs. potential dependence in the UV–vis region reported by Tucceri et al. [31]. As the maximum absorbances of both bands (750 nm [31] and 1638 cm^{-1}) appear approximately at the same potential, this was considered to be indicative of the existence of two redox processes in the oxidation of POAP. Thus, Raman [30] and UV–vis [31] measurements seem to suggest that the third species could be a cation radical. A redox mechanism of POAP was proposed by Salvagione et al. [30] where the first step involves mainly the anion exchange and the second step involves the insertion/expulsion of protons.

Evidence about the existence of cation radical species during the redox conversion of POAP was also reported by Ortega [3]. Ortega [3] studied the conducting potential range of POAP by employing CV and electron spin resonance (ESR) measurements. POAP films deposited on a Pt electrode were introduced into a solution at *pH* 0.9, which was free of monomer and then ESR spectra were recorded at different potentials, scanning forwards and backwards from −0.250 to 0.55 V (Ag/AgCl).

Figure 1.16 shows a typical signal at negative potentials, which starts decreasing until it reaches a very small value at 0.55 V. The maximum in the ESR

Fig. 1.16   a Typical electron spin resonance (ESR) spectrum of an 80 nm thick poly-*o*-aminophenol (POAP) film on a Pt electrode at *pH* 0.9. Plot (**b**) illustrates the change in the ESR intensities as a function of potential. The maximum intensities are shown between the dotted straight lines [3]
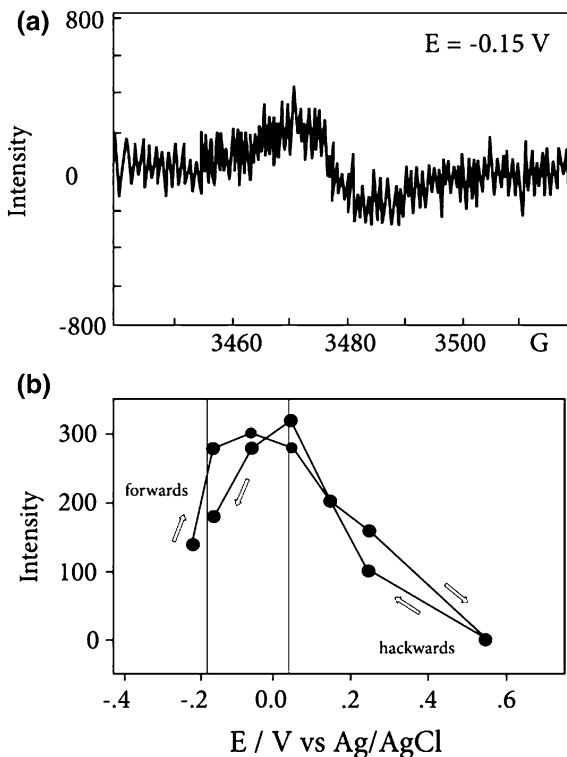
spectra occurs in the potential ranging from -0.24 to approximately 0.0 V (SCE). The decrease and further absence of a detectable ESR signal at higher potentials than 0.55 V was attributed to a combination of radicals to give rise to dication species, which are not ESR active because of their paired spin. Ortega [3] concludes that, at high positive potential values, the creation of bipolarons by a combination of polarons is possible at POAP films.

The existence of charged intermediate species together with structural changes during the redox process of POAP was also reported by Holze et al. [13]. They investigated the potentiostatic electrochemical polymerization of *o*-AP at different electrode potentials by employing in situ Raman spectroscopy. In situ Raman spectra in the potential range between the reduced state ($E = -0.2$ V vs. SCE) and the oxidized state ($E = 0.5$ V vs. SCE) of POAP in 0.5 mol/L H_2SO_4 solution were compared by Holze et al. [13] for both potentiostatically and potentiodynamically synthesized POAP films. The various bands together with their possible assignments are shown in Table 1.2. The bands at 1598, 1472, and 1170 cm^{-1} were associated to quinoid groups, whereas the bands at 1522 and 578 cm^{-1} were attributed to benzoid rings. The band at 1330 cm^{-1} was assigned to a semiquinone species with an intermediate structure between amines –C–NH– and imines –C=N– resulting in polarons. However, Holze et al. [13] also observed an additional

Table 1.2 Vibrational bands in Raman spectra ($\lambda_o = 647.1$ nm) for a poly(*o*-aminophenol) (POAP) film in a 0.5 mol/L H_2SO_4 solution [13]

Wavenumber/cm^{-1}	Description
1645	C=N stretching of quinonimine units
1598	C=C stretching of quinoid units
1522	C=C stretching in the aromatic ring
1472	C=N stretching of quinoid units
1402	C—N$^{\bullet+}$ stretching of radical semiquinone
1330	C—N$^{\bullet+}$ stretching
1170	C—H bending in plane
982 and 1050	Sulfate modes
578	Ring deformation of benzeniod units

band at 1402 cm^{-1} that was completely missing in the spectra reported by Salvagione et al. [30]. It was assigned to the radical semiquinone C–N•+ formed during the partial oxidation of *N,N*-diphenyl-1,4-phenylenediamine. The bands located at 982 and 1050 cm^{-1} were assigned to the internal modes of the sulphate anion of the electrolyte solution. Holze et al. [13] observed that the intensity of some of the bands depends on the applied potential. For instance, the band located at 1170 cm^{-1} grew in intensity when the potential was shifted up to $E = 0.2$ V, beyond this value it diminished with a further increase of the potential. The dependence of the intensity of this band on electrode potential was considered to be a characteristic feature of the oxidized form of POAP and was attributed to the CH-bending vibrational mode of the quinoid-like rings formed during electro-oxidation. The bands in the frequency range 1300–1400 cm^{-1} were associated mainly with the stretching vibrations of charged C$\sim$N+ segments ($\sim$ denotes the bond intermediate between the single and double bonds). Although the Raman features of the POAP films potentiostatically and potentiodynamically synthesized by Holze et al. [13] were similar, some marked differences with respect to the potential dependence of some bands were observed. A difference was observed in particular with respect to the potential dependence of the band around 1645 cm^{-1}. The intensity of this band sharply increased at 0.3 V and slowly decreased at more positive potentials for the POAP film synthesized potentiostatically. However, in the case of the potentiodynamically prepared POAP this band attained the intensity maximum at about $E = 0.2$ V. The band located at 1645 cm^{-1} was assigned [13] to –C=N– in quinonimine units, and was considered to correspond to the C–N–C bond of a heterocyclic six-membered ring structure arising from *ortho*-coupling rather than *para*-coupling during the electropolymerization, resulting in a ladder polymer. As this band did not disappear even at the highest applied potential, the oxidation of fully reduced POAP synthesized potentiostatically to fully oxidized POAP was assumed to proceed via an intermediate half-oxidized state. This assumption is supported by the fact that the maximum intensity of the band at 1645 cm^{-1} was observed at a roughly middle potential between the two redox processes observed on the cyclic voltammograms of POAP shown in Ref. [13].

The effect was associated with the maximum polaron concentration in the polymer. The increase of potential beyond the maximum intensity, which leads to the fully oxidized state of the polymer, was attributed to a lowering in the polaron concentration, probably by the coupling into bipolarons. The band observed around 1598 cm^{-1} was assigned to the quinoid units and grew in intensity with increasing electrode potential. The band at 1472 cm^{-1} was only observed at electrode potentials within the range 0.3 V $< E <$ 0.4 V.

Structural changes during the redox process for chemically synthesized POAP were also analyzed by employing ex situ and in situ UV–vis measurements. POAP was chemically synthesized by treatment of an acid solution of *o*-AP with CuCl$_2$, and the oxidative polymerization was followed by UV–vis spectroscopy [8]. Prior to the addition of CuCl$_2$, two absorption peaks were found on the monomer solution spectra at 258 and 460 nm that were assigned to the $\pi \rightarrow \pi^*$ transition of the aromatic structure (benzene structure) and the oxidized form of *o*-AP, respectively. A new absorption peak at 410 nm was developed after the addition of Cu(II) and its intensity increased with time at the expense of the peak at 460 nm. The peak at 410 nm was assigned to the radical cation (oxidized form) of POAP. The solid polymer synthesized by Zhang et al. [8] was also examined by X-ray photoelectron spectroscopy (XPS). The authors remarked that the C1s, N1s, and O1s spectral features were similar to those reported for POAP electrochemically prepared in other works [32]. The carbon spectrum was deconvoluted to estimate the extent of carbon involved in the C–C, C–N, and C=O bonds. A ratio of 3:2:1, indicating a good degree of polymerization, was obtained by Zhang et al. [8]. They [8] concluded that polymer growth proceeds mainly through the reactions between the growing polymer (POAP) and the oxidized monomer units, and subsequent cyclization of the functional units in the polymer leads to a ladder structure. The relative reflectance change ($\Delta R/R$) as a function of the wavelength within the visible spectrum region was also employed by Zhang et al. [8] to study the structure of electrochemically synthesized POAP films. The wavelength dependence of $\Delta R/R$ for a POAP film electrochemically deposited on Pt when it is polarized at various potentials is shown in Ref. [8]. A broad absorption band extending from 410 to 532 nm was observed for polarization within the range 0.1–1.1 V (SCE). The band intensity increased with increasing potential, turning the film dark brown. In addition, a slight blue shift simultaneous with the intensity increase was noted. The absorption band was assigned to the formation of radical cations at POAP as the polymer matrix became oxidized. The blue shift with the increase in potential was attributed to a larger fraction of radical cation species contained in the polymer as it becomes more oxidized. According to Zhang et al. [8] the oxidation of POAP is not complete even at 0.5–0.6 V (SCE); therefore, the broad band at 410 nm was considered to be composed of $\pi \rightarrow \pi^*$ transitions proceeding from both the oxidized (quinonoid) and reduced (*N*-phenyl-*p*-phenylenediamine) units (Fig. 1.9).

UV–vis spectra of POAP films synthesized potentiostatically at different electrode potentials were analyzed by Holtze et al. [13]. Figure 1.17a, b show UV–vis spectra of a POAP film at different electrode potentials within the range
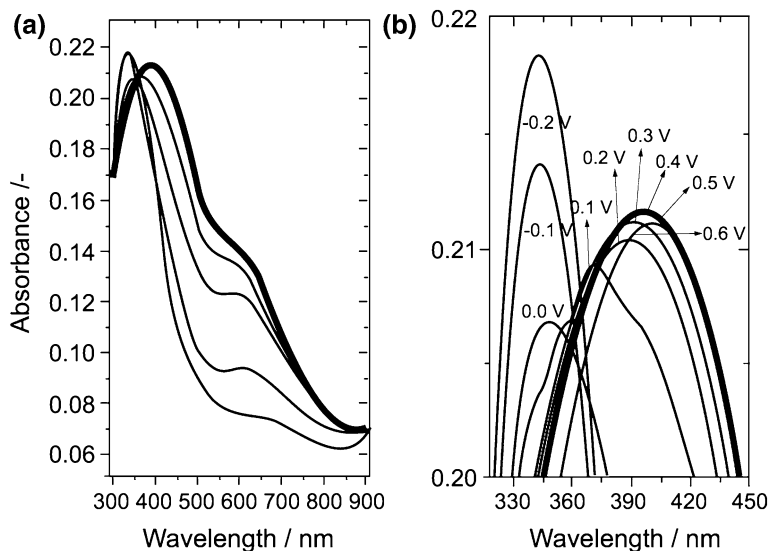
Fig. 1.17 a In situ UV–vis spectra of poly-*o*-aminophenol (POAP) at different applied electrode potentials. The POAP film was prepared on indium thin oxide (ITO)-coated glass at 0.8 V (1 h electrolysis) from a solution containing 0.05 mol/L o-AP in 0.5 mol/L H_2SO_4 solution. **b** Enlarged spectra of (**a**) between 320 and 450 nm [13]

-0.2 V $< E <$ 0.6 V (SCE). Three absorption peaks located at $\lambda =$ 350, 410, and 610 nm were observed. At $E = -$ 0.2 V the polymer is in its reduced state, and the corresponding spectra show an absorption band located at approximately at $\lambda =$ 350 nm. This band was attributed to the phenoxazine structure. With increasing potential, the oxidation of POAP takes place, leading to the formation of radical cations. Holtze et al. [13] observed that, as the potential is increased from -0.2 to 0.1 V, the intensity of the band at $\lambda =$ 350 nm decreases and, at 0.1 V, it split into at least two bands. With a further increase of the potential the intensity of one of these bands was diminished, while the other one started to shift to lower energies and changed into a broad maximum around $\lambda =$ 410 nm. The absorption band at $\lambda =$ 610 nm increased in intensity up to 0.2 V and then it became nearly constant with a further increase of potential. The behaviour of the in situ UV–vis spectra of the potentiostatically synthesized POAP films presented in Ref. [13] was considered as a verification of previous results reported by Ortega [3] indicating that the redox transition of POAP from its completely reduced state to its completely oxidized state proceeds though two consecutive reactions in which a charged intermediate species takes part.

A spectroelectrochemical study of the redox process of POAP was reported by Tucceri et al. [31]. Absorbance changes in the wavelength region between 300 and 800 nm, at different *pH* values and in the presence of different supporting electrolytes, were recorded and analyzed at different degrees of oxidation of POAP.

Fig. 1.18 Absorbance as a function of wavelength at fixed electrode potentials (*E*) in 0.4 mol/L NaClO$_4$ + 0.1 mol/L HClO$_4$. −0.2 V, (— · · —); 0.0 V, (— - - —); 0.1 V, (-x-); 0.2 V, (-o-); 0.5 V, (—); 0.7 V, (- - -) [31]
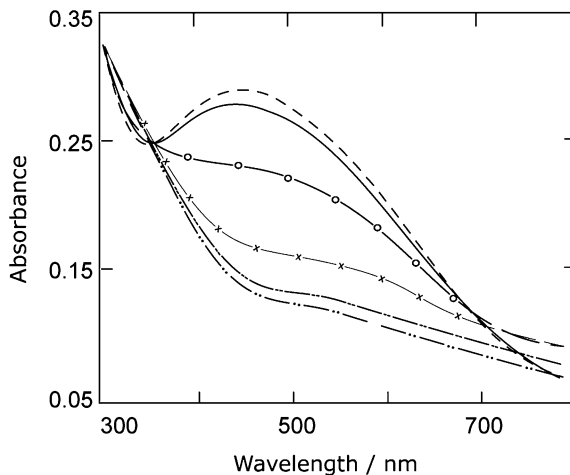
Two types of experiments were carried out by Tucceri et al. [31]: (i) at a fixed wavelength, the electrode potential was swept at scan rates between 0.005 and 0.03 V s^{-1} and (ii) at a fixed electrode potential the wavelength was scanned. Figure 1.18 shows the spectra of POAP films at different electrode potentials in the region where the film is electrochemically active (−0.2 V < *E* < 0.7 V vs. SCE). The absorbance of the film at the negative potential limit (−0.2 V) was attributed to the tail of the UV band related to the $\pi \rightarrow \pi^*$ transition of the basic aromatic structure of the phenoxazine units.

A reaction scheme for the POAP redox switching, which also includes protonation reactions, is shown in Ref. [31]. The redox switching of POAP was interpreted in terms of the oxidation of amine groups to imine groups. As POAP is progressively oxidized, several changes in the spectral response were observed by Tucceri et al. [31]: (*i*) a decrease of the absorbance in the wavelength region at about 340 nm; (*ii*) a broad maximum was developed at 450 nm; and (*iii*) in the region of $\lambda > 750$ nm, the absorbance first increased with a potential up to *E* = 0.1 V and then, for *E* > 0.1 V, the absorbance decreased. The broad band growing at 450 nm as the potential increases in the positive direction was assigned to the partially oxidized phenoxazine structure. While the decreases of the absorbance at $\lambda = 340$ nm, as the potential increases in the positive direction, was attributed to the disappearance of the reduced form of POAP, the increase of the absorbance at $\lambda = 450$ nm was associated with the increase of the oxidized form with the potential scan. For $\lambda = 750$ nm, the absorbance presents a maximum at *E* = 0.15 V, which was considered to be indicative of the existence of a transient species. The spectra of reduced (*E* = −0.2 V) and oxidized (*E* = 0.7 V) states of POAP were also found to be dependent on *pH*. The absorbance difference ($\Delta A = A\text{ox} - A\text{red}$; *A*ox, absorbance of the oxidized state; *A*red, absorbance of the reduced state) was analyzed [31] and represented, at different *pH*, as a function of the wavelength while the polymer goes from the reduced state to the oxidized one. A slight increase of the UV tail was observed under these conditions and it

was attributed to poor protonation of the polymer as it becomes oxidized. This effect was associated with the conversion of one protonated amino group to a nonprotonated imino group. Tucceri et al. [31] concluded that, as the *pH* increases, the reduction of the oxidized species becomes progressively hindered and, consequently, the amount of oxidable species available in the film decreases. Experiments carried out by Tucceri et al. [31] in the presence of different anions (perchlorate, sulfate, and benzenesulfonate) at *pH* 1, showed that the absorbance with potential at 440 nm decreases in the sequence $ClO_4^- > HSO_4^- >$ benzenesulfonate. That is, the absorbance decreases with increasing the anion size, because the anion size follows the sequence $ClO_4^- \leq HSO_4^- <$ benzenesulfonate. The transient response at 750 nm was also dependent on the nature of the anion of the supporting electrolyte; thus, for benzenesulfonate the change was smaller, but the decay was slower than for perchlorate and bisulfate.

The UV–vis absorption spectra of the oxidized and reduced forms of a POAP-film-coated ITO electrode were analyzed by Oyama et al. [7]. The maximum absorption peak of the oxidized form was observed at 400 nm and that of the reduced one at 600 nm. A reversible colour change of the film between brown and pale green was observed when the electrode potential was cycled between -0.7 and 0.7 V versus SCE. Figure 1.19 shows the response of the current and

Fig. 1.19 The responses of current and transmittance at 440 nm of the poly-*o*-aminophenol (POAP) film ($\phi = 0.2\ \mu$m) coated indium thin oxide (ITO) electrode to a potential pulse between -0.7 and 0.7 V in 0.2 mol/L NaClO$_4$ aqueous solution (*pH* 1). Electrode area, 0.20 cm^2 [7]
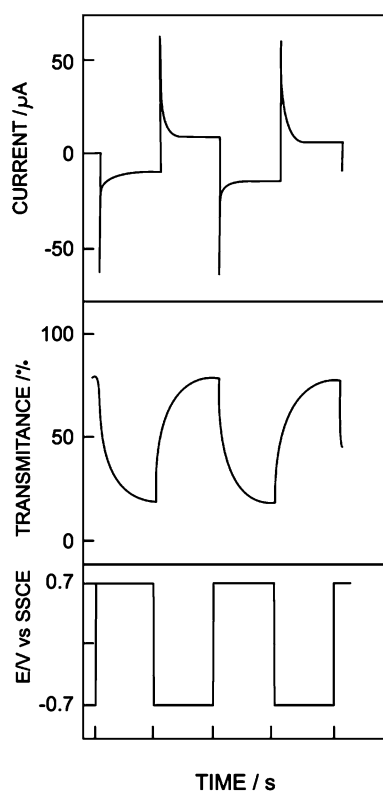
transmittance at 440 nm of the electrode during the potential step within the electrochromic region. The colour accumulated in the anodic step was bleached in the cathodic one. No substantial change in the transmittance response of the electrode was observed, even after a potential stepping of 100 cycles. The brown colour of the oxidized form remained substantially unchanged even after standing in air at open circuit for a period of 6 months. On the other hand, the reduced form was gradually oxidized by oxygen in air and consequently became coloured. The colourlessness of the reduced form was held under an atmosphere of nitrogen gas.

Barbero et al. [33] reported a spectrophotometric and ellipsometric study of POAP formed by electropolymerization of *o*-AP on Au and Pt surfaces. POAP films of different thickness (*d*) were synthesized by CV in Ref. [33]. The films were subjected to different polarization conditions (reduced and oxidized states), and the ellipsometric readings of the polarizer and analyzer (Δ and ψ values, respectively) at $\lambda = 541.6$ nm were obtained. It was observed that up to one particular film thickness (50 nm), reversing the potential from the oxidized to the reduced state and vice versa, resulted in the same ellipsometric readings for each state (i.e., oxidized and reduced), thus showing that the film behaves reversibly from the optical viewpoint. Experimental values of Δ and ψ for both states, for the different thicknesses at one wavelength, were fitted by a single film model in which it was assumed that the complex refractive index of the film ($\tilde{n}$) for each state (oxidized ($\tilde{n}_{ox}$) or reduced ($\tilde{n}_{red}$)) was independent of the film thickness. The best fit allowed for the determination of $\tilde{n}$ and k (real part of the complex refractive index) common to all thicknesses for each state. The corresponding $\tilde{n}$ values were $\tilde{n}_{red} = 1.704 - i\,0.02$ and $\tilde{n}_{ox} = 1.699 - i\,0.175$, where i is the imaginary unit for the complex numbers, at $\lambda = 546.1$ nm. These values indicate that the film is transparent in the reduced state and opaque in the oxidized one. As the value of the real part of $\tilde{n}$ was common to both states and it was slightly higher than that reported for PANI, Barbero et al. [33] inferred that the structure of POAP is similar to that proposed for PANI. Also, from the determination of ψ versus Δ dependence, it was concluded that POAP in the oxidized state should have a higher thickness (d_{ox}) than in the reduced (d_r) one. From the poor fitting at $d > 50$ nm it was suggested that thick POAP films exhibit a less densely packed structure or an increasing surface roughness or both, as compared with thin POAP films. Similar experiments as those described were carried out by Barbero et al. [33] at different wavelengths within the range 350 nm $< \lambda <$ 650 nm. In this regard, by repeating the same fitting procedure, the n and k values together with the thickness were determined for both film conditions (oxidized and reduced states). It was observed that, for low thicknesses, d_{ox} was bigger than d_r. However, this difference tended to disappear for high film thicknesses. A voltammetric cathodic charge vs. ellipsometric thickness relationship for POAP was also reported by Barbero et al. [33]. They observed that the charge (Q) increased linearly with the film thickness obtained by ellipsometry during the negative potential scan. However, as d increased beyond 40 nm, the slope of the Q versus d dependence became smaller. This fact was considered to be indicative of a decrease in the film density,

i.e., the ellipsometric thickness would be bigger than the electrochemically active portion of the film.

1.4.3 Spectroscopic Studies of POAP Films Synthesized in Basic and Neutral Media

Kudelski et al. [34] studied the chemical and electrochemical oxidation of *o*-AP over a wide *pH* range. A mixture of at least eight different compounds obtained from the chemical oxidation of *o*-AP were separated chromatographically [34] and then their surface-enhanced Raman scattering (SERS) spectra were compared. 3APZ was identified as the main product by recording an IR spectrum, and the second product of the chemical oxidation of *o*-AP was identified as DHAB. 3APZ is formed by the simultaneous N–C and O–C coupling of *o*-AP monomer units. The N–N coupling yields DHAB. With regard to the solution *pH*, DHAB was formed mainly in neutral and basic solutions of *o*-AP, whereas at low *pH* values, 3APZ was considered to be the main oxidation product. Also, the two main products identified by Kudelski et al. [34] after electrochemical oxidation of *o*-AP were 3APZ and DHAB. 3APZ could be oxidized at the electrode forming a ladder structure polymer.

Figure 1.20 shows SERS spectra of a silver electrode immersed in *o*-AP at different *pH* and electrode potential values. A band at 1395 cm^{-1} is clearly observed in all spectra. This band was assigned to nitrosophenol. As demonstrated in Fig. 1.20, this band exhibits a strong intensity in alkaline solutions, but is weaker in the acidic medium. By comparing the behaviour of this band with the band at 1390 cm^{-1} observed in the SERS spectra of nitrosobenzene, it was concluded that at open-circuit potential, the *o*-AP on the silver electrode was already oxidized into two major products, 3APZ and DHAB. The SERS spectrum of the *o*-AP solution also depends on the applied electrode potential.

At *pH* 3.0 (Fig. 1.20a), the spectrum is most intense at the stationary potential electrode $E = 0.01$ V, weak at -0.2 V, and almost absent at -0.4 V after the reduction of 3APZ. At *pH* 7.5 (Fig. 1.20b), the overall intensity of the spectrum significantly diminishes at more negative potential values (about -0.6 V). In alkaline solutions (Fig. 1.20c), the main band ascribed to 3APZ and DHAB disappear at -0.7 V after a reduction of azo compounds to hydrazo compounds. The spectrum observed at more negative potential values in neutral and alkaline *pH* was attributed to the hydrazo species, which are products of the reduction of DHAB.

The electropolymerization of *o*-AP in alkaline media (*pH* 12) on copper electrodes was studied by Guenbour et al. [16]. IR spectrometry was employed to characterize the polymer films. The IR spectrum of the POAP film and that of the 2-aminophenol compound were compared [16]. The film spectrum did not present the O–H band (3375 cm^{-1} for the stretching vibration and 1268 cm^{-1} for the
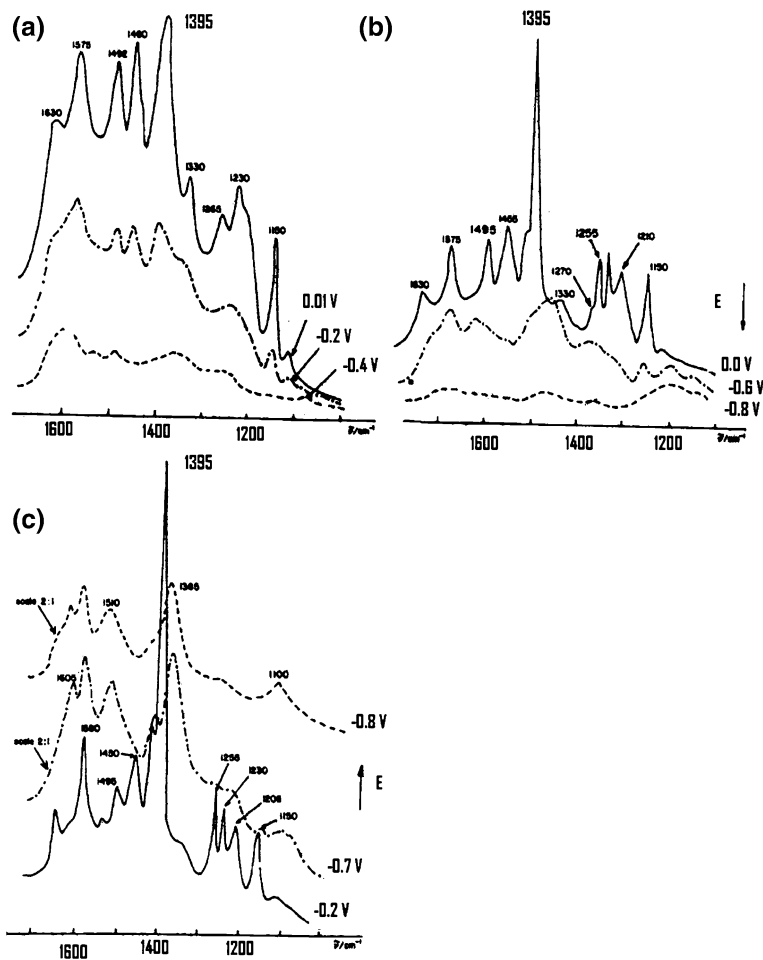
Fig. 1.20 Surface-enhanced Raman scattering (SERS) spectra of *o*-aminophenol (*o*-AP) solutions at **a** *pH* 3.0, **b** *pH* 7.5, and **c** *pH* 9.7 for different electrode potentials [34]

bonding vibration), characteristics of the 2-aminophenol. Instead of these bands, that of C–O–C at 1297.7 cm^{-1} was observed. This spectral difference was considered to be consistent with an electropolymerization process of *o*-AP, which proceeds through the anodic oxidation of the monomer. The absence of the band at 1700 cm^{-1}, assigned to C=O groups, confirmed the only formation of a polyether compound. The presence of the characteristic strong absorptions corresponding to the bands of the –NH$_2$ group in the ranges 300–3500 cm^{-1} and 1590–1610 cm^{-1} were observed in the IR spectra of the films. Electron spectroscopy for chemical analysis (ESCA) of the POAP films was also carried out by Guenbour et al. [16]. The spectrum of the oxygen 1s was interpreted as being composed of different peaks, 531.5, 532.9, and 533.9 eV, attributed, respectively, to the oxygen bonding

to a metal in an oxide, to the oxygen of water adsorbed molecules, or to hydroxide group (OH) and to C–O–C bonds. The third component at high energy (286.5 eV) of the C1s spectrum was assigned to C–O–C bonds and the low-energy components were considered to be characteristics of C–C bonds (284.6 eV) and C–N bonds (285.5 eV). The N1s spectrum was assigned to the three types of bonds of the 2-aminophenol: O–N, N–H, and C–N (389.9, 400.3, and 401.2 eV). Copper in its oxidized forms was also observed in the film: Cu_2O (932.6 eV) and CuO (933.7 eV). The higher energy component (934.5 eV) was attributed to a complex formed with the organic compounds. IR studies were also carried out by Guenbour et al. [16] and they seemed to indicate that the POAP film growing process in alkaline media involves the deprotonation of the aminophenol molecule, which is probably chemisorbed at the metal surface, followed by oxidation and electropolymerization reactions. In this whole process, the polymerization affects the –OH group by the formation of C–O–C bonds while the $–NH_2$ groups are preserved.

1.5 Formation Mechanism of Poly(*o*-aminophenol) Films

On the basis of the electrochemical and spectroscopic studies reported in Ref. [1], Barbero et al. explained the formation of POAP films in acid medium employing the generalized mechanism of anodic oxidation of anilines in aqueous media solutions. These authors proposed that a radical cation *o*-AP•+ is formed in a first charge transfer step and then it may follow the reaction paths shown in Fig. 1.21. The *o*-AP•+ radical may dimerize by either C–C coupling or C–N coupling to give species (I) and (II), respectively (Fig. 1.21). The dimers oxidize to the corresponding dications. The oxidized dimer II can suffer a cyclization reaction to give species III, which is oxidized further to 3APZ. The product distributions analyzed by Barbero et al. [1] allowed the authors to establish that the rate constants for the dimer formation follow the order $k_{dI} < k_{dII}$ and both rate constants are higher than the cyclization rate (k_c), to give species III. However, the rate of polymerization (k_p), to obtain the immobilized couple on the electrode surface, was lower than k_c. The possibility that the dication of compound II can polymerize was not disregarded. Therefore, the formation of a composite of two different films, one of linear chain structure similar to PANI and the other with a phenoxazine-like chain structure, was assumed to be possible. The latter product was considered to be the predominant one by Barbero et al. [1].

Bulhoes et al. [5] postulated that electrochemical oxidation of *o*-AP consists of a first oxidation step involving a two electron transfer to form radical cations followed by chemical couplings of radical cation—radical cation or radical–monomer species (E(CE)) mechanisms to form a ladder polymer with phenoxazine units. However, radical cations can also react quickly near the electrode surface, and after the first step involving two electrons, soluble products are easily formed by hydrolysis (Fig. 1.22).
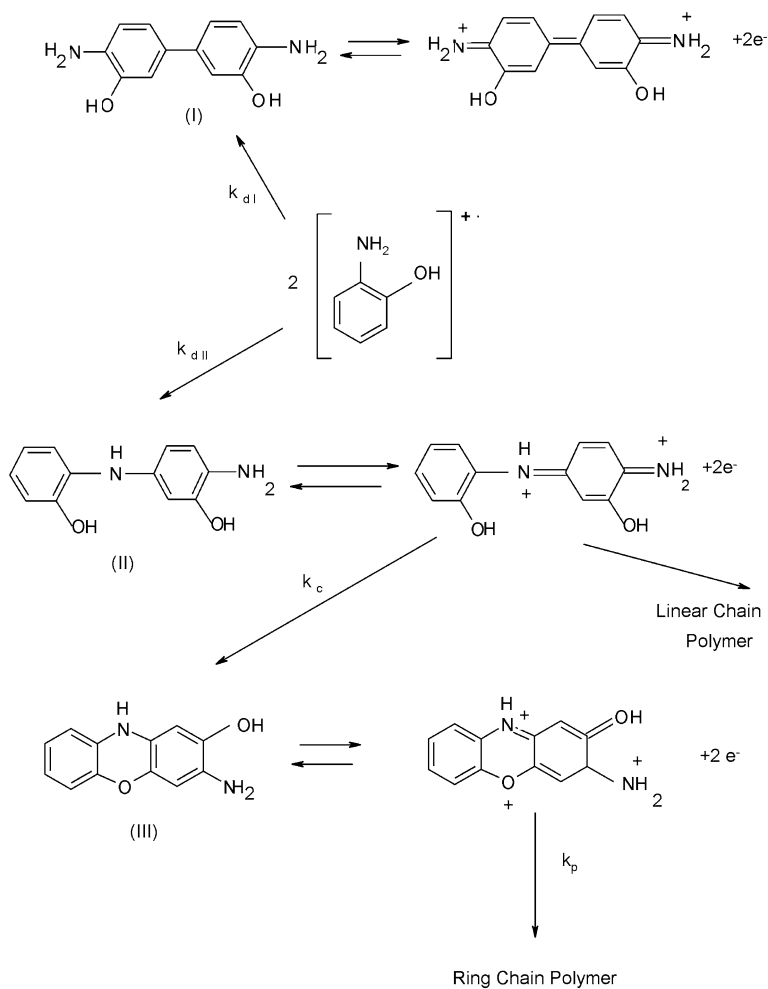
Fig. 1.21 Mechanism of anodic oxidation of *o*-aminophenol (*o*-AP) [1]

Thus, besides a film with a ladder structure, Bulhoes et al. [5] proposed that oxidation of *o*-AP can produce intermediate benzoquinone monoamine after successive cycling. Particularly at less controlled conditions such as at higher final potentials and lower scan rates, monoamines can react with neutral *o*-AP giving an intermediate (2-amino-*o*-indophenol) prior to cyclization to APZ. The low solubility of POAP films was attributed to the stiffness of the ladder phenoxazine backbone, which also seems to justify the low conductivity of POAP (10^{-7} S cm^{-1}) as compared with that of PANI (1 S cm^{-1}).

Kudelski et al. [34, 35] combined CV and SERS measurements to study the formation mechanism of POAP at different *pH*. The SERS results [35] from a
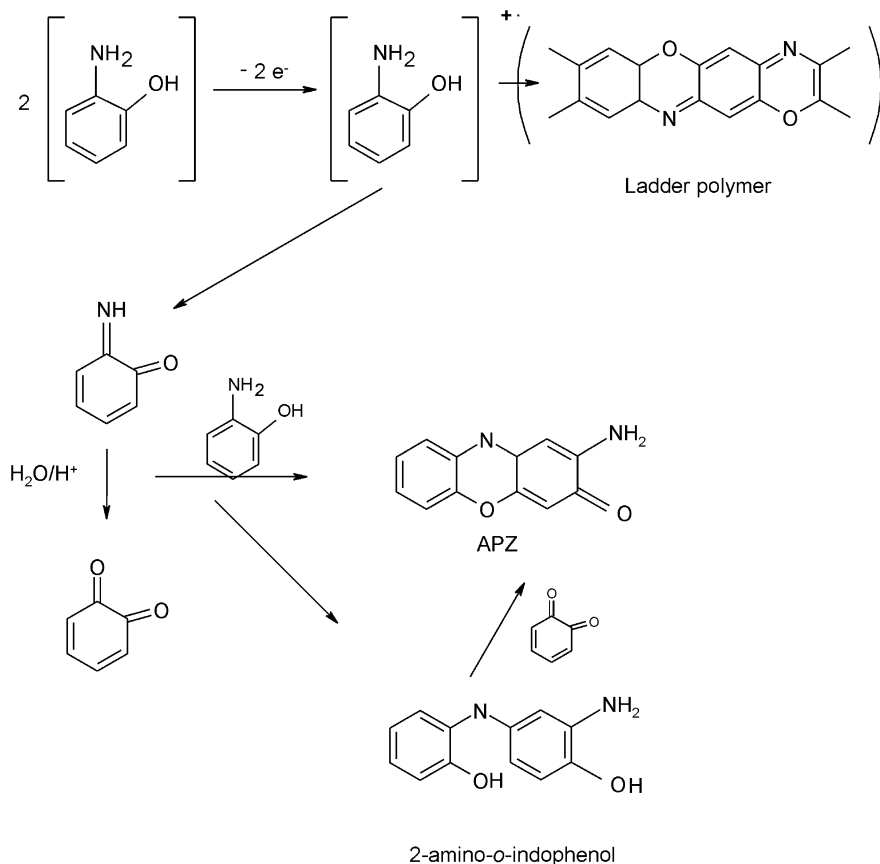
Fig. 1.22 Mechanism of *o*-aminophenol (*o*-AP) electro-oxidation in aqueous acidic medium [5]

roughened silver electrode in contact with an *o*-AP solution had suggested the presence of at least two oxidation products (nitrophenol and nitrosophenol) on the electrode surface at open-circuit potential.

Typical cyclic voltammetric curves obtained for a silver electrode in 0.1 mol/L LiClO4 solutions of *o*-AP at different *pH* values are shown in Ref. [35]. In all cases one pair of redox peaks was observed. However, two *pH* ranges with different curve features could be distinguished. Within the range of moderate *pH* (9.1 and 7.2), potentials of anodic (*E*pa) and cathodic (*E*pc) peaks changed slightly with *pH*. However, within the second *pH* range (*pH* 3.6 and below) *E*pa and *E*pc were strongly *pH*-dependent. These different features of the CV curves within these two *pH* ranges were attributed to the presence of two different electroactive oxidation products on the surface of the silver electrode. To identify products formed during the potential cycling, cyclic voltammograms were recorded in different solutions of 0.1 mol/L LiClO₄: (*i*) saturated with nitrosobenzene (*pH* 10, 6.7, 3.6, and 1.3),

(*ii*) saturated with azoxybenzene (*pH* 10, 7.0, 3.7, and 2.0), and (*iii*) on a roughened silver electrode modified with 3APZ. In the first two cases no redox peaks were found in the potential range from 0.15 to -0.5 V (SCE) for nitrosobenzene (*pH* 1.3) and azoxybenzene (*pH* 2.0) solutions. However, for nitrosobenzene solutions with *pH* values in the range 10 to 3.6, two pairs of slightly *pH*-dependent redox peaks were recorded. The first pair of redox peaks was assigned to the well-known reduction reaction of nitrosobenzene (C_6H_5NO) to phenylhydroxylamine (C_6H_5NHOH) and the re-oxidation of C_6H_5NO to C_6H_5NHOH. The second pair of redox peaks was attributed to the reduction of azoxy species, which are formed by the chemical reaction of C_6H_5NO and C_6H_5NHOH to hydrazobenzene and re-oxidation of hydrazobenzene to azobenzene. In solutions containing azoxybenzene only one pair of redox peaks was recorded. As it is well known that azoxybenzene can undergo irreversible reduction to azobenzene followed by a two-electron reversible reduction to hydrazobenzene, the observed pair of redox peaks was ascribed to an azo-hydrazo redox reaction. CV curves for nitrosobenzene, azoxybenzene, and *o*-AP solutions at moderate *pH* (about 7) were also compared by Kuldelski et al. [34]. As a pair of redox peaks was obtained for *o*-AP solutions in neutral and alkaline media, they were attributed to the azo–hydrazo couple. Thus, Kudelski et al. [34] assumed that, after oxidation of *o*-AP to *o*-AP•+ in neutral and alkaline media, dimerization of *o*-AP•+ by N–N coupling takes place. Then, the formation of azo species from *o*-AP on the silver electrode in an alkaline medium was postulated, and the reaction path was considered to be similar to that proposed for the formation of azobenzene from the aniline molecule (Fig. 1.23). To interpret the CV curves for *o*-AP solutions at *pH* < 4, cyclic voltammograms for a roughened silver electrode modified with 3APZ (Ag/3APZ) were analyzed in the potential range from -0.2 to -0.4 V (SCE). Only one pair of reversible redox peaks was observed on the curves. The dependence of the peak potentials on *pH* indicated that protons are essential for the electrode reaction. It was not possible to determine Epa and Epc precisely for the Ag/3APZ electrode at *pH* < 2, since Ep is in the potential range of silver oxidation, but data obtained for Pt/3APZ electrode at *pH* < 3 suggested that Ep changes at a rate about 60 mV/*pH*. This relationship indicated that protons and electrons take part in the electrode reaction of 3APZ in a
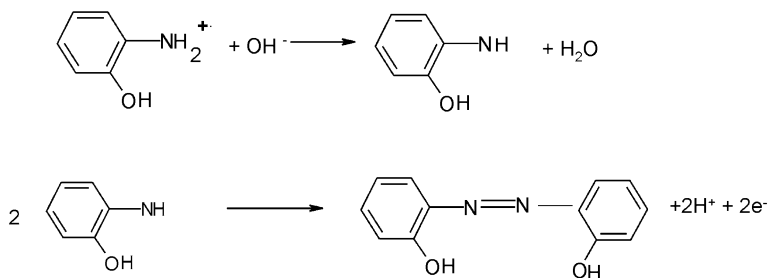
Fig. 1.23 Formation of azo species from *o*-aminophenol (*o*-AP) on the silver electrode in an alkaline medium [34]

Table 1.3 Electropolymerization of *o*-aminophenol on different electrode materials and in different electrolyte media

Electrode materials	Electrolyte medium	Electrosynthesis method	Reference
Pt, Au and glassy carbon	0.1 M HClO$_4$ + 0.4 M NaClO$_4$ + 1 × 10^{-3} M *o*-AP (1 < pH < 7)	Potentiodynamic cycling −0.25 V and 0.70 V (SCE)	[1]
Pt electrode	0.4 mol cm^{-3} of NaClO$_4$ + 10^{-2} mol dm^{-3} of *o*-AP	Potentiodynamic cycling −0.25 V and 0.75 V (SCE)	[3]
Carbon paste electrode	5 mM *o*-AP + 0.5 M HClO$_4$ In the presence and in the absence of sodium dodecyl sulphate	Potentiodynamic cycling −0.1 V and 0.7 V(Ag/AgCl/KCl 3 M)	[4]
Platinum and glassy carbon electrodes	0.2 M NaClO$_4$ + 0.1 M HClO$_4$ +5 × 10^{-3} M *o*-AP solution	Potentiodynamic cycling 0.2 V and 1.3 V (RHE)	[5]
Glassy carbon electrodes chemically (nitric acid (67 % wt/wt) and sulphuric acid (98 % wt/wt) for 10 min) and electrochemically (1.85 V (SCE) for 5 min) pre-treated before electropolymerization of *o*-AP	0.1 M H$_2$SO$_4$ + 0.05 M *o*-AP	Potentiodynamic method (−0.2 V and 0.7 V vs. SCE)	[6]
Basal-plane pyrolytic graphite and In-Sn oxide conducting glass	0.5 M Na$_2$SO$_4$ solution (*pH* 1) + 50 mM *o*-AP	Potentiodynamic cycling (−0.4 and 1.0 V vs. sodium chloride saturated calomel electrode)	[7]
Glassy carbon	1 M SO$_4$H$_2$ + 0.5 M Na$_2$SO$_4$ +50 mM *o*-AP solution	Potentiodynamic cycling (−0.2 V and 1.0 V vs. SCE)	[8]
Glassy carbon and Pt electrodes	0.05 M *o*-AP in a mixture of 1 M H$_2$SO$_4$ and 0.5 M Na$_2$SO$_4$	Potentiodynamic cycling (−0.2 V to 0.8 V vs. SCE)	[9]
Pt and Au electrodes	0.05 M *o*-AP + 0.5 M H$_2$SO$_4$ solution	Potentiostatic method (*E* = 0.7 V; 0.8 V and 0.9 V vs. SCE	[13]
Pt and GC electrodes	0.05 M *o*-aminophenol solution in 0.5 M HClO$_4$ + 10 mM sulfonated nickel phtalocyanine	Potentiodynamic cycling (−0.25 and 0.7 V vs. SCE)	[14]

(continued)

Table 1.3 (continued)

Electrode materials	Electrolyte medium	Electrosynthesis method	Reference
GC electrodes	0.10 M HClO$_4$ + 0.10 M *o*-AP	Potentiodynamic (-0.10 V and 1.00 V vs. SCE) and potentiostatic (E = 1.0 V for a given time) methods	[15]
Vitreous carbon, platinum and copper	0.3 M NaOH hydroalcoholic solution (70 vol % H$_2$O, 30 vol % CH$_3$OH) + 0.1 M *o*-AP	Potentiodynamic cycling	[16]
Glassy carbon electrode or on a glass plate covered with semi-conducting indium thin oxide	1 M phosphate buffer *pH* 5.55 solution containing 25 μg/ml of laccase and 10 mM *o*-AP	Potentiodynamic cycling (−0.1 V and 0.9 V vs. Ag/AgCl)	[24]

1:1 ratio. Therefore, it was postulated that in more acidic solutions the favoured path after oxidation of *o*-AP to *o*-AP•+ is dimerization of *o*-AP•+ with N–C coupling resulting in the cyclic dimer 3APZ.

1.6 Concluding Remarks

Table 1.3 lists the electrode materials, electrosynthesis methods and electrolyte composition employed by different authors to obtain POAP films.

POAP films have been synthesized by electrochemical oxidation of acid and basic *o*-AP solutions. While 2-2′dihydroxyazobenzene (DHAB) is formed mainly in neutral and basic solutions, at low *pH* values, 3-aminophenoxazone (3APZ) was considered to be the main electrooxidation product. 3APZ is formed by the simultaneous N–C and O–C coupling of *o*-AP monomer units and it can be oxidized at the electrode forming a ladder polymer with a phenoxazine-like chain structure. The N–N coupling yields DHAB in basic media.

On the basis of spectroscopic measurements, different structures have been proposed for POAP. Besides a completely ring-closed structure with phenoxazine units other two structures, a partially ring opened and another partially hydrolyzed, have been formulated for POAP. In situ Raman Spectroscopy measurements suggest that the POAP matrix contains alternating oxidized (quinonoid) and reduced (N-phenyl-*p*-phenylenediamine) repeating units. The 1,4-substituted molecular structure of POAP proposed by Zhang et al. allows explaining the interaction of the polymer with metal cations. The cation capturing process by POAP was attributed to simultaneous presence of hydroxyl and amino groups of the polymeric backbone, in which the lone pair electrons are available to coordinate with metal cations.

With regard to mechanisms of POAP formation, most authors postulate that in acidic solutions the favoured path after oxidation of *o*-AP to o-AP$^{\bullet+}$ is dimerization of o-AP$^{\bullet+}$ with N–C coupling resulting in the cyclic dimer 3-APZ. Oxidation of 3APZ leads a ladder structure polymer with phenoxazine units. However, the o-AP$^{+\bullet}$ radical may also dimerize by C–C coupling. Thus, the formation of a composite of two different films, one of linear chain structure similar to polyaniline (PANI) and the other with a phenoxazine-like chain structure, was assumed to be possible for POAP. Bulhões et al. postulate that electrochemical oxidation of *o*-AP consists in a first oxidation step involving a two-electrons transfer to form radical cations followed by chemical couplings of radical cation-radical cation or radical-monomer species to yield a ladder polymer with phenoxazine units. However, the radical cations can also react quickly near the electrode surface to produce soluble products by hydrolysis. Then, besides a film with a ladder structure, Bulhões et al. propose that oxidation of *o*-AP can produce intermediate benzoquinone monoamine after successive cycling. Spectroscopic measurements demonstrate the formation of azo species from alkaline solutions of *o*-AP. Kudelski et al. postulate that after oxidation of *o*-AP to o-AP$^{\bullet+}$, dimerization of

o-AP$^{\bullet+}$ by N–N coupling takes place and the reaction path in basic media was assumed to be similar to that proposed for the formation of azobenzene from the aniline molecule.

It was demonstrated that some substances, such as sodium dodecyl sulphate, increase the rate of polymerizaton of o-aminophenol in acid media because in its presence the monomer can more easily reach the electrode surface and produce more monocation radical, than in its absence. Also, some electrode surface pre-treatments affect the electropolymerization rate of o-aminophenol. It was proved that the electron-transfer rate from a POAP film to a glassy carbon electrode is twice when the glassy carbon surface was previously electrochemically pre-treated (electrode subjected to 1.85 V (SCE) for 5 min in a 0.1 M H_2SO_4 solution), as compared with an untreated surface.

The redox switching of POAP from the totally reduced form to the completely oxidized one in acid medium was also studied by employing UV–Vis and Raman spectroscopies and ERS measurements. The existence of transient species during the redox process of POAP was demonstrated analyzing the potential dependence of some spectral bands. In this regard, the redox process of POAP was interpreted in terms of the oxidation of amine groups to imine groups. To this end absorbance changes in the wavelength region comprised between 300 and 800 nm, at different pHs values were recorded and analysed at different degrees of oxidation of POAP. Three bands were studied: 340 nm, 450 nm and 750 nm. The band at 340 nm was attributed to the phenoxazine structure of the polymer. The band at 450 nm was assigned to the partially oxidized phenoxazine structure. At $\lambda = 750$ nm the absorbance presents a maximum at $E = 0.15$ V (SCE), which was considered to be indicative of the existence of a transient species. The same conclusion was reached by studying the potential dependence of some bands of the Raman spectra of POAP. For instance, the intensities of the band at 1638 cm^{-1} attributed to –C=N– in quinonimine units the band at 1474 cm^{-1} assigned to the –C=N– stretching, were analyzed as functions of the applied electrode potential. It was found that when the potential increases, the band at 1474 cm^{-1} increases and the band at 1638 cm^{-1} also increases until a potential about 0.2 V and there after, it diminishes. This behaviour was considered indicative of the existence of an intermediate species. The existence of intermediate species was associated to an oxidation process that occurs through two consecutive reactions through a charged species, which was considered to be a cation radical. From other point if view, the effect was also associated to the maximum of polaron concentration in the polymer. The increase of potential beyond the maximum intensity was attributed to a lowering in the polaron concentration probably by coupling into bipolarons. In the same sense, although the Raman features of the POAP films synthesised potentiostatically and potentiodynamically were similar, marked differences respect to the potential dependence of some bands were observed. A difference was observed particularly with respect to the potential dependence of the band around 1645 cm^{-1} assigned to the C=N stretching of quinonimine units. The intensity of this band sharply increased at 0.3 V and slowly decreased at more positive potentials for POAP films synthesized potentiostatically. However, in the case of

POAP films potentiodynamically prepared this band attained the intensity maximum at about $E = 0.2$ V. Thus, the oxidation of POAP synthesised potentiostatically was assumed to proceed via an intermediate half-oxidized state. The behaviour of the in situ UV–Vis spectra of POAP films potentiostatically synthesized, also demonstrate that the redox transition of POAP proceeds though two consecutive reactions in which a charged intermediate species takes part. Evidence about the existence of cation radical species during the redox conversion of POAP was also obtained by ERS measurements.

References

1. Barbero, C., Silber, J.J., Sereno, L.: Formation of a novel electroactive film by electropolymerization of orthoaminophenol. Study of its chemical structure and formation mechanism. Electropolymerization of analogous compounds. J. Electroanal. Chem. **263**, 333 (1989)
2. Salvagione, H.J., Arias, J., Garces, P., Morallon, E., Barbero, C., Vazquez, L.: Spectroelectrochemical study of the oxidation of aminophenols on platinum electrode in acid medium. J. Electroanal. Chem. **565**, 375 (2004)
3. Ortega, M.: Conducting potential range of poly(o-aminophenol). Thin Solid Films **371**, 28 (2000)
4. Ojani, R., Raoof, J.B., Fathi, S.: Poly(o-aminophenol) film prepared in the presence of sodium dodecyl sulphate: Aplication for nickel-ion dispersion and the elecctrocatalytic oxidation of methanol and ethylene glycol. Electrochim. Acta **54**, 2190 (2009)
5. Goncalves, D., Faria, R.C., Yonashiro, M., Bulhoes, L.O.S.: Electrochemical oxidation of *o*-aminophenol in aqueous medium: formation of film and soluble products. J. Electroanal. Chem. **487**, 90 (2000)
6. Yong, Y., Zugeng, L.: Effects of surface oxide species on the electropolymerization of o-aminophenol on pretreated glassy carbon electrodes. Synth. Met. **78**, 111 (1996)
7. Kunimura, S., Ohsaka, T., Oyama, N.: Preparation of thin polymeric films on electrode surfaces by electropolymerization of o-aminophenol. Macromolecules **21**, 894 (1988)
8. Zhang, A.Q., Cui, C.Q., Chen, Y.Z., Lee, J.Y.: Synthesis and electrochromic properties of poly-*o*-aminophenol. J. Electroanal. Chem. **373**, 115 (1994)
9. Zhang, A.Q., Cui, C.Q., Lee, J.Y.: Metal-polymer interactions in the Ag(I)|poly-o-aminophenol system. J. Electroanal. Chem. **413**, 143 (1996)
10. Zhang, A.Q., Chen, Y.Z., Tian, Z.W.: Metal|polymer interactions in the Cu(I)-poly(o-aminophenol) system. Acta Phys. Chem. China **9**, 523 (1993)
11. Yano, J., Kawakami, H., Yamasaki, S., Kanno, Y.: Cation capturing ability and the potential response of a poly(o-aminophenol) film electrode to dissolved ferric ions. J. Electrochem. Soc. **148**, E61 (2001)
12. Jano, J., Kawakami, H., Yamasaki, S.: Potential response of poly(o-aminophenol) film electrode to dissolved ferric ion. Synth. Met. **102**, 1335 (1999)
13. Ul-Haq, A., Shah, A., Holze, R.: Poly(o-aminophenol) with two redox processes: A spectroelectrochemical study. J. Electroanal. Chem. **597**, 95 (2006)
14. Miras, M.C., Badano, A., Bruno, M.M., Barbero, C.: Nitric oxide electrochemical sensors based in hybrid films of conducting polymers and metal phtalocyanines. Portugaliae Electrochim. Acta **21**, 235 (2003)
15. Golabi, S.M., Nozad, A.: Electrocatalytic oxidation of methanol at lower potentials on glassy carbon electrode modified by platinum and platinum alloys incorporated in poly(o-aminophenol) films. Electroanalysis **15**, 278 (2003)

16. Guenbour, A., Kacemi, A., Benbachir, A., Aries, L.: Electropolymerization of 2-aminophenol. Electrochemical and spectroscopic studies. Progr. Org. Coatings **38**, 121 (2000)
17. Kursun, S., Ekinci, B.Z., Pasahan, A., Ekinci, E.: Preparation and properties of amperometric uric acid sensor based on poly(2-aminophenol). J. Appl. Polym. Sci. **120**, 406 (2011)
18. Tao, W., Pan, D., Liu, Y., Nie, L., Yao, S.: An amperometric glucose biosensor based on poly(o-aminophenol) and Prussian blue films at platinum electrodes. Anal. Biochem. **338**, 332 (2005)
19. Tao, W., Liu, Y., Pan, D., Nie, L., Yao, S.: Study of enhancement of catalytic activity for hemoglobin by quinhydrone in poly(o-aminophenol) film. Bioelectrochemistry **65**, 51 (2004)
20. Pan, D., Chen, J., Nie, L., Tao, W., Yao, S.: Amperometic glucose biosensor based on immobilization of glucose oxidase in electropolymerized o-aminophenol film at Prussian blue-modified platinum electrode. Electrochim. Acta **49**, 795 (2004)
21. Miland, E., Miranda Ordieres, A.J., Tunon Blanco, P., Smyth, M.R., Fagain, C.O.: Poly(o-aminophenol)-modified bienzyme carbon paste electrode for the detection of uric acid. Talanta **43**, 785 (1996)
22. Lobo Castañon, J., Miranda Ordieres, A.J., Tunon Blanco, P.: A bienzyme-poly-(o-phenylenediamine)-modified carbon paste electrode for the amperometric detection of L-lactate. Anal. Chim. Acta **346**, 165 (1997)
23. Lobo, M.J., Miranda, A.J., Lopez-Fonseca, J.M., Tunon, P.: Electrocatalytic detection of nicotinamide coenzymes by poly(o-aminophenol) and poly(o-phenylenediamine)-modified carbon paste electrodes. Anal. Chim. Acta **325**, 33 (1996)
24. Palys, B., Marzec, M., Rogalski, J.: Poly-o-aminophenol as a laccase mediator and influence of the enzyme on the polymer electrodeposition. Bioelectrochemistry **80**, 43 (2010)
25. Pan, D., Chen, J., Yao, S., Tao, W., Nie, L.: An amperometric glucose biosensor based on glucose oxidase immobilized in electropolymerized poly(o-aminophenol) and carbon nanotubes composite film on a gold electrode. Anal. Sci. Jpn. Soc. Anal. Chem. **21**, 367 (2005)
26. Zhang, Z., Liu, H., Deng, J.: A glucose biosensor based on immobilization of glucose oxidase in electropolymerized o-aminophenol film on platinized glassy carbon electrode. Anal. Chem. **68**, 1632 (1996)
27. Li, J., Lin, X.: Glucose biosensor based on immobilization of glucose oxidase in poly(o-aminophenol) film on polypyrrole-Pt nanocomposite modified glassy carbon electrode. Biosens. Bioelectron. **22**, 2898 (2007)
28. Tucceri, R.I.: J. Specularity change of a thin gold film surface coated with poly(o-aminophenol) during the polymer redox conversion. The pH affect on the redox sites distribution at the metal‖polymer interface. Electroanal. Chem. **543**, 61 (2003)
29. Ohsaka, T., Kunimura, S., Oyama, N.: Electrode kinetics of poly(o-aminophenol) film prepared by electro-oxidative polymerization of o-aminophenol and its electrochromic properties. Electrochim. Acta **33**, 639 (1988)
30. Salvagione, H.J., Arias-Padilla, J., Perez, J.M., Vazquez, J.L., Morallon, E., Miras, M.C., Barbero, C.:Study of the redox mechanism of poly(o-aminophenol) using in situ techniques: evidence of two redox processes. J. Electroanal. Chem. **576**, 139 (2005)
31. Tucceri, R.I., Barbero, C., Silber, J.J., Sereno, L., Posadas, D.: Spectroelectrochemical study of poly-o-aminophenol. Electrochim. Acta **42**, 919 (1997)
32. Chen, Y.Z., Zhang, A.Q., Tian, Z.W.: Poly(o-aminophenol) studied by X-ray Photoelectron Spectroscopy. Chem. J. Chin. **12**, 519 (1991)
33. Barbero, C., Zerbino, J., Sereno, L., Posadas, D.: Optical properties of electropolymerized orthoaminophenol. Electrochim. Acta **32**, 693 (1987)
34. Jackowska, K., Bukowska, J., Kudelski, A.: Electro-oxidation of o-aminophenol studied by cyclic voltammetry and surface enhanced Raman scattering (SERS). J. Electroanal. Chem. **350**, 177 (1993)
35. Jackowska, K., Bukowska, J., Kudelski, A.: Poly-ortho-aminophenol modified electrodes. Structure and electrochemical properties. Polish J. Chem. **68**, 141 (1994)

Chapter 2
The Charge Conduction Process
at Poly(o-aminophenol) Film Electrodes

2.1 Introduction

Electroactive polymers contain electron donor and acceptor sites that usually consist of up to hundreds of molecular layers. Oxidation and reduction of fixed sites introduce charged sites into the polymer, which, to achieve charge neutrality, require the ingress of counter-ions from the contacting electrolyte solution and, according to the Donnan relation, the egress of co-ions. Electron hopping is believed to be the mechanism for electron transport, but it is also possible that ion motions may partially or totally control the rate of charge transport. Thus, the charge-transport rate in electroactive polymer films is quantitatively characterised by a heterogeneous constant of charge transfer and an effective (or apparent) diffusion coefficient for charge transport across the film. The factors governing the magnitude of these parameters are not well understood. Furthermore, in general, these transport parameters depend on different variables such as degree of oxidation of the polymer, polymer film thickness, type of electrolyte, ionic strength and pH of the solution in contact with the polymer film. A combination of different techniques was employed to determine the rates of the charge-transfer and charge-transport processes in electroactive polymers, such as Cyclic Voltammetry (CV), Rotating Disc Electrode Voltammetry (RDEV), Normal Pulse Voltammetry (NPV), Potential Step Chronoamperometry (PSCA), Potential Step Chronocoulometry (PSCC), EQCM measurements, Electron Spin Resonance (ESR), Probe Bean Deflection (PBD), Surface Resistance (SR) and Electrochemical Impedance Spectroscopy (EIS).

The electropolymerization of o-AP in acid medium yields a conducting polymer. The electroactivity of POAP was explained by a redox mechanism that involves an addition/elimination of protons coupled with a reversible electron transfer. However, POAP shows a relatively low conductivity as compared with other conjugated polymers. The charge-transport process at poly(o-aminophenol) (POAP) films was found to depend not only on the medium used for the electrosynthesis, but also on the polymer oxidation state, the polymer film thickness and pH and type of ions of the external solution in contact with the polymer.

Particularly, the electro-oxidation of *o*-AP in neutral buffer solutions leads to the formation of a non-conducting and permselective thin film of POAP. The permselectivity of a non-conducting POAP film synthesized at *pH* values over 3 was found to be suitable to reduce the effect of interferents in amperometric determinations of different biologically important substances. In this chapter of this book concerns charge-transfer and charge-transport processes occurring in the curse of redox reactions of POAP film electrodes. This chapter first deals with the case where the solutions contacting POAP films only contain ions that do not possess a redox activity ("background electrolyte"). Thus, the counter-ion is able to cross the film|solution interface to retain the bulk film electroneutrality. Then, the transport properties of POAP films contacting redox active solutions are treated. In this last case, redox species inside the electrolyte solution participate in an interfacial electron exchange with the polymer at the polymer|solution boundary. In practical applications of POAP is necessary to maintain the conducting properties of the polymer unaltered. However, in some of them the polymer is subjected to extreme conditions that can cause its partial deactivation. In this regard, it seems to be important to know the fundamental nature of the charge propagation in poly(o-aminophenol) film electrodes.

2.2 The Charge Conduction Process at Poly(o-aminophenol) (POAP) Film Electrodes in Contact with Inactive Electrolytes

A study about the electrochemical properties of POAP, determining its thermodynamical properties and some of the kinetic and charge transport parameters, is reported in Ref. [1]. A mechanism of charge transport for the charging and discharging process of POAP is also proposed [1]. POAP was obtained [1] by electrooxidation of the monomer on platinum and glassy carbon (GC) electrodes in aqueous solution. The electrochemical behavior of POAP films was studied by cyclic voltammetry (CV) under different experimental conditions. On both, platinum and GC, the POAP response is highly asymmetric (see Fig. 1.2 of Chap. 1). It presents anodic and cathodic peak potential separations ($E_{pa} - E_{pc}$) independent of the sweep rate (v) for values of v between 1 and 100 mV s^{-1}(0.1 M HClO$_4$ + 0.4 M NaClO$_4$ solution). However, at $v > 100$ mV s^{-1} E_{pc} shifts to more negative values, indicating a non-ideal behavior. Since the presence of the film does not inhibit the proton reduction, the negative potential limit for the film depends on the base electrode, being about -0.5 V (SCE) over Pt and Au and -1.0 V (SCE) over GC. On the other hand, the positive potential limit is about 1.0 V and independent of the bare electrode. Beyond these limits irreversible modifications with formation of electroinactive films are produced. The anodic peak, as well its E_{pa}, does not vary with v or with *pH* in the range 1–3. On the other hand, the cathodic peak shape and E_{pc} show variations with these variables, which indicate additional

kinetic effects in the reduction cycle. The effect of the scan rate on the maximum current of the anodic voltammetric peak current (i_{pa}) was also studied [1]. A plot of ln i_{pa} versus ln v (where i_{pa} is the anodic peak current and v is the potential scan rate) showed, for values of v less than 0.5 V s^{-1}, a slope that approaches unity as predicted theoretically for an adsorbed species of film-modified electrodes with thin-layer behaviour. For v values greater than 2.5 V s^{-1}, the slope was 0.5, which indicates semi-infinite diffusion behaviour. The intermediate zone, between 0.5 and 2.5 V s^{-1}, was shown to correspond to finite diffusion behaviour. Similar results were obtained for the cathodic peak but with the difference that the thin-layer behaviour was restricted to values of v lower than 0.3 V s^{-1}, revealing that the cathodic process is slower than the anodic one. Plots of i_{pa} versus $v^{1/2}$ were linear for values of v as high as 10 V s^{-1}. By assuming that these plots follow the Randles–Sevcik or the equivalent Nicholson and Shain equation [2], the slope was proportional to $cD^{1/2}$. The concentration of active sites, c, was calculated for a homogeneous film considering the film thickness known from ellipsometric data [3] and employing Eq. (2.1):

$$Q_T = nFAc\,d \qquad (2.1)$$

where $n = 1$ is the number of exchanged electrons during the redox reaction of the polymer and d is the film thickness. Q_T is either the anodic or the cathodic charge corresponding to voltammograms obtained at $v < 0.10$ V s^{-1} in order to ensure the completion of the redox process in the film. Besides, F is the Faraday constant and A the electrode area in Eq. (2.1). A value of $c = 4.7$ M was obtained in [1]. Then, an apparent diffusion coefficient for the anodic process D was calculated from the $cD^{1/2}$ slope. A D value of 4.0×10^{-11} cm^{2}s^{-1} was obtained in [1]. The close fit to the i_{pa} versus $v^{1/2}$ plot with the Randles–Sevcik equation suggested that the anodic charge transport within the film might be by electron hopping with the necessarily charge-compensating counter-ion motion [4]. Since the reduction peak was affected by kinetic effects, this invalidates the previous calculation on the basis of CV in the reduction process. A value of the conductivity of POAP by using the formalism of Nicholson [5] was also calculated in Ref. [1]. The obtained value, with the assumption of fast charge transfer at the electrode/film and film|solution interfaces, was 1.34×10^{-4} S cm^{-1}. However, as the proton diffusion at POAP-coated electrodes depends on the base electrode, then, it was considered to be possible that both D and the film conductivity are affected by proton transport. As the proton diffusion process seems to occur, allowing them to reach the metal electrode surface, this fact was explained [1] considering that protons reach the electrode surface by permeation through pores in the film. However, these pores should be very small since other cations do not diffuse [1]. Another reasonable explanation given in Ref. [1] was to consider a fast assisted Grotthus-like diffusion of protons through the polymer matrix.

As the POAP film behaves as a thin-layer cell in equilibrium, at sweep rates lower than 0.10 V s^{-1} [1], then its electrochemical behavior should obey to the

Nernst's law [2]. For an n-electron redox reaction involving reversible charge transfer, Nernst's equation for the POAP cathodic process was written in Ref. [1] as:

$$a_O/a_R = \gamma_O c_O/\gamma_R c_R = \exp\left[nF(E - E^0)/RT\right] \tag{2.2}$$

where a_i and γ_j are the activity and activity coefficient of the species, respectively, and E^0 is the standard potential of the redox reaction. To a first approximation the activity coefficients were considered independent of the concentration and equal to unity [1]. With this assumption [1], the relationship between i_p and v was written as:

$$i_{pa} = i_{pc} = nFQv/4RT \tag{2.3}$$

where $Q\ (= nFcAd)$ is obtained by integration of the voltammetric peak, A is the film area and $c = c_O + c_R$ (where c_O and c_R are the concentration of oxidized and reduced redox sites, respectively). As can be seen from Fig. 2.1, the values of i_{pa} and i_{pc}, although linear with v, the slopes are not equal to values predicted by Eq. (2.3). This fact confirms a non-ideal behavior of POAP suggested in [1], which is actually expected considering the rather high concentration of active sites on the film ($c = 4.7$ M). The deviation from the ideal behavior was explained [1] considering that the redox process produces notable physical and probably structural changes in the polymer matrix. To account for the non-ideal behavior of POAP, interaction between active sites in the film was assumed in Ref. [1]. Thus, to evaluate such interaction quantitatively, the activity coefficients were defined, following the Frumkin's isotherm, as:

$$\gamma_O = \exp\left[-(r_{OO}c_O + r_{OR}c_R)\right] \tag{2.4}$$

$$\gamma_R = \exp\left[-(r_{RR}c_R + r_{RO}c_O)\right] \tag{2.5}$$

Fig. 2.1 Plots of i_p versus v for a POAP-modified electrode on Pt. $A = 0.159$ cm^2. (•) anodic; (o) cathodic. Film thickness, $d = 38$ nm [1]
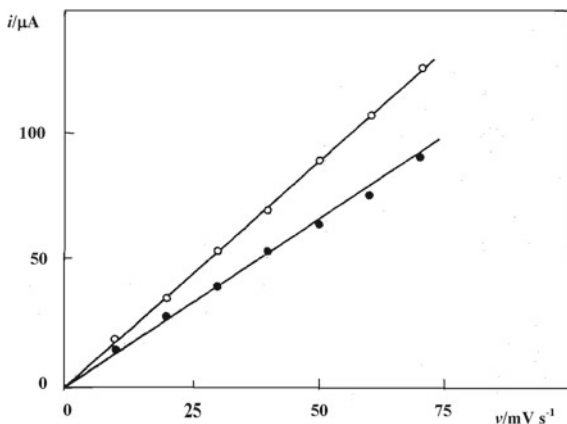
where r_{ij} and r_{ji} are the interaction parameters, which describe the mutual inter-action between sites i and i and i and j, respectively. The corresponding expression for non-ideal behavior deduced for the i_p–v relationship was expressed as Ref. [1]:

$$i_p = nFQv/(4 - 2cr)RT \qquad (2.6)$$

where $r = (r_O + r_R)$, $r_O = (r_{OO} + r_{RO})$ and $r_R = (r_{RR} + r_{OR})$ assuming that $r_{RO} = r_{OR}$.

From data of the type shown in Fig. 2.1 and using Eq. (2.6), the parameters cr_a and cr_c, for the anodic and cathodic response, respectively, were calculated for various films in [1]. Different values of the interaction coefficients, r_a and r_c were obtained in Ref. [1]. Both are negative, thus involving a repulsive energy of interaction. However, while for the cathodic process a value of r_c around -0.13 M^{-1} was obtained, for the anodic process r_a resulted about -0.5 M^{-1}. Other measurements, peak width, charge needed to oxidize or reduce the film at a given potential, directly related to the interaction parameters were also performed in Ref. [1], and the corresponding interaction parameters were calculated. Then, it was concluded in Ref. [1] that POAP films exhibit a Nernstian behavior with interaction between the active redox sites.

Temperature and pH effects on the POAP charge conduction process were also analyzed in Ref. [1]. With regard to temperature effects, it was observed that in the tin-layer domain, both i_{pa} and i_{pc} increase with increasing the temperature. Considering the ideal behavior (Eq. (2.3)) an opposite effect should be expected. Thus, the observed POAP response with temperature was attributed to the effects of temperature on the interaction parameters. To quantify these effects a current function was calculated for each temperature. It was found that interaction parameters become more negative (more repulsive) when the temperature decreases. Concerning pH effects, the POAP response is highly dependent on the pH, being optimal at pH 3. At $pH > 7$ no response was observed. The pH effect was considered as an indication that protons and electrons take part in the electrode reaction of POAP. The redox response of thin POAP films ($d < 30$ nm) at different pH in HClO$_4$ solutions of variable concentration and 0.4 M NaClO$_4$ was studied in Ref. [1]. All measurements were performed at $v < 0.1$ V s^{-1} to ensure thin-layer behavior. As the pH is increased the voltammetric peaks maintain the shape, but the peak current decreases, particularly the cathodic peak. At pH close to 5, the cathodic response disappears completely, while this occurs for the anodic peak at pH 7. Although a response of POAP is not observed at $pH > 7$, the film is not destroyed and recovers its original response when pH is restored to 1. The behavior of E_{pa} and E_{pc} at low pH values is shown in Fig. 2.2. As can be observed, E_{pa} does not vary with pH until a value of 2.3 is reached. However, E_{pc} varies significantly in the same pH range and the plot of gives straight lines with different slopes. This complicated behavior was not explained in Ref. [1]. An attempt to quantify the observed pH effects was made in [1]. In this respect, the change of the formal potential ($E^{0\prime}$) with the pH, was measured. On the assumption that the redox process of POAP can be represented by reaction (2.7) [1]:

$$R_pH_x \Leftrightarrow O_p + xH^+ + ne \qquad (2.7)$$
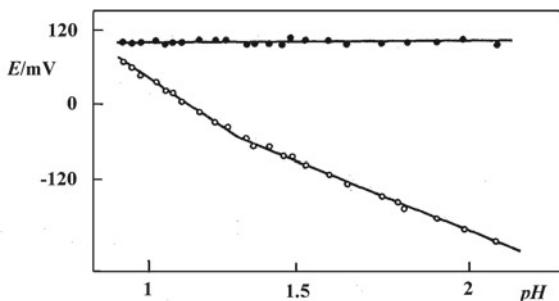
The relation between $E^{0\prime}$ and *pH* was written as:

$$E^{0\prime} = E^0 + 2.303\,(RT/nF)\,\log\left\{\left[\,O_p\,\right]/\left[\,R_pH_x\,\right]\right\} - 2.303\,(RT\,x/nF)pH \quad (2.8)$$

As the concept of $E^{0\prime}$ is not easily applicable in the case of POAP, an operational formal potential ($E^{\#\prime}$) was adopted in [1], defined and measured as the equilibrium potential of a film-modified electrode when half of the charge required for total film conversion, has been passed. Using this assumption, the dependence of $E^{\#\prime}$ on the *pH* was measured in the range 1–6. At *pH* between 1 and 2.3, no variation of $E^{\#\prime}$ was observed. At *pH* > 2.3 the film showed a variation of $E^{\#\prime}$ with *pH* with a slope around 50 mV/decade. The latter is close to the theoretical slope for a reaction in which protons and electrons take part in the electrode reaction in the film in a 1:1 ratio ($n = x$ in Eq. (2.8)). The breakpoint (*pH* 2.3) was considered to correspond to the apparent pK_a of the film (Fig. 2.2).

Kinetic effects on the reduction process of POAP were also studied in Ref. [1]. Kinetic effects are shown in Fig. 2.3, where it is observed that while E_{pa} is independent of v, E_{pc} depends on v.

This behaviour was explained by assuming a chemical reaction coupled with the charge transfer. The theoretical model available for EC processes in surface

reactions proposed by Laviron [6] was employed in Ref. [1] to explain the linear relation of E_{pc} with log v observed in Fig. 2.3. This model leads to the peak potential versus potential scan rate dependence represented by Eq. (2.9) [6]:

$$E_p = E^{0\prime} + 2.303\,(RT/nF)\,\log\,(RT\,k/nFv) \tag{2.9}$$

where k is the pseudo-first-order rate constant for the coupled chemical reaction. However, the experimental slope obtained in [1] is higher than that predicted by Eq. (2.9). This discrepancy was attributed to repulsive interactions, which affect the reduction wave. The coupled chemical reaction with the charge transfer process was considered to be the protonation of the oxidized film [1]. The protonation reaction of POAP was considered as the rate-controlling step due to the constrains of H^+ diffusion through the film matrix. Some experiments were also performed in Ref. [1] varying the ClO_4^- concentration between 0.1 and 1.7 M. While the anodic peak was not affected, the cathodic peak showed a positive variation. Also, it was observed that i_{pc} increases when the concentration of proton is increased. It is indicated that the high concentration of perchlorate produces the same effect as a high proton concentration, making POAP more easily reducible. However, no noticeable changes were observed for other species, such as SO_4^{2-}, PO_4^{3-} and Cl^- or cations such as Li^+, K^+ and Cs^+.

A redox mechanism of POAP films was proposed in Ref. [1] (Fig. 2.4). In this mechanism the redox reaction of POAP involves a process of addition/elimination of protons coupled with a reversible electron transfer. As there is no influence of the nature of cation in the electrolyte solution, it was concluded that the proto-electronic oxidation reaction (I ↔ II ↔ III) is fast and reversible. On the other hand, the kinetic and strong *pH* effects observed in the reduction process seem to indicate that the protonation and corresponding counter-ion motion (III ↔ IV) could be rate-determining. As it is observed in Ref. [1], these processes are favoured by high proton and/or counter-ion concentrations. Also, the protonation reaction is considered to require a demanding polymeric matrix reorganization in the reduction process.

A comparative study of the conduction properties of polyaminoarene films was performed in Ref. [4]. The charge transport in the case of POAP is diffusion-limited and a linear dependence of peak current on the square root of the sweep rate $\left(i_p - v^{1/2}\right)$ was observed. The dependence was explained on the basis of Eq. (2.10):

$$i_p = 2.69\,10^5 n^{3/2} A D_{ef}^{1/2} v^{1/2} c \tag{2.10}$$

with c given by Eq. (2.11):

$$c = Q/nFAd \tag{2.11}$$

where n is the number of electrons participating in the redox process, A the area of the film in cm^2, c is the concentration of active centers in the film (mol cm^{-3}), Q the total charge calculated by the integration of the anodic or cathodic cyclic
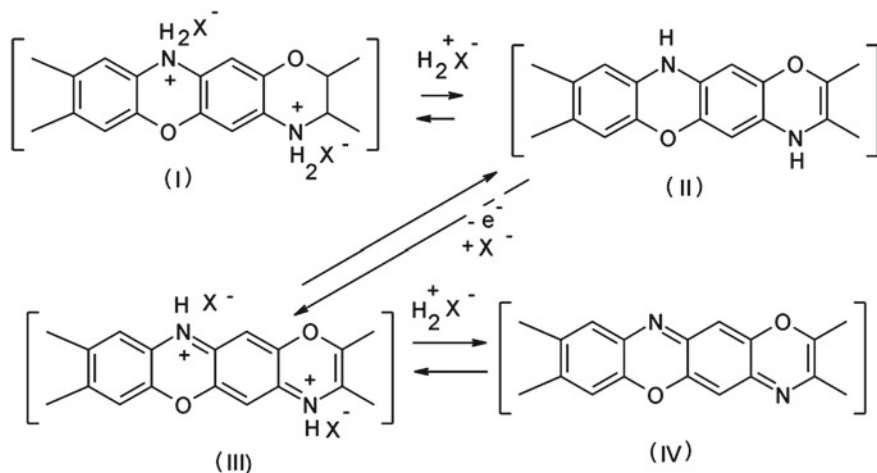
Fig. 2.4   Redox mechanism of POAP [1]

voltammetric currents at slow sweep rate, d is the film thickness and F is the Faraday's constant. From this feature the authors of Ref. [7] calculated an effective diffusion coefficient, D_{ef}, using a model of semi-infinite diffusion developed in Ref. [8]. The calculated D_{ef} values for polyaminophenol films in acid electrolytes are listed in Table 2.1. These parameters of charge transport correlate with the absolute mobility of anions [9]. For the rigid ladder polymer structure of POAP the values of D_{ef} are 2–3 orders of magnitude lower as compared with PANI, indicating a low rate of charge transport in POAP films. The strong difference between diffusion coefficient values of polyaminophenols and PANI films was attributed to the different molecular structure and segment mobility of polymer chains. The presence of electron-donor substituents in the benzene rings was considered to cause some loss of conductivity and electron-transport rate [10].

The effect of the electrolyte composition on the conduction properties of POAP film electrodes was studied by CV in [11]. Measurements were performed in $LiClO_4$ and $HClO_4$ solutions at different pH values and constant ionic strength (1 M). It was assumed that CV curves for POAP films result from two different processes. The former corresponds to a background film conduction, similar to that observed for the unmodified base electrode, while the latter is determined only by redox activity of the film. In order to separate the contributions of such processes from the total CV trace, subtraction of a base current $I_f(E)$, from the total one $I(E)$, was performed in Ref. [11]. Anodic and cathodic peak currents ($I^{(p)}$), as computed by the background subtraction, were found not to be proportional to $v^{1/2}$. Also, the slope of $\ln I^{(p)}$ versus $\ln v$ was 0.9. This result was attributed to the fact that injection of one or two types of charge carriers into the film is the limiting step of the total charge-transfer process under the conditions of the CV measurements.

Table 2.1 Absolute mobilities of anions (u_c) and effective diffusion coefficients (D_{ef}) of polyaminoarene films in acid solutions [7]

Polyaminoarene film, area and thickness	Electrolyte	u_c, m²/V s	D_{ef} 10¹⁰, cm² s⁻¹
Poly-o-aminophenol $A = 3.4$ cm², $d = 0.25$ μm	CH₃COOH (1 M)	3.7	0.08 ± 0.02
	HCl (1 M)	6.8	0.15 ± 0.02
	H₂SO₄ (0.5 M)	7.1	0.23 ± 0.04
Poly-m-aminophenol $A = 4.0$ cm², $d = 0.28$ μm	HCl (1 M)	6.8	1.17 ± 0.07
	H₂SO₄ (0.5 M)	7.1	1.56 ± 0.07
	CH₃COOH (1 M)	3.7	40.2 ± 0.5
Polyaniline $A = 4.0$ cm², $d = 0.28$ μm	HClO₄ (1 M)	6.7	73.7 ± 0.5
	H₂SO₄ (0.5 M)	7.1	90.2 ± 0.5

D_{ef} values extracted from the method reported in Ref. [8]. A and d represent the electrode area and film thickness, respectively

Kinetic and charge transport parameters for POAP (the standard rate constant, k^0, the transfer coefficient, α, and the apparent diffusion coefficient, D_{app}) were obtained in [12] by employing different electrochemical techniques, such as CV, PSCA (potential-step chronoamperometry), PSCC (potential-step chronocoulometry) and NPV (normal pulse voltammetry). Anodic and cathodic peak currents of the voltammetric response were found to scale linearly with the square root of the potential scan rate within the range 5–200 mV s⁻¹. Thus, both anodic and cathodic charge-transport processes within POAP films were considered to be diffusion-controlled [12]. Potential Step Chronoamperometric and Chronocoulometric responses for the oxidation and reduction of POAP films were employed in Ref. [12] to obtain Cottrell plots ($i - t^{-0.5}$ (Eq. (2.12)) and $Q - t^{0.5}$ (Eq. (2.13)). These plots were found to be linear for POAP, indicating that, in agreement with CV results, the charge-transport processes within POAP films follow Fickian diffusion laws [2].

$$i = nFA\, D_{app}^{Ox} C\pi^{-0.5\cdot}t^{-0.5} \tag{2.12}$$

$$Q = Q_{dl} + (2nFA\, D_{app}^{Ox} C\pi^{-0.5}t^{-0.5}) \tag{2.13}$$

Equations (2.12) and (2.13) are expressed for the oxidation process. D_{app}^{ox} is the apparent diffusion coefficient for the oxidation process, n is the number of electrons involved in the heterogeneous electron transfer reaction, F is the Faraday constant and A is the electrode area. C is the volume concentration of the redox sites and Q_{dl} represents the charge corresponding to the double layer. The slopes of the linear chronoamperometric and chronocoulometric Cottrell plots give the D_{app} values for the diffusion-like charge transport process within POAP films. The D_{app} values obtained in [12] are summarized in Table 2.2. With regard to NPV, normal pulse voltammograms for the oxidation and reduction of a POAP film were recorded at various sampling times. Plots of the cathodic and anodic limiting currents (i_{lim}) of normal pulse voltammograms against the inverse of the square root of the sampling time (τ) were found to be linear, as expected for a diffusion-

Table 2.2 Apparent diffusion coefficient values for the homogeneous charge transport within POAP films and kinetic parameters for the heterogeneous electron transfer at the electrode|POAP film interface [12]

Method[a]	$10^{10} D_{app}^{ox} (D_{app}^{red})^a$ cm^2 s^{-1}	$10^4 k^o$ cm^2 s^{-1}	α[b]
PSCA	4.0 ± 0.5 (A)		
	5.8 ± 0.6 (C)		
PSCC	3.3 ± 0.4 (A)		
	5.2 ± 0.6 (C)	1.1 ± 0.3	0.75 ± 0.02 (A)
NPV	1.3 ± 0.2 (A)		
	2.6 ± 0.3 (C)		0.21 ± 0.03 (C)

The measurements were carried out in 0.2 M NaClO$_4$ aqueous solution (pH 1) where the $E'_{1/2}$ values of the POAP film were estimated to be 0.044 V versus SSCE from the average of the anodic and cathodic peak potentials of the cyclic voltammograms for the oxidation–reduction reaction of the POAP film. Other parameters are: the thickness (0.60 ± 0.06) μm and the concentration of electroactive site (4.5 ± 0.04) M for POAP deposited on BPG electrode [12]

[a] *PSCA*, Potential-step chronoamperometry; *PSCC*, Potential-step chronocoulometry; *NPV*, Normal pulse voltammetry

[b] "A" and "C" are used for the anodic and cathodic processes, respectively

controlled limiting current. Thus, D_{app} values were also obtained from the slope of i_{lim} versus $\tau^{-0.5}$ plots by using the normal pulse voltammetric Cottrell equation (Table 2.2). The kinetic parameters (k^0 and α) of the heterogeneous electron-transfer reaction were extracted from the rising part of the normal pulse voltammograms [2] (Table 2.2).

At this point it is interesting to compare results reported in Refs. [11, 12]. In this regard, transient currents for POAP-modified electrodes as a function of the reciprocal of the square root of time were also recorded in Ref. [11].

Authors of Ref. [11] remark that current relaxation for POAP films does not satisfy the Cottrell equation. It is indicated that the main part of the recorded current responses well fits a two-exponential time dependence, which most likely indicates a limiting influence of the charge carrier injection processes at both interfaces of POAP films. Thus, results reported in Ref. [11] seem to indicate that charge transfer through POAP films is complicated by irreversible injection processes at the film interfaces.

Electrochemical Impedance Spectroscopy (EIS) was employed in Ref. [13] to obtain transfer and transport parameters of POAP films of different thickness in contact with a 0.1 M HCO$_4$ + 0.4 M NaClO$_4$ (pH1) solution. Impedance measurements were made within the potential range $0.125 < E < 0.7$ V (vs. NHE). Impedance diagrams were interpreted through a simple charge-transfer resistance in parallel with a constant capacity at high frequencies and the redox capacity (C_{lf}) in series with the film resistance at low frequencies. The electrochemical rate constant ($k_{s, h}$), the concentration of redox centres (c), the film conductivity (σ_{lf}) and the diffusion coefficient of electrons (D_e) for POAP were obtained in Ref. [13]. The charge transfer resistance, R_c, was obtained by fitting experimental data to a semicircle, and it was expressed by Eq. (2.14):
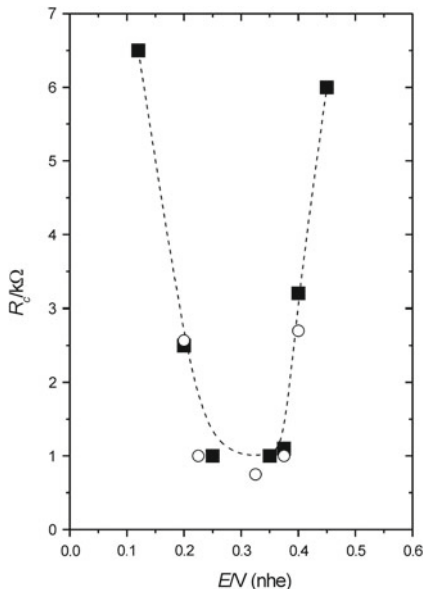
α and β are the charge transfer coefficients for the anodic and cathodic partial processes, respectively, A the electrode area, $k_{s, h}$ the standard rate constant for the charge transfer process (cm s^{-1}), $c_T = C_O + C_R$ the sum of the concentrations of the oxidized and reduced forms, respectively, and $\phi = nF(E - E_0)/RT$ where E_0 is the standard potential of the redox couple. A plot of R_c versus E is shown in Fig. 2.5. No thickness dependence of the semicircle radius was observed in Ref. [13]. With c_T values extracted from a previous work [1] and assuming $\alpha = \beta = 0.5$, a $k_{s, h}$ value about 2.3×10^6 cm s^{-1} was obtained from Eq. (2.14). A high-frequency capacitance (C_{dl}) value about 8×10^{-6} F cm^2 was obtained in Ref. [13] and it was roughly independent of E and d. The redox capacity (C_{lf}) was obtained from $-Z''$ versus ω^{-1} plots at sufficiently low frequencies. C_{lf} versus potential dependence exhibits a maximum value around $E = 0.3$ V (Fig. 2.6). As can be seen from Fig. 2.6, C_{lf} increases with the film thickness, d. The low-frequency resistance, R_{lf} versus E dependence obtained in [13] is shown in Fig. 2.7. As R_{lf} is related to the conductivity (σ_{lf}) through:

$$\sigma_{lf} = d/(R_{lf}A) \tag{2.15}$$

a σ_{lf} value of $(4.55 \pm 0.2) \times 10^{-7}$ ohm^{-1} cm^{-1} was obtained at E_0. In this connection, authors of [13] remark that POAP exhibits a lower conductivity as compared with PANI. An electron-diffusion coefficient value D_e of about 1.3×10^{-11} cm^2 s^{-1} was also obtained by employing the formalism of Chidsey and Murray [14]:

$$R_c = 2RT(e^{\beta\phi} + e^{-\alpha\phi})/An^2F^2k_{s, h}c_T \tag{2.14}$$

Fig. 2.6 C_{lf} versus E for (o)
$d = 30$ nm and (▼) 300 nm
[11]
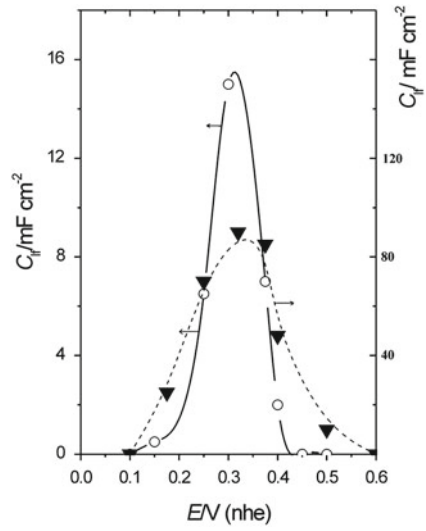
Fig. 2.7 The R_{lf} versus
E dependence for POAP at
different thickness: (o)
$d = 30$ nm and (▼) 300 nm
[13]
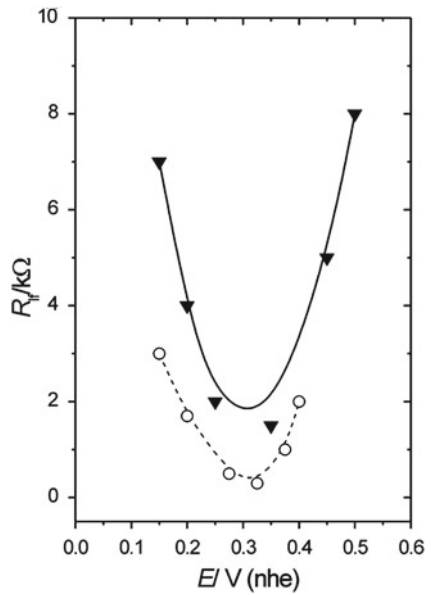
$$D_e = \sigma_{lf}/C_{lf} \tag{2.16}$$

D_e results nearly independent of E (Fig. 2.8).

Impedance measurements were performed in Ref. [15] to obtain charge transport parameters of POAP films and their dependence on solution *pH*. Impedance data were interpreted on the basis of the general expression of the faradaic

Fig. 2.8 Potential dependence of D_e calculated from Eq. (2.16) [13]

impedance of redox polymers with the diffusion–migration transport of two mobile species derived by Mathias and Haas [16]. The low-frequency capacitance, C_L was written as:
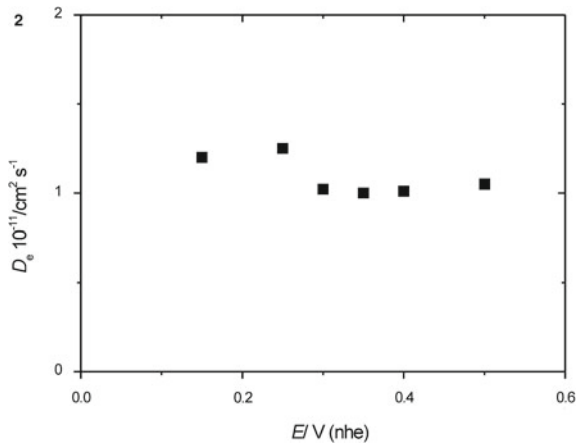
$$C_L = \left(F^2 A d / RT\right) \left\{ \beta \left[n^2 x(1-x)c\right]^{-1} + \left(z_i^2 c_i\right)^{-1} \right\}^{-1} \tag{2.17}$$

where $\beta = 1 - Gx(1-x)$, G is an interaction parameter, x is equals the proportion of oxidized sites to the total electroactive sites, c is the total redox-site concentration, c_i is the concentration of ions with a charge number z_i, n is the number of electrons exchanged in a homogeneous reaction, d is the film thickness and A, the electrode area. The other symbols have their usual meanings. As according to the Mathias and Haas theory [16], Eq. (2.17) can be transformed into:

$$C_L = A d \kappa t_e t_i D^{-1} \tag{2.18}$$

where κ is the film conductivity, $D(= D_i t_e + D_e t_i)$ is the coupled diffusion coefficient, which is expressed in terms of the electron (D_e) and mobile ions (D_i) diffusion coefficients and the transference numbers for electrons (t_e) and ions (t_i), respectively, then, the resistance of the bulk films, R_p, was written as:

$$R_p = d(A\kappa)^{-1} = d^2 (DC_L)^{-1} t_e t_i \tag{2.19}$$

The low-frequency resistance, R_L, was also expressed in terms of the coupled diffusion coefficient D:

$$R_L = d^2 (3DC_L)^{-1}(1 - 3t_e t_i) \tag{2.20}$$

The high-frequency charge-transfer resistance R_c, was related to the exchange current (i_0) of the redox couple at the metal/film interface by means of Eq. (2.21):

$$R_c^{-1} = nF(RT)^{-1} i_0 = (nF)^2 (RT)^{-1} A k_s c_o^{(1-\alpha)} c_R^\alpha \tag{2.21}$$

where k_s is apparent standard heterogeneous rate constant, α is the transfer coefficient, c_o and c_R are the concentrations of the oxidized and reduced species, respectively. Equation (2.21) predicts that R_c reaches a minimum at nearly equal concentrations of the oxidized and reduced species in case of $\alpha = 0.5$ (Fig. 2.9). As the experimental dependence of the low-frequency resistance, R_L, on potential (Fig. 2.10) was basically similar to that of the charge-transfer resistance, R_c (Fig. 2.9) authors of Ref. [15] conclude that charge transport in the polymer occurs by a diffusion-like process due to molecular electron exchange, as suggested by Gabrielli et al. [4]. On the basis of relationships between R_L and the polymer resistance, R_p, the rate-determining step in charge transport through POAP films was discussed in [15]. Table 2.3 shows the two combinations of transport parameters in the extreme cases of ion-transport control, electron-transport control and mixed control. With regard to experimental data extracted from impedance plots showed in Ref. [15], R_p/R_L was very low (see Table 2.3), since R_L values were within the range 0.2–2 kΩ at a thickness film of $d = 0.1$ μm and R_p resulted very small (less than 2 ohm).

It was concluded in Ref. [15] from parameters listed in Table 2.3, that $t_e \gg t_i$ or $t_e \ll t_i$. Then, one of the two carriers moves much faster than the other at POAP. In order to shed light on this point, the authors of Ref. [14] calculated the D versus E dependence from experimental R_L (Fig. 2.10) and C_L values (Fig. 2.11). In spite of the error in the D values (near 50 %), it was found that D depends on E, that is, on the oxidation level of the polymer. The calculated D versus E dependence shows a maximum near the formal potential of POAP (Fig. 2.12).

Fig. 2.9 Changes of the charge-transfer resistance with applied potential at different pH values: 0.5 (○); 1.3 (□); 2.5 (◇); 3.5 (△). Electrode area, $A = 0.071$ cm^2 [15]
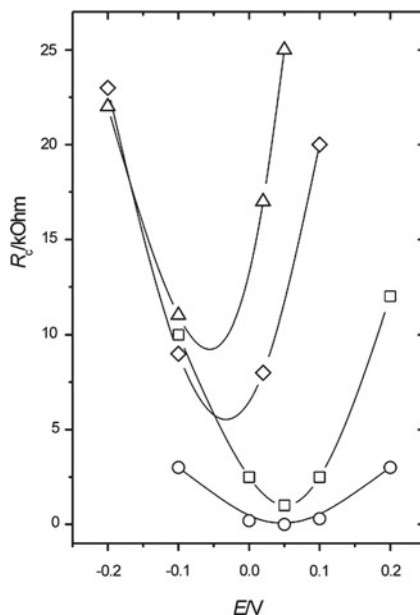
Fig. 2.10 Changes in the width of the Warburg region with applied potential at different pH values: 0.5 (o); 1.3 ($\square$); 2.5 ($\diamond$); 3.5 ($\triangle$). Electrode area, $A = 0.071$ cm^2 [15]
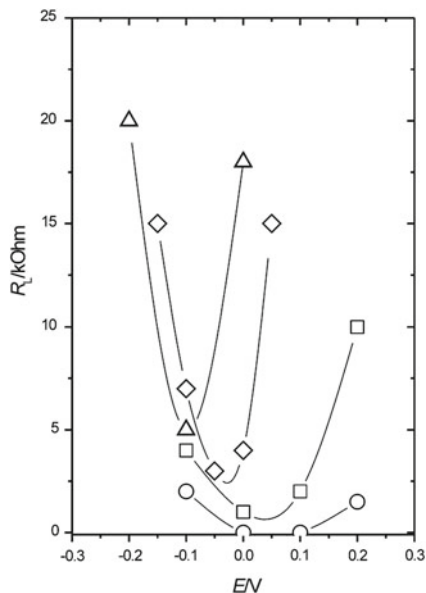
Table 2.3   Values of two combinations of transport parameters in the extreme cases of ion-transport control, electron- transport control and mixed control [15]

	Ion-transport control $t_e = 1,\ t_i = 0$	Electrón-transport control $t_e = 0,\ t_i = 1$	Mixed control $t_e = t_i = 0.5$
R_p/R_L	0	0	3
C_L/R_L	$d^2(3D)^{-1}$	$d^2(3D)^{-1}$	$d^2(12D)^{-1}$

Relationships extracted from the impedance model described in Ref. [15].

By comparing the D versus E dependence extracted from experimental R_L and C_L values with the D versus E dependence extracted from theoretical models [17], the existence of an electron-transport control in POAP was established. In this regard, authors of Ref. [15] consider the interaction between electroactive sites employing the coupled diffusion coefficient in electron-hopping conductive materials derived in [16], that is,

$$D = D_i t_e + \beta D_e t_i \tag{2.22}$$

where D_e and D_i are the diffusion coefficients of electrons and ions, respectively. At the extreme of ion-control ($t_e = 1$, $t_i = 0$), D becomes equal to D_i, which is potential independent. On the other hand, for electron-transport control ($t_e = 0$, $t_i = 1$), authors of Ref. [15] consider the expression,

$$D = D_e[1 - Gx(1 - x)] \tag{2.23}$$

Fig. 2.11 Changes in the low-frequency capacitance with E at different pH values. 0.5 (o); 1.3 ($\square$); 2.5 ($\diamond$); 3.5 (Δ). Electrode area, $A = 0.071$ cm^2 [15]

where if D is independent of the oxidation level, D will show a maximum of $D_e(1 - G/4)$ at $x = 0.5$. This expectation corresponds to experimental results shown in Ref. [15] (Fig. 2.12) with a G value of -10 and $D_e = 3.7 \times 10^{-9}$ cm^2 s^{-1}.

Fig. 2.12 Changes in coupled diffusion coefficients with applied potential in HCl–KCl solution (pH 1.3). ($\square$) obtained from R_L and C_L; (o) estimated from method of Armstrong [17]; (- - -) calculated from the expression of the high-frequency capacitance, $C = F(RT)^{-1} Q_m x(1 - x)$ $[1 - Gx(1 - x)]^{-1}$ and $D_e = k\lambda^2 c/6$, where k is the intermolecular electron-transfer rate constant and λ is the mean distance between two adjacent redox sites. $E^{o'} = 0$ V and $G = -10$ [15]
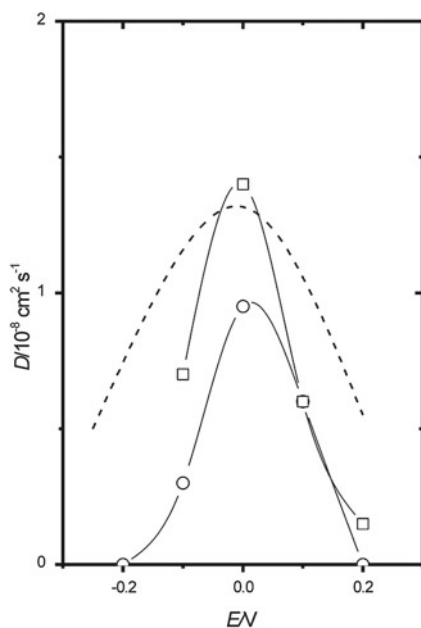
In the case of electron-transport control, the D_e value was found to be $D_e = 6 \times 10^{-9}$ cm^2 s^{-1} in 0.2 M HCl, from the estimated D maximum and a G value of -10. The D_e value obtained in Ref. [15] was very small in comparison with a D_i value of $(0.9–5\ 6 \times 10^{-6}$ cm^2 s$^{-1})$ reported for PANI films.

EIS was also employed in Ref. [18] to study the effect of the electrolyte solution on the transport properties of POAP. Different 0.1 M HClO$_4$ + x M NaClO$_4$ solutions were employed, where x was varied between 0.4 and 2. The dependence of the characteristic impedance quantities at low frequency on the electrolyte concentration was interpreted on the basis of two models: a transmission line [19, 20] and a modified electron-hopping model described in Ref. [21]. Figure 2.13a, b shows the low-frequency capacitance (C_{LF}) and the low-frequency resistance (R_{LF}) vs potential dependences, respectively, for solutions of different ionic strengths. With regard to the transmission line model, impedance quantities obtained in Ref. [18] from experimental impedance spectra were employed in the Albery's Model [19, 20] to obtain different transport parameters of POAP films. Two separate distributed resistances are used in this model to represent the transport of electrons (R_e) and counter-ions (R_i) within the polymer [19, 20]:

$$R_e = RTc\phi_p/F^2abAD_e(1/p + 1) \tag{2.24}$$

$$R_i = RT\phi_p(1 + p)/F^2bAD_i \tag{2.25}$$

D_e and D_i are the diffusion coefficients for electronic species and ions, respectively; c is the total concentration of redox sites in the polymer; a, is the concentration of the reduced sites; and b the concentration of the oxidized ones $(a + b = c)$. The parameter p represents the ratio of the volume of the polymer film to that of the aqueous pores; ϕ_p is the polymer film thickness; and A the geometric electrode area. The other constants have their usual meanings. The parameter p changes between 1 for a completely compact film and 0 for a completely porous one.

At low frequency the impedance expression given by the transmission line model, allowed to authors [18] to calculate $R_\Sigma(= 3R_{LF})$ from:

$$Z_{LF} = R_\Sigma/3 - i/\omega C_\Sigma \tag{2.26}$$

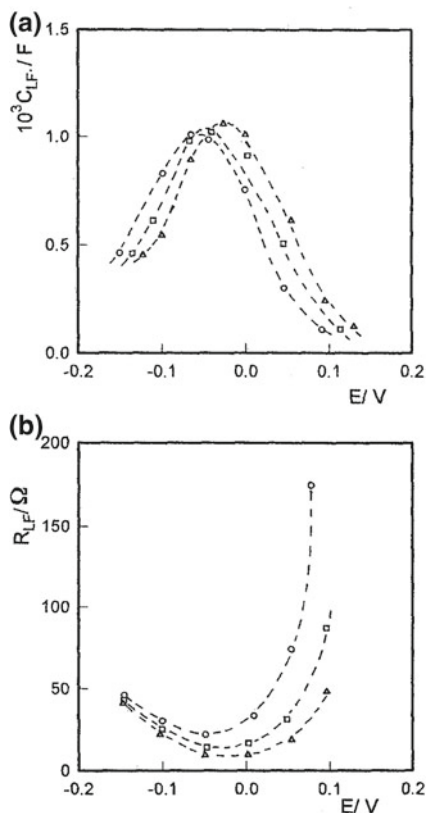where R_Σ is the sum:

$$R_\Sigma = R_e + R_i \tag{2.27}$$

and C_Σ is related to D_e through:

$$C_\Sigma^{-1} = C^{-1} + (D_e/\phi_p^2)\Psi \tag{2.28}$$

where C^{-1} describes the Feldberg capacitance and Ψ is:

$$\Psi = R_e[1 + (1 + \theta^{ox})]/[1 + (2s/\theta^{ox}pc)^2]^{1/2} \tag{2.29}$$

In this last equation s is the salt concentration of the external electrolyte phase
and $\theta^{ox} = b/c$ is the degree of oxidation of the polymer. When the polymer is
completely oxidized authors [18] estimated p from:

$$Q_T^o = FAc\phi_p[p/(1+p)] \tag{2.30}$$

Q_T^o in Eq. (2.30) is the voltammetric charge for the oxidation process of POAP.
With values of c, $\theta^{ox}(= b/c)$ and ϕ_p; D_i and D_e and p were employed as fitting
parameters in order to obtain the best fit of Eq. (2.27) to experimental R_Σ versus
θ^{ox} curves (continuous lines in Fig. 2.14). Despite p was estimated from Eq.
(2.30), it was also employed as a fitting parameter in Eq. (2.27). The parameter
p was considered as representative of the polymer porosity in this simple
impedance model. In this regard, while D_i and D_e were considered to depend on
film thickness and electrolyte composition, p was only considered to vary with the
film thickness. Application of the electron-hopping model developed in [21] only
gave an effective diffusion coefficient, D_{eff}. Figure 2.15 shows the D_{eff} versus θ_{ox}
dependence for different ionic strengths of the electrolyte solution. At the different
electrolyte concentrations, D_e obtained from the transmission line model was

Fig. 2.14 Plots of the low-frequency resistance (R_Σ vs. θ_{ox}) for a 30 nm thick POAP film in 0.1 M $HClO_4$ + x M $NaClO_4$ solutions: (Δ) $x = 1.9$ M, ionic strength, $\mu = 2$ M; ($\square$) $x = 0.4$ M, ionic strength, $\mu = 0.5$ M; (o) $x = 0$ M, ionic strength, $\mu = 0.1$ M. Symbols represent experimental values and *dashed lines* theoretical fit using the transmission line model [19, 20]
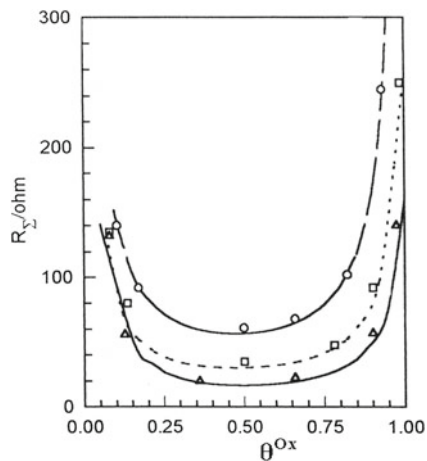
Fig. 2.15 D_{eff} versus θ_{ox} dependence for a 30 nm thick POAP film at different μ values: (o) 0.1 M, ($\square$) 0.5 M, (Δ) 2 M. D_{eff} values were obtained from the model given in [21]
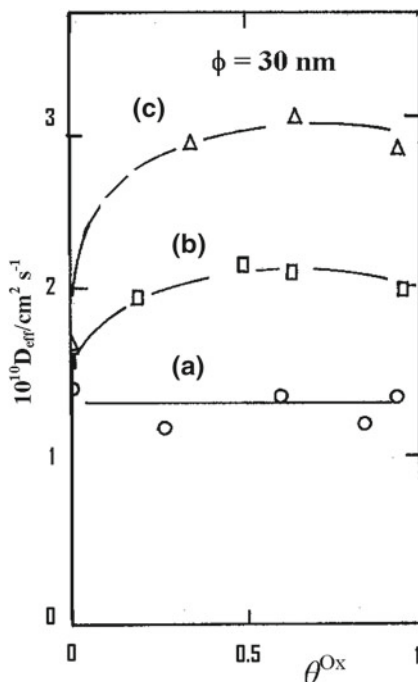
always two orders of magnitude lower than D_i. Also, as D_{eff} was very close to D_e, this was considered as indicative of a conduction mechanism at POAP films dominated by electron transport.

2.2.1 Conducting Potential Range of Poly(o-aminophenol)

POAP shows a relatively low conductivity as compared with other conjugated polymers. Table 2.4 lists the conductivity of some typical electroactive polymers.

On the basis of "polaron–bipolaron" model [29] of charging processes at polymer films, Ortega [30] investigated POAP by cyclic voltammetry and ESR measurements to determine the conducting potential range of the polymer. POAP films deposited on a Pt electrode were studied at *pH* 0.9, where spectra were recorded at different potentials, scanning forwards and backwards from −0.250 to 0.55 V (vs. SCE). The maximum in ESR spectra occurs in the potential range from −0.24 to approximately 0.0 V (see Fig. 1.16, Chap. 1). The decrease and further absence of a detectable ESR signal at potentials higher than 0.55 V suggests a combination of radicals to give rise to dication species, which are not ESR active because of their paired spin. The determined *g* value was 2.00710 for the spectra recorded from −0.2 to 0.05 V and 2.0076 for the one at 0.15 V. The slight change in *g*, due to the change in the nature of the electrostatic interactions between the charges in the polymer, was attributed to the combination of polarons at positive potentials to give rise to dications. Thus, it was concluded that at high positive potential values, the creation of bipolarons by a combination of polarons is possible at POAP films [30]. This conclusion is supported by other spectroscopic studies. Raman spectroscopy and voltammetry were coupled in [31] to identify structural changes in POAP during its redox process. Raman spectra of POAP contacting a 1 M $HClO_4$ solution exhibit bands whose intensities depend on the applied potential. For instance, the band associated with quinoid groups (1474 cm^{-1}) and the band assigned to –C=N– in quinoneimine units (1638 cm^{-1}) depend on the potential (Fig. 2.16).

The behaviour of these bands with the potential shows that when the potential increases, the band at 1474 cm^{-1} increases and the band at 1638 cm^{-1} also increases until a potential of about 0.2 V and thereafter, it diminishes. The fitting of these bands by employing Lorentz curves allowed the authors of [31] to quantify the evolution with the potential of the species related to these bands. The integrated intensity of the band at 1638 cm^{-1} increases until a potential around 0.15 V and then decreases. However, the integrated intensity of the band at

Table 2.4 Conductivity of some typical electroactive polymers

Polymer	[a]Conductivity (S cm^{-1}) of the oxidized polymer	References
Poly(o-aminophenol)	10^{-7}–10^{-6}	[1, 13, 15, 21–24]
Polyacetylene	3–1000	[25]
Polyaniline	0.01–5	[25]
Polypyrrole	0.3–100	[26]
Polythiophene	2–150	[27]
Poly(p-phenylene)	10–500	[28]

[a] Significantly higher conductivity has been published for the polymers listed but not in the context of their practical applications

Fig. 2.16 Dependence of the relative area of 1474 cm^{-1} (•) and 1638 cm^{-1} (◇) Raman bands on the electrode potential for a POAP modified Au electrode in 1 M HClO$_4$ electrolyte solution [31]
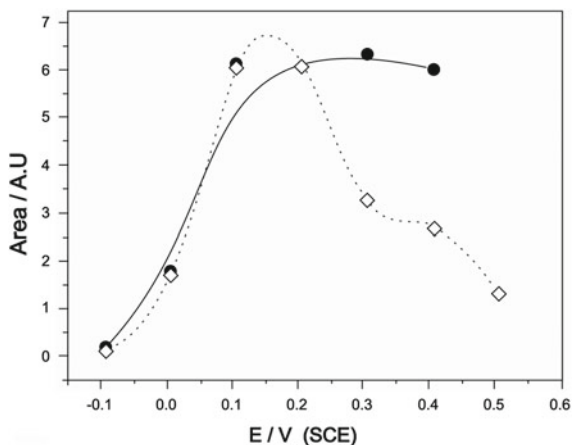
1474 cm^{-1} increases until 0.15 V, and then it is maintained. Thus, the behaviour of the band at 1638 cm^{-1} corresponds to a typical intermediate species. Since POAP has a conductivity maximum at about 0.04 V versus SCE, the intermediate species was related to the polymer conductivity and then, it was assigned to a charged species. The authors of Ref. [31] indicate that the existence of an intermediate species suggests that the oxidation of POAP occurs through two consecutive reactions from the totally reduced phenoxazine form to the completely oxidised one, through a charged species, which could be a cation radical. Authors of Ref. [31] remark that the behaviour of the integrated Raman intensity of the band at 1638 cm^{-1} is similar to that of the band at 750 nm observed in the absorbance *versus* potential dependence in the UV-Vis region reported in [32]. Then, Raman and UV-Vis measurements suggest that the third species could be a cation radical, in agreement with the results obtained by EPR [30].

EIS was employed in Ref. [13] to obtain dependences of charge transfer and charge transport parameters of POAP films on the electrode potential within the range 0.125 V $< E <$ 0.7 V (versus NHE). A conductivity value of 4.55 ± 0.2) × 10^{-7} ohm^{-1} cm^{-1} was obtained for POAP at $E = 0.3$ V (NHE). Authors of Ref. [13] remark that POAP exhibits a lower conductivity as compared with PANI. An electron-diffusion coefficient value D_e of about 1.3 × 10^{-1} cm^2 s^{-1} was also obtained.

Dynamic Monte-Carlo simulations were employed in order to find the morphological effect of the insulating–conducting (I–C) transition of a POAP film [33]. In these calculations it was assumed that the polymer has a random distribution of electroactive and electroinactive sites. The electrochemical switching potential (I–C) of the polymer and its percolative nature [34–36] under potential changes, was analyzed in Ref. [33]. The model of electrochemical system used in Ref. [33] consists in a conductive polymer film in a solution containing a large excess of supporting electrolyte and dopant ions. The film was considered to be conductive in the oxidized state and nonconductive in the reduced state. It was assumed that the

zone composed of only the conductive species is fully conductive and that the mass transfer of counter-or dopant ions associated with the charge transfer has only a minor effect on the propagation of the conductive zone. The conductive polymer film was simulated by means of a two-dimensional lattice of which each element was a regular rectangle. Each element was attributed to a conductive, a non-conductive or an electro-inactive site. A substrate electrode was allocated randomly on the lattice so that the ratio of the area of electroactive sites to that of the lattice was a given value, p (p is the percolation probability). On the basis of the cyclic voltammetry (CV) technique and the theory of propagation, the growth rate of the conductive zones was considered as an exponential function of the electrode potential. The dimensionless amount of interconverted conductive zones, X, was expressed in terms of the theoretical linear sweep voltammetry [37] as:

$$X = \int \kappa e^{\beta\xi}\Big\{[1 + \Phi(e^{\beta\xi} - \beta/\kappa)^{1/\beta}]^{-1} - (1 + e^{\xi})^{-1}\Big\}d\xi \qquad (2.31)$$

where, $\xi = (nF/RT)(E - E^{0r})$ is the dimensionless electrode potential, β is the chatodic transfer coefficient, κ is the dimensionless kinetic parameter given by $\kappa = k^{o}RT/nFv\delta$ and Φ is a function defined as:

$$\Phi(z) = z \text{ for } z \geq 0 \text{ and } 0 \text{ for } z < 0 \qquad (2.32)$$

k^0 is the charge-transfer constant, δ is the thickness of the polymer film and v is the potential sweep rate. It was assumed that at the electrode/film interface, and under the Nernst boundary condition, $1/(1 + e^{-\xi})$ fraction of the total electrode area is converted at any increment $\Delta\xi$. Therefore, the amount of conversion, $X(\xi + \Delta\xi) - X(\xi)$ was written as:

$$X(\xi + \Delta\xi) - X(\xi) = \Delta\lambda/(1 + e^{-\xi i}), \text{ for } i \in [1, \infty). \qquad (2.33)$$

$\Delta\lambda$ is the side length of the square element and the value of ξ_i was obtained numerically for a given value of the initial potential, ξ_0 The initial potential, ξ_0 was estimated from Eq. (2.31) by taking $\Phi = 0$. Then, a series of $\{\xi_i\}$ was computed. Electroactive sites were assigned to the lattice by the Monte-Carlo method so that that the total area of the active sites was p-times the area of the lattice. The number n_i of the conductive sites converted at ξ_i was considered to be proportional to the faradaic charge at the step ξ_i to ξ_{i+1}. As the lattice consists of $N \times M$ rectangles, hence the dimensionless current was written as $n_i/[N \times M(\xi_{i+1} - \xi_i)]$ Various patterns of the conductive zones were observed in Ref. [33] at p ranging from 0.5 to 0.61. A two-dimensional patter of the conductive sites ($\xi = -4$ and $p = 0.50$) was observed when the current vanishes in linear sweep voltammetry. The sites have a very low electrical contact with the electrode under this condition. This effect was explained by assuming that under an insufficiently positive potential there are a few conductive sites on the electrode. The growth began at the sites on the first layer activated by the Nernst condition, (for $\xi = -2$, $p = 0.55$). In this case, the zones consist of a number of clusters, which are disconnected electrically from each other. Some of these patterns result

fractal. In this case, the zone grew not only in direction parallel to the electrode and toward the film/solution interface, but also in the direction toward the electrode. Further, growth yielded electrical percolation at $\xi = -0.50$ from the electrode to the top of the film. The fractal pattern occurs at percolation threshold ($p = 0.59$). The final converted pattern involved various sizes of islands after percolation threshold ($p = 0.61$) at $\xi = 0.5$. Since the islands consisted of not only electroinactive zones, but also nonconductive zones, the conversion ratio was less than p. Figure 2.17 shows the average linear sweep voltammogram corresponding to the patterns reported in Ref. [33]. From the peak current and the conversion ratio with p, the voltammogram was classified into the three controlled processes: Nernsian condition control ($0 < p < 0.55$), morphological control ($0.55 < p < 0.61$) and charge-transfer control at the interface between conductive and nonconductive sites ($p > 0.61$). The morphological effects are specific to the peak potential. The comparison of the simulated patters obtained in Ref. [36] with the corresponding linear sweep voltammogram shown in Fig. 2.17, reveals that the peak potential of linear sweep voltammetry could be considered as a first approximation of the percolation threshold potential of the electrochemically deposited conductive polymer film. In order to verify this assumption, authors of Ref. [33] performed an independent analysis to determine the percolation threshold potential of a conductive POAP film and compared it with the peak potential of a cyclic sweep voltammogram. Thus, POAP films in Ref. [33] were deposited on glassy carbon electrodes by multiple potential cycling between -0.2 and 0.9 V versus Ag/AgCl at a scan rate of 50 mV s^{-1} in a sulfuric acid solution (*pH* 5) containing *ortho*aminophenol at a concentration of 0.1 M. The POAP coated electrode was stepped in the positive potential direction and the growth of the conductive zone was investigated through examining the chronoamperometric behavior.

Figure 2.18 shows the chronoamperograms of the film/H$_2$SO$_4$ interface recorded at *pH* 5 at various potential steps in the range of 0.01–0.2 V/Ag/AgCl. The electrochemical activity of POAP begins at around 0.11 V, as indicated by the sharply rising initial current (I) and its relatively slow decay with time (t) (Fig. 2.18). Plots of I–$t^{-1/2}$ and I–t^{-1} were recorded at various potential step values. Below 0.15 V, linear dependency of I–$t^{-1/2}$ was observed indicating the dominance of the diffusion controlled processes giving rise to the development of the conducting conductive zone. Above 0.15 V, no linear dependency of I–$t^{-1/2}$ was observed over any appreciable period of time. On the other hand, good to fair linear plots of I–t^{-1} were obtained over a large time period. Interestingly, the slope of this dependency increases as the magnitude of the potential step increases to 0.17 V and decreases upon further increase of the size of the potential step.

An explanation of this behavior is given in Ref. [33]. It was considered that linear I–t^{-1} plots correspond to the production of finite quantities of material conducting form of the polymer under a potential step of finite height. The polymeric film is initially in the insulating mode, then, upon stepping the potential into the electrochemically active region, the polymer immediately in contact with the metallic surface is oxidized and converted to the conducting mode while the rest is still
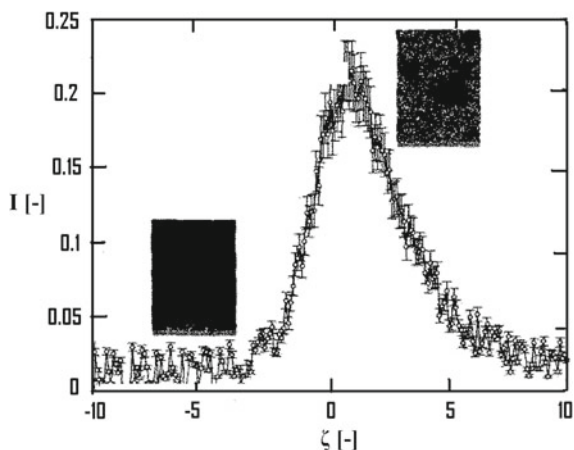
Fig. 2.17 Dimensionless voltammogram ($iRT/n^2F^2c^*\delta vp$ vs. ξ) simulated for distribution of the electroactive sites. Inset shows distribution for conductive zones at $\xi = -4$ (*lower*) and at $\xi = -0.59$ (*upper*), i is the current density, c^* is the concentration of the electroactive species, v is the potential sweep rate, p is the ratio of the area of electroactive sites to that of the lattice and δ is the thickness of the polymer film [33]
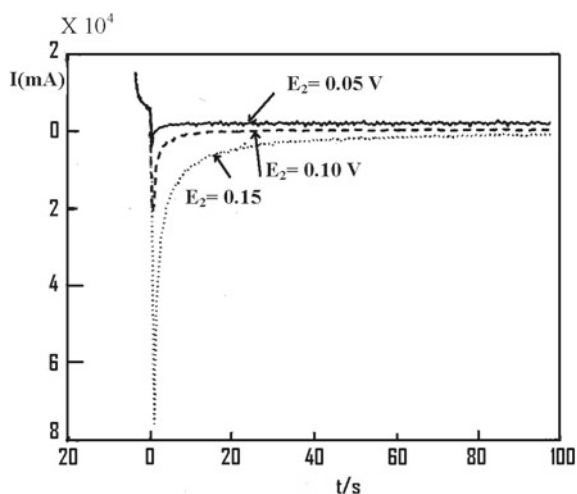
Fig. 2.18 Chronoamperograms of the POAP film/H_2SO_4 interface at various potential steps [33]

insulating. Further conversion has to continue at the partially metal-like progressive conducting zone. The size of the conducting zone (cluster) is certainly controlled by the charge delivered onto the electrode (film) at the specified potential step. The deposited film is converted into the conducting mode by repeating this process. Some of the conducting clusters keep growing and some are probably transported

Fig. 2.19 Cyclic voltammogram of a POAP film in the presence of sulfate anions (*pH* 5). Scan rate: 50 mV/s [33]
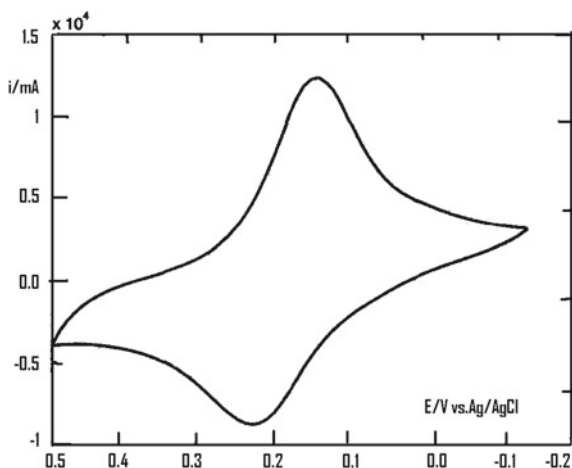
trough the film by diffusion. It is believed that the rate of enlargement of the conducting cluster is slowed down by the depletion of the wandering (migrating off the metallic back contact) of the already existing small conducting clusters giving rise to the t^{-1} dependency of the current rate. However, the linearity was found to be limited to the potential range of $0.15\ V < E_c < 0.17\ V$. In the opinion of the author [33], E_c is definitely in the range of $0.15\ V < E_c < 0.17\ V$ near the peak potential of the corresponding voltammogram (Fig. 2.19).

This fact was confirmed by the Monte Carlo simulation results. Both the simulated linear sweep voltammetry and the potential step experiments show an extremely rapid drop in the current during C–I conversion. That is, the film changes from the conducting form to the insulating one, once the conversion yield reaches a threshold during the phase transition. Since, the transition is based on fractal formation, slight fluctuations, such as movement of the sites may change the cluster size. Therefore, the abrupt growth of the C zone and the onset of the current at E_c correspond to a rapid rise in the anodic voltammogram when the film is sufficiently reduced. Then, authors of Ref. [33] conclude that the percolation threshold during insulating/conducting transition of electrochemically deposited POAP films is in the range 0.15–0.17 V (Ag, AgCl).

2.2.2 Effect of the Solution pH on the Charge-Transport Process at POAP Films

The electrochemical response of POAP is highly dependent on the solution *pH*. The *pH* effects on the voltammetric response of POAP were described in Ref. [1] (see Eqs. (2.7) and (2.8), and Fig. 2.2). Also, a redox reaction of POAP was proposed in Ref. [1] (Fig. 2.4), which involves a process of addition/elimination of

protons coupled with a reversible electron transfer. The protonation of the oxidised form of POAP was considered as the coupled chemical reaction in the mechanism proposed in Ref. [1].

Electrochemical Impedance Spectroscopy was used in Ref. [21] to study the effect of the solution *pH* on the charge conduction at POAP films. An *a.c* impedance expression was derived on the basis of a model that considers a chemical reaction influencing the dynamics of the charge-transport process by electron hopping between redox sites. The model described in Ref. [21] considers a protonation reaction (Eq. (2.34)) coupled with a self-exchange process between oxidized and reduced sites (Eq. (2.35)):

$$O + [H^+]_{film} \underset{k'_{-1}}{\overset{k'_1}{\longleftrightarrow}} HO^+ \tag{2.34}$$

$$OH^+ + e^- \underset{k_b}{\overset{k_f}{\longleftrightarrow}} RH \tag{2.35}$$

The analytical expression for the impedance derived in Ref. [21] is

$$Z(\omega) = R_{Qt} + (RT/nF^2Ac) [k_f + k_b(K+1)/K]A(\omega, D_e, k) \tag{2.36}$$

R_{Qt} in Eq. (2.36) is a charge-transfer resistance, which is given by the expression

$$R_{Qt} = (RT/nF^2Ac) \left[(k_f + k_b) (k_f k_b)^{-1} + 1/K \ k_f \right] \tag{2.37}$$

In Eqs. (2.36) and (2.37), A is the electrode area, c the volumetric redox site concentration, and K an equilibrium constant that can be explicitly written in terms of the solution *pH* as

$$K = (k'_1/k'_{-1})K_p 10^{-pH} \tag{2.38}$$

K also depends on the k'_1 and k'_{-1} constants involved in step (2.34) and a partition coefficient K_p, which determines the ratio between the proton concentration inside the film ($[H^+]_{film}$) and the actual proton concentration in solution ($[H^+]_{sol}$), i.e.,

$$[H^+]_{film} = K_p[H^+]_{sol} \tag{2.39}$$

k_f and k_b in Eq. (2.36) are the forward and backward electrochemical rate constants involved in step (2.35), respectively, and $A(\omega, D_e, k)$ is a function of the frequency, ω, which also contains an affective diffusion coefficient (D_e) to describe the charge-transport process within the polymer film and the constant $k = k'_{-1} + [H^+]_{film} k'_1$. OH^+ and RH (steps (2.34) and (2.35)) are the protonated oxidized and reduced forms of the polymer confined redox couple, respectively. Other chemical equilibria following the self-exchange (2.35) were ignored in Ref. [21]. Concerning step (2.35), the electroactive centres OH^+ and RH can exchange

electrons with the electrode at the metal/polymer interface following a Buttler–Volmer kinetics, with k_f and k_b given by the expressions

$$k_f = k_{sh} \exp \left[b_f \left(E - E^0 \right) \right] \tag{2.40}$$

$$k_b = k_{sh} \exp \left[-b_b \left(E - E^0 \right) \right] \tag{2.41}$$

E^0 in expressions (2.40) and (2.41) is the standard potential of the redox couple, b_f and b_b are the Tafel coefficients, $b_f = \alpha nF/RT$ and $b_b = (1 - \alpha) nF/RT$, and k_{sh} is the electrochemical standard rate constant. The other constants have their usual meanings. The redox centres are uniformly distributed throughout the polymer with a total concentration, c, given by

$$c = [O] + [HO^+] + [RH] \tag{2.42}$$

Eq. (2.36) was employed in [21] to fit experimental impedance diagrams of POAP films in solutions of different pH. In the model the equilibrium constant (K) (Eq. (2.38) for the protonation reaction appears in the different impedance quantities (Warburg coefficient (σ_{Qc}), low-frequency resistance ($R_{Q, LF}$), low-frequency capacitance ($C_{Q, LF}$), electron diffusion coefficient (D_e), etc.). Then, a comparison between experimental and theoretical impedance quantities at different pHs values was made in Ref. [21].

Figures 2.20 and 2.21 show some results of the fitting (continuous lines) of the theoretical impedance quantities derived in Ref. [21] to experimental (discrete points) data. It was found that the low-frequency capacitance and the conductivity decrease with pH. A conductivity value of about 3.2×10^{-6} S cm^{-1} at pH 0 was reported for POAP in Ref. [21]. Also, as the pH affects the dynamics of the electron-hopping process through reduction of the redox centre density, from the fitting it was possible to extract an electron-diffusion coefficient that decreases from 2.1×10^{-10} to 5×10^{-11} cm^2 s^{-1} as the pH increases from 0 to 2. Also, a pKa value about 2.3 for the proposed protonation reaction could be estimated from the model developed in Ref. [21].

Another *ac* impedance study of POAP-coated electrodes was performed in Ref. [15] to establish how the kinetic parameters of the charge-transport process are affected by the protonation levels and also by the degree of oxidation of the polymer. Impedance data were analysed on the basis of the electron-hopping transport accompanied with intermolecular proton exchange. The dependence of the charge-transfer resistance (R_c) on the potential (E vs. Ag/AgCl) at different pH values was evaluated from experimental impedance spectra (Fig. 2.9). R_c values obtained at a given pH reach a minimum at the formal potential of POAP, which was evaluated as the average of the voltammetric anodic and cathodic peak potentials. The minimum of R_c considerably increased with increasing pH. Also, the R_c *versus* E curve shifts to the negative potential with a rate of -0.06 V/pH as pH increases. This effect was considered as indicative of a proton participation in the redox reaction of POAP. With regard to low frequencies of impedance data, the capacitance (C_{LF}) was evaluated from the slope of Z'' versus ω^{-1} plot. C_{LF}

Fig. 2.20 Low-frequency
capacitance $C_{Q,LF}$ versus *pH*
at $(E - E^0) = -0.05$ V. (o)
Experimental points extracted
from the Nyquist diagrams
obtained at different *pH*
values. Thickness of the film
30 nm. Bathing electrolyte:
$HClO_4 + NaClO_4$, ionic
strength 1 M [21]
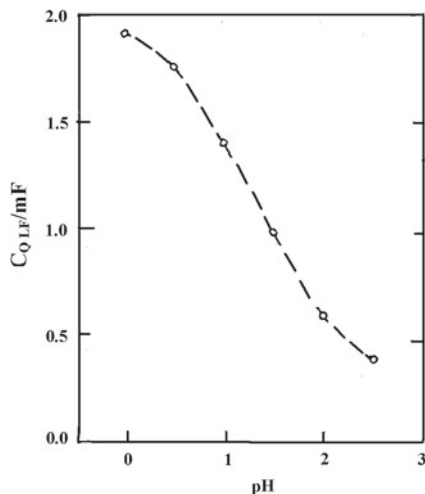
Fig. 2.21 Warburg
coefficient σ_{Qc} versus *pH* at
$(E - E^0) = -0.05$ V. (o)
Experimental points extracted
from the Nyquist diagrams
obtained at different *pH*
values. Thickness of the film
30 nm. Bathing electrolyte:
$HClO_4 + NaClO_4$, ionic
strength 1 M [21]
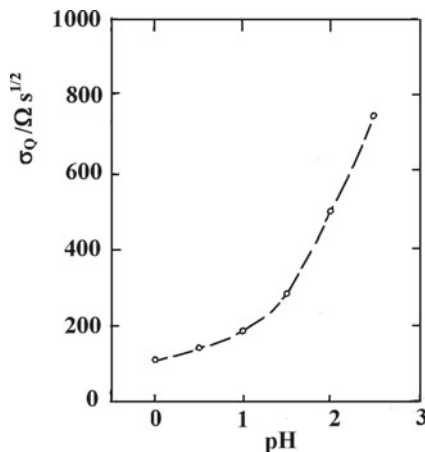
obtained at a given *pH* shows a maximum near the formal potential. The C_{LF}
versus E curve shifts to the negative potential with increasing *pH*, whereas the
maximum of C_{LF} was independent of *pH* (17 ± 1 mF cm^{-2} at a film thickness of
0.14 μm) (Fig. 2.11). As *pH* increases, it was also observed in Ref. [15] that the
formal potential of POAP shifts to the negative direction with a rate of -0.06 V/
pH in the *pH* range below 6. This shift was considered to indicate that one proton
is released for each electron transferred in the oxidation process, thus electro-
chemical oxidation of the polymer was considered equal to its dehydrogenation. In
this sense, it was considered in Ref. [15] that when the polymer including elec-
troactive nitrogen atoms is oxidized, anions are inserted into the polymer (Eq.
(2.43)), or else protons are released from the polymer (Eq. (2.44)) to maintain its
electroneutrality:

$$P + Cl^-(s) \rightarrow P^+Cl^- + e \ (m) \tag{2.43}$$

$$PH \rightarrow P + H^+(s) + e(m) \tag{2.44}$$
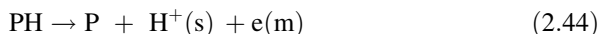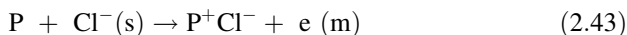
where both P and PH denote the monomer unit in polymer chains, in disregard for its protonation. On the basis of the acid dissociation constant of phenazine, it was concluded in Ref. [15] that all species of the different oxidation states of POAP should be protonated in acid solutions. The redox reaction of the protonated POAP was expressed as indicated in Fig. 2.22.

The reduced form $-NH_2^+-$ or $-NH-$ (for the non-protonated polymer) has one hydrogen atom more than the oxidized form $-NH^{\bullet+}-$ or $-N^\bullet-$ (for the non-protonated polymer) where $-NH_2^+-$, $-NH-$, $-NH^{\bullet+}-$ and $-N^\bullet-$ represent hydrogen atoms in the heterocyclic rings. The adjacent two oxidized species combine to produce stable imines $-NH^+=$ or $-N=$ in the polymer chains (Fig. 2.22). From an electronic equilibrium at the metal/polymer interface and an ionic equilibrium at the polymer/solution interface, for reaction (2.44) the following relationship between the potential and the oxidation level was obtained in Ref. [15]:

$$E = E^0 - 2.3RTF^{-1}pH + RTF^{-1}\ln x(1-x)^{-1} \tag{2.45}$$

where x equals the proportion of oxidized sites to the total electroactive sites. Eq. (2.45) shows the formal potential shift with pH. Employing Eqs. (2.45) and (2.46) which defines the redox capacitance,

$$C_{LF} = dQ/dE = Q_m dx/dE \tag{2.46}$$

where Q is the charge required to oxidize the fully reduced polymer, Q_m is its maximum and x is the oxidation level evaluated as Q/Q_m, the low-frequency capacitance was written as:
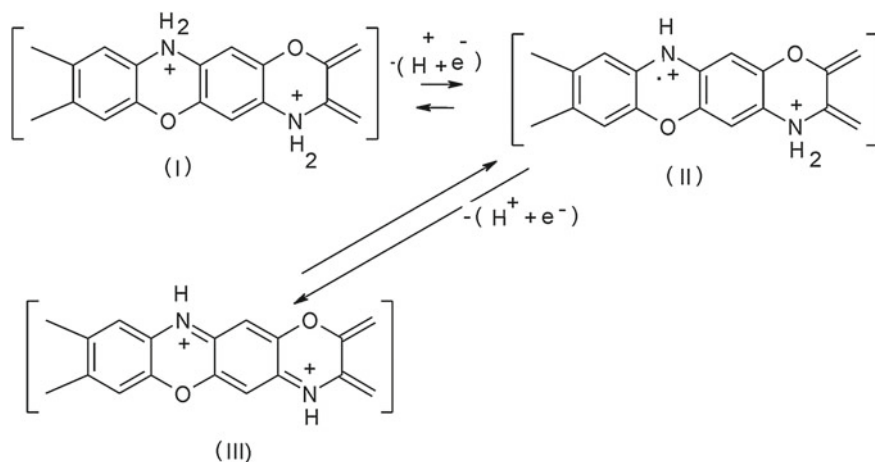

Fig. 2.22 Probable redox reaction of the protonated POAP proposed in [15]

$$C_{LF} = F(RT)^{-1} Q_m x(1-x) \tag{2.47}$$

Equations (2.45) and (2.47) predict that the capacitance is directly proportional to the film thickness through Q_m, and shows a maximum at a medium oxidation level and C_{LF} versus E curve shifts to the negative potential with increasing pH, as it experimentally observed. However, the calculated C_{LF} versus E curve has a smaller width of the capacitance peak as compared with the experimental data. The discrepancy was ascribed to activity effects involving an interaction between electroactive sites of the polymer. The theoretical curve was well fitted to experimental data by using a negative interaction parameter, which means a repulsive interaction between electroactive sites (see Eq. (2.23)). The charge-transport process in Ref. [15] was also expressed in terms of a coupled diffusion coefficient D (= $D_i t_e + D_e t_i$, where D_e and D_i are the electron and ion diffusion coefficients, and t_e and t_i are the transference numbers for electrons and ions, respectively). The D versus E dependence was calculated from experimental R_L and C_{LF} values (see Eq. (2.20)). It was observed that D decreases with pH (Fig. 2.23). In order to explain this dependence, it was considered that only protons are the ionic charge carriers in POAP. In this sense, the homogeneous electron transfer in the film should be accompanied with proton transfer from the reduced sites to the oxidised ones. This transport mechanism implies that electronic conductivities (κ_e) of the polymer probably decrease with its deprotonation. In this regard, authors of Ref. [15] measured κ_e of a POAP film at different oxidation levels with a symmetrical cell. It was effectively found that the electronic conductivity decreases with pH. As κ_e depends on D_e [16], authors of Ref. [15] attributed the κ_e decrease with increasing pH to the corresponding decrease of D_e. In this connection, in the electron hopping between adjacent redox sites in different oxidation states, D_e was expressed as a function of the intermolecular electron-transfer rate constant (k) and the mean distance (λ) between two adjacent redox sites [38]. Then, the D_e decrease with pH was attributed to a decrease of k with the polymer deprotonation.

EIS measurements were also performed in $LiClO_4$ and $HClO_4$ solutions at different pH values and constant ionic strength (1 M), to elucidate the role of protons in the conduction mechanism of POAP [11]. The simplified theory of polymer film impedances of Mathias and Haas [16] was applied in [11] to estimate an effective diffusion coefficient (D_{eff}) value of charge carriers inside POAP films. However, the estimation of D_{eff} was hardly possible, because of the absence of a well-defined Warburg region in the impedance spectra. Also, the low-frequency dependences of the imaginary component of POAP impedance spectra at different potentials exhibit curves that consist of two lines and an intermediate region in between. Only the first lines approximately satisfy the impedance theory, since their intercepts are near zero. The second intercepts are non-zero. Also, impedance measurements for POAP became very difficult for frequencies lower than 0.1 Hz due to the noise fluctuations observed in this frequency region. Thus, it was not possible in Ref. [11] to obtain real low-frequency capacity (C_{lf}) values of the POAP films and then, only estimations were obtained. Apparent capacities $C_{lf}^{(ap)}$

Fig. 2.23 The *pH*
dependence of the
D maximum obtained at a
given *pH* [15]
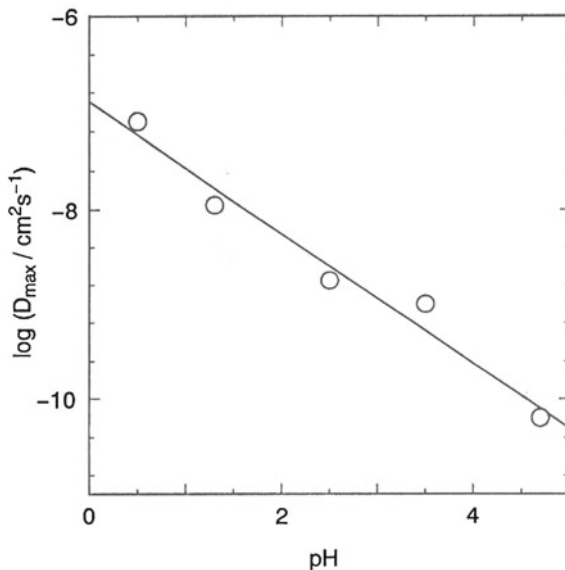
were calculated from $d(-ImZ)/d(f^{-1})$ slopes and they were compared with the C_{lf} values extracted from CV. The latter values are nearly three times higher than the former. Thus, impedance data presented in Ref. [11] demonstrate the capacity dispersion in the low-frequency region. Even when this phenomenon at the low-frequency region can be attributed to porosity effects of POAP films, the authors of Ref. [11] are rather disposed to explain the observed capacity dispersion as a consequence of the binding of hydrogen ions with polymer nitrogen-containing groups.

Interfacial resistance measurements [39] were also employed to study the redox mechanism of POAP and its dependence on the solution *pH* [40, 41]. The experimental arrangement in these investigations [39–41] was one in which a POAP film is supported on a thin gold film of thickness 30 nm. Interfacial resistance is not only sensitive to the presence of scattering centres but also to their distribution at the surface of a metal film. In this connection, it is demonstrated in Ref. [40] that the oxidation–reduction process of a POAP film, deposited on a thin gold film electrode, has a significant effect on the electronic transport of the base metal film. While Cyclic Voltammetry was used to quantitatively characterise the redox species transformation on the gold film surface contacting the polymer film, the resistance change $(\Delta R/R)$ was employed to investigate changes in the electronic properties at the gold|POAP interface during the redox conversion of the polymer [40]. Resistance changes with potential $(\Delta R/R - E)$ of a gold film free of and coated with a POAP film, both of them contacting a 0.1 M $HClO_4$ + 0.4 M $NaClO_4$ solution, were compared within the potential range –0.2 V < E < 0.5 V (*E* vs. SCE) where POAP exhibits its maximal electroactivity (Fig. 2.24). As

Fig. 2.24 $\Delta R/R$ versus
E response for POAP coated
gold film electrodes. POAP
thickness: ϕ_p(—) 0 nm,
(···)5 nm, (- - -) 10 nm, (·–·–·)
60 nm. Scan rate:
$v = 5 \times 10^{-3}$ V s^{-1},
$d = 30$ nm. Electrolyte:
0.1 M HClO$_4$ + 0.4 M
NaClO$_4$ [39]
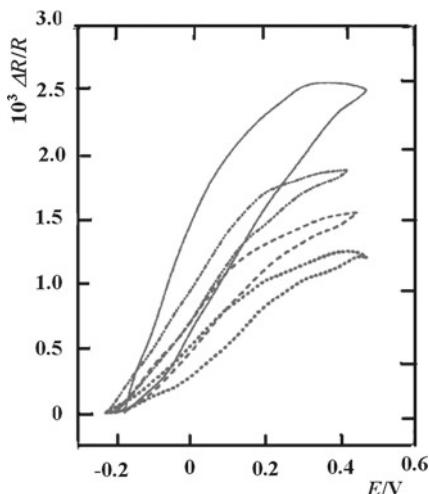
POAP becomes conductive at positive potentials (oxidized state) the $\Delta R/R$ versus E changes were referred to the potential value $E = -0.2$ V where POAP is its reduced state. The increase of the resistance of the naked gold film electrode (free of polymer) going from –0.2 V to 0.5 V was ascribed to ClO$_4^-$ adsorption (Fig. 2.24). Also, within the same potential region a resistance increase was observed for the gold film modified with POAP.

However, the observed $\Delta R/R$ change appears attenuated respect to the gold film free of POAP and this attenuation becomes more pronounced as thicker is the polymer film. However, for high polymer thickness (thickness, $\phi_p > 60$ nm) the $\Delta R/R$ change becomes independent of ϕ_p. Furthermore, for $\phi_p > 60$ nm the resistance behaviour of the base gold film is independent not only of the polymer thickness but also of the external electrolyte composition (Fig. 2.25). The $\Delta R/R$ increase going from the reduced to the oxidized state of POAP (curves in Fig. 2.25b) was ascribed in Ref. [39] to the proper redox conversion of the POAP film.

Author of Ref. [39] explains the observed increase of resistance considering that during polymer oxidation generation of charged electronic entities at the polymer chains near the gold surface occurs by electron transfer across the polymer-metal interface. In this regard, the author remarks that the redox switching of POAP was interpreted in a previous work [32] in terms of the oxidation of the amino groups to imine. Thus, it should be expected that imine sites act themselves as different scattering centres compared with amine sites, increasing in this way the diffuse reflection (increase of ΔR) of conduction electrons on the gold film surface during POAP oxidation. With regard to Fig. 2.25 (b), the author of Ref. [40] indicates that it is possible that by means of resistance measurements on a gold film surface blocked with an enough thick POAP film the attention is paid to only one process, that is, the redox transformation of the

Fig. 2.25 $\Delta R/R$ versus
E response for a gold film
electrode ($d = 30$ nm) coated
with **a** a 0.12 mC cm^{-2} and
b a 2.8 mC cm^{-2} thick POAP
film, in the presence of
different electrolytes: (*1*)
0.1 M HClO$_4$ + 0.4 M
NaClO$_4$, (*2*) 0.1 M
H$_2$SO$_4$ + 0.4 M Na$_2$SO$_4$ and
(*3*) 0.4 M sodium
benzenesulphonate + 0.1 M
benzenesulphonic acid. Scan
rate: $v = 10^{-2}$ V s^{-1} [39]
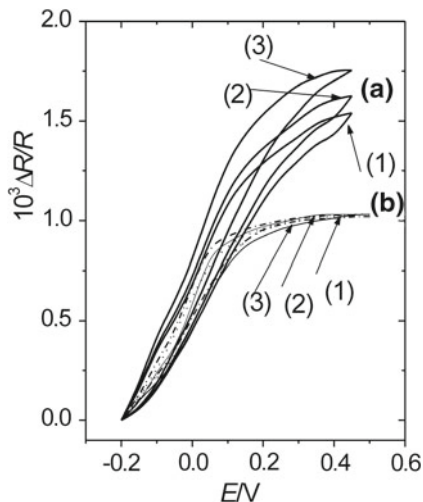
polymer film due to its interfacial exchange with the metal surface. However, the
same resistance measurements employed to study gold films coated with thinner
POAP films ($Q_{red} = 0.2$ mC cm^{-2}) (Fig. 2.25a), which could not be sufficiently
compact at the gold-POAP interface to prevent the interaction of species pro-
ceeding from the external electrolyte with the gold film surface, show some anion
adsorption effects on the gold surface. Then, author of Ref. [39] concludes that for
thin POAP films resistance changes could reflect interfacial effects (metal-polymer
interface) due to a competition between the adsorption of different species pro-
ceeding from the external electrolyte and the own redox transformation at the
metal-polymer interface. It is possible that at very low POAP thickness
(<0.15 mC cm^{-2}) either polymer islands (a continuous film is formed by fusion of
these islands) or polymer layers with imperfections exist on the gold surface.
However, the resistance response of a gold film electrode coated with a thick
POAP film becomes unique and independent of the type of external electrolyte
contacting the polymer. Under these conditions, a linear increase of ΔR as a
function of the degree of oxidation θ_{ox} of the POAP film was also observed in Ref.
[40]. This ΔR change of the gold film coated with POAP was expressed in Ref.
[40] as

$$\Delta R = -3/8G(\rho_b l_0/d^2)\Delta p \tag{2.48}$$

where ρ_b and l_0 represent the bulk resistivity of the massive gold and the mean free
path of the conduction electrons of gold, respectively, G is a geometrical constant
given by the ratio length/with for a rectangular film of thickness, d and Δp is the
change of the specularity parameter, p [40]. On the assumption that the decrease of
the specularity parameter $(-\Delta p)$ of the gold film surface going from the reduced to
the oxidized state of POAP is proportional to the degree of oxidation (θ_{ox}) of the
polymer film deposited on it, $\Delta p = -k\theta_{ox}$, Eq. (2.48) was written as:

Fig. 2.26 ΔR versus θ^{Ox} dependences for different gold film thicknesses coated with the same POAP film. Film thickness, d, indicated on the figure. Different symbols represent different electrolytes: (O) 0.1 M $HClO_4$ + 0.4 M $NaClO_4$, (Δ) 0.1 M H_2SO_4 + 0.4 M Na_2SO_4 and ($\square$) 0.4 M sodium benzenesulphonate + 0.1 M benzenesulphonic acid [39]
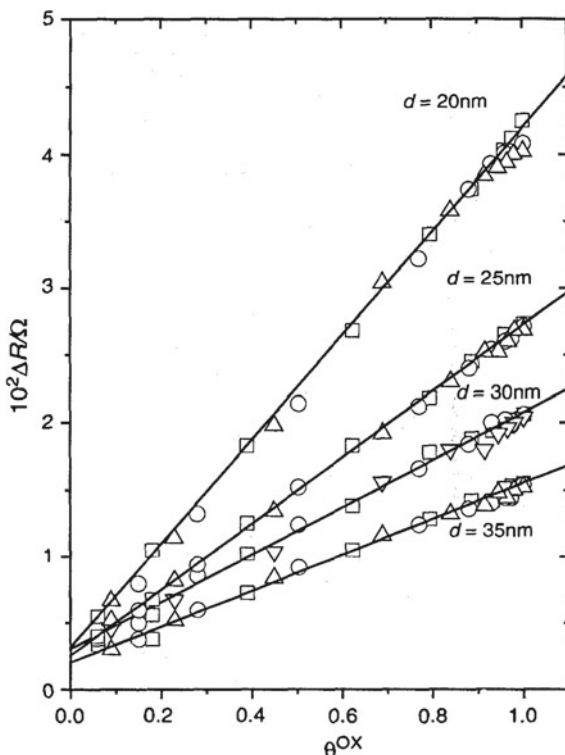
$$\Delta R = 3/8G(\rho_b l_0/d^2)k\theta_{ox} \tag{2.49}$$

Figure 2.26 shows $\Delta R - \theta_{ox}$ dependence for different film gold film thicknesses.

The observed linearity was explained in Ref. [40] in terms of an interfacial distribution of scatterers (imine sites) in the oxidized state with a spacing among them constant and larger than that corresponding to amine sites in the reduced state. In this connection, during POAP oxidation only one in every four or five amine sites are converted to the corresponding imine sites [32]. This gives rise to gaps which eventually would yield a distribution of oxidized sites less compact than the corresponding distribution of reduced ones. Another confirmation remarked by the author [39] about the different reflecting properties of the oxidized and reduced state of POAP is related to the different values of the site interaction parameters (r) obtained from the cathodic and anodic voltammetric responses of POAP in Ref. [1]. In this regard, the following values of anodic and cathodic site interaction parameters: $r_a = -0.55$ M^{-1} and $r_c = -0.18$ M^{-1}, respectively, are reported in Ref. [1]. Both are negative, thus involving a repulsive energy of interaction. As a higher repulsion is observed between oxidized sites than reduced ones at POAP films, then a more extended configuration of oxidized sites should

be expected as compared with the corresponding distribution of reduced sites. Then, according to author of Ref. [40], it would also be expected that the distribution of oxidized sites reflects electrons more diffusely than the distribution of reduced sites.

A study about the distribution of redox sites of POAP as the solution pH increases employing CV and resistance measurements was carried out in Ref. [41]. The increasing difficulty in reduce the polymer from its oxidised state with increasing the pH, is shown in Fig. 2.27 and it was attributed to the fact that amine species become less protonated as the pH increases. The resistance response of the gold film coated with POAP is also affected as the solution pH increases (Fig. 2.28). Author of Ref. [41] also studied the ΔR versus θ_{ox} dependence as the solution pH is changed. However, the $\Delta R/R$ change was referred in Ref. [41] to the potential value $E = 0.5$ V, where POAP is assumed to be oxidised (imine groups not protonated) and the different j–E curves for the different pHs coincide (see Fig. 2.27). Consequently, starting at $E = 0.5$ V towards the negative potentials direction, that is, going from the oxidised to the reduced state of POAP, an attenuation in the $\Delta R/R$ response was observed with the increasing of the pH (Fig. 2.28) [41].

The resistance change going from the oxidised to the reduced state of POAP (Fig. 2.28) was correlated in [41] to the degree of reduction ω^{-1} of the polymer at each pH value. In this case, θ_{Red} was defined by the ratio $\theta_{Red} = Q_{Red}/Q_{T,Red}$. $Q_{T,Red}$ is the maximal voltammetric reduction charge, achieved at each pH. This is obtained by integration of the voltammetric current from $E = 0.5$ V to the lowest

Fig. 2.27 j versus E responses for a gold film ($\phi_m = 30$ nm) coated with a 2.8 mC cm^{-2} thick POAP film contacting HClO$_4$ + NaClO$_4$ solutions of different pH's. Constant ionic strength, v pH values indicated on the figure [41]
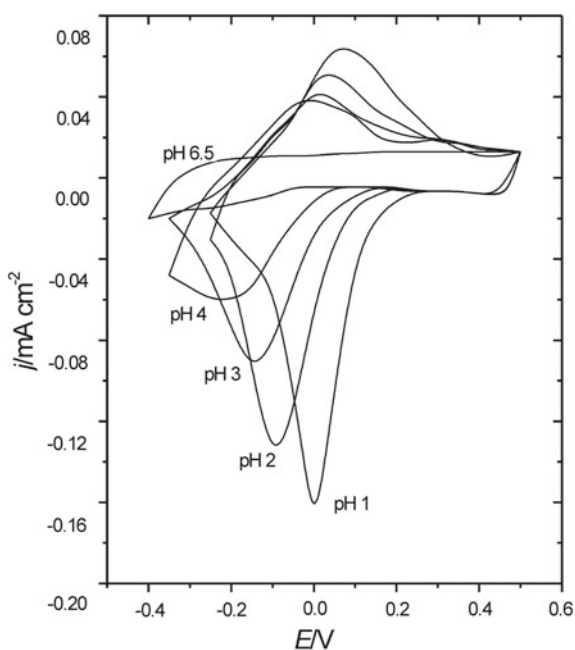
Fig. 2.28 $\Delta R/R$ versus E responses for the same POAP coated gold film and solutions indicated in Fig. 2.27 [41]
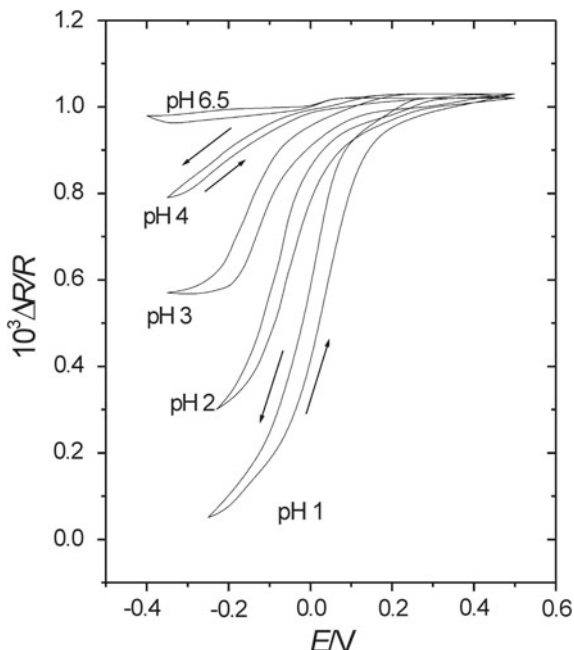
negative potential limit reached (see Fig. 2.27). Q_{Red} is the reduction charge at each E value, also assessed from $E = 0.5$ V toward the negative potential direction.

As can be seen from Fig. 2.27, $Q_{T,Red}$ decreases as the pH increases. It was assumed in Ref. [41] that at $pH = 1$ the polymer achieves its maximum degree of reduction ($\theta_{Red}^{max} = 1$ for $Q_{T,\ Red} = 2.8$ mC cm^{-2}), then, taking $Q_{T,\ Red} = 2.8$ mC cm^{-2} as the reference charge, lower θ_{Red}^{max} values are achieved with increasing the pH (Fig. 2.29). Thus, the $\theta_{Red} - E$ dependence (Fig. 2.29) was correlated with $\Delta R/R - E$ dependence (Fig. 2.28) going from the oxidised to the reduced state of POAP, at each pH value. This correlation leads to ΔR vs. θ_{red} dependences showed in Fig. 2.30. It is observed that the gold film resistance decreases nearly linearly during the POAP reduction. However, different slopes are observed depending on the solution pH.

Author of Ref. [41] considers as reference the $\Delta R/\theta_{Red}$ slope at pH 1, then, he remarks that as the higher is the solution pH the higher is the $\Delta R/\theta_{Red}$ slope. An explanation is given in Ref. [41] in relation to the change of the $\Delta R/\theta_{Red}$ slope with pH (Fig. 2.30). Author indicates that even when the reflection of conduction electrons on the gold film surface becomes more specular with increasing the degree of reduction of the polymer film at the different pH's, for a given θ_{Red} value (Fig. 2.30) the final reflection is more diffuse as pH increases. If only the amount of reduced sites decreases with increasing the pH, only one slope should be obtained. However, the effect of scattering centres on conduction electrons in

Fig. 2.29 θ_{red} versus
E dependence for the same
POAP coated gold film
electrode and solutions
indicated in Fig. 2.27.
Different symbols correspond
to different *pH* values [41]
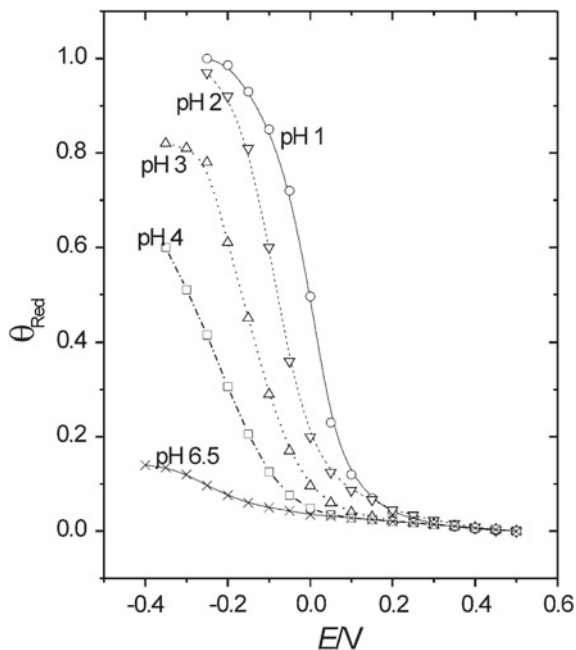
Fig. 2.30 ΔR *versus*. θ_{red}
dependences for the same
POAP coated gold film
electrode and solutions
indicated in Fig. 2.27. The
same symbols as in Fig. 2.29
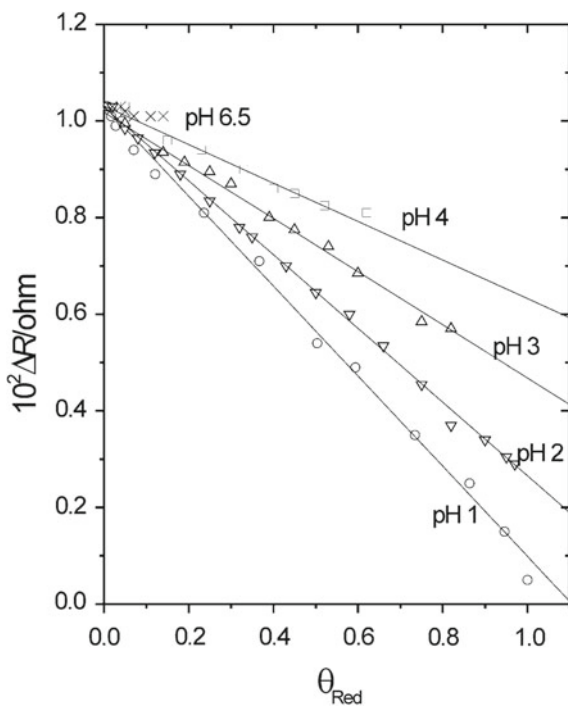
metal films is governed not only by the number of scatterers but also by its distribution over the metal surface [41]. In this sense, as mutual distances between scattering charges on a metal surface decreases towards the value corresponding to the wavelength of the conduction electrons of the metal ($\lambda_{Fermi} = 0.5$ nm in gold), the distribution of scatterers should reflect electrons more specularly [41]. Then, considering the increase of the slope in Fig. 2.30, it seems to be probable that as *pH* increases, the lower number of reduced sites at the polymer|metal interface forms surface distributions that scatter electrons more diffusely than that at *pH* 1. If the resulting surface structure of reduced sites at *pH* > 1 is thought as identical scatterers with a spacing that is equal to that at *pH* 1, again only one slope should be obtained. Then, the more immediate conclusion extracted by the author of Ref. [41] from resistance data at different *pH*'s is that the lower number of reduced sites formed as *pH* increases, also forms distributions with mutual distances between them that are larger as higher is the *pH* of the external solution. That is, reduced sites at the gold|POAP interface should form less compact distributions on the gold surface as *pH* increases, which reflect electrons not so specularly as the same amount of reduced sites at *pH* 1, does. According to author of Ref. [41], this effect could be attributed to a low degree of swelling of a polymer at high *pH* values. At high *pH* values the ability of the inner solution (incorporated into the polymer matrix) to reduce the electrostatic repulsion of the charged sites is limited. Under these conditions redox sites would adopt an extended configuration so as to minimise the coulombic repulsions.

2.2.3 Effects of the Type and Concentration of Ions of the External Solution on the Charge-Transport Process at POAP Films

Effects of the type and concentration of ions of the supporting electrolyte on the electrochemical response of POAP films were studied in several papers [1, 11, 18, 31, 42]. Some voltammetric experiments were performed in Ref. [1] by varying the ClO_4^- concentration between 0.1 and 1.7 M. While the anodic peak was not affected, the cathodic peak showed a positive variation. In this sense, a high concentration of perchlorate produces the same effect as a high proton concentration, making POAP more easily reducible. However, no noticeable changes were observed for anions such as SO_4^{2-}, PO_4^{3-} and Cl^- or cations such as Li^+, K^+ and Cs^+.

The participation of the supporting electrolyte anions in charge-transfer processes through POAP films was studied in $LiClO_4$ and $HClO_4$ solutions at different *pH* values and constant ionic strength (1 M) by employing CV and EQCM [11]. CV experiments with POAP-modified electrodes uncovered and covered with Nafion thin films were performed [11]. Nafion is known to hinder anionic permeability due to its own negative charge, so the films covered with this material

should significantly change their electrical properties, as compared to the uncovered ones, when supporting electrolyte anions participate in the redox activity of the films. No significant effect of Nafion on the redox response of POAP was observed. This finding allowed the authors [11] to conclude that no perchlorate anions are involved in the redox reactions of POAP. In order to confirm this conclusion, EQCM measurements on POAP films were carried out in Ref. [11]. The microbalance frequency change Δf_{cm} in the presence of the POAP films was measured simultaneously with their current responses under the electrode potential cycling. The $\Delta m/\Delta Q(E)$ ratio, where $\Delta m = \Delta f_{cm}/k$ (k is the constant of the Sauerbrey law) and $\Delta Q(E)$ is the charge consumed during the oxidation/reduction process, gave a mass number of about 3–5 in the main range of the cycling potential of 0.0–0.3 V (vs. Ag/AgCl). This mass number was considered very low, as compared with the molecular weight of ClO_4^- anion. Then, it was concluded that an insignificant insertion of the anions into the POAP films occurs during the redox reaction of the polymer.

The ionic exchange of POAP in the presence of perchlorate anions was studied by using Probe Bean Deflection (PBD) [31]. During the reduction scan only a positive deflection of the PBD signal was observed, which was indicative of a simultaneous expulsion of perchlorate and insertion of protons, the latter process being dominant. To check this conclusion, a PBD profile was simulated by convolution of the current response using parameters reported in the literature [43] and considering that only protons are exchanged between the solution and POAP. The simulated profile fits reasonably well the negative scan but differs significantly in the positive direction, suggesting that not only protons but also perchlorate anions are exchanged during the positive scan.

The effect of the ionic strength (μ) of the solution on the transport properties of POAP was studied employing EIE [18]. To this end 0.1 M $HClO_4$ + x M $NaClO_4$ solutions were employed, where the concentration of perchlorate anions, x, was varied in order to change the ionic strength.

Experimental complex impedance plots of POAP at constant potential and different ionic strengths were recorded (Figs. 2.31 and 2.32). It was observed that when POAP is in its oxidised state, impedance diagrams depend strongly on the electrolyte concentration (Fig. 2.31). However, when POAP is in its reduced state ($E = -0.1$ V vs. SCE), the impedance response does not exhibit a significant dependence on the bathing electrolyte concentration (Fig. 2.32).

Dependences of the characteristic impedance quantities, at low frequency, on μ were interpreted on the basis of two models: a transmission line model [19, 20] and a modified electron-hopping model [21]. From the former model it was possible to separately extract an electron (D_e) and an anion (D_x) diffusion coefficient. From the latter [21] only an effective diffusion coefficient, D_{eff}, was obtained. It was observed that the low-frequency capacitance C_{LF} does not depend much on the ionic strength (Fig. 2.13a). However, the low-frequency resistance, R_{LF}, depends markedly on μ at constant E value, for potential values higher than 0.0 V (SEC) (Fig. 2.13b). R_{LF} versus E curves pass through a minimum value, which depends on the electrolyte concentration. The fitting of experimental low-frequency

Fig. 2.31 Complex
impedance plots for a 30 nm
thick POAP film at
$E = 0.1$ V (SCE) in 0.1 M
$HClO_4$ + x M $NaClO_4$
solutions: (a) $x = 1.9$ M,
ionic strength, $\mu = 2$ M; (b)
$x = 0.4$ M, ionic strength,
$\mu = 0.5$ M; (c) $x = 0$ M,
ionic strength, $\mu = 0.1$ M.
The inset is a comparison of
the experimental (o) and
calculated (—) points
employing the model of the
electron hopping reported in
[18]
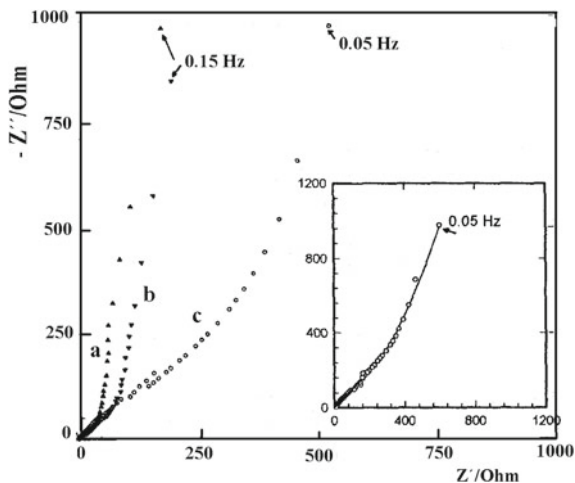
Fig. 2.32 Complex
impedance plots for a 30 nm
thick POAP film at $E =$
-0.1 V (SCE) in 0.1 M
$HClO_4$ + x M $NaClO_4$
solutions: (□) $x = 0.4$ M,
ionic strength, $\mu = 0.5$ M;
(Δ) $x = 0.9$ M, ionic
strength, $\mu = 2$ M. The inset
is a magnification of the low-
frequency region [18]
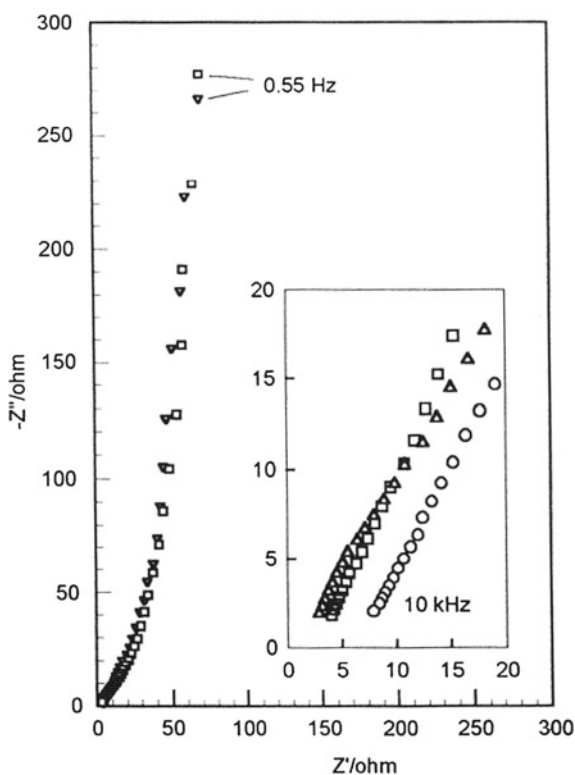
resistance expressed as $R_\Sigma (= 3R_{LF})$ as a function of the degree of oxidation (θ_{ox}) by employing the transmission line model (Fig. 2.14), allowed the authors [18] to obtain D_e and D_x versus θ_{ox} dependences for different μ values. Also, application of the electron-hopping model described in Ref. [21] allowed the authors to obtain the (κ_e) dependence for different μ values (Fig. 2.15). Diffusion coefficient values for different ionic strengths obtained in Ref. [18] are shown in Table 2.5. Several explanations have been given to account for the dependence of the transport process at POAP films on external electrolyte concentration [18]. It has been suggested that an excess of supporting electrolyte can be incorporated into the polymer phase during the redox process. If the incorporated ions act as counterions, an increase in their concentrations within the film would cause a decrease in the resistance of charge transport through it or an equivalent increase in the diffusion coefficient. Another explanation invokes reduction of the electrostatic repulsion between redox centres as the electrolyte concentration increases, which allows a sufficiently facile ion transport. Another study about the effects of the electrolyte concentration and degree of oxidation on the conduction properties of POAP films by employing EIS is reported in Ref. [42].

The participation of different anions in the charge-transport process of POAP films was studied by employing fractal dimensions [44]. Fractal dimensions of POAP films doped with different anions were determined using CV and EIS experiments. The formalism developed by Stromme et al. [45] was employed in Ref. [44] to obtain the fractal dimensions. According to this formalism, α (called fractal parameter) is related to the fractal dimension, D_f, through Eq. (2.50):

$$\alpha = (D_f - 1)/2 \qquad (2.50)$$

POAP films were deposited on glassy carbon in acidic media and in the presence of different anions. The film thickness was measured by assessing the voltammetric charge. Film thicknesses around 0.1 μm were employed in Ref. [44]. Voltammetric responses of POAP in the presence of different anions used in Ref. [44] are shown in Fig. 2.33. Correlations between the size of the anions, the length scales and the yardstick for scaling of the fractal surfaces with the fractal dimensions of the surfaces, were found in Ref. [44]. The fractal dimensions of the films in the presence different anions, ClO_4^-, SO_4^{2-}, NO_3^- and Cl^-, were 2.46, 2.46, 2.46 and 2.32, respectively. The fractal dimension in the presence of chloride

Table 2.5 Electronic D_e and ionic D_x, diffusion coefficients calculated from the transmission line model [19, 20] for a 30 nm thick POAP film at different ionic strengths. D_{eff} extracted from the model given in Ref. [21]. $pH = 1$, $c = 4.5$ M, $A = 0.081$ cm^2, $E = 0.1$ V, $p/(1+p) = 0.96$ [18] (see Eq. (2.28))

μ (Ionic strenght)/M	$10^{10} D_{eff}$/cm^2 s^{-1}	$10^{10} D_e$/cm^2 s^{-1}	$10^8 D_x$/cm^2 s^{-1}
0.1	1.32	1.03[a] 1.2[b]	1.27
0.5	1.92	1.67[a] 2.20[b]	1.83
2	2.93	3.14[a] 3.18[b]	2.42

[a] Values extracted from the R_Σ versus θ_{ox} dependence
[b] Values extracted from the C_Σ^{-1} versus Ψ dependence

Fig. 2.33 Cyclic voltammograms of POAP films in the presence of different anions. *The inset* presents the voltammetric responses recorded at the indicated sweep rates for a POAP film in the presence of NO_3^- anions [44]
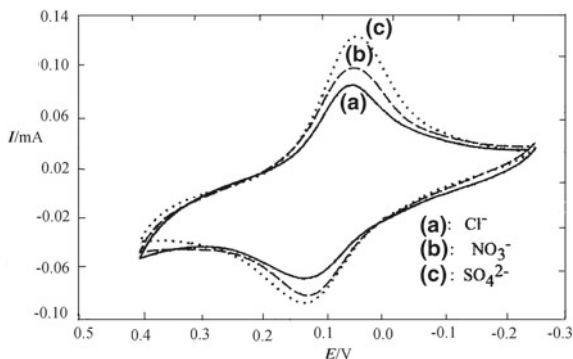
differs from the others. In order to shed light on the physical significance of the fractal dimension values, diffusion layer widths were employed as a yardstick to estimate the length scales traversed by anions on the surface at the condition of the maximum currents.

As according to the Fick's first law, the diffusion-limited current is proportional to the magnitude of the concentration gradient of the electroactive species, then, the width of the diffusion layer, ΔX, was expressed as:

$$\Delta X = z\,FAD\,C_b/i_{peak} \tag{2.51}$$

where C_b is the difference between bulk concentration of the anions inside the polymeric film and that of its surface at time τ (where the voltammetric peak current is reached). The diffusion coefficient value, D, was estimated using the Randles–Sevcik equation [2]. The width of the diffusion layer and the diffusion coefficient of selected anions are shown in Table 2.6. It was concluded from the results summarized in Table 2.6 that the distance sensed in the presence of different anion varies on the 11.7–2.98 Å range, and the possible cutoff of the fractal region investigated by employing the peak current method occurs at the length scales larger than 11.7 Å.

The fractal dimension of POAP was also obtained in [44] from EIE measurements. The impedance response of POAP films doped with different anions was obtained. An equivalent circuit compatible with the experimental impedance response was employed in [44]. The following Z versus ω dependence was used:

$$Z(\omega)\ = R + B(j\omega)^{-n} \tag{2.52}$$

The expression (2.52) corresponds to the electrical characteristics of a so called constant phase element (CPE) with $n < 1$ and B is a constant related to the capacitive nature of the interface. From the impedance response and equivalent circuits, the fractal dimensions were derived by using the Eq. (2.53):

$$D_f =\ (n+1)/n \tag{2.53}$$

Table 2.6 Diffusion coefficients and diffusion layer thickness for different anions [44]

Anion	$10^{13} D_a/cm^2 s^{-1}$	$10^{13} D_b/cm^2 s^{-1}$	[a]Diffusion layer thickness	[b]Diffusion layer thickness
SO_4^{2-}	2.4	8.1	3.18	2.98
ClO_4^-	6.5	7.4	10.70	3.02
NO_3^-	6.8	8.0	11.32	3.05
Cl^-	5.8	6.6	11.72	3.90

[a] Slow scan
[b] Fast scan

The D_f values obtained were 2.45, 2.43, 2.41 and 2.33, for ClO_4^-, SO_4^{2-}, NO_3^- and Cl^-, respectively. To determine the length scales used in the fractal scaling, Eq.(2.54), relating the electrode capacitance C_0, film resistance R and the frequency f of measurement, to the length scale λ, was employed:

$$\lambda = 1/(2\pi f C_0 R) \tag{2.54}$$

The capacitance C_0 at the frequency of f was obtained from C versus log f plots. Results are shown in Table 2.7. As can be seen from Table 2.7, the length scale in the 1.43–7.3 Å range was found. There is a partial overlap of the results obtained by employing both CV and EIE measurements. The smaller fractal dimension in the presence of chloride was attributed to its smaller size and has the consequence of providing larger yardstick for scaling of the surface.

The doping process of electrodeposited POAP films with different anions under the regime of CV was analyzed by the application of "Chaotic Logistic Map" [46]. Quadratic logistic map presentations of the current density versus charge for POAP films doped with different anions and under both, negative and positive potential scans were analyzed in Ref. [46]. The electrochemical data were fitted to a quadratic logistic map of the type [47, 48]:

$$x_{n+1} = r x_n (1 - x_n) \quad 0 < r < 4 \tag{2.55}$$

Eq. (2.55) describes the effect of feedback on the magnitude of some property x, as well as the effect of the parameter r that determine the occurrence of oscilatory and chaotic nature of the result. The magnitude x_n behaves chaotically for $3.45 < r < 4$, while for $3 < r < 3.45$, x_n gradually approaches a periodic motion of period 2. Only partial fittings were observed [46], then, authors conclude that the system is more complicated than a simple non-linear system with a feedback to

Table 2.7 Length scales and cutoff frequency region for the different anions [44]

Anion	Length scale/A	Frequency cutoff region
SO_4^{2-}	1.4–5.3	50 kHz–100 Hz
ClO_4^-	1.6–5.8	10 kHz–30 Hz
NO_3^-	1.8–6.1	100 kHz–1 Hz
Cl^-	2.3–7.3	1 kHz–100 Hz

Fig. 2.34 *I* (Current density) versus *Q* (Voltammetric charge). The goodness of fit to the logistic map during positive potential cycles of POAP in the presence of different anions: (□) Cl^-, (o) NO_3^-, (Δ) SO_4^{2-}, (—) theoretical plot [46]
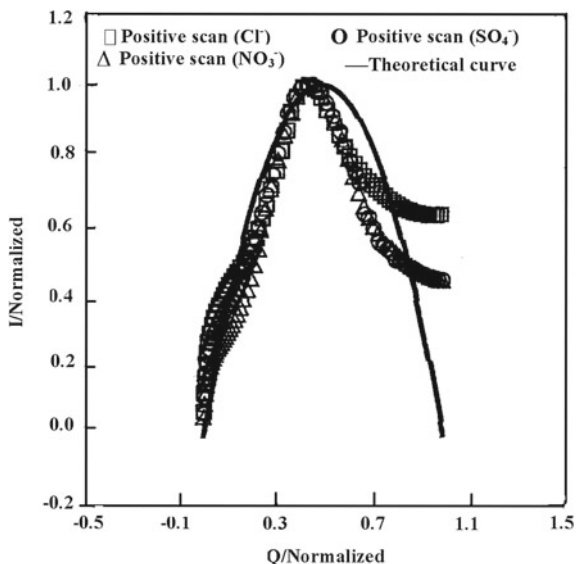
withstand a perfect fit to the quadratic logistic equation in the entire domain of *x*. Thus, other contributions, such as charge/discharge of the double layer capacitance (in general, any intervening phenomena other than the flux generated by diffusion), were considered as factors that complicate the behaviour of the doping process and cause deviation from a perfect fit.

A better fit was observed for the positive potential sweep, where participation of anions is the main phenomenon. However, it was observed that the increase of the positive potential sweep rate is accompanied by a decrease in anion-insertion in the polymer matrix (anion-insertion/movement cannot respond quickly enough to the increasing field). Thus, the doping process is no longer a dissipative one and a feedback-controlled phenomenon appears which is observed in the form of a more poor fit to the logistic map (Fig. 2.34). Furthermore, it was observed that the chloride/POAP system exhibits the least satisfactory fit. This fact was attributed to topological structural differences between a film doped with Cl^- and other one doped with other anions, as revealed by the differences of their fractal dimensions [44]. It is indicated that the Cl^- doped film possesses a self affine structure with less available regions in the film capable of participate in the transport process. Then, the dissipative processes occur less favourably in Cl^--doped films which cause the breakdown of the applicability of the logistic equation and a poorer fit, especially in the region of higher charges.

2.2.4 *Effect of the Film Thickness on the Charge Conduction Process of POAP*

While in some papers it is reported that only thin POAP films could be electrochemically synthesised [11, 13, 18, 21], in other ones thick films were manufactured [15]. POAP films synthesized in Ref. [11], for instance, did not exceed 50 nm due to the self-limiting effect caused by the low polymer film conductivity. Film thicknesses in the range 0.05–0.5 μm were examined in Ref. [15]. Also, while in some studies voltammetric charge values were employed for POAP film thickness estimation [11, 49], in other ones the ellipsometric thickness was considered [18].
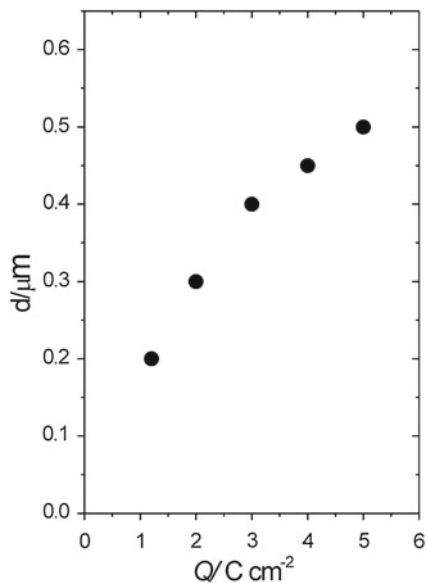
Surface resistance was applied [49, 50] to study the interaction of different anions, such as perchlorate, sulphate and benzene sulphonate, and also a cation such as Cu(II), with a gold film surface when it is blocked with a POAP film. The dependence of the resistance change on the external electrolyte composition for POAP thickness lower than 0.25 mC cm^{-2} was attributed to a competition at the gold film surface, between the proper redox process of the polymer and the adsorption of the different species contained in the electrolyte solution on the gold surface. This result points to a discontinuous character of POAP for thicknesses lower than 0.25 mC cm^{-2}. For POAP thicknesses higher than 0.8 mC cm^{-2} the resistance response becomes independent of both the film thickness and electrolyte composition. This result is indicative of the presence of a compact polymer layer at film thicknesses higher than 0.8 mC cm^{-2}.

POAP films synthesized on ITO (In–Sn oxide conducting glass) electrodes seem to be continuous and have a fairly smooth surface and the thickness is almost uniform over the whole film [22]. Scanning electron micrographs of the POAP film surface revealed non-specific amorphous surface features. Morphology of POAP seems to be granular rather fibrous. The size of the nodules resulted about 0.1 μm. Plots of film thickness (d) and surface concentration of electroactive sites (Γ) versus the amount of charge (Q) passed to prepare the POAP films are shown in Figs. 2.35 and 2.36, respectively [22].

The film thickness, d, increases with increasing Q in the same way as the relation between Γ and Q does. The volume concentration of electroactive sites in the POAP films, with different thicknesses, was estimated as (Γ/d) from Γ and d given at a constant Q value [22]. The obtained volume concentration of electroactive sites value was $(5.0 \pm 0.5) \times 10^{-3}$ mol cm^{-3} irrespective of d. This result was indicative of a uniform distribution of electroactive sites in the films of different d values. Results reported in Ref. [22] indicate that POAP film thickness can be arbitrarily controlled by the charge passed during the film synthesis.

The effect of the film thickness on the POAP charge-transport process was treated in several papers [13, 15, 18]. EIS was employed in Ref. [13] to obtain transport parameters of thin POAP film electrodes. Impedance measurements were performed in the frequency range 0.01–10 kHz and at two different film

thicknesses ($d = 30$ and 300 nm). Nyquist diagrams at high frequency exhibit a depressed semicircle (Fig. 2.37) [13].

It was observed that the change of the film thickness does not affect the size of the semicircle. This fact was considered as indicative of the existence of an

Fig. 2.37 Nyquist diagrams for POAP at different thickness: (O) 30 nm, (●) $d = 300$ nm. $E = 0.375$ V [13]
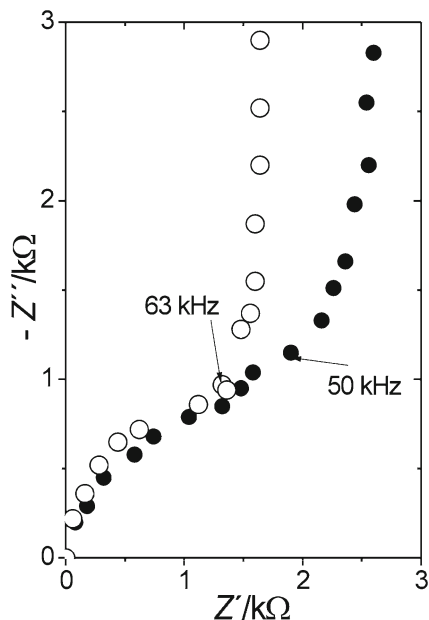
interfacial charge-transfer process at the metal|polymer interface (see Eq. (2.14) and Fig. 2.5). However, the pseudo-capacitive rise of Z'' at low frequencies occurs at larger Z' values for thicker films (Fig. 2.37). This effect means that the film resistance at low frequencies depends on the film thickness, d (see Eq. (2.15) and Fig. 2.7). The redox capacity was obtained from $-Z''$ *versus* ω^{-1} plots at sufficiently low frequencies. Despite the redox capacity increases with d, the dependence was not linear (Fig. 2.6). The low-frequency capacity for thick POAP films (0.05–0.5 μm), at a given potential and pH, was also found to be proportional to the film thickness [15].

Dependences of different characteristic impedance quantities on film thickness were also studied in Ref. [18]. Results were interpreted on the basis of two models, a modified electron-hopping model [21] and a transmission line one [19, 20]. While the former only allowed the authors [18] to obtain an effective diffusion coefficient, D_{eff}, the latter allowed the authors to obtain electron (D_e) and ion (D_x) diffusion coefficient values for different film thickness.

Table 2.8 shows the dependences of the respective diffusion coefficients on film thickness for POAP. The low conductivity of thin POAP films was explained in Ref. [18] in terms of a structure that changes as the film thickness increases. In this connection, during the synthesis of a polymer film, two or more stages of the polymerisation process have been distinguished: first, islands of the polymer are formed at the substrate surface, then a continuous film, compact (non-porous), is formed by fusion of these islands, and then, further growth takes place above this compact layer giving rise to the external, porous part of the film. In this regard, a

Table 2.8 Electronic D_e and ionic D_x, diffusion coefficients calculated from the transmission line model [19, 20] for different film thickness (ϕ). D_{eff} extracted from the model given in [21]. $\mu = 2$ M ($pH = 1$), $c = 4.5$ M, $A = 0.081$ cm^2, $E = 0.1$ V, $p/(1+p) = 0.96$ [18]

ϕ (thickness)/nm	10^{10} D_{eff}/cm^2 s^{-1}	10^{10} D_e/cm^2 s^{-1}	10^8 D_x/cm^2 s^{-1}
10	0.163	0.17	0.22
30	2.93	3.14	2.42
60	24.3	27.7	23.2

high permeability of thick films, as compared with thin ones, should allow the incorporation of electrolyte solution into the polymer matrix. Electrolyte incorporated into the film should affect the polymer conduction, increasing the rate of the charge-transport process.

2.3 The Charge Transport Process at Poly(o-aminophenol) (POAP) Film Electrodes in the Presence of Redox Active Solutions

The conduction properties of electroactive polymer films are often tested by analysing the electrochemical behaviour of the films contacting different redox active solutions. To this end, techniques such as CV, Rotating Disc Electrode Voltammetry and EIS have been employed. Redox mediation and redox solute permeabilities at film-coated rotated-disc electrodes are determined from the variations of limiting currents with the electrode rotation rate, film thickness and redox couple concentration. Complete mechanism diagnosis criteria from steady-state polarisation curves for redox mediation at electroactive polymers coated electrodes are discussed in Ref. [51]. Authors of Ref. [51], also present a review [52] about the theoretical basis for the electrochemical rectification in mediated redox reactions at redox polymer-modified electrodes.

Steady-state current–potential curves for the oxidation of Fe(CN)$_6^{4-}$ at bare and POAP film-coated rotating BPG (Basal-plane Pyrolytic Graphite) disk electrodes were compared in Ref. [12]. The comparison of the formal redox potential ($E^{0\prime}$) values of POAP (0.044 V vs. SSCE) with that of FE(CN)$_6^{4-/-3}$ couple (0.350 V vs. SSCE) in a 0.2 M NaClO$_4$ aqueous solution (pH 1) indicates that the oxidation of Fe(CN)$_6^{4-}$ is not thermodynamically mediated by POAP films. Then, the observed anodic currents in the presence of POAP were assigned to the oxidation of Fe(CN)$_6^{4-}$ ions that penetrate the POAP film to reach the electrode surface [12]. The quantitative analysis of the experiments reported in Ref. [12], were made employing the Koutecky–Levich equation [2]:

$$i_{lim}^{-1} = i_{Lev}^{-1} + i_s^{-1} \tag{2.56}$$

with

$$i_{\text{Lev}} = 0.62nFAD_{\text{sol}}^{2/3}v^{-1/6}C^b\Omega^{0.5} \tag{2.57}$$

$$i_s = nFAC^bD_s\kappa\phi^{-1} \tag{2.58}$$

where i_{lim} is the limiting current, i_{Lev} is the Levich current, i_s is the "permeation current" of $Fe(CN)_6^{4-}$ through the POAP film, D_{sol} is the diffusion coefficient of $Fe(CN)_6^{4-}$ in the bulk solution, D_s is the diffusion coefficient of $Fe(CN)_6^{4-}$ into the POAP films, v is the kinematic viscosity of the solution, C^b is the bulk concentration of $Fe(CN)_6^{4-}$, κ is the partition coefficient of $Fe(CN)_6^{4-}$ between the film and the bulk of the solution and Ω is the rotation rate of the disk electrode. Experimental Koutecky–Levich plots i_{lim}^{-1} versus $\Omega^{-1/2}$ resulted linear, as expected from Eq. (2.56), and the slopes matched that at the bare electrode. Thus, D_{sol} and D_s were estimated: $D_{\text{sol}} = (6.7 \pm 0.4) \times 10^{-6}$ $\text{cm}^2 \text{ s}^{-1}$ and $D_s\kappa = (1.2 \pm 0.3) \times 10^{-9}$ $\text{cm}^2 \text{ s}^{-1}$. It is remarked in [12] that for POAP, $D_s\kappa > D_{\text{app}}$ (see Table 2.2), that is, the overall charge-transport within the film is slower than the physical diffusion rate of a dissolved ion ($Fe(CN)_6^{4-}$) through the film.

Another study employing CV and RDEV about the electrochemistry of POAP-modified electrodes in the presence of different redox couples ($Fe(CN)_6^{4-/3-}$, hydroquinone/benzoquinone (HQ/Q), Sn^{2+}) was carried out in Ref. [53]. Different POAP film thicknesses between 10 and 70 nm were employed in Ref. [53] to study the diffusion process of electroactive species across POAP films. The diffusion process of the electroactive species through POAP was interpreted on the basis of the membrane-diffusion theory [54]. The electron hopping model was also employed in order to obtain the diffusion constant for the electron transport [4]. The effects of the electrode rotation rate (Ω) film thickness (ϕ), charge and concentration (c) of the electroactive species and acid concentration (x) of the solution, on the steady-state current–potential curves (I–E), were quantitatively analyzed in Ref. [53].

Steady-state current–potential (I–E) curves, at different Ω values, for a 60 nm thick POAP film contacting a x M $HClO_4$ + $(2 - x)$ M $NaClO_4$ + c (HQ/Q) solution where $x = 0.1$ and $c = 3 \times 10^{-3}$ M are shown in Fig. 2.38 [53]. Diffusion limited currents are observed at $E > 0.8$ V (vs. SCE) for HQ oxidation and at $E < 0.0$ V (vs. SCE) for the Q reduction. Besides, these main anodic and cathodic plateaux, the presence of a pre-plateau (0.2 V $< E < 0.4$ V) during Q reduction was also observed. At Ω and c fixed, I–E curves are film thickness (Fig. 2.39) and acid concentration (Fig. 2.40) dependent [53]. As HQ oxidation is not thermodynamically mediated on POAP, then, the observed anodic currents (Fig. 2.38) were assigned to the oxidation of HQ species that penetrate through the POAP films to reach the gold surface.

Benzoquinone (Q) is reduced in two waves (Fig. 2.38). The first one was attributed to the penetration of reactants into the film coupled with their subsequent discharge at the metal/polymer interface. The limiting current for the second wave ($E < 0.0$ V) is independent of ϕ and follows the Levich equation. This second wave was adjudicated to the rapid electron-transfer mediation at the POAP/redox active solution interface. Similar experiments were carried out in Ref.

Fig. 2.38 *I–E* curves for
different Ω values: $\Omega = 500$
(o), 1500 (□) and 3650 (△)
rpm. $\phi = 60$ nm. Electrolyte:
0.1 M HClO$_4$ + 1.9 M
NaClO$_4$ + 3 × 10^{-3} M
(HQ/Q) [53]
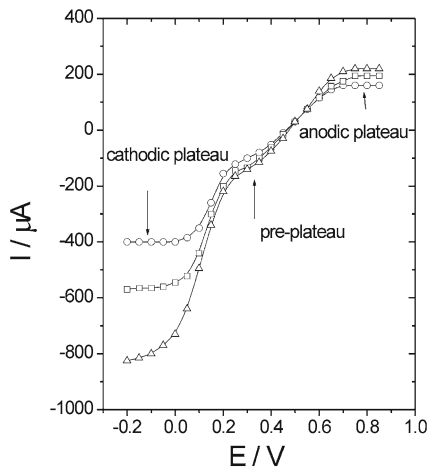
Fig. 2.39 *I–E* curves for
different ϕ values: $\phi = 0$ (o),
13.7 (□) and 60 (△) nm.
$\Omega = 1800$ rpm. Electrolyte:
0.1 M HClO$_4$ + 1.9 M
NaClO$_4$ + 3 × 10^{-3} M (HQ/
Q) [53]
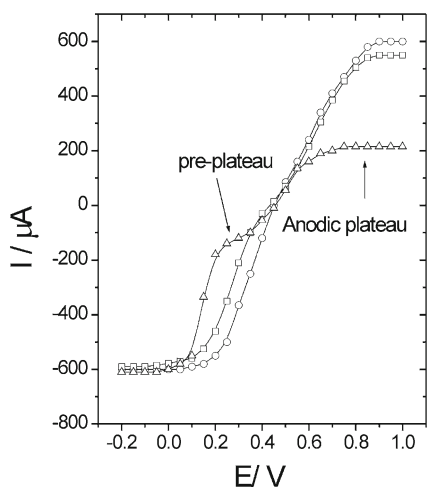
[53] with POAP films contacting anionic Fe(CN)$_6^{4-/3-}$ and cationic Sn^{2+} redox active species. The permeation characteristics of POAP films at potential values $E > 0.8$ V (vs. SCE) were evaluated employing Eq. (2.59):

$$I_{\lim}^{-1} = \phi(nFA\kappa D_s c)^{-1} + (0.62nFA\,D^{2/3}\nu^{-1/6}\Omega^{1/2}c)^{-1} \tag{2.59}$$

In order to use Eq. (2.59) it was assumed that electroactive species dissolves into the polymer film with a partition equilibrium $\kappa = c_{\mathrm{pol}}/c$ at the film/solution interface where c_{pol} and c are the respective concentrations of the species in the polymer and solution. D_s and D are the diffusion coefficients of the electroactive species in the polymer and solution, respectively. $I_{\lim}$ is the limiting current for the oxidation of electroactive species and the other terms have their usual meanings.

Fig. 2.40 *I–E* curves obtained in different *x* M $HClO_4 + (2 − x)$ M $NaClO_4 + 3 \times 10^{-3}$ M (HQ/Q) solutions. $x = 0.1$ (o), 0.01(□) and 0.001 (Δ). Electrode rotation rate: $\Omega = 800$ rpm. $\phi = 60$ nm. *Inset* cyclic voltammograms [53]
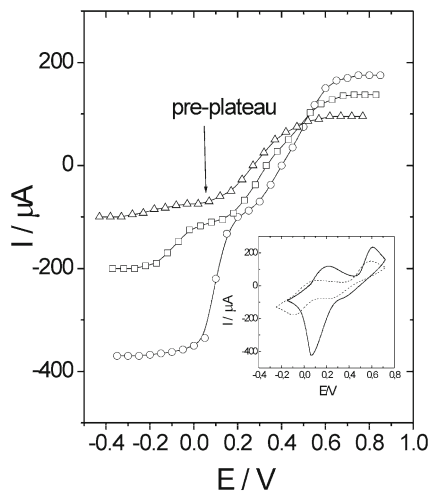
At constant c, x and ionic strength of the solutions, experimental I_{lim}^{-1} versus $\Omega^{-1/2}$ representations for different film thickness, give linear diagrams with nearly the same slope but different intercepts on the ordinate axis (Fig. 2.41) [53]. Thus, for the different oxidation processes studied in Ref. [53] and the Q reduction (first wave), κD_s values were extracted from the first term of Eq. (2.59). With regard to the film thickness, κD_s decreases as ϕ increases for the oxidation process of HQ.

The same behaviour was observed for the Q reduction (first wave) and oxidation of Sn^{2+} and $Fe(CN)_6^{4-}$ species at POAP films [53]. However, it was observed in Ref. [53] that in all cases, for film thickness higher than 60 nm, κD_s becomes independent of ϕ. Thus, extrapolated κD_s values for high film thickness

Fig. 2.41 Koutecky–Levich plots for different ϕ values: $\phi = 8$ (□), 41 (+), 60 (×) and 69 (Δ) nm. Electrolyte: a 0.1 M $HClO_4$ +1.9 M $NaClO_4 + 3 \times 10^{-3}$ M (HQ/Q) solution [53]
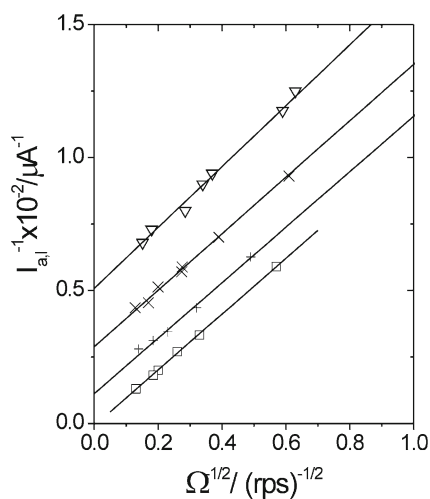
Fig. 2.42 Levich
representations for the
cathodic plateau $E < 0.0$ V.
$\phi = 41$ nm(+) and 60 nm
(X). Electrolyte: a
0.1 M HClO$_4$ +
1.9 M NaClO$_4$ + 3 ×
10^{-3} M (HQ/Q) solution.
Inset $I_{\text{lim,c}}$ versus $\Omega^{1/2}$ for a 60
thick POAP film [53]
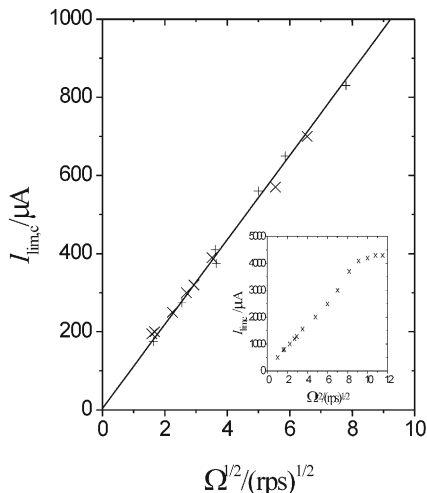
were considered as true permeation rates for the different species studied [53]. The
resultant extrapolated values were: $\kappa D_s(\text{HQ}) = (0.92 \pm 0.2) \times 10^{-8} \, \text{cm}^2 \, \text{s}^{-1}$,
$\kappa D_s(\text{Fe(CN)}_6^{4-}) = (0.62 \pm 0.2) \times 10^{-9} \, \text{cm}^2 \, \text{s}^{-1}$ and $\kappa D_s(\text{Sn}^{2+}) = (1.42 \pm 0.2) \times 10^{-10} \, \text{cm}^2 \, \text{s}^{-1}$ for the oxidation processes and $\kappa D_s(\text{Q}) = (0.42 \pm 0.2) \times 10^{-8} \, \text{cm}^2 \, \text{s}^{-1}$ for the Q reduction.

A comparison of redox solutes permeabilities at POAP films with transport rate
of electroinactive anions, such as perchlorate, was also made in Ref. [53]. It was
observed that the electroinactive ions transport process within the POAP film is
faster than the physical diffusion process of a dissolved electroactive species
through the film. In the presence of HQ/Q species, the limiting current at
$E < 0.0$ V depends linearly on $\Omega^{1/2}$ (Fig. 2.42). This wave was associated with the
electron-transfer mediation at the POAP/solution interface where Q diffusion in
solution limits the current [53]. However, it was observed in Ref. [53] that for
thick POAP films contacting solutions of high concentration of HQ/Q
($c > 0.01$ mol dm^{-3}), the limiting current at $E < 0.0$ V was independent of the
electrode rotation rate for $\Omega > 7000$ rpm (see inset in Fig. 2.42).

Such a constant value of the current was attributed to a slow electron transport
across the POAP film to mediate in the electron-transfer reaction at the polymer/
solution interface. The limiting current at which $I_{\text{lim, c}}$ ($=I_e$) was independent of Ω,
was considered as a representation of the maximum flux of redox species confined
in the polymer. This fact was interpreted on the basis of Eq. (2.60) [53]:

$$I_e = nFAD_e c^* / \phi \tag{2.60}$$

where c^* is the concentration of redox species of the polymer and D_e represents a
measure of the electron hopping rate. The n value expresses the number (fractions)
of unit charges per monomer unit of the polymer. Equation (2.60) was employed
in Ref. [53] to estimate the electron diffusion coefficient, D_e. The obtained value

Fig. 2.43 Koutecky–Levich plots for different acid concentrations: x M $HClO_4 + (2 - x)$ M $NaClO_4 + 3 \times 10^{-3}$ M (HQ/Q) solutions, $x = 0.1$ ($\square$), 0.01(o) and 0.001 (∇). $\phi = 60$ nm [53]
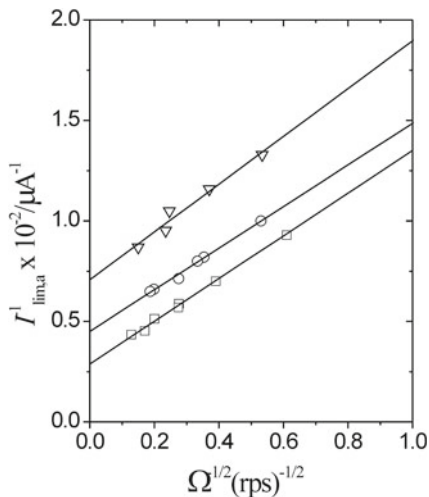
was $D_e = 2.4 \times 10^{-10}$ cm^2 s^{-1}. The effect of the acid concentration on the charge transport process of POAP films was also analyzed in Ref. [53].

Figure 2.43 shows that at c and ϕ fixed, experimental I_{lim}^{-1} versus $\Omega^{-1/2}$ dependences for HQ oxidation are linear plots with different intercepts at $\Omega \to \infty$ dependent on the acid concentration (x) in solution. The same behaviour was observed for Q reduction in the potential range corresponding to the pre-plateau (Fig. 2.38). Then, again by fitting of Eq. (2.59) to experimental data, κD_s values were obtained in Ref. [53] for both HQ oxidation and Q reduction at different x values.

Figure 2.44 shows $I_{lim, c}$ versus $\Omega^{-1/2}$ dependences corresponding to the main cathodic wave for a 60 nm thick POAP film contacting solution of different x values between 0.1 and 0.001. It was observed that after a certain Ω value, which depends on x, the liming current $I_{lim, c}$, becomes independent of Ω [53]. The values of Ω at which the limiting current becomes constant, is lower as x decreases. This effect was attributed to a slow electron transport across the polymer as x decreases [53]. By employing Eq. (2.60), values of D_e for different x values, were obtained (Table 2.9). This last result allowed the authors of Ref. [53] to conclude that POAP is less conductive as it becomes less protonated.

The redox mediation reaction of POAP films in the presence of the $Fe^{2+/3+}$ and $Fe(CN)_6^{3-/4-}$ redox couples was also studied employing RDEV in Ref. [52]. The i–E responses of the two external redox couples on both a naked Au and a POAP coated electrodes at an electrode rotation rate of 1200 rpm, are shown in Fig. 2.45. These i–E responses for POAP modified electrodes show no anodic currents, for both solutions. Authors of Ref. [52] remark that in the case of $Fe^{2+/3+}$ system (Fig. 2.45a), the cathodic limiting current is independent of the film thickness but it depends on the concentration of Fe^{3+}. However, for the case of $Fe(CN)_6^{3-/4-}$ solutions (Fig. 2.45b), the cathodic limiting current was independent of the

Fig. 2.44 I_{lim}^{-1} versus $\Omega^{½}$ for the 60 nm thick POAP film contacting a x M $HClO_4 + (2 - x)$ M $NaClO_4 + 0.01$ M (HQ/Q) solution, $x = 0.1$ (×), 0.01 (□) and 0.001 (△) [53]
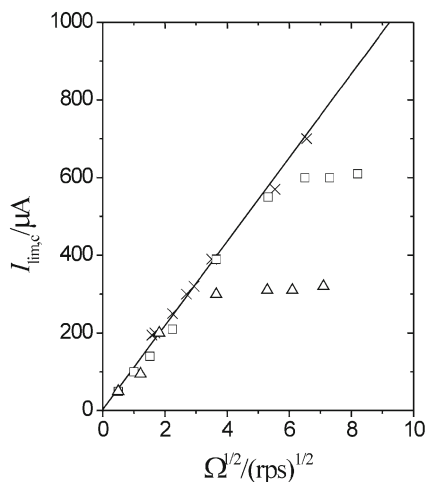
Table 2.9 D_e values obtained for POAP films from Eq. (2.60) [a][53]

x	$10^{10} D_e/cm^2\ s^{-1}$
0.1	2.4
0.01	0.34
0.001	0.17

[a] Q reduction (second wave) xM $HClO_4 + (2 - x)$ M $NaClO_4 + 10 \times 10^{-3}$M (HQ/Q) solutions. Electrode area, $A = 0.23\ cm^2$, $n = 0.44$, $c^* = 4.7$ M, $\phi = 60$ nm
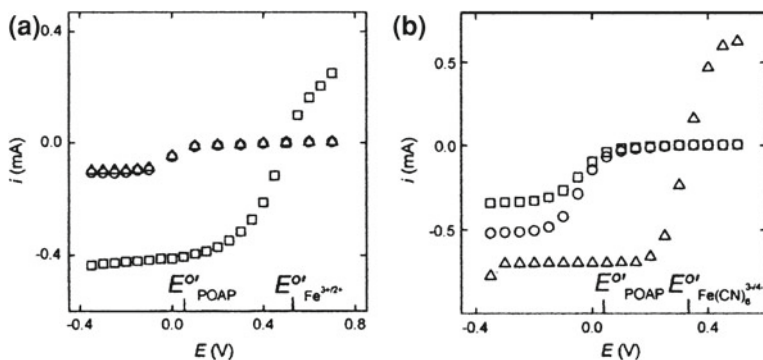
Fig. 2.45 Current–potential curves: **a** Naked Au electrode (□) and coated with a POAP film 88 nm thick (o) and 125 nm thick (△). Electrolyte: $HClO_4$ 0.1 M + $Fe^{2+/3+}$ 5 mM. **b** Naked Au electrode (△) and coated with a POAP film 88 nm thick (o) and 125 nm thick (□). Electrolyte: $HClO_4$ 0.1 M + $Fe(CN)_6^{3-/4-}$ 5 mM. The rotation rate was 1200 rpm [52]

concentration of $Fe(CN)_6^{3+}$ and increases with decreasing the film thickness. Furthermore, in this last case, for relatively high rotation speeds, the cathodic limiting current was independent of the rotation speed. This was considered as an indication of current control by charge transport in the film. The independence of the cathodic limiting current of the film thickness for the $POAP/Fe^{2+/3+}$ system was considered as an indication that the electronic transport in the POAP film is not the rate-determining step of the transport process.

On the other hand, the permeation of Fe^{3+} in the film was ruled out in Ref. [52], because it is indicated that otherwise the half-wave potential for the coated electrode should be the same as that for the naked electrode. Then, authors of Ref. [52] conclude that according to the theoretical basis of the electrochemical rectification developed by themselves in a previous work [51], the cathodic limiting current must be controlled by the kinetic of the electron transfer between the redox species in solution and those from the polymer. Then, the observed *i-E* response was attributed to a slow kinetics for the mediated oxidation of Fe^{2+}. Concerning the $POAP/Fe(CN)_6^{3-/4-}$ system, the electronic transport was considered to be the responsible for the observed cathodic limiting currents [52]. As the self-exchange in $Fe(CN)_6^{3-/4-}$ is much faster than in the $Fe^{2+/3+}$ system, then authors of Ref. [50] conclude that the electron exchange reaction between $Fe(CN)_6^{3-/4-}$ and POAP to be much faster than that between $Fe^{2+/3+}$ and POAP.

In order to analyze the conducting potential range of POAP, Ortega [30] carried out experiments with POAP films contacting different redox active solutions. The behavior of POAP-modified electrodes in contact with a 0.4 mol dm^{-3} $NaClO_4$ solution (*pH* 9) containing 10^{-3} mol dm^{-3} $Fe(CN)_6^{3-}$ was firstly studied. Ortega [30] attributed the strong dependence of the redox potential (E_0) of the $Fe(CN)_6^{3-} + e^- \Leftrightarrow Fe(CN)_6^{4-}$ reaction on the solution *pH* to the formation of $HFe(CN)_6^{3-}$. Ortega [30] remarks that E_0 for $Fe(CN)_6^{3-}$ is 0.36 V (vs. SCE), at *pH* 9, and then it is located in the region where the applied potential is more positive than the formal potential of the polymer $E_f = 0.05$ V (vs. SCE), which is defined as the average of cathodic and anodic peak potentials. The voltmmograms corresponding to the redox process of $Fe(CN)_6^{4-}$ at POAP-modified Pt electrode (Fig. 2.46) did not show peak ascribable to hexacyanoferrate ion in the region ranging from 0.0 to 0.75 V (vs. SCE).

Increasing concentrations of $Fe(CN)_6^{4-}$ were used in Ref. [30] as well as different thickness of films, but no peak was observed. However, a light increase in the cathodic peak current of polymer was observed as the concentration of $Fe(CN)_6^{4-}$ increased. Ortega [30] attributes this effect to a very small amount of $Fe(CN)_6^{3-}$ that could be oxidized during the forward scan through pores formed from the swollen reduced form of the film, however, during the reverse scan, the polymer becomes more compact and the $Fe(CN)_6^{3-}$ is reduced when the polymer becomes conducting. This assumption is consistent with a higher conductivity of POAP in the negative potential range comprised between -0.25 and 0.0 V (vs. SCE). $FeCl_2$ solutions were also employed by Ortega [30] to study the conduction potential range of POAP. Ortega [30] remarks that as the oxidation of Fe(II) to

Fig. 2.46 Voltammograms corresponding to 60 nm thick POAP film in KCl (0.4 mol dm^{-3}) at pH 9 in presence and absence of Fe(CN)$_6^{4-}$ [30]
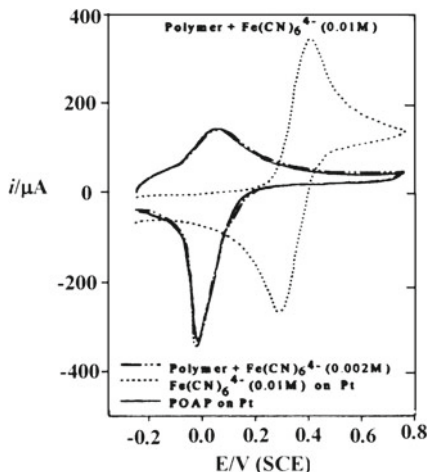
Fe(III) is reported to take place at the formal potential of 0.8 V (vs. NHE) in acid medium, and no peak ascribable to oxidation of Fe(II) is observed in the voltammetric response of POAP, then, he concludes that POAP is not conductive in the potential range more positive than the polymer formal potential.

Paraquat (1,1$'$-dimethyl-4,4$'$ bipyridylium or methyl viologen) was also employed by Ortega [30] to test the conductivity of POAP at negative potentials. Ortega remarks that paraquat was reported to exhibits two reversible peaks at –0.7 V (vs. Ag/AgCl) in aqueous solutions at pH 4 [55]. Then, reduced paraquat (0.5 × 10^{-3} mol dm^{-3}) was synthesized by Ortega and a voltammogram of this redox species on bare Pt was recorded in a neutral solution to avoid hydrogen evolution (Fig. 2.47). Ortega compared voltammograms of POAP in the presence and the absence of paraquat and he observed an additional current when POAP contacts paraquat within the negative potential range of POAP, exactly in the region where POAP is in a lower oxidation state (Fig. 2.47). Such additional current was not observed in absence of the radical methyl viologen, which was considered by Ortega as a signal of a higher conductivity of the film in that region as compared with more positive potential values.

Copper was also utilized by Ortega [30] to demonstrate the conductivity of POAP at negative potentials. The voltammograms corresponding to copper deposition from an acid solution containing Cu(ClO$_4$)$_2$ onto bare Pt and POAP-modified electrode are compared in Fig. 2.48.

The voltammogram of a POAP-modified electrode in contact with a Cu(II) solution clearly shows the oxidation and reduction peaks corresponding to the polymer and Cu(II)/Cu couple. The copper reduction peak appears at more negative potentials on POAP, probably due to the resistivity of the film while the cathodic current does not change significantly. However, the oxidation peak is not significantly affected by the presence of the POAP film. Voltammograms recorded at different scan rates showed that the reduction peak of copper depends on this

Fig. 2.47 Voltammograms of POAP in KCl (0.4 mol dm^{-3}) at *pH* 9 in presence and absence of paraquat. Area of working electrode 1.9×10^{-3} cm^2. Reduced paraquat was produced in situ on a mercury pool electrode (12 cm^2) [30]
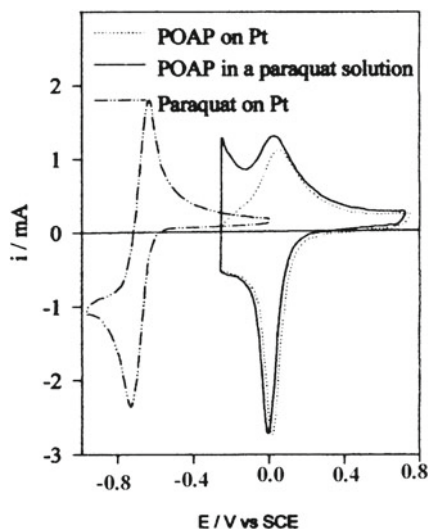
Fig. 2.48 Voltammograms of **a** 70 nm thick POAP film immersed in a 3.5×10^{-3} mol dm^{-3} in Cu(II) and 0.4 mol dm^{-3} NaClO$_4$ solution at *pH* 9. $v = 20$ mV s^{-1}. **b** Cu(II) on bare Pt in the same medium as **a** [30]
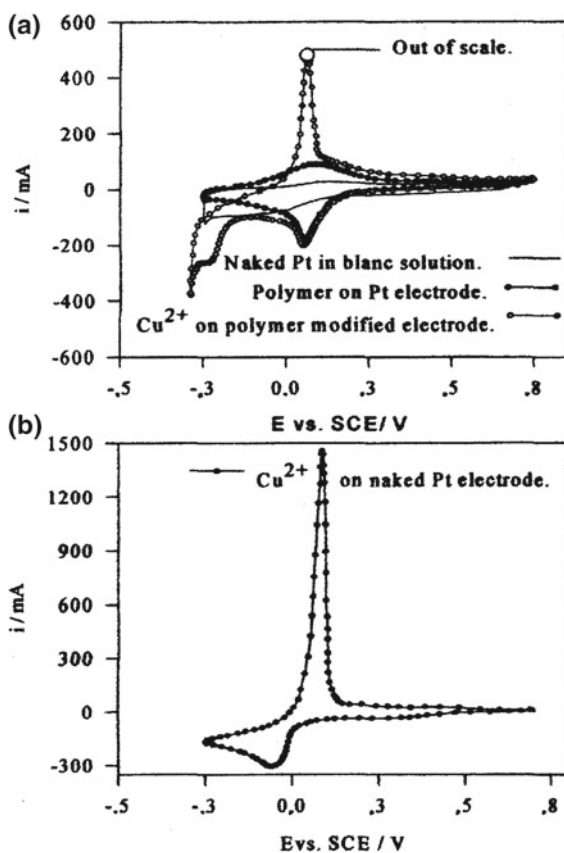
parameter in the same way as the POAP reduction peak. That is, it moves to more negative potential as the sweep rate increases. However, changes in the scan rates do not affect the oxidation peak potentials of the polymer and copper. According to Ortega [30], the more reasonable explanation for this behaviour is that the POAP film is conductive at negative potentials lower than −0.250 V (vs. SCE).

In this regard, Ortega [30] assumes that it is possible that the shift of the reduction peak of copper on POAP-modified electrode, with respect to the one observed from the naked Pt electrode originates from the different nature of the substrate, that is, from the potential-dependent resistance of the POAP film. Ortega also observed that reduction currents at the modified electrode were also very similar to those recorded when the bare Pt electrode is used. These features allow Ortega to conclude that the deposition of copper takes place on the polymer-solution interface, otherwise, an appreciable decrease in the current because of the diffusion of copper through the film would be observed. This assumption is supported by scanning electron micrographs of POAP films, where no pinholes were visible [30]. Then, the difference between current–potential profiles for the reduction of copper on POAP-modified electrode and naked Pt was attributed by Ortega to the resistance of the polymer film, expressed as:

$$R = \rho L/A \qquad (2.61)$$

where R and L are the resistance and the thickness of the film, respectively, A is the area of the electrode and ρ is the resistivity of the film. Knowing that conductivity (σ) is $1/\rho$, and $R = \Delta E/i$, Eq. (2.61) becomes:

$$\sigma = iL/\Delta EA \qquad (2.62)$$

where i is the current and ΔE is the difference of potential between points with the same magnitude of current for the reduction of copper curves on POAP-modified and naked Pt electrode.

RDEV was also employed by Ortega to study the copper deposition process [30]. Voltammograms of modified rotating disc electrode were recorded at different rotation rates. No change was observed in the voltammograms at a rotation rate lower that 50 rad/s because the process is controlled by charge transfer in the polymer matrix. The voltammograms were recorded at low scan rates (3 mV/s) so that steady-state conditions were kept during the experiments. Under such conditions, it was assumed by Ortega that the polymer should also have time to reach its equilibrium conductivity at each potential. The voltammograms corresponding to the reduction of copper on naked Pt and POAP-modified Pt electrodes are shown in Fig. 2.49. The smaller hump observed in the i–E curve for the reduction of copper on the modified electrode represents the reduction of the polymer while the larger one involves the reduction of the metal ion on the polymeric material.

Ortega remarks that small changes in the potential produce large changes in the current for the reduction of copper on naked Pt at 0.0 V. However, the curve corresponding to the POAP-modified electrode is less steep, which was attributed to the potential-dependent resistance of the film that controls the copper
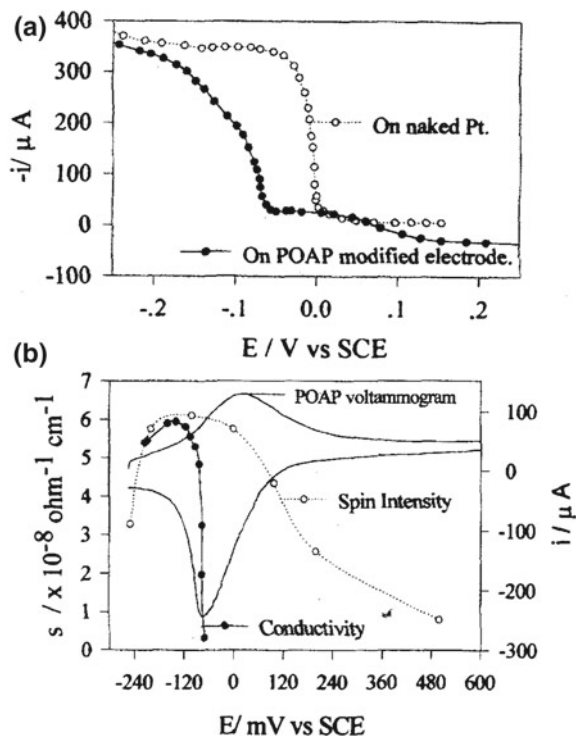
Fig. 2.49 **a** Voltammograms on the rotating Pt-POAP and Pt naked disc electrode in aqueous solution containing 3.5×10^{-3} mol dm^{-3} in Cu(II) at *pH* 9. Scan rate $v = 3$ mV/s and rotation rate 3 rad/s. **b** Changes in the conductivity of the film as a function of potential and its correlation with spin intensity (*see* Chap. 1) [30]

deposition. Ortega [30] determined the conductivity of the film as a function of polarization potential by using Eq. (2.62) and employing a surface area of the electrode of 0.33 cm^2 and a thickness of the film of 80 nm. The resulting $\sigma - E$ plot (Fig. 2.49 (b)), was compared with the spin intensity-E characteristic (see Fig. 1.16, Chap. 1). Ortega indicates that the conductivity increases very sharply at approximately -67 mV, peaks at approximately -120 mV and starts decreasing at more negative potentials. The conductivity and the spin intensity both exhibit maximum at -0.120 V, which according to Ortega shows the polaronic nature of the conductivity of the film at that potential range. At more positive potentials the number of polarons decreases, but no so steeply as the conductivity. This fact was explained by Ortega by assuming that when the concentration of polarons is high they start to combine to give rise to bipolarons, some of these bipolarons are converted to a higher oxidized state of the polymer, that is, the ones with opened structure, which decreases the conductivity in the polymer. Some polaron islands surrounded by fully oxidized units can still be present in segments of the chains so that the conductivity of the film is strongly reduced while ESR spectra still show

the presence of radicals. Values of conductivity for POAP calculated by Ortega are of the order 1.0×10^{-8} S/cm.

A voltammetric study about the conduction process through POAP-coated platinum electrodes employing neutral and charged species was carried out in Ref. [1]. With regard to positive charges species, it was observed in Ref. [1] that chemical substances, which are reduced on the bare electrode at potentials lower than the E_{pa} (anodic peak potential) of POAP, such as, Cr^{3+}, Cu^{2+} and Cd^{2+} could not be reduced above it with exception of protons. However, couples which have a formal potential value more positive than the E_{pa} of the POAP film could be easily oxidized [1]. With regard to neutral and negative charges species, three couples (ascorbic acid, hydroquinone and $K_4Fe(CN)_6$) were oxidized over POAP films Ascorbic acid suffers irreversible oxidation at a bare and a POAP electrode but the latter shows an increase of the total current, which was attributed to a catalytic effect of the film. Hydroquinone oxidizes reversibly at a modified electrode showing a negative catalytic effect, which was assigned to the film resistance. $K_4Fe(CN)_6$ oxidation shows, at low film thickness, a reversible behaviour. However, with a film thickness greater than 200 nm, quasi-reversible behaviour was observed. This effect was attributed to the film resistance [1]. A resistance value of POAP was calculated in Ref. [1]. The value obtained, with the assumption of fast charge transfer at the electrode/film and film/solution interfaces, was 15 ohms, which corresponds to a conductivity value of 1.34×10^{-4} S cm^{-1}. Authors of Ref. [1] conclude that POAP is conductive in the oxidized state and non-conductive in the reduced one.

2.4 POAP Deactivation and its Effect on the Charge-Transport Process

Partial oxidation of POAP films was studied by employing CV and EIS [56].

The voltammetric response of a fresh POAP film shows one peak at about 0.1 V (versus SCE) (Fig. 2.50a) and its impedance response for a potential corresponding to the peak potential shows a Warburg behaviour at high frequencies and a capacitive increase at low frequencies (Fig. 2.51a).

The early increase in the imaginary component of the impedance and the absence of a high-frequency semicircle in the impedance plots of POAP are indicative of fast interfacial charge transfer processes. POAP gives the same electrochemical response with potential cycling for more than 1 day provided that the positive potential does not exceed 0.5 V (versus SCE). However, after cycling the potential during several days POAP starts to show the characteristics of deactivation. Also, as the positive potential limit is increased beyond 0.5 V, the voltammetric response (Fig. 2.50b) and, more clearly, the impedance response (Fig. 2.51b) starts to change. In the latter case, a semicircle appears in the Nyquist plot, after deactivation (Fig. 2.51b). Deactivation is accompanied by a decrease in
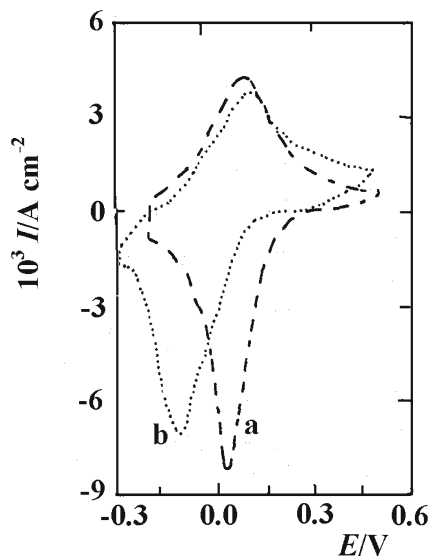
Fig. 2.50 Voltammetric response of POAP in a 0.1 M $HClO_4$ + 0.4 M $NaClO_4$ solution. $v = 0.1$ V s^{-1}. **a** Recently prepared and **b** after partial oxidation [56]
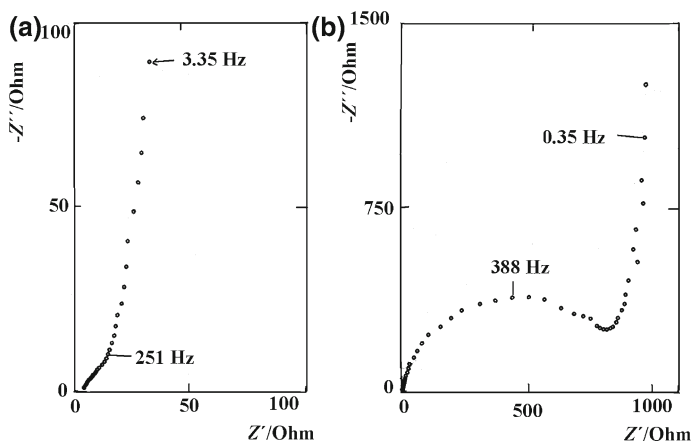
Fig. 2.51 Nyquist plots for POAP in a 0.1 M $HClO_4$ + 0.4 M $NaClO_4$ solution. $E = 0.1$ V versus SCE. **a** Recently prepared and **b** after partial oxidation [56]

the film conductivity. The total conductivity of the POAP films synthesized in Ref. [56] was calculated by extrapolating the pseudocapacitive behaviour to the real axis and subtracting the resistance of the electrolyte. The conductivity of an

immediately prepared POAP film decreased from 1×10^{-6} to 4×10^{-7} S cm^{-1} after its deactivation [56].

The irreversible deactivation of POAP films when the positive potential limit (E_{upl}) exceeds 0.5 V was also studied in the presence of a redox active solution employing CV, Rotating Disc Electrode Voltammetry (RDEV) and EIS in Ref. [57]. CV was employed to prepare and deactivate POAP films. Then, the electrochemical behaviours of the freshly prepared (nondeactivated) and deactivated POAP films were studied by RDEV and EIS in the presence of p-benzoquinone/hydroquinone, that is, when a redox mediation reaction is taking place at the polymer–solution interface. The reduced state of POAP (-0.2 V $< E <$ 0.0 V vs. SCE) was employed to compare the behaviour of nondeactivated and deactivated POAP films. The experimental impedance diagrams of POAP films contacting the p-benzoquinone/hydroquinone redox couple, were interpreted on the basis of the homogeneous impedance model described in Ref. [58]. Eleven POAP coated electrodes, all of the same polymer thickness, were consecutively manufactured in Ref. [57] to carry out the experiments. Each one of the 11 POAP coated electrodes was successively used as the working electrode in an individual experiment. The eleven POAP coated gold electrodes were split into three different groups. While the first group, including three samples, was subjected to a potential cycling where the positive potential limit E_{upl} was 1.0 V, the second and third ones, each involving four samples, were subjected to potential cycles where E_{upl} values were 0.8 and 0.65 V, respectively.

The different dependencies of the charge transfer and charge transport parameters on the degree of deactivation of the polymer films ($\theta_{Red,Max}$) were obtained in [57]. The parameter $\theta_{Red,Max}$ [57] was defined in such a way that $\theta_{Red,Max} = 1$ for a nondeactivted film, that is, for the film only subjected to potential cycles within the potential range -0.2 V $< E <$ 0.5 V (SCE). Then, $\theta_{Red,Max}$ values lower than 1 are representative of deactivated films and as the lower is $\theta_{Red,Max}$, the higher is the degree of deactivation of the polymer film. The different features of some of these dependencies (for instance, bulk electronic and ionic transport on $\theta_{Red,Max}$) were explained in terms of the different mechanisms of electron and ion transport in polymeric materials. The charge-transfer resistance at the metal-polymer interface, R_{mlf}, as a function of $\theta_{Red,Max}$ extracted from the fitting procedure employed in [57], is shown in Fig. 2.52.

R_{mlf} exhibits a strong increase from the beginning of the deactivation, that is, as (θ_{ox}) goes from 1 to 0. The ion-transfer resistance R_i^{fls} at the polymer-solution interface results almost one order of magnitude lower than R_{mlf}. Also, R_i^{fls} as a function of $\theta_{Red,Max}$ exhibits a different feature as compared with R_{mlf} (Fig. 2.53).

That is, while R_i^{fls} remains nearly constant ($R_i^{f|s} \sim 10\,\Omega\,cm^2$) within the range $0.6 < \theta_{Red,Max} < 1.0$, a marked increase in R_i^{fls} is observed from $\theta_{Red,Max} \sim 0.6$ towards $\theta_{Red,Max} \sim 0.2$ In the same way as R_{mlf}, a pronounced increase in the resistance related to the electron interfacial exchange R_e^{fls} at the polymer-solution interface, is observed from the beginning of the polymer deactivation (high $\theta_{Red,Max}$ values) (Fig. 2.54).
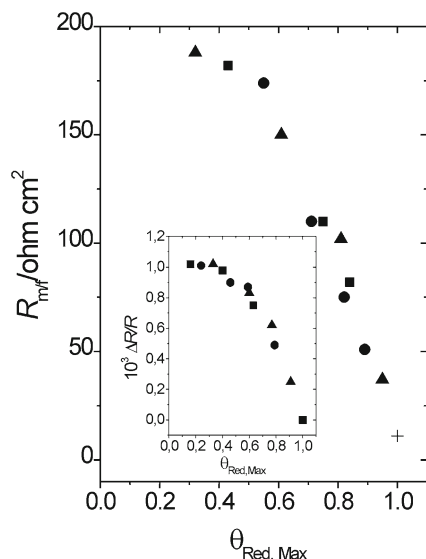
Fig. 2.52 Metal-polymer interfacial electron-transfer resistance ($R_{m/f}$) as a function of the degree of degradation, $\theta_{Red,\ Max}$ for eleven deactivated POAP films: (■) films of the first group; (▲) films of the second group; (●) films of the third group; (+) Value corresponding to the nondeactivated POAP film. Electrolyte: 0.1 M HClO$_4$ + 0.4 M NaClO$_4$ + 2 × 10^{-3} M (HQ/Q) solution. *Inset* Surface resistance change $\Delta R/R$ as a function of $\theta_{Red,Max}$ for same eleven deactivated POAP films indicated above [57]: (■) films of the first group; (▲) films of the second group; (●) films of the third group. The same electrolyte solution above indicated. Scan rate: $v = 0.01$ V s^{-1}[57]

However, R_e^{fls} values are nearly one order of magnitude lower than $R_{m|f}$ values. Then, concerning the polymer-solution interface, a slow ion transfer process is observed for POAP as compared with the electron transfer process at this interface (compare Figs 2.53 and 2.54). With regard to the high-frequency capacity, C_H, starting at a value around 17 μF cm^{-2} for a nondeactivated film, C_H decreased with increasing the degree of degradation of the polymer, reaching a value about 5 μF cm^{-2} for a almost completely deactivated POAP film.

Diffusion coefficients for electron (D_e) and ion (D_i) transport as functions of $\theta_{Red,Max}$ are shown in Figs. 2.55 and 2.56, respectively. As can be seen, while D_e is strongly affected even at low degree of degradation $0.8 < \theta_{Red,Max} < 1.0$, D_i changes are more pronounced for $\theta_{Red,Max} < 0.6$ Authors indicate that taking into account that transfer and transport parameters obtained in Ref. [57] correspond to the reduced state of POAP ($E < 0.0$ V), it is possible that R_i^{fls} and D_i only reflect the proton movement through the polymer-electrolyte interface and inside the polymer film, respectively.

Authors [57] also remark that D_e values extracted from the Vorotyntsev's model [58] are near two orders of magnitude higher than D_i for POAP. Thus, these relative diffusion coefficient values contrast with those reported in other works,
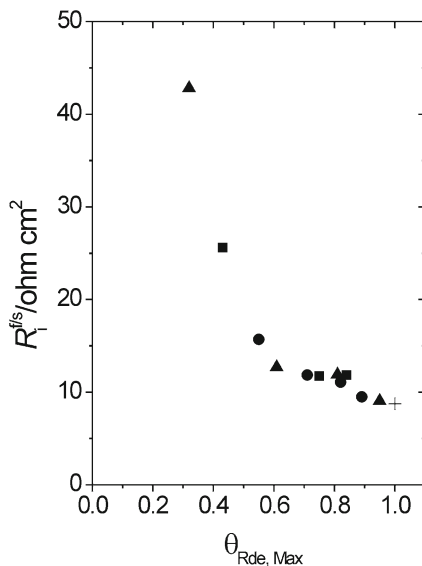
Fig. 2.53 Polymer-solution interfacial ion-transfer resistance ($R_i^{f/s}$) as a function of the degree of degradation, $\theta_{Red,\ Max}$ for the 11 deactivated POAP films synthesized in Ref. [57]: (■) films of the first group; (▲) films of the second group; (●) films of the third group. (+) value corresponding to a nondeactivated POAP film. Electrolyte: 0.1 M HClO$_4$ + 0.4 M NaClO$_4$ + 2 × 10^{-3} M (HQ/Q) solution [57]

Fig. 2.54 Interfacial electron-transfer resistance ($R_e^{f/s}$) at the polymer-solution interface as a function of the degree of degradation, $\theta_{Red,Max}$ for the 11 deactivated POAP films described in Ref. [57]: (■) films of the first group; (▲) films of the second group.(●) films of the third group. (+) Value corresponding to the nondeactivated POAP film. Electrolyte: 0.1 M HClO$_4$ + 0.4 M NaClO$_4$ + 2 × 10^{-3} M (HQ/Q) solution [57]
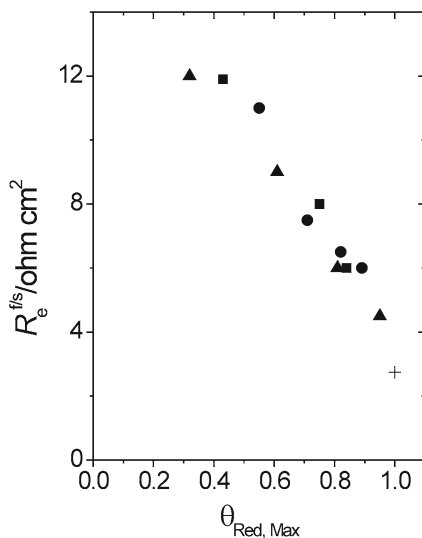
where electron motion was considered slow relative to the ion motion [40]. An interesting comparison between the transversal charge transfer resistance at the metal–polymer interface R_{mlf} (obtained from EIE) and the lateral resistance $\Delta R/R$ along the electrode (obtained by Surface Resistance measurements [39, 40], as functions of $\theta_{Red,Max}$. (see inset in Fig. 2.52) was established in Ref. [57]. Similar features in R_{mlf} versus $\theta_{Red,Max}$ and $\Delta R/R$ versus $\theta_{Red,Max}$ dependencies were

Fig. 2.55 The electron diffusion coefficient (D_e) as a function of the degree of deactivation, $\theta_{Red,Max}$ for the 11 deactivated POAP films described in Ref. [57]: (■) films of the first group; (▲) films of the second group; (●) films of the third group. (+) Value corresponding to the nondeactivated POAP film. Electrolyte: 0.1 M $HClO_4$ + 0.4 M $NaClO_4$ + 2 × 10^{-3} M (HQ/Q) solution [57]
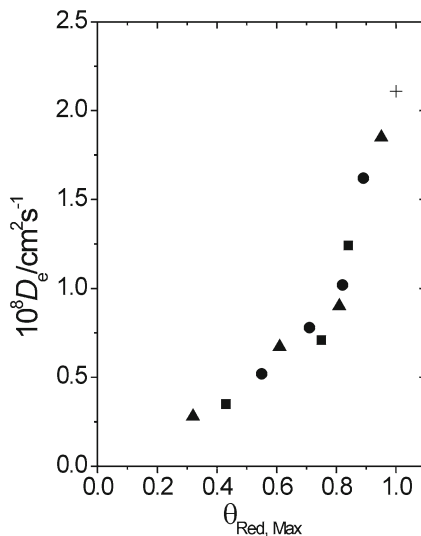
observed, which was explained in terms of two different aspects of the electron motion at metal surfaces contacting a polymeric material. However, while $R_{m|f}$ is a transversal resistance at the metal-polymer interface related to the electron transfer process during the redox reaction of the polymer, $\Delta R/R$ changes are attributed to the scattering of conduction electrons from the inside of the metal to the metal-polymer interface, caused by changes in the translational symmetry parallel to the interface due to the presence of different distributions of redox sites at this interface (a more expanded distribution of redox sites as more deactivated becomes the polymer) [39]. In this sense, $\Delta R/R$ changes are not considered as the direct result of the electron transfer between the species on the metal surface electrode and the electrode, but rather that they originate from the effect of foreign surface particles on the conduction electrons of the metal itself [39]. Thus, despite the different origins of these two electron resistances at the polymer-metal interface and the different type of measurements employed to obtain them (*ac* impedance measurements and potentiodynamic potential scans at low scan rates $v = 5 \times 10^{-3}\,\mathrm{V\,s^{-1}}$), similar behaviours are observed as a function of the polymer deactivation. This observation is interesting because it seems that a given surface process on the electrode affects in a similar way both the electron transport along (parallel) the metal surface and the electron transfer across the electrode-polymer interface. Authors indicate that the results reported in Ref. [57] demonstrate that when POAP is subjected to rough conditions (excessive positive potential limits or prolonged potential cycling), as in some of its practical applications does (see Chap. 3), ion and electron diffusion inside the polymer and rates of interfacial charge transfer processes, are strongly affected, which should reduce drastically the efficiency of the material.

Fig. 2.56 The ion diffusion coefficient (D_i) as a function of the degree of deactivation, $\theta_{Red,Max}$ for the eleven deactivated POAP films synthesized in Ref. [57]: (■) films of the first group; (▲) films of the second group; (●) films of the third group. (+) Value corresponding to the nondeactivated POAP film. Electrolyte: 0.1 M HClO$_4$ + 0.4 M NaClO$_4$ + 2 × 10^{-3} M (HQ/Q) solution [57]
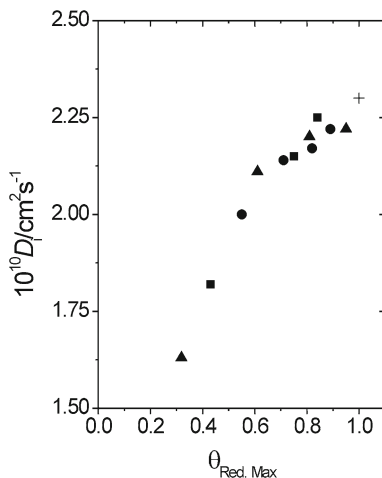

The electroactivity of a POAP film can be reduced by soaking in a 50 mM Fe$_2$(SO$_4$)$_3$ solution [59]. This deactivation was attributed to the interaction of iron ions with the redox sites of POAP, which impedes the protonation reaction of the polymer. A series of eight electrodes were prepared in [59] (see first column in Table 2.10) and each one of them was successively deactivated in an individual experiment by soaking in a ferric cation solution.

Each POAP film, after being equilibrated within the potential region $-0.2 < E < 0.5$ V in the supporting electrolyte solution (j–E response shown in dashed line in Fig. 2.57), was soaked in a 0.1 M H$_2$SO$_4$ + 0.05 M Fe$_2$(SO$_4$)$_3$ solution for different time periods (see second column in Table 2.10). Then, each

Table 2.10 Voltammetric reduction charge $Q_{Red, c}$ and degree of deactivation, θ_c^d, of different POAP films

POAP films[a]	[b]Soaking time/h	$Q_{Red,c}^c$/mC cm^{-2}	θ_c^d
1	2	2.44	0.13
2	4	2.04	0.27
3	5	1.87	0.33
4	10	1.57	0.44
5	16	1.32	0.53
6	21	1.15	0.59
7	24	1.12	0.60
8	33	1.06	0.62

[a] Numbers *1* to *8* represent different deactivated POAP films
[b] Different soaking times in a 0.1 M H$_2$SO$_4$ + 0.05 M Fe$_2$(SO$_4$)$_3$ solution
[c] Voltammetric reduction charge of the different deactivated POAP films after being subjected to the soaking process in the presence of the ferric cation solution
[d] Degree of deactivation of the different POAP films calculated from $\theta_c = 1 - (Q_{Red,c}/Q_{Red,T})$. $Q_{Red,T}(= 2.8$ mC cm$^{-2})$ is the voltammetric reduction charge of a non-deactivated film [59]

Fig. 2.57 Voltammetric (j–E) responses for 2.8 mC cm^{-2} thick POAP films: **a** (- - - -) a freshly prepared POAP film. Numbers (*1*), (*4*), (*7*) correspond to POAP films with different degrees of deactivation (θ_c): (*1*): $\theta_c = 0.13$; (*4*): $\theta_c = 0.44$; (*7*): $\theta_c = 0.60$. Electrolyte: 0.1 M HClO$_4$ + 0.4 M NaClO$_4$. Scan rate: $v = 0.01$ V s^{-1} [59]
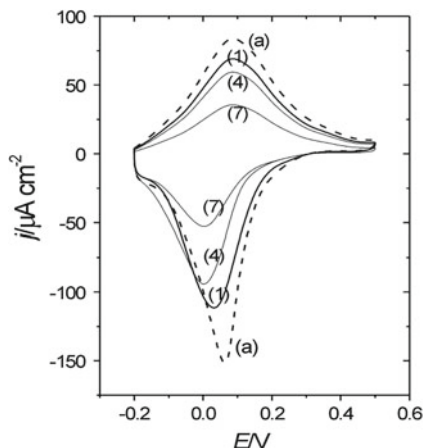
one of these electrodes was extracted from the solution containing ferric ions and it was copiously washed with the supporting electrolyte solution, then the electrode was again transferred to the electrochemical cell containing the supporting electrolyte solution.

The corresponding *j*–*E* responses were again recorded for each one of the 8 POAP films. Figure 2.57 shows voltammetric responses corresponding to the films (1), (4) and (7) (see also Table 2.10), respectively, after being subjected to the soaking process previously described. With each one of these deactivated POAP films, RDEV experiments were performed in the presence of a solution containing equimolar concentrations of *p*-benzoquinone (Q) and hydroquinone (HQ) species (0.1 M HClO$_4$ + 0.4 M NaClO$_4$ + 2 × 10^{-3} M Q/HQ). Then, stationary current–potential curves (*I*–*E*) at different electrode rotation rates Ω were recorded. From these curves, cathodic and anodic limiting current *versus* electrode rotation rate (I_{lim} versus $\Omega^{1/2}$) dependences were obtained. Also, with some of these deactivated POAP films, *ac* impedance measurements, in the presence and in the absence of the HQ/Q redox couple in solution, were performed. In some experiments the HQ/Q redox couple concentration in solution was varied. In order to reactivate some deactivated POAP films, which had been initially treated with the ferric cation solution, they were treated with a 0.1 M NH$_4$OH solution [59]. The more attenuated voltammetric response of a POAP film with increasing soaking time in the ferric cation solution (Fig. 2.57) was considered as representative of a higher degree of deactivation of the polymer film [59]. In this regard, voltammetric reduction charge values corresponding to the completely reduced POAP films were compared for both non-deactivated films ($Q_{Red,T} = 2.8$ mC cm^{-2}) and films subjected to the soaking process in the presence of the Fe(III) solution ($Q_{Red,c}$) (see column 3 in Table 2.10); then, a degree of deactivation (column 4 of Table 2.10) was defined in Ref. [59] as

$$\theta_c = 1 - \left(Q_{Red,c} / Q_{Red,T} \right) \tag{2.63}$$
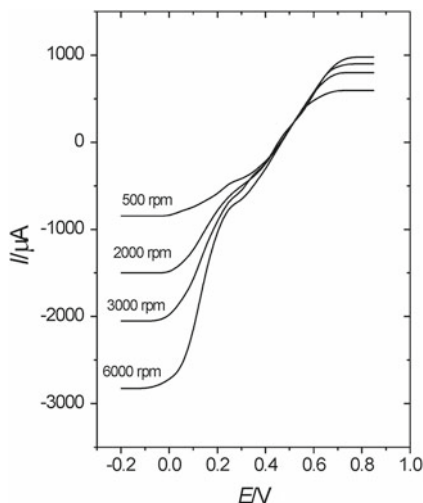
where $Q_{Red,c}$ is the total reduction charge assessed by integration of the corresponding j-E response from $E = 0.5$ V towards the negative potential direction for a deactivated film and $Q_{Red, T} = 2.8$ mC cm^{-2} is the total reduction charge for the non-deactivated film. In this way, for a non-deactivated POAP film (dashed curve in Fig. 2.57) the degree of deactivation was $\theta_c = 0$, taking $Q_{Red, T} = 2.8$ mC cm^{-2} as reference charge. However, values of $\theta_c > 0$ are indicative of POAP films that have been deactivated. Figure 2.58 shows stationary current–potential curves (I–E) at different electrode rotation rates Ω for a freshly prepared (nondeactivated) POAP film contacting a 0.1 M $HClO_4$ + 0.4 M $NaClO_4$ + 2×10^{-3}M Q/HQ solution. (I–E) curves at different Ω values were obtained for each one of the POAP films

Fig. 2.60 Levich representations $I_{lim,c}$ versus $\Omega^{1/2}$ for POAP films contacting a 0.1 M $HClO_4$ + 0.4 M $NaClO_4$. + 2×10^{-3} M (HQ/Q) solution. (●) A non-deactivated POAP film. (1), (4) and (7) correspond to the three films indicated in Fig. 2.1. Inset: steady-state (I–E) curves for potential values $E < 0.2$ V at $\Omega = 3000$ rpm [59]
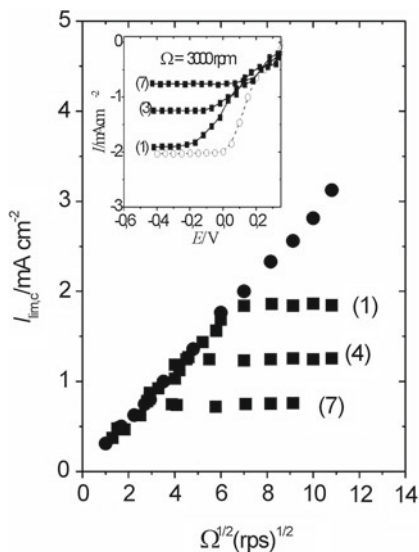
indicated in Table 2.10. Figure 2.59 shows this representation for a POAP film with $\theta_c = 0.13$. As can be seen by comparing Figs. 2.58 and 2.59, at each electrode rotation rate, the anodic limiting current for a deactivated POAP film is lower than that for a non-deactivated one. Also, after a given electrode rotation rate, which depends on the degree of deactivation, the cathodic limiting current for a deactivated film becomes independent of this variable.

Then, at potential values $E < 0.0$ V, $I_{lim,c}$ versus $\Omega^{1/2}$ dependences, for a non-deactivated film and also for each one of the deactivated POAP films indicated in Table 2.10, were extracted in Ref. [59]. For a non-deactivated POAP film a linear $I_{lim,c}$ versus $\Omega^{1/2}$ dependence, which follows the Levich equation, was obtained within a wide range of Ω values (Fig. 2.60). However, for POAP films that have been deactivated, after a certain Ω value, a constant cathodic limiting current value $I_{lim,c}$ independent of Ω is achieved.

Authors [59] remark that the transition, at which the cathodic limiting current becomes independent of Ω occurs at lower Ω values as the degree of deactivation increases. Interpretation of this effect was made on the basis of the electron-hopping model. Limiting current values at which $I_{lim, c}$ ($=I_e$) becomes constant were considered as a representation of the maximum flux of electrons confined in the polymer, according to Eq. (2.64)

$$I_e = n F A D_e c / \phi_p \qquad (2.64)$$

In Eq. (2.64), c is the concentration of redox sites of the polymer and ϕ_p the polymer film thickness. D_e represents a measure of the electron hopping rate and n expresses the numbers (fractions) of unit charges per monomer unit of the polymer. A is the electrode area and F the Faraday's constant.
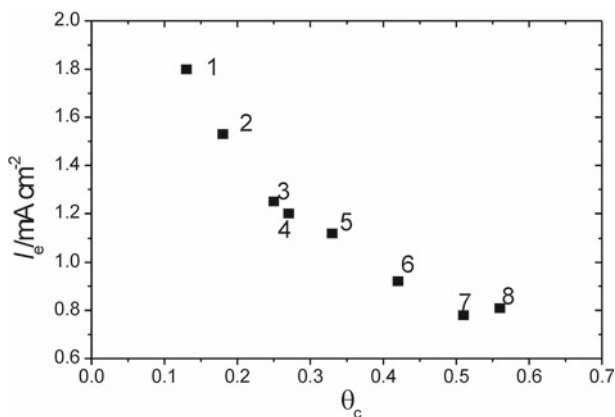
Fig. 2.61 Electron current I_e (Eq. (2.63)) as a function of θ_c. Numbers *1* to *8* correspond to each one of the POAP films indicated in Table 2.10 [59]

Experimental I_e values, corresponding to each one of the eight deactivated POAP films contacting a 2×10^{-3} M HQ/Q solution, were extracted from the cathodic plateau and they were represented as a function of θ_c (Fig. 2.61).

As can be seen, I_e decreases with increasing θ_c. In this regard, such a constant value of the current (I_e) at a given Ω value for deactivated POAP films was related to a slow electron transport across the POAP film to mediate in the electron-transfer reaction at the polymer|solution interface, as compared with a non-deactivated POAP film [59]. Author explains this effect indicating that as one increases the flux of Q (increase of Ω) from the bulk solution, then if the flux exceeds the supply of electrons from the electrode through the polymer to the electrolyte interface, the rate-limiting step will shift from the limiting transport of Q to the limiting transport of the charge through the polymer. In order to verify this limiting charge-transport process across the POAP film, the HQ/Q concentration in solution was increased in Ref. [59].

Figure 2.62 shows the $I_{\text{lim, c}}$ versus $\Omega^{1/2}$ dependence for the same films indicated in Fig. 2.60, but contacting a 3×10^{-3} M HQ/Q solution. The inset in Fig. 2.62 shows the same dependence for a 4×10^{-3} M HQ/Q solution. As can be seen by comparing Figs. 2.60 and 2.62, the constant current for a given deactivated film remains unchanged with increasing redox couple concentration in solution. However, this constant current is reached at a lower electrode rotation rate as the concentration of HQ/Q in solution is increased. On the basis of Eq. (2.64), the slower electron transport in deactivated films, as compared with non-deactivated ones, was attributed to a decrease of D_e. From data shown in Fig. 2.61 for I_e, and using the parameter values $c = 4.7$ M, $A = 1$ cm^2, $n = 0.44$ reported in other works, and $\phi_p = 60$ nm in Eq. (2.64), authors obtained a relative decrease of D_e from 5.4×10^{-11} to 2.4×10^{-11} cm^2 s^{-1} for a relative increase of θ_c from 0.13 to 0.62.

The decrease of D_e was attributed to an increase of the hopping distance between remnant active redox sites after deactivation. The increase of the hopping

Fig. 2.62 Levich representations $I_{lim,c}$ versus $\Omega^{1/2}$ for POAP films contacting a 0.1 M $HClO_4$ + 0.4 M $NaClO_4$ + 3×10^{-3} M (HQ/Q) solution. (●) A non-deactivated POAP film. (*1*), (*4*) and (*7*) correspond to the three films indicated in Fig. 2.60. Inset: $I_{lim,c}$ versus $\Omega^{1/2}$ representations for the same films indicated in Fig. 2.60, but contacting a 0.1 M $HClO_4$ + 0.4 M $NaClO_4$ + 4×10^{-3} M (HQ/Q) solution [59]
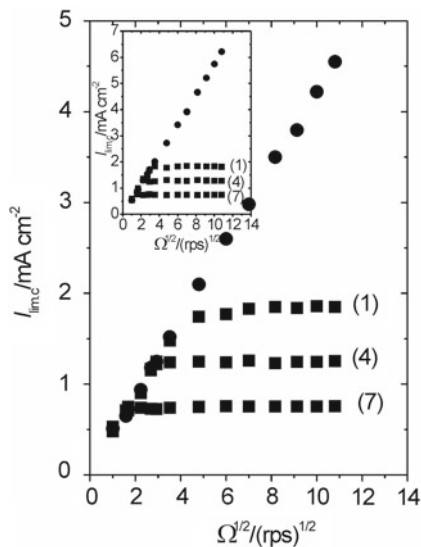
distance with deactivation was explained assuming that the electronic interaction of iron ions with redox sites of POAP impedes the protonation of redox sites, and then they become inactive for the redox reaction of the polymer. This point was clarified in Ref. [59] by increasing the *pH* of the external solution contacting a nondeactivated POAP film. In this regard, when the concentration of perchloric acid was decreased from 0.1 to 10^{-4} M in a solution containing a constant HQ/Q concentration, the cathodic plateau on the *I–E* dependences at different electrode rotation rates was affected in a similar way as the increase of θ_c does. That is, after a certain Ω value, which depends on the acid concentration, a constant current (I_e) independent of the electrode rotation rate was observed [59].

Figure 2.63 shows $I_{lim,c}$ versus $\Omega^{1/2}$ dependences for a POAP film contacting an HQ/Q solution at different perchloric acid concentrations. Thus, the higher the solution *pH* is, the lower the electrode rotation rate value at which the current becomes constant. Then, the observed I_e decrease with increasing the solution *pH* allowed the authors to conclude that the effect of iron ions on the charge transport of POAP is similar to a deprotonation of the polymer. Another experiment was performed in [59] with POAP films that, after being deactivated by treatment with the ferric cation solution, were treated with an ammonium solution. Figure 2.64 compares the voltammetric response of a non-deactivated film with those of the same film, firstly deactivated by soaking in a ferric cation solution and then reactivated by treatment with a 0.1 M NH_4OH solution. An enhancement of the redox response was observed after reactivation. Figure 2.65 compares the $I_{lim,c}$ versus $\Omega^{1/2}$ dependence for the non-deactivated film (plot (a)) with those of the same film firstly deactivated (plot (b)) and then, reactivated (plot (c)) by alkaline treatment. As can be seen from Fig. 2.65 also, an enhancement of the constant

Fig. 2.63 Levich representations $I_{lim,c}$ versus $\Omega^{1/2}$ for a non-deactivated POAP film contacting x M $HClO_4 + (2 - x)$ $NaClO_4 + 2 \times 10^{-3}$ M HQ/Q solutions, (*a*) $x = 10^{-2}$ M; (*b*) $x = 10^{-3}$ M; (*c*) $x = 10^{-4}$ M. (●) $x = 0.1$. $E = -0.3$ V [59]
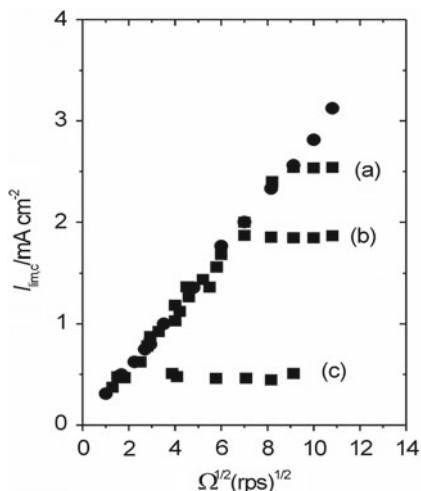
Fig. 2.64 Voltammetric (*j*–*E*) responses of: (*a*) A non-deactivated POAP film, $\theta_c = 0$; (*b*) the same film deactivated, $\theta_c = 0.62$; (*c*) the same film after reactivation, $\theta_c = 0.43$. Electrolyte: 0.1 M $HClO_4$ + 0.4 M $NaClO_4$. Scan rate: $v < 0.10$ V s^{-1} [59]
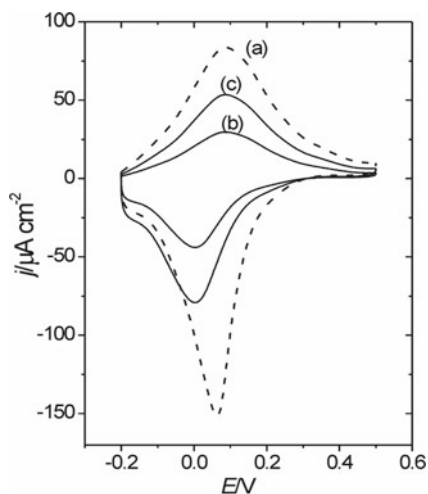
cathodic limiting current value is obtained with reactivation, but the Levich dependence corresponding to a non-deactivated film is not totally recovered. Then, authors conclude that the electron conduction of a deactivated POAP film can only be partially recovered with reactivation by treatment with an alkaline solution.

The HQ oxidation at potential values $E > 0.8$ V (vs. SCE) on both nondeactivated and deactivated POAP films was also studied in Ref. [59]. It was observed that at each electrode rotation rate, the anodic limiting current for a given deactivated film is lower than that corresponding to the same non-deactivated film (compare Figs. 2.58 and 2.59). Then, expression (2.65) was also employed in Ref. [59] to evaluate the blocking characteristics of the deactivated POAP films, during HQ oxidation. Equation (2.65) assumes that the electroactive species dissolves into

Fig. 2.65 Levich representations $I_{lim,c}$ versus $\Omega^{1/2}$ for the same POAP film indicated in Fig. 2.64 contacting a 0.1 M HClO₄ + 0.4 M NaClO₄ + 2 × 10⁻³ M (HQ/Q) solution. E = −0.2 V. (a) $\theta_c = 0$; (b) $\theta_c = 0.62$; (c) $\theta_c = 0.43$
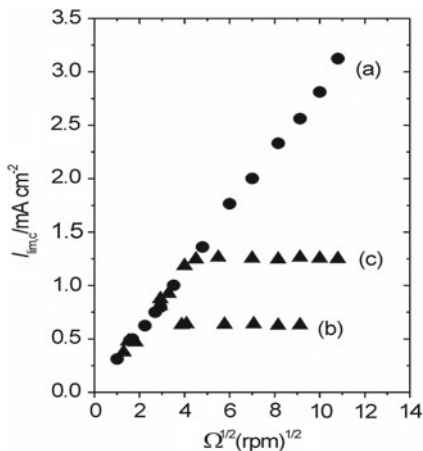
the polymer film with a partition equilibrium $\kappa = c_{pol}/c_o$ at the film|solution interface, where c_{pol} and c_o are the concentrations of the species in the polymer and in the solution, respectively.

$$I_{a,l}^{-1} = \phi_p \left(nFA\,\kappa D_{pol}c_o \right)^{-1} + \left(0.62\,nFA\,D^{2/3}v^{-1/6}\Omega^{1/2}c_o \right)^{-1} \qquad (2.65)$$

D_{pol} and D are the diffusion coefficients of the electroactive species in the polymer and in the solution, respectively, $I_{a,l}$ is the anodic limiting current for the oxidation of HQ species and the other terms have their usual meanings. Then, Eq. (2.65) was applied to POAP films with different degrees of deactivation in order to obtain the parameter κD_s, which represents a measure of the rate of diffusion of redox species incorporated into the deactivated film. It was observed in [59] that at constant c_o, experimental $I_{a,l}^{-1}$ versus $\Omega^{-1/2}$ representations for deactivated POAP films give linear diagrams with the same slope but different intercepts on the ordinate axis (Fig. 2.66).

By using a linear regression method authors determined the intercept at $\Omega \rightarrow \infty$ of these Koutecky–Levich plots at different θ_c values, and then κD_s was extracted from the first term of Eq. (2.65). Table 2.11 shows that the parameter κD_s decreases with the increase of the deactivation.

Authors were not able to separate κ from D_s. However, they attribute the κD_s decrease to the κ decrease. In this regard, authors assumed that the high degree of swelling, as a direct result of solvent ingress to compensate changes in the charge density within the film (proton inclusion and/or anion exclusion during reduction and the reverse during oxidation), are absent in a deactivated film. Then, as θ_c increases the poor electrolyte permeation would lead to low κ values, which would make the solute electroactive diffusion within the film difficult.

Besides RDEV experiments, *ac* impedance measurements were performed in Ref. [59] with nondeactivated POAP films and POAP films with different θ_c

Fig. 2.66 Koutecky–Levich plots ($I_{a,l}$ vs. $\Omega^{-1/2}$) for different deactivated POAP films. (a) $\theta_c = 0$; (b) $\theta_c = 0.13$; (c) $\theta_c = 0.27$. Film thickness: 60 nm. Electrolyte: 0.1 M HClO$_4$ + 0.4 M NaClO$_4$ + 2 × 10^{-3} M (HQ/Q) solution. $E = 0.8$ V [59]
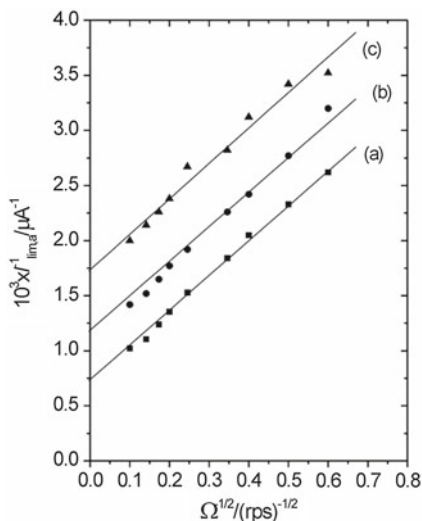
Table 2.11 Diffusion rate, κD_s, of hydroquinone species at different degrees of deactivation, θ_c

θ_c	$10^8 \ \kappa D_s^a / cm^2 \ s^{-1}$
0	2.0
0.13	1.24
0.42	0.88

^{a} Diffusion rate values of hydroquinone species extracted from Koutecky–Levich plots
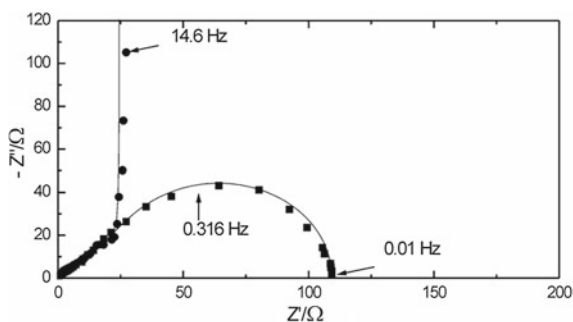
Fig. 2.67 *Ac* Impedance diagrams in the Nyquist co-ordinates ($-Z''$ vs. Z) obtained at $E = -0.3$ V for a non-deactivated POAP film (●) contacting a 0.1 M HClO$_4$ + 0.4 M NaClO$_4$ solution. The same POAP film (■) contacting a 0.1 M HClO$_4$ + 0.4 M NaClO$_4$ + 2 × 10^{-3} M (HQ/Q) solution. Rotation rate, $\Omega = 300$ rpm *Discrete points* are experimental data and *continuous lines* represent the fitting by using the theory given in Ref. [59]

values. The measurements were carried out, firstly, only in the presence of the supporting electrolyte solution, and then, in a solution of equimolar concentrations of *p*-benzoquinone (Q) and hydroquinone (HQ) species (0.1 M HClO$_4$ +

0.4 M NaClO$_4$ + 2 × 10^{-3}M (Q/HQ). A potential value $E < 0.0$ V was selected to obtain impedance diagrams, where POAP acts as mediator in the reduction process of *p*-benzoquinone. In the supporting electrolyte, Nyquist diagrams of a nondeactivated POAP film show a Warburg region at high frequency followed by a pseudo-capacitive increase (Fig. 2.67).

However, for a deactivated POAP film, a high-frequency semicircle appears on the impedance diagram (Fig. 2.68). The presence of a high-frequency semicircle on the Nyquist diagram of deactivated POAP films was considered indicative of a lower value of the standard electrochemical rate constant k_{sh} (high charge-transfer resistance at the gold|POAP interface), as compared with the value corresponding to a nondeactivated film. Authors remark that this high charge-transfer resistance is consistent with the low reactivity of the redox sites in a deactivated film, as found by stationary current–potential measurements. In the presence of the HQ/Q redox couple, impedance diagrams of a deactivated POAP film exhibit two loops (Fig. 2.68). However, a nondeactivated POAP film only shows one loop at low frequency (Fig. 2.67).

For deactivated POAP films, it was found that while the loop at low frequency is Ω dependent (Fig. 2.69), the high-frequency semicircle is independent of this variable. However, the size of the high-frequency semicircle depends on the degree of deactivation (θ_c). In this regard, at a given Ω value, the higher the θ_c value is, the greater the high-frequency semicircle becomes. In Fig. 2.70, impedance diagrams of a non-deactivated POAP film are compared with those of the same film, firstly deactivated by soaking in a ferric cation solution to reach a θ_c value of 0.43 and then, reactivated by treatment with a 0.1 M NH$_4$OH solution, where θ_c was reduced to 0.27. A larger high-frequency semicircle is observed for $\theta_c = 0.43$ as compared with that for $\theta_c = 0.27$.

The impedance results reported in Ref. [59] were quantitatively interpreted in another work of the same author [60], on the basis of the general theory of *ac*
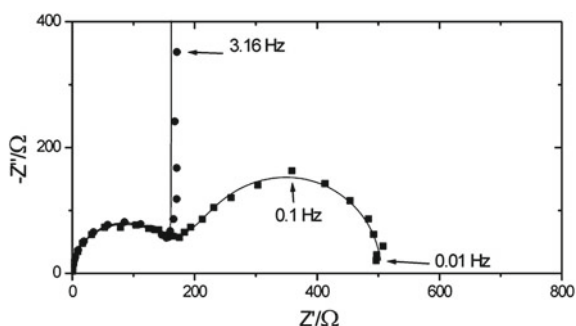
Fig. 2.68   *Ac* Impedance diagrams in the Nyquist co-ordinates ($-Z''$ vs. Z) obtained at $E = -0.3$ V for a deactivated POAP film (●) contacting a 0.1 M HClO$_4$ + 0.4 M NaClO$_4$ solution. The same POAP film (■) contacting a 0.1 M HClO$_4$ + 0.4 M NaClO$_4$ + 2 × 10^{-3} M (HQ/Q) solution. Rotation rate, $\Omega = 600$ rpm. $\theta_c = 0.27$ *Discrete points* are experimental data and *continuous lines* represent the fitting by using the theory given in Ref. [59]
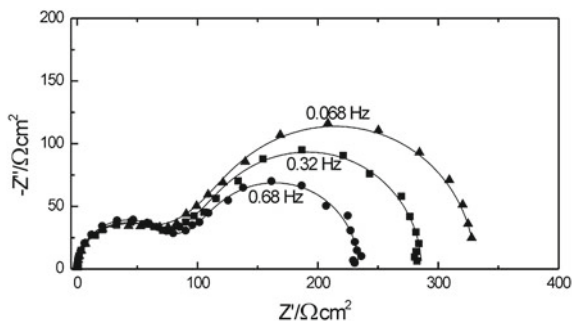
Fig. 2.69 *Ac* Impedance diagrams in the Nyquist co-ordinates ($-Z''$ vs. Z) obtained at $E = -0.3$ V for the film (*1*) of Table 2.1, $\theta_c = 0.13$. The different diagrams correspond to different electrode rotation rates, Ω : (▲) 1000 rpm; (■) 1500 rpm: (●) 2600 rpm. Electrolyte: 0.1 M HClO$_4$ + 0.4 M NaClO$_4$ + 2 × 10^{-3}M (HQ/Q) solution. *Discrete points* are experimental data and *continuous lines* represent the fitting by using the theory given in Ref. [59]

impedance described in Ref. [58] (see continuous lines on impedance diagrams of Figs. 2.67, 2.68, 2.69 and 2.70). This theory was developed within the framework of the assumption that the redox active species are present in the solution phase and they participate in the interfacial electron exchange with the polymer at the film|solution boundary. In this way, a complete series of charge-transport parameters, electron and ion diffusion coefficients, interfacial resistances and capacitances as a function of the degree of deactivation were obtained in Ref. [60].

The theory described in Ref. [58] is based in Eq. (2.66):

$$Z_{m|film|es} = R_{m|f} + R_f + R_s + \left[Z_e^{f|s} R_i^{f|s} + W_f Z_{12}^m \right] \left(Z_e^{f|s} + R_i^{f|s} + 2W_f \coth 2v \right)^{-1} \quad (2.66)$$
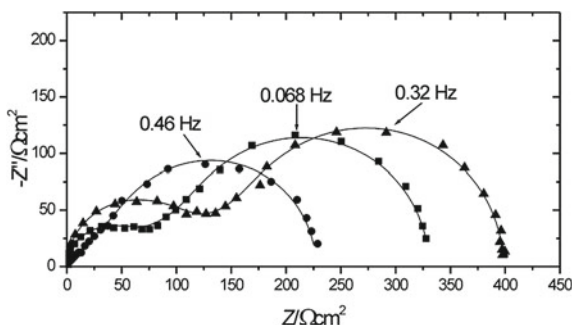
Fig. 2.70 *Ac* Impedance diagrams in the Nyquist co-ordinates ($-Z''$ vs. Z) obtained at $E = -0.3$ V and a constant electrode rotation rate, $\Omega = 1000$ rpm, for: (●) a non-deactivated POAP film ($\theta_c = 0$); (▲) the same film after deactivation ($\theta_c = 0.43$) and (■) the same film after reactivation ($\theta_c = 0.27$). Electrolyte: 0.1 M HClO$_4$ + 0.4 M NaClO$_4$ + 2 × 10^{-3}M (HQ/Q) solution. *Discrete points* are experimental data and *continuous lines* represent the fitting by using the theory given in Ref. [58]

where

$$Z_{12}^m = Z_e^{f|s}[\coth v + (t_e - t_i)^2 \tanh v] + R_i^{f|s} 4t_i^2 \tanh v + W_f 4t_i^2 \qquad (2.67)$$

In Eqs. (2.66) and (2.67):

$v = \left[\left(j\omega\phi_p^2\right)\big/4D\right]^{1/2}$ is a dimensionless function of the frequency ω, ϕ_p is the film thickness, D is the binary electron–ion diffusion coefficient, and t_i and t_e are the migration (high frequency) bulk-film transference numbers for anions and electrons, respectively. D is defined as $D = 2D_iD_e(D_e + D_i)^{-1}$ and $t_{i,e} = D_{i,e}(D_e + D_i)^{-1}$, where D_e and D_i are the diffusion coefficients for the electrons and ion species, respectively.

$W_f = \left[v/j\omega\phi_pC_p\right] = \Delta R_f/v$ is a Warburg impedance for the electron–ion transport inside the polymer film. $\Delta R_f(= \phi_p/4DC_p)$ is the amplitude of the Warburg impedance inside the film, and C_p is the redox capacitance per unit volume.

$R_f(= \phi_p/\kappa)$ is the high-frequency bulk-film resistance, R_s the ohmic resistance of the bulk solution (κ is the high-frequency bulk conductivity of the film), $R_{m|f}$ is the metal|film interfacial electron-transfer resistance, and $R_i^{f|s}$ is the film|solution interfacial ion-transfer resistance.

$Z_e^{f|s} = (R_e^{f|s} + W_s)$ is the electronic impedance, where $R_e^{f|s}$ is the interfacial electron-transfer resistance at the film|solution interface and W_s is the convective diffusion impedance of redox species in solution, which contains the bulk concentrations of ox(red) forms, $c_{ox}(c_{red})$, and their diffusion coefficients inside the solution, $D_{ox}(D_{red})$. Also, it contains the Nernst layer thickness, δ.

$R_e^{f|s}$ is defined as

$$R_e^{f|s} = RT\left(nF^2k_0c_{red}\right)^{-1} \qquad (2.68)$$

where k_0 is the rate constant of the reaction between the film and the redox active forms in solution. Diffusion of the redox forms from the bulk solution to the film|solution interface can be regarded as stationary through the diffusion layer thickness, expressed in cm by

$$\delta = 4.98D_{ox,red}^{1/3}\eta^{1/6}\Omega^{-1/2} \qquad (2.69)$$

where η is the kinematic viscosity of the solution in the same units as $D_{ox,red}$, and Ω the rotation rate of the disk electrode in rpm. The rest of the constants have their usual meaning. This model also includes the impedance behavior of the polymer contacting the inactive electrolyte (absence of the redox couple in solution) by considering $Z_e^{f|s} \to \infty$ in Eq. (2.66).

In the simulations used in Ref. [60], the number of transferred electrons, n, was assumed to be 0.44, and diffusion coefficient values of the redox species (Q and HQ) were considered equal, $D_{ox,red} = 1.5 \times 10^{-5}$ cm^2 s^{-1}. Also, the bulk concentrations of the redox substrate species were considered equal

($c_{ox} = c_{red} = 2 \times 10^{-6}$ mol cm^{-3}). The polymer thickness was considered as $\phi_p = 60$ nm. The value of the total redox site concentration of POAP was considered as $c_o = 4.7 \times 10^{-3}$ mol cm^{-3}. Then, the other parameters contained in Eq. (2.66) (R_{mlf}, R_i^{fls}, R_e^{fls}, C_p, D_e and D_i) were calculated from the experimental impedance data employing a fitting procedure based on the CNLS (Complex Nonlinear Squares) method. The first three parameters (R_{mlf}, R_i^{fls} and R_e^{fls}) were varied without restraints during the fitting. However, some reference values were considered for C_p, D_e and D_i. In this regard, for the film thickness used in Ref. [60] ($\phi_p = 60$ nm) and solution $pH = 1$, D_e and D_i values were allowed to vary within the range 10^{-7}–10^{-11} cm^2 s^{-1}, in such a way that diffusion coefficient values lower than 10^{-11} were considered not realistic. Concerning C_p, reference values were extracted from experimental $-Z''$ versus ω^{-1} slopes of impedance diagrams at sufficiently low frequency (in the absence of the redox substrate in solution). A contribution of the interfacial capacitance, C_H, also considered as a fitting parameter, was included in order to represent the actual impedance diagrams from the calculated ones.

The dependences of the different charge-transport and charge-transfer parameters on θ_c, extracted from the fitting procedure described in [60], are shown in Figs. 2.71, 2.72, 2.73, 2.74, 2.75, 2.76, and 2.77.

C_p versus θ_c dependence is shown in Fig. 2.71. Starting from a C_p value of about 27 F cm^{-3}, for a nondeactivated film, a decrease of C_p with increasing θ_c is observed.

The author of Ref. [60] remarks that C_p values correspond to the reduced state of POAP. R_{mlf} exhibits an almost continuous increase from the beginning of the deactivation, that is, from $\theta_c = 0$ to $\theta_c = 0.6$ (Fig. 2.72). This increase was considered consistent with an increasing number of inactive sites at the metal|polymer interface, as the deactivation becomes more pronounced [59]. R_i^{fls} as a function of θ_c (Fig. 2.73) exhibits a different feature as compared with R_{mlf}.

While a strong R_i^{fls} increase is observed within the range $0 < \theta_c < 0.35$, a less pronounced increase is obtained at values of $\theta_c > 0.4$. Author [60] indicates that it is possible that the R_i^{fls} increase was related to the inhibition of the protonation reaction of surface redox sites during POAP deactivation. Also, the increase in the diameter of the HF loop of the impedance diagrams observed with increasing θ_c in [59] was assigned not only to a R_{mlf} increase but also to a marked contribution of R_i^{fls}. R_e^{fls} values were extracted from Eq. (2.68) using k_o as fitting parameter ($0.1 < k_0 < 1$ cm s^{-1}). Within the whole range of θ_c values, the electron-transfer resistance R_e^{fls} at the polymer|solution interface (Fig. 2.74) shows a similar feature to that of R_{mlf}.

However, R_e^{fls} results almost one order of magnitude lower than both R_{mlf} and R_i^{fls}. With regard to C_H values, starting at a value of around 17 μF cm^{-2} for a nondeactivated, it decreases in a nearly continuous way as the degree of deactivation increases, reaching a value of about 5 μF cm^{-2} for the maximum $\theta_c(\sim 0.6)$ value (Fig. 2.75). The C_H decrease, in the same way as the R_{mlf} increase, was attributed to the creation of inactive gaps in the redox site configuration at the polymer|metal interface with deactivation.

Fig. 2.71 Redox capacitance (C_p) as a function of θ_c: Deactivated (■) and reactivated (▲) films. (+) Value corresponding to the freshly prepared POAP film. Electrolyte: 0.1 M HClO$_4$ + 0.4 M NaClO$_4$ + 2 × 10^{-3}M (HQ/Q) solution [60]
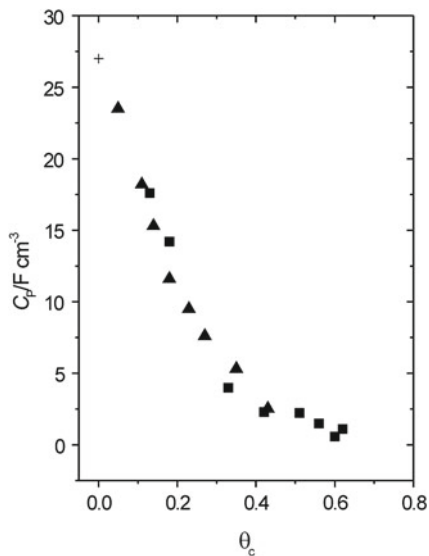
Fig. 2.72 Metal–polymer interfacial electron-transfer resistance ($R_{m/f}$) as a function of θ_c. The same symbols and conditions as indicated in Fig. 2.71
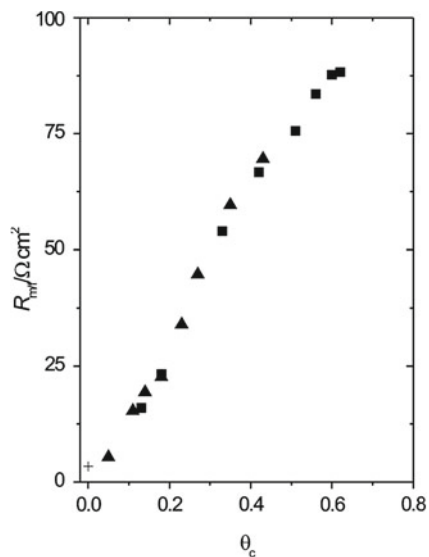
The author of Ref. [60] remarks that when deactivated POAP films are reactivated by alkaline treatment, all dependences $(C_p, R_{m|f}, R_e^{f|s}, R_i^{f|s}$ and C_H versus θ_c) (Figs. 2.71, 2.72, 2.73, 2.74 and 2.75) do not exhibit hysteresis within the whole θ_c range. All these dependences exhibit a univocal correspondence between deactivation and subsequent reactivation. However, this is not the case for

Fig. 2.73 Polymer–solution interfacial ion-transfer resistance ($R_i^{f/s}$) as a function of θ_c. The same symbols and conditions as indicated in Fig. 2.71
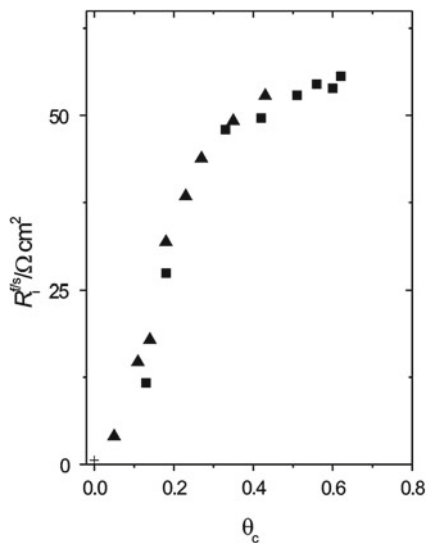
Fig. 2.74 Interfacial electron-transfer resistance ($R_e^{f/s}$) as a function of θ_c. The same symbols and conditions as indicated in Fig. 2.71
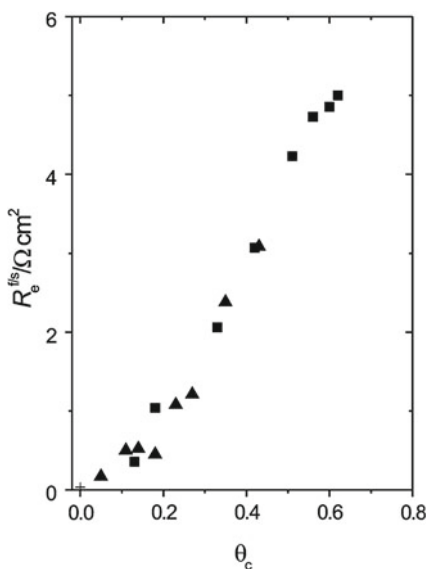
the dependences that involve diffusion coefficients for electron (D_e) and ion (D_i) transport. These dependences are shown in Figs. 2.76 and 2.77, respectively. Even though both dependences seem to show a univocal correspondence between deactivation and subsequent reactivation for θ_c values lower than 0.4, a hysteresis phenomenon is observed after the reactivation of films with θ_c values higher than 0.5.

Fig. 2.75 Interfacial capacitance (C_H) at the metal–polymer interface as a function of θ_c. The same symbols and conditions as indicated in Fig. 2.71
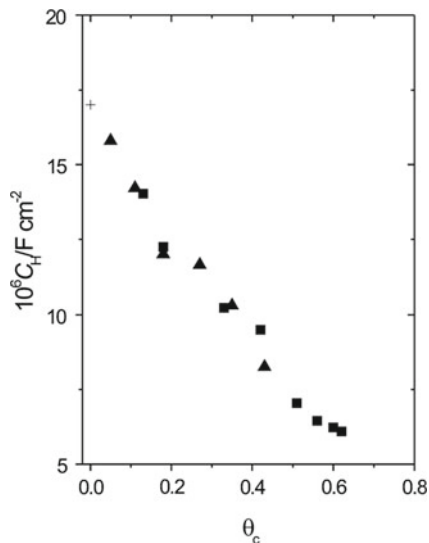
Fig. 2.76 Electron diffusion coefficient (D_e) as a function of θ_c. Numbers 1 to 8 represent each one of the eight films listed in Table 2.10. The same symbols and conditions as indicated in Fig. 2.71
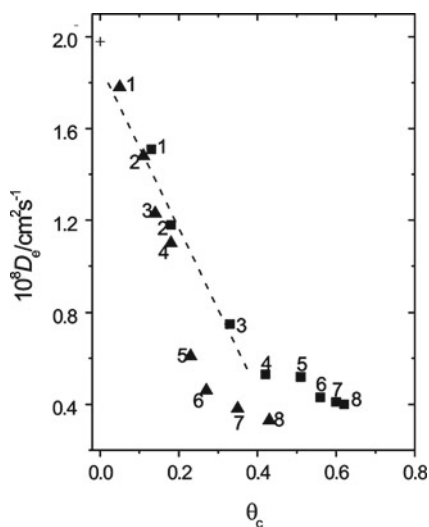
The univocal D_e versus θ_c dependence within the deactivation range $0 < \theta_c < 0.4$ was linear with a slope $\Delta D_e / \Delta \theta_c = -1.6 \times 10^{-8}$ cm^2 s^{-1}. The decrease of D_e with the increase of θ_c shown in Fig. 2.76 was attributed to an increase of the hopping distance between remnant redox active sites after deactivation [60]. In order to explain the D_e decrease with θ_c, the author [60] invokes the expression of the electron diffusion coefficient, $D_e = a^2 k_0$, which is given in terms of the mean distance a, between adjacent redox sites and k_o is the

Fig. 2.77 Ion diffusion coefficient (D_i) as a function of θ_c. Numbers *1* to *8* represent each one of the eight films listed in Table 2.10. The same symbols and conditions as indicated in Fig. 2.71
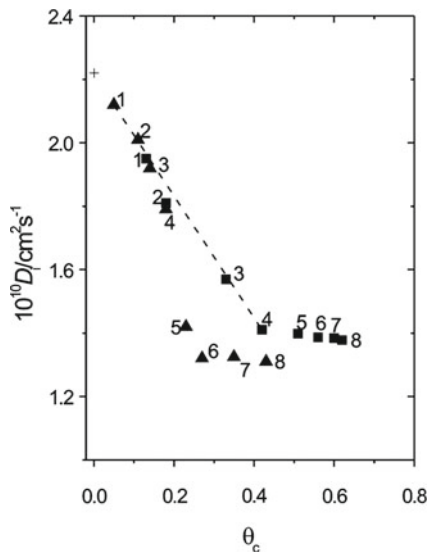
intermolecular electron-transfer rate constant that exhibits an exponential dependence on *a*.

The hysteresis phenomenon during the reactivation process was attributed in Ref. [60] to a lack of relaxation of the configuration of redox sites of a film that was strongly deactivated ($\theta_c > 0.5$). This lack of relaxation was associated with the poor swelling effect at the reduced state of the polymer. With regard to ion transport, the D_i versus θ_c dependence (Fig. 2.77) exhibits the same characteristics as the D_e versus θ_c dependence.

A univocal correspondence was observed between deactivation and reactivation, for θ_c values lower than 0.4 with a slope value of $\Delta D_i / \Delta \theta_c = -2.0 \times 10^{-10} \, \text{cm}^2 \, \text{s}^{-1}$. A change of slope was also observed at about $\theta_c \sim 0.5$. D_i was related to proton movements inside the polymer film rather than to anion transport.

2.5 Concluding Remarks About the Charge Conduction at POAP Films

Different electrochemical techniques applied to studying the charge conduction through POAP film electrodes indicate the existence of a charge-transport process that is diffusion-limited. It was suggested that this charge transport might be electron hopping with the necessarily charge-compensating counter-ion motion. In this regard, effective or apparent diffusion coefficient values were extracted from electrochemical measurements. Particularly, from impedance techniques it was possible to separate the charge transport process within POAP films in terms of ion

(D_i) and electron (D_e) contributions. D_e values are nearly two orders of magnitude lower than D_i values. This is indicative of a conduction mechanism dominated by electron transport. The conductivity of POAP was also interpreted on the basis of percolation theories. In this connection, a charge-transfer diffusion-controlled process within the potential range 0.11–0.15 V (Ag|Ag/Cl) was observed. Other kinetic parameters, such as the electrochemical standard rate constant, k^0, and the charge transfer coefficient, α, were also determined for POAP film electrodes. Values of k^0 within the range 10^4–10^6 cm s^{-1} have been reported. In some papers it was indicated that charge transfer through POAP films is complicated by irreversible injection processes at the film interfaces.

The conductivity potential range of POAP was explained on the basis of the polaron-bipolaron model. By employing ESR measurements, the existence of a conductivity maximum within the potential range -0.24 to 0.0 V (SCE) was established. The decrease and further absence of a detectable ESR signal, at potential values above 0.55 V (SCE), was attributed to a combination of radicals to give rise to dication species. EIS measurements also seem to indicate the existence of a conducting potential range between 0.1 and 0.6 V (NHE). On the basis of percolation theories, the percolation threshold during insulating-conducting transition was found to be in the range 0.15–0.17 V (Ag|Ag/Cl).

Effective diffusion coefficient values for POAP are two or three orders of magnitude lower than those determined for polyaniline. This was attributed to the different molecular structure and segment mobility of polymer chains. The presence of electron-donor substituents in the benzene rings of POAP should cause some loss of conductivity.

Voltammetric and *ac* impedance measurements show that the electrochemical response of POAP depends strongly on the solution *pH*. A redox mechanism was proposed for the polymer, in which the redox reaction involves a process of addition/elimination of protons coupled with a reversible electron transfer. The protonation of the oxidised form of POAP was considered as the coupled chemical reaction. Some impedance measurements seem to indicate that one proton is released for each electron transferred in the oxidation process, thus electrochemical oxidation of the polymer was considered equal to its dehydrogenation. It was suggested that the *pH* affects the dynamics of the electron-hopping process through reduction of the active redox centre density. In this connection, the decreasing electron conductivity observed for POAP as the *pH* increases was explained considering a decrease of the intermolecular electron-transfer rate constant between two adjacent redox sites with the polymer deprotonation.

The participation of supporting electrolyte anions in the charge-transport process of POAP was also studied. While some techniques, such as EQCM, seem to indicate that perchlorate anions do not participate in the redox reaction of the polymer, others, such as PBD, show that even when the insertion of protons is the dominant process during the reduction scan, during the positive direction not only protons but also perchlorate anions are exchanged between the solution and the polymer. By EIS it was observed that electron and ion coefficient values increase as the concentration of perchlorate anions increases.

With regard to the film thickness effect on the charge conduction process of POAP, it was observed that thin films exhibit a lower conductivity as compared with thick ones. This effect is clearly reflected in the ion and electron diffusion coefficient values extracted from EIS. Both parameters increase as the film thickness increases. This effect of the film thickness on the conduction properties was explained in terms of a polymer structure that changes when the film thickness increases. In this connection, while thin films are continuous, compact and non-porous, thick films are porous and more permeable to external electrolyte solution. Thus, electrolyte incorporated into a thick film should give rise to a higher rate of the charge-transport process as compared with that in a thin film.

The redox mediation of POAP on different redox couples in solution was analyzed by employing Cyclic Voltammetry and Rotating Disc Electrode Voltammetry. In some cases cathodic limiting currents, which are independent of the concentration of the redox couple in solution, are observed but they depend on the polymer film thickness. This was considered as an indication of current control by charge transfer across the polymer film. Conversely, in other cases limiting currents independent of the polymer thickness but dependent on the redox substrate concentration in solution were observed. In this latter case limiting currents must be controlled by the kinetics of the electron transfer at the polymer|solution interface. Anodic currents corresponding to oxidation of redox species that penetrate through POAP films to reach the metal surface were also observed. These anodic currents were employed to calculate physical diffusion rates of redox species across POAP films. It was observed that the electron transport through POAP is slower than the physical diffusion of redox species into the polymer. However, the physical diffusion rate of some redox active species across POAP films is comparable with the transport rate of electroinactive ions (perchlorate) into the polymer. The conducting potential range of POAP was analysed in the presence of redox active species. Some authors indicate that positive species that are reduced at potentials lower than the formal potential of POAP could not be reduced above such potential, with the exception of protons. However, species that have formal potential values more positive than the formal potential of POAP could be oxidised easily. Thus, it was concluded that the polymer is conductive in the oxidised state and non-conductive in the reduced one. Other authors have demonstrated that POAP is conductive at negative potentials. In this connection, it was reported that the conductivity of POAP as a function of potential increases sharply at approximately -0.067 V (SCE), peaks at approximately -0.120 V (SCE) and starts to decrease at more negative potential values.

With regard to the stability POAP film electrodes, they maintain their voltammetric response, at least for a day, provided that the positive potential limit does not exceed 0.5 V (SCE). However, after continuous cycling during several days, the polymer starts to show the characteristics of degradation. Also, if a freshly prepared film is subjected to a positive potential limit beyond 0.5 V (SCE), the voltammetric response, and more clearly the impedance response, shows a decrease in the film conductivity.

2.6 Some Critical Viewpoints About Charge Transport Parameter Values of Poly(o-aminophenol) Film Electrodes

It is evident that application of electrochemical models to interpret experimental results in the field of electroactive polymers is often complicated by concurrent difficulties that are not only theoretical but also experimental. In this connection, most of the impedance models employed to obtain transport parameters of POAP films assume the existence of a homogeneous (uniform) polymer layer on a smooth electrode surface. However, from the theory of porous electrodes and relevant electrochemical studies, it is known that their impedance behaviour differs from that of electrodes with a smooth surface. In some papers [39–41, 57, 59, 60] a thin gold film deposited under high vacuum conditions (10^{-7} Torr) was employed as base metal to deposit POAP films. In this way it was expected to reduce, at atomic scale, surface defects of the base electrode. On studying "size effects" [39] on thin gold films employed in Refs. [39–41] a value of the specularity parameter, $p \sim 0.91$, was estimated. The p value correlates with the roughness of the metal surface topography and the presence of surface defects. More precisely, this parameter represents the probability of an electron being reflected specularly or diffusely (due to the presence of defects) at the metal film surface. The p value ranges from 0, for complete diffuse scattering, to 1 for complete specular scattering. Thus, imperfections should lead to experimental p values much lower than 1. In this connection, p values of gold films employed in Refs. [36–41, 59, 60] are high enough ($p \sim 0.91$) to assume a low amount of surface defects on an atomic scale, as compared with the surface of a bulk electrode mechanically polished to deposit the polymer film.

With regard to the structure of the polymer layer, it was proved [49, 50] that when a 2.8 mC cm^{-2} thick POAP film covers a metal surface, ions from the electrolyte solution do not interact with the metal electrode, which should be indicative of the existence of a relatively compact polymer layer on the metal surface. Then, some papers as in Ref. [59, 60], where a thin gold film deposited by vacuum evaporation was employed as base electrode to deposit a thick POAP film on it, seem to justify the application of a homogeneous electrochemical impedance model to interpret experimental impedance diagrams. However, the thickness of the polymer film is always a critical parameter. In general, thickness is estimated from the charge consumed in reducing the polymer film [13, 15]. In some papers, the films were grown to approximately the desired thickness by employing a reduction charge versus ellipsometric thickness working curve [3, 21, 40–42]. In this connection, it was indicated that voltammetric responses of POAP result from two different processes. The former corresponds to a background film conduction, similar to that observed for the base electrode (unmodified electrode), while the latter is determined by the proper redox process of the film. Charge values corresponding to these different contributions are not always easy to separate in order to estimate film thickness values. It was suggested that the background conductance of the films most likely results from some residual charge in their bulk and their porosity.

There is evidence about the dependence of transport parameters of POAP on both film thickness and concentration of the external electrolyte solution [18]. This effect was explained considering that the polymer structure changes as the film thickness increases. In this regard, while thick POAP films seem to exhibit open structures that allow incorporation of the electrolyte into the polymer layer, thin films are compact enough to prevent the electrolyte incorporation. In this regard, the high permeability of some polymer films to transport redox species from the solution in contact with the polymer to the metal substrate was attributed to dispersed polymer structures with imperfections (*e.g.* pinholes and large channels) with large dimensions compared to those of species present in solution [54]. This effect should be taken into account when mechanism diagnosis criteria from steady-state polarisation curves for redox mediation at electroactive polymer-coated electrodes are considered, because redox species in solution could reach the metal surface by transport through pores in the polymer layer.

Complex impedance is one of the major techniques for the experimental study of electroactive polymer films. However, it should be taken into account that the estimation of transport parameters values of POAP, such as diffusion coefficient values, D, is often hardly possible on the basis of impedance spectra, because of the absence of a well-defined Warburg region for this polymer. In this connection, D values were obtained with an error of 50 % [15]. Besides, in some papers it is indicated that impedance measurements cannot be performed for frequencies lower than 0.1 Hz due to the noise fluctuations observed in this frequency region. In this regard, it was indicated that the estimated error in the values of the low-frequency resistance obtained from impedance spectra was around 30 % because of the overlap of the charge-transfer and the diffusion-controlled regions. The observed peculiarities at low-frequency impedance of POAP films were attributed to porosity effects [11].

With regard to impedance models, the general theory of *ac* impedance described by Vorotyntsev [58] was applied in Refs. [59, 60] to interpret experimental impedance spectra of POAP in the presence of active redox species in solution. However, this theory was developed within the framework of the assumption that the redox active species is only present in the solution phase but not inside the polymer film, and they participate in the interfacial electron exchange with the polymer at the film|solution boundary. However, it should be taken into account that this theory is strictly valid when charging of the interfacial double layers is negligible, that is, the theory does not account for charging the film|substrate and the film|solution layers in parallel with the process of injection of charge carriers. If this is not the case, a more complete model such as that developed by Vorotyntsev in Ref. [61] should be used. In Ref. [61], besides the traditional "double layer" capacitance and interfacial charge transfer resistances, two additional parameters for each boundary, "interfacial numbers" for each species and "asymmetry factors", are introduced. However, it should be indicated that even when the authors of Ref. [59] attempted to fit experimental impedance spectra by means of the *ac* impedance model presented in Ref. [61], the fitting was not much more precise than that obtained by applying the theory given in Ref.

[58]. Furthermore, the increasing mathematical difficulty of determining the numerous parameters of the model given in Ref. [61] from experimental data was remarked. Also, from the physical viewpoint, in some cases diffusion or incorporation of different species into polymer films could alter the molecular structure of the polymeric film, and then, its physical properties. Thus, application of models in these cases should only allow obtaining fitting parameters that do not represent the real physical properties of the system. Even when different authors do not expect a complete coincidence of the electrochemical properties of the polymer film with those predicted by theoretical models, qualitative agreements are often considered satisfactory enough to obtain information about electroactive polymers.

References

1. Barbero, C., Silber, J.J., Sereno, L.: Electrochemical properties of poly-*ortho*-aminophenol modified electrodes in aqueous acid solutions. J. Electroanal. Chem. **291**, 81 (1990)
2. Bard, A.J., Faulkner, L.R.: Electrochemical Methods. Fundamentals and Applications. Wiley, New York (1980)
3. Barbero, C., Zerbino, J., Sereno, L., Posadas, D.: Optical properties of electropolymerized orthoaminophenol. Electrochim. Acta **32**, 693 (1987)
4. Gabrielli, C., Takenouti, H., Haas, O., Tsukada, A.: Impedance investigation of the charge transport in film-modified electrodes. J. Electroanal. Chem. **302**, 59 (1991)
5. Nicholson, R.S.: Theory and application of cyclic voltammetry for measurements of electrode reaction kinetics. Anal. Chem. **37**, 1351 (1965)
6. Laviron, E.: Theoretical study of a reversible reaction followed by a chemical reaction in thin layer linear potential sweep voltammetry. J. Electroanal. Chem. **39**, 1 (1972)
7. Konopelnik, O.I., Aksimentyeva, O.I., Grytsiv, M.Ya.: Electrochromic transitions on polyaminoarene films on the transparent electrodes. Mater. Sci. **20**, 49–59 (2002)
8. Maksimov, Y.M., Khaldum, M., Podlovchenko, B.I.: Electrocatalysis on polymer-modified electrodes. Elektrokhimiya **27**, 739 (1991)
9. Dobosh, D.: Electochemical Constants. Ed. Mir., Moscow (1980)
10. Foot, P.J.S., Simon, R.: Electrochromic properties of conductiong polyanilines. J. Phys. D: Appl. Phys. **22**, 159 (1989)
11. Levin, O., Kondratiev, V., Malek, V.: Charge transfer processes at poly-o-phenylenediamine and poly-o-aminophenol films. Electrochim. Acta, **50**, 1573 (2005)
12. Ohsaka, T., Kunimura, S., Oyama, N.: Electrode kinetics of poly(o-aminophenol) film prepared by electro-oxidative polymerization of o-aminophenol and its electrochromic properties. Electrochim. Acta **33**, 639 (1988)
13. Barbero, C., Tucceri, R.I., Posadas, D., Silber, J.J., Sereno, L.: Impedance characteristics of poly(o-aminophenol) electrodes. Electrochim. Acta, **40**, 1037 (1995)
14. Chidsey, C.E.D., Murray, R.W.: Redox capacity and direct current electron conductivity in electroactive materials. J. Phys. Chem. **90**, 1479 (1986)
15. Komura, T., Ito, Y., Yamaguti, T., Takahasi, K.: Charge-transport processes at poly-o-aminophenol film electrodes: electron hopping accompanied by proton exchange. Electrochim. Acta **43**, 723 (1988)
16. Mathias, M.F., Haas, O.: An alternating current impedance model including migration and redox-site interactions at polymer-modified electrodes. J. Phys. Chem. **96**, 3174 (1992)
17. Armstrong, R.D.: Impedance plane display for an electrode with diffusion restricted to a thin layer. J. Electroanal. Chem. **198**, 177 (1986)

18. Rodríguez Nieto, F.J., Posadas, D., Tucceri, R.: Effect of the of the bathing Electrolyte Concentration on the Charge Transport Process at Poly(o-aminophenol) Modified Electrodes. An ac Impedance study. J. Electroanal. Chem. **434**, 83–91 (1997)
19. Albery, W.J., Elliot, C.M., Mount, A.R.: A transmission line model for modified and thin layer cells. J. Electroanal. Chem. **288**, 15 (1990)
20. Albery, W.J., Mount, A.R.: A further development of the use of transmission lines to describe the movement of charge in conducting polymers. J. Electroanal. Chem. **388**, 1 (1995)
21. Rodríguez Nieto, F.J., Tucceri, R.: The pH Effect on the Charge Transport at Redox Polymer-Modified Electrodes. An ac Impedance Study applied to Poly(o-aminophenol) Film Electrodes. J. Electroanal. Chem. **416**, 1–24 (1996)
22. Kunimura, S., Ohsaka, T., Oyama, N.: Preparation of thin polymeric films on electrode surfaces by electropolymerization of o-aminophenol. Macromolecules **21**, 894 (1988)
23. Tucceri, R.: A review about the charge conduction process at poly(o-aminopenol) film electrodes. Open Phys. Chem. J. **4**, 62 (2010)
24. MacDiarmid, A.G., Kaner, R.B.: In: Handbook of Conducting Polymers, T.A. Skotheim (ed.), vol. 1, p. 689. Marcel Dekker, New York (1986)
25. Huang, W.S., Hamphrey, B.D., MacDiarmid A.J.: Polyaniline, a novel conducting polymer. Morphology and chemistry of its oxidation and reduction in aqueous electrolytes. J. Chem. Soc. Faraday Trans. 1, **82**, 2385 (1986)
26. Chattaraj, A.P., Basumallik, I.N.: Improved conducting polymer cathodes for lithium batteries. J. Power Sources **45**, 237 (1993)
27. Tanaka, K., Shichiri, T., Yamabe, T.: Influence of polymerization temperature on the characteristics of polythiophene films. Synth. Met. **16**, 207 (1986)
28. Satoh, M., Kaneto, K., Yoshino, K.: Electrochemistry preparation of high quality poly(*p*-phenylene) film. J. Chem. Soc., Chem. Commun. **25**, 1629 (1985)
29. Chance, R.R., Boudreaux, D.S., Bredas, J.L., Silbey, R. In: T.A. Skotheim (ed.), Handbook of Conducting Polymers, vol. 2, p. 825. Marcel Dekker, New York (1986)
30. Ortega, M.: Conducting potential range of poly(o-aminophenol). Thin Solid Films **371**, 28 (2000)
31. Salvagione, H.J., Arias-Padilla, J., Pérez, J.M., Vázquez, J.L., Morallón, E., Miras, M.C., Barbero, C.: Study of the redox mechanism of poly(o-aminophenol) using in situ techniques: evidence of two redox processes. J. Electroanal. Chem. **576**, 139 (2005)
32. Tucceri, R.I., Barbero, C., Silber, J.J., Sereno, L., Posadas, D.: Spectroelectrochemical study of poly-o-aminophenol. Electrochim. Acta **42**, 919 (1997)
33. Malek, K.: Dynamic Monte-Carlo simulation of electrochemical switching of a conducting polymer film. Chem. Phys. Lett. **375**, 477 (2003)
34. Aoki, K.: Nernst equation complicated by electric random percolation at conducting polymer-coated electrodes. J. Electroanal. Chem. **310**, 1 (1991)
35. Aoki, K.: Simulation of electrochemical slow relaxation at electrically conducting polymer-coated electrodes based on the concept of percolation. J. Electroanal. Chem. **373**, 67 (1994)
36. Aoki, K., Teragashi, Y., Tokeida, M.: Light scattering of polyaniline films responding to electrochemical switching. J. Electroanal. Chem. **460**, 254 (1999)
37. Odin, C., Nachtschein, M.: Slow relaxation in conducting polymers. Phys. Rev. Lett. **67**, 1114 (1991)
38. Buck, R.P.: Electron hopping in one dimension: mixed conductor membranes. J. Phys. Chem. **92**, 4196 (1988)
39. Tucceri, R.: A review about the surface resistance technique in electrochemistry. Surf. Sci. Rep. **56**, 85 (2004)
40. Tucceri, R.I.: Surface resistance measurements on thin gold film electrodes coated with poly(o-aminophenol) films. J. Electroanal. Chem. **505**, 72 (2001)
41. Tucceri, R.I.: Specularity change of a thin gold film surface coated with poly(*o*-aminophenol) during the polymer redox conversion. The pH affect on the redox sites distribution at the metal‖polymer interface. J. Electroanal. Chem. **543**, 61 (2003)

42. Rodríguez, F.J., Tucceri, R.: Influencia del grado de oxidación y de la concentración del electrolito soporte sobre el transporte de carga de un polímero electroactivo. Información Tecnológica **9**, 109 (1988)

43. Rudnicki, J.D., Brisard, G.M., Gasteiger, H.A., Russo, R.E., McLarnon, F.R., Cairns, E.J.: Effect of the supporting electrolyte and beam diameter on probe beam deflection experiments. J. Electroanal. Chem. **362**, 55 (1993)

44. Gobal, F., Malek, K., Mahjani, M.G., Jafarian, M., Safarnavadeh, V.: A study of the fractal dimension of the electrodeposited poly-*ortho*-aminophenol films in presence of different anions. Synth. Met. **108**, 15 (2000)

45. Stromme, M., Niklasson, G.A., Granqvist, C.G.: Determination of fractal dimension by cyclic *I-V* studies: The Laplace-transform method. Phys. Rev. B **52**, 14192 (1995)

46. Malek, K., Gobal, F.: Application of chaotic logistic map for the interpretation of anion-insertion on poly-*ortho*-aminophenol films. Synth. Met. **113**, 167 (2000)

47. González, E.R.: Interpretation of the Power Response of a Fuel Cell with a Quadratic Logistic Differential Equation. J. Electrochem. Soc., **143**, L 113 (1996)

48. Rasband, S.N.: Chaotic Dynamics of Nonlinear Systems. Wiley, New York (1990)

49. Tucceri, R.: Application of the Surface Resistance technique to detect the different interactions of ClO_4^-, SO_4^{2-} and $C_6H_5SO_3^-$ anions and Cu(II) cation with a gold surface partially blocked with poly(o-aminophenol). J. Argent. Chem. Soc. **94**, 55 (2006)

50. Tucceri, R.: The metal/electroactive polymer interface studied by surface resistance. J. Surf. Eng. Mater. Adv. Technol. **3**, 205 (2013)

51. Ybarra, G., Moina, C., Florit, M.I., Posadas, D.: Redox mediation at electroactive polymer coated electrodes: Mechanistic diagnosis criteria from steady state polarization curves. J. Electroanal. Chem. **609**, 129 (2007)

52. Ybarra, G., Moina, C., Florit, M.I., Posadas, D.: Current rectification by mediating electroactive polymers. Electrochim. Acta **53**, 3955 (2008)

53. Bonfranceschi, A., Pérez Córdoba, A., Keunchkarian, S., Zapata, S., Tucceri, R.: Transport across poly(o-aminophenol) modified electrodes in contact with media containing redox active couples. A study using rotating disc electrode voltammetry. J. Electroanal. Chem. **477**, 1 (1999)

54. Ikeda, T., Schmehl, R., Denisevich, P., Willman, K., Murray, R.W.: Permeation of electroactive solutes through ultrathin polymeric films on electrode surfaces. J. Am. Chem. Soc. **104**, 2683 (1982)

55. Pinilla Macías, J.M., Hernández Hernández, L., Moreno Sobrino, J.M., Sevella Escribano, M.T.: Determination of paraquat by cathodic stripping voltammetry after accumulation through the formation of an ion pair on a hanging mercury drop electrode. Electroanalysis **79**, 5 (1993)

56. Rodríguez Nieto, F.J., Tucceri, R., Posadas, D.: EIS Detection of the Partial Oxidation of Polymers derived from Aryl Amines. J. Electroanal. Chem. **403**, 241 (1996)

57. Tucceri, R.: The effect of high positive potentials on the different charge transport and charge transfer parameters of poly(o-aminophenol) modified electrodes. A study using cyclic voltammetry, rotating disc electrode voltammetry and ac impedance measurements. J. New Mater. Electrochem. Syst. **8**, 305 (2005)

58. Vorotyntsev, M.A., Deslouis, C., Musiani, M.M., Tribollet, B., Aoki, K.: Transport across an electroactive polymer film in contact with media allowing both ionic and electronic interfacial exchange. Electrochim. Acta **44**, 2105 (1999)

59. Tucceri, R.I.: Redox mediation and permeation processes at deactivated poly(*o*-aminophenol) films. A study applying rotating disc electrode voltammetry and electrochemical impedance spectroscopy. J. Electroanal. Chem. **633**, 198 (2009)

60. Tucceri, R.I.: Charge transfer and charge transport parameters at deactivated poly(o-aminophenol) film electrodes. A study applying Electrochemical Impedance Spectroscopy. J. Electroanal. Chem. **659**, 83 (2011)

61. Vorotyntsev, M.A.: Impedance of thin films with two mobile charge carriers. Interfacial exchange of both species with adjacent media. Effect of the double layer charges. Electrochim. Acta **47**, 2071 (2002)

Chapter 3
Applications of Nonconducting Poly(*o*-aminophenol) Films in Bioelectrochemistry and Electrocatalysis

3.1 Introduction

Electron-conducting polymers can easily be switched between different states, just by changing the potential, i.e. by electrochemical oxidation and reduction. During this transformation a new polymeric material, which has chemical and physical properties substantially different from the initial one, is created. In these materials, besides the transport of species throughout the polymer film and the ion exchange at the polymer film-solution interface, a faradaic process occurs at the metal surface contacting the polymer film by electron transfer with the metal. These different processes are affected not only by the change of potential but also by changes in composition of the contacting fluid medium, e.g. varying H^+ concentration and film thickness [1] (see Chap. 2).

Poly(*o*-aminophenol) (POAP) [2–7] is a ladder polymer whose redox reaction was considered as an internal conversion between oxidized and reduced units that can be represented by the stoichiometry shown in Fig. 3.1 [8].

The polarization of POAP, at potentials more positive than 0.1 V (SCE), transforms the polymer predominantly into the quinonoid form, whereas the reduced units predominate only at negative potentials. This redox conversion of POAP must be accompanied by the proton exchange between the polymer and the solution. In this regard, the voltammetric response of POAP is highly dependent on the *pH*, being optimal at *pH* 3. At *pH* close to 5, the cathodic peak disappears completely, while for the anodic peak this occurs at *pH* 7 [9]. Parameters characterizing charge-transfer and charge-transport processes at POAP films and their dependences on the external electrolyte contacting the polymer have been estimated using different techniques [10–20] (see Chap. 2). On the basis of impedance measurements, it was found that both ion and electron conductivities of POAP decrease as the solution *pH* increases [12, 15]. The potential is another critical external variable that affects the electrochemical behavior of POAP. It was demonstrated that POAP remains electroactive when the potential is cycled from −0.2 V to 0.5 V (vs. SCE). However, POAP suffers irreversible deterioration when the positive potential limit is extended to values higher than a threshold
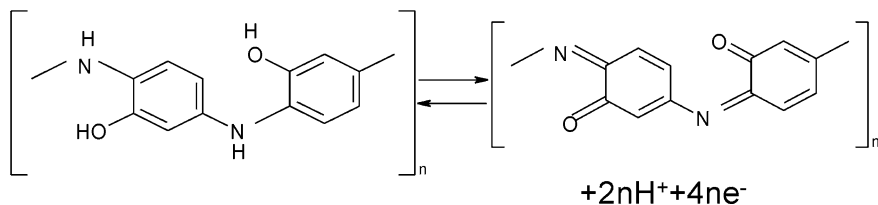
Fig. 3.1 Stoichiometry of redox reactions of POAP film electrodes [8]

value of 0.5 V (vs. SCE) [14]. Rotating Disc Electrode Voltammetry experiments demonstrated that the electron conductivity of POAP decreases as the polymer becomes more degraded [21]. On the basis of the Surface Resistance (SR) technique, this effect was attributed to a more extended configuration of redox sites at the metal-POAP interface after degradation, as compared with that of a film cycled only between $-0.2\ V < E < 0.5\ V$ (vs. SCE) [14]. With regard to POAP film thickness, it was observed that POAP films (thickness between 0.2 and 0.5 μm) deposited on ITO electrodes are compact and continuous with a uniform thickness over the whole film [3]. Also, by employing POAP-coated gold film electrodes it was possible to ensure that species of the external electrolyte do not interact with the thin gold film employed as base metal to deposit the polymer [12]. In the same sense, a study [22] about the permeability of POAP films to different redox ion species (Br^-, I^-, Tl^+, $Fe(CN)_6^{3-}$, Cu^{2+}, Cd^{2+}, Mn^{+2}, Co^{2+} and Cr^{3+}) showed that all the redox ions analyzed were unable to penetrate into POAP films, other than the Tl^+ ion which was able to partly permeate the films.

Despite a great number of studies reported in the literature about POAP synthesized in acidic media [2, 3, 5–8, 10–21], there is relatively little work that has been reported about electrochemistry of poly(*o*-aminophenol) in neutral and alkaline solutions [23]. POAP formed in neutral media leads to a nonconducting film that exhibits some advantages over the conducting film formed in acidic media. The film thickness of a nonconducting polymer is self controlled during electropolymerization, and a very thin and uniform film can be obtained. Also, nonconducting films prevent the diffusion of electroactive species from the electrolyte solution. These characteristic properties of POAP synthesized in neutral media (thickness uniformity and compactness, and low permeability) have practical applicability. POAP has usefully been employed in the development of different types of sensors, mainly biosensors based on immobilized enzymes and also, in the field of electrocatalysis. In biosensor applications, thin nonconducting POAP films are combined with different electroactive materials (carbon nanotubes, other polymers such as poly(*o*-phenylenediamine) and polypyrrole, hemoglobin, Prussian blue, etc.) in such a way that POAP acts as an effective barrier to protect the sensor from the interference of electroactive species. The permselectivity of a nonconducting POAP film synthesized at *pH* values over 3 was found to be suitable to reduce the effect of interferents, such as ascorbic acid, uric acid and acetaminophen, in different biosensors. Concerning the film thickness, a small

number of polymerization cycles (15 cycles) is found to be sufficient to obtain a compact and permselective film. In electrocatalysis, even though POAP has no apparent electrocatalytic activity by itself, POAP films have been employed to improve the activity of some electrocatalysts by increasing their active surface area. Another interesting characteristic of POAP in electrocatalysis is the presence of the electron-donating OH group next to the amine nitrogen that increases the electron density at amine sites. The OH group is also a potential coordinating site. These factors combine to provide a strong acceptor binding of POAP to several metal cations. In this regard, POAP was employed to develop stable electrocatalysts for oxygen reduction.

In this Chapter, the more relevant uses of poly(*o*-aminophenol) in the fields of sensors and electrocatalysis are presented. Special attention is paid to the influence of different external variables (applied potential, *pH* of the solution and film thickness) on the electrochemical performance of this polymer as a sensor component. Some properties of POAP such as morphology and thickness uniformity, which improve the catalytic activity of other catalysts, as well as its own catalytic activity to decrease the oxidation overpotential of some biological macromolecules, are discussed.

Although this Chapter is not comprehensive it brings together much of the work around POAP and is intended to be of particular in biosensors applications, particularly in the analysis of real samples, e.g. human serum and milk. Also, some results from basic research are included to explain the behavior of biosensors in their practical applications.

3.2 Biosensors Based on POAP

3.2.1 Glucose Biosensors

Recently, the development of glucose biosensors has received considerable attention because the determination of glucose concentration is very important in clinical applications. Most glucose measurements are based on the immobilization of glucose oxidase (GOx) for detecting hydrogen peroxide concentration, which is produced from the GOx enzyme reaction. Since GOx can recognize glucose target molecules quickly and accurately in complicated systems, a suitable matrix on the base electrode surface should be well designed for the immobilization of GOx while maintaining its highly enzymatic activity. The entrapment of GOx in electropolymerized films is a simple and efficient way to develop glucose sensors with high sensitivity, good stability and fast response. The entrapping technique should control the layer thickness and enzyme loading, while keeping the enzyme highly bioactive. So far, most work in this area has focused on the use of electropolymerized conducting films of polypyrrole (Ppy) [24, 25] and its derivatives [26] and polyaniline (PANI) [27]. However, the recent literature seems to show increasing

attention to some electropolymerized nonconducting polymers such as POAP. Biosensors based on POAP generally have the advantages of fast response and high sensitivity because of relatively high enzyme loading. Besides, the nonconducting POAP films are generally found to be more effective than the conducting ones in both preventing the biosensor from fouling and eliminating the interference from electroactive species such as ascorbic acid and uric acid.

Several glucose biosensors based on POAP are reported in the literature [28–32]. In most cases, hydrogen peroxide liberated by the enzymatic reaction is detected by measuring its oxidation current on the base electrode material (platinum, gold, glassy carbon, carbon paste, etc.). Glucose amperometric measurements are in general carried out with the sensor under stirred conditions, and the response current is considered in terms of the relationship between the steady-state current and background current (without glucose) changes. The composition of each one of these biosensors is described in this section. Table 3.1 shows the response characteristics of the biosensors.

Experimental conditions related to the preparation and characteristics of the Pt/PB/POAP/GOx amperometric glucose biosensor, which is based on the immobilization of glucose oxidase (Gox) in an electrochemically polymerized POAP film at a Prussian blue (PB)-modified platinum (Pt) microelectrode, are described in [28]. While PB acts as a typical electroactive film that exhibits catalytic properties for H_2O_2 oxidation, the nonconducting POAP film acts as an effective barrier to protect the electrode from fouling. PB in the Pt/PB/POAP/GOx biosensor leads to a lower detection limit and a larger response current as compared with the Pt/POAP/GOx electrode (Table 3.1). This difference was attributed to PB, which allows a higher surface coverage of enzyme to be obtained due to the high surface roughness of the PB film. Also, PB molecules can be oxidized to Berlin green at high potentials, which electrocatalyzes the oxidation of hydrogen peroxide. However, the Pt/PB/POAP/GOx biosensor has a narrower linear range than the Pt/POAP/GOx electrode. This characteristic was attributed to the poor operational stability and high decrease in sensitivity of the PB film.

A GC/BCNT/POAP-GOx glucose biosensor has been reported and is based on boron-doped carbon nanotubes (BCNT) and POAP films [29]. GOx was immobilized on the BCNT-modified glassy carbon electrode (GC/BCNT) by electrochemical copolymerization of GOx and *o*-AP. The GC/BCNT/POAP-GOx electrode exhibits better characteristics for glucose determination as compared with GC/BCNT and GC/BCNT/POAP electrodes. The better performance of the former biosensor was attributed to the presence of POAP that improves the stability and the anti-interferent ability of the electrode.

The Au/POAP/CNT/GOx amperometric glucose biosensor that is based on the immobilization of GOx in a composite film of POAP and carbon nanotubes (CNT), which are electrochemically copolymerized at a gold electrode, has been described [30]. Compared with the Au/POAP/GOx biosensor, the Au/POAP/CNT/GOx biosensor has a lower detection limit and a larger response current. While POAP can efficiently avoid the interference of electroactive compounds, CNT has the property of increasing the electron transfer.

Table 3.1 Detection solutions and response characteristics of the different biosensors based on poly(*o*-aminophenol)

Biosensor	Detection solution	Electrochemical conditions and response characteristics	Detection limit	Ref.
Pt/PB/POAP/GOx	1/15 M phosphate buffer solution (*pH* 7) containing different glucose concentrations (0–35 mM)	Operating potential, $E = 0.6$ V (vs. SCE). Linear dependence of the current on glucose concentration up to 5 mM	0.01 mM	[28]
Pt/POAP/GOx	1/15 M phosphate buffer solution (*pH* 7) containing different glucose concentrations (0–60 mM)	Operating potential, $E = 0.6$ V (vs. SCE). Linear dependence of the current on glucose concentration up to 10 mM	0.02 mM	
GC/BCNT/ POAP-GOx	1/15 M phosphate buffer solution (*pH* 7) containing different glucose concentrations (0–25 mM)	Operating potential, $E = 0.6$ V (vs. SCE). Linear dependence of the current on glucose concentration up to 8 mM	3.6 μM	[29]
Au/POAP/CNT/ GOx	1/15 M phosphate buffer solution (*pH* 7) containing different glucose concentrations (0–50 mM)	Operating potential, $E = 0.75$ V (vs. SCE). Linear dependence of the current on glucose concentration up to 5 mM	0.01 mM	[30]
Au/POAP/GOx	1/15 M phosphate buffer solution (*pH* 7) containing different glucose concentrations (0–50 mM)	Operating potential, $E = 0.75$ V (vs. SCE). Linear dependence of the current on glucose concentration up to 10 mM	0.02 mM	[30]
PGCE/POAP/ GOx	A stirred, air-saturated 0.05 M phosphate buffer (*pH* 7) solution, where aliquots of glucose were added.	Operating potential, $E = 0.6$ V (vs. SCE), The linear response of the enzyme electrode to glucose was from 1×10^{-6} to 1×10^{-3} M	5×10^{-7} M	[30]
POAP-GOx/PPy-Pt/GCE	Stirred solution containing 25 ml air-aturated 0.1 M PBS, *pH* 7, where glucose was injected using a micro-syringe	Operating potential, $E = 0.60$ V (vs. SCE). Linear dependence of the current on glucose concentration from 0.0015 mM to 13 mM	0.45 μM	[32]
POAP-GOx/Pt/ GCE	Stirred solution containing 25 ml air-aturated 0.1 M PBS, *pH* 7, where glucose was injected using a micro-syringe	Operating potential, $E = 0.60$ V (vs. SCE). Linear dependence of the current on glucose concentration from 0.0042 mM to 12 mM	0.90 μM	[32]

(continued)

Table 3.1 (continued)

Biosensor	Detection solution	Electrochemical conditions and response characteristics	Detection limit	Ref.
POAP-GOx/PPy/GCE	Stirred solution containing 25 ml air-aturated 0.1 M PBS, *pH* 7, where glucose was injected using a micro-syringe	Operating potential, $E = 0.60$ V (vs. SCE). Linear dependence of the current on glucose concentration from 0.0055 mM to 12 mM	0.95 µM	[32]
Hb/POAP/FeCoHCF/Au	Aliquots of a standard solution of H_2O_2 added to an acetate buffer solution (*pH* 5.29)	Operating potential, $E = -0.25$ V (vs. SCE). Linear dependence of the current on the H_2O_2 concentration within the range 1.73×10^{-5} M–4.03×10^{-3} M	1.2×10^{-5} M	[22]
HRP-ferrocene/POAP	Batch mode: Hydrogen peroxide in 0.1 M phosphate solution (*pH* 8)	Rotating Disc Electrode Voltammetry (RDEV). Linear dependence of the current on the H_2O_2 concentration within the range 1×10^{-8} M-1 × 10^{-5} M. Detection potential: 0.050 V (Ag/Ag/Cl)	8.5×10^{-9} M	[34]
	Flow Injection mode (FIA): Hydrogen peroxide in 0.1 M phosphate solution (*pH* 8)	Consecutive injections (50 injections per day for six days). Linear dependence of the current on the H_2O_2 concentration within the range 1×10^{-8} M-2 × 10^{-6} M. Detection potential: 0.050 V (Ag/Ag/Cl)	8.5×10^{-9} M	[34]
Carbon paste/HRP-Uricase/POAP	A stirred 0.1 M solution of phosphate buffer (*pH* 7.5) containing uric acid	Operating potential, $E = 0.050$ V (vs. Ag/AgCl). Linear response up to 1×10^{-4} M of urate	3.14×10^{-6} M	[35]
Carbon paste/HRP-Uricase/POAP	Flow injection system: carrier stream was 0.1 M phosphate buffer (*pH* 7.5)	Operating potential, $E = 0.050$ V (vs. Ag/AgCl). Linear response up to $1 \times 2 \times 10^{-4}$ M of urate. Flow rate 0.85 ml min^{-1}	6.8×10^{-6} M	
Carbon paste/GPT- LDH-NAD$^+$/PPD-POAP	0.1 M phosphate, 0.01 M glutamate solution, *pH* 9.5, containing lactate	Operating potential, $E = 0.0$ V (vs. Ag/AgCl). Linear response to lactate up to 8.5×10^{-5} M	6×10^{-7} M	[36]
Carbon paste/POAP	0.1 M acetate buffer (*pH* 5) solution or 0.1 M phosphate buffer (*pH* 7) solution, where NADH was added in increments of 1×10^{-8} M	Operating potential, $E = 0.15$ V (vs. Ag/AgCl). Linear response of the catalytic oxidation current from 0 M to 1×10^{-7} M (NADH)	1.0×10^{-9} M	[45]

The PGCE/POAP/GOx glucose biosensor based on the immobilization of GOx in an electropolymerized *o*-aminophenol (*o*-AP) polymer film on a platinized glassy carbon electrode is described in [31]. The porous platinum particle matrix of PGCE provided not only a large microscopic surface area for higher enzyme loading but also a desirable microenvironment to transform the enzymatically produced H_2O_2 more efficiently to an electronic signal. The POAP film acts as a permselective material in this sensor.

The fabrication and characterization of the POAP-GOx/PPy-Pt/GCE glucose sensor based on a polypyrrole-platinum (PPy-Pt) composite-modified glassy carbon electrode (GCE), which was covered by a layer of POAP-GOx, are reported in [32]. The generated H_2O_2 can penetrate through the POAP film and be electrocatalytically oxidized at the PPy-Pt conducting nanocomposite. The fast response of this biosensor was attributed to the thin POAP film and the high dispersion of embedded Pt nanoclusters. The presence of the PPy-Pt nanocomposite in the POAP-GOx/PPy-Pt/GCE electrode leads to a lower detection limit and high sensitivity as compared with those of POAP-GOx/Pt/GCE and POAP-GOx/PPy/GCE electrodes (Table 3.1).

3.2.1.1 Influential Factors in the Response Characteristic of Glucose Biosensors Based on POAP

The amperometric response characteristics of the enzyme electrodes based on POAP are affected by the thickness of the polymer film (polymerization cycle number), the *pH* of the detection solution, applied potential used in the determination, and the presence of electroactive (interfering) compounds. The effects of these factors on the behavior of glucose biosensors based on POAP are separately described.

Effect of the Polymerization Cycle Number of POAP Films

Thickness and morphology characteristics of electrochemically synthesized POAP films play an important role in the response current of glucose biosensors. In this regard, POAP synthesized in acidic media has some advantages over PANI. SEM examination shows that POAP deposits are denser and have a smoother appearance than PANI, deposited under similar experimental conditions [33]. Furthermore, thin POAP films have a characteristic smooth, continuous and denser appearance, which contrasts with electrochemically polymerized thin PANI films, which are not smooth but show a spot-like morphology. In the respect of thickness control, the vertical sectional profile of POAP films shows that they are continuous with the thickness being almost uniform over the whole film [3]. It has, however, been demonstrated that the compactness of POAP morphology prevents the diffusive penetration of dissolved oxygen, and POAP oxidation does not occur to the same extent as in PANI [33]. Also, in some cases the POAP film can be easily regenerated after use.

With the Pt/PB/POAP/GOx biosensor [28], it has been observed that the response current is affected by the film thickness of Prussian blue (PB) and POAP. In general, thick films show a long response time and low sensitivity, but result in a wider linear response range. When the polymerization cycle number was 15 for both PB and POAP, the maximum value of the response current was obtained. Also, for the POAP-GOx/PPy-Pt/GCE biosensor [32], the maximum current response was obtained when the polymerization cycle number for POAP-GOx was 15. The response current of the Au/POAP/CNT/GOx biosensor [30] also increases with the increase of the polymerization cycle number, until a maximum value of 15 cycles (Fig. 3.2). It has been suggested that when the number of cycles is lower than 15, then the amount of enzyme entrapped in the POAP film gradually increases with the increase of the polymerization cycle number. However, when the number of cycles is higher than 15, GOx may be covered by the POAP film, decreasing the available amount of GOx.

Morphologic studies of the PGCE/POAP/GOx biosensor [31] revealed the presence of a three-dimensional porous open structure. The aggregates of the electrodeposited Pt on the GC surface were fairly uniform and roughly spherical. The porous open structure provided a greatly enhanced effective electrode surface for high enzyme loading. When the PGCE was coated with an electropolymerized POAP film, the porous open structure was maintained, although the aggregates got bigger and the surface became smoother because of the deposited POAP film. The polymerization of *o*-AP and immobilization of GOx were done either by holding them at a constant potential or by applying cyclic voltammetry (CV). Biosensors prepared by CV were more reproducible and more effective in rejecting

Fig. 3.2 Effect of the polymerization cycle number on the response current of the Au/POAP/CNT/GOD electrode. Steady-state currents are measured at 0.75 V (SCE) in 1/15 M phosphate buffer solution (*pH* 7) containing 2 mM glucose (*n* = 3) [30]
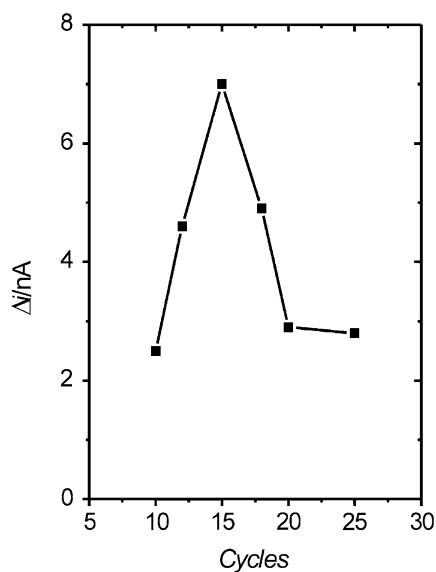
interferents. This was attributed to the fact that the film formed by CV was more uniform and compact than that formed at constant potential.

Effect of the Solution *pH*

In general, neutral buffer solutions (*pH* 7) are selected for glucose detection with most of the biosensors based on POAP (Table 3.1).

The response current of the GC/BCNT/POAP-GOx sensor [29] increases with the increase of the *pH* value, and the maximum response was observed at *pH* 7.0. Also, for the POAP-GOx/PPy-Pt/GCE electrode [32], the current increased from *pH* 4.5 to 7.0, while it decreased sharply above *pH* 7.0. The maximum current at *pH* 7.0 was attributed to the entrapment of GOx in the POAP film, which made GOx more active in neutral solution. However, other biosensors show response currents as a function of *pH* where different maximum current values are observed. Figure 3.3 shows the response current of the Pt/PB/POAP/GOx electrode [28] as a function of *pH*. As can be seen, even though the biosensor can be used over a wide *pH* range (*pH* 4.5–8), the maximum of the response current was observed at *pH* 7. Again, this was attributed to the entrapment of GOx in the POAP film, making GOx more active in neutral media. However, at *pH* 5.6 a high response current was also observed.

Effect of the Applied Potential

The response current of most glucose biosensors based on POAP [28–30, 32] increases rapidly with the increase of the applied potential, and then, after a given potential value, the response current remains constant. The response current as a function of the applied potential for the Au/POAP/CNT/GOx biosensor [30] is shown in Fig. 3.4. When the applied potential is below 0.75 V (vs. SCE) (0.5–0.75 V vs. SCE), the response current increases rapidly with the increase of the applied potential. The response of the enzyme electrode in this potential range is controlled by the electrochemical oxidation of hydrogen peroxide. When the potential was over 0.75 V, the response current remained almost the same. This effect was explained by the rate-limiting process of enzyme kinetics and substrate diffusion. However, it was also found that the higher the applied potential, the easier it is for the electroactive interferents to be oxidized and to cause an additional response current, and the easier it is for the polymer film to be damaged. Potential values lower than 0.8 V (SCE) are often therefore selected for the oxidation operation of the different enzyme electrodes (Table 3.1).

Effect of the Interferents

Selectivity is one of the major characteristics of an amperometric glucose biosensor. The response of the sensor should be specific to a given analyte and should not involve other electroactive substances in the sample. With regard to the effects of interferents, the magnitude of the interferent current (I_{G+I}) relative to the analytical signal (I_G) produced by the analyte (glucose) was considered in different biosensors [28–30]. The interferences of electroactive compounds in the glucose response were examined in the presence of their physiological normal levels (0.1 mM ascorbic acid (AA), 0.5 mM uric acid (UA) and 0.1 mM acetaminophen

Fig. 3.3 Effect of *pH* on the steady-state response current on the Pt/Prussian blue/poly(*o*-aminophenol)/glucose oxidase electrode at 0.6 V in 1/15 M phosphate buffer solution (*pH* 7) containing 2 mM glucose (*n* = 3) [28]
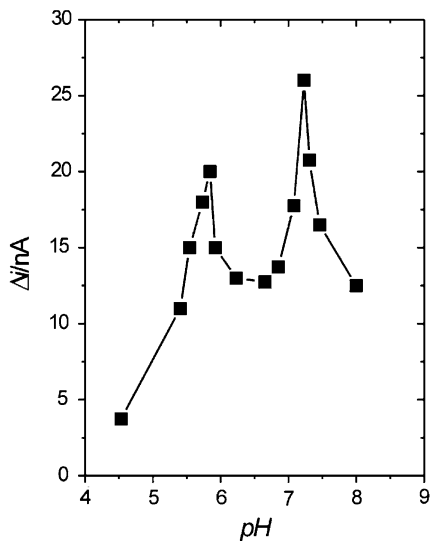
(AMP)) with a glucose concentration of 5.6 mM. It was observed that the influence of AA, UA and AMP on the glucose response was always small under the testing conditions. The ratio I_{G+I} to I_G for different biosensors is shown in Table 3.2. The improved interferent behavior of these biosensors [28–30] was attributed to POAP films, which could efficiently avoid the interference of the above-mentioned electroactive compounds.

Fig. 3.4 Effect of applied potential on the response current of the Au/POAP/CNT/GOD electrode. Steady-state currents are measured in 1/15 M phosphate buffer solution (*pH* 7) containing 2 mM glucose [30]
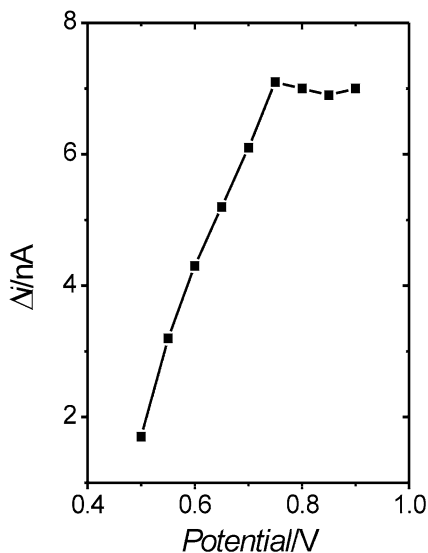
With the PGCE/POAP/GOx biosensor [31], it has been shown that POAP films can prevent the access of interferents such as AA, UA, and $Fe(CN)_6^{4-}$ to the platinum surface, while allowing 60 % of H_2O_2 to penetrate it. However, even though the interference from electroactive species such as AA and UA was significantly reduced by the use of the POAP film, the response of the sensor to ascorbate gradually increased when the sensor was stored for more than 3 months. This was attributed to the falloff or dissolution of the film into the solution. Nevertheless, the rejection efficiency could be restored by redeposition of POAP onto the electrode surface from a GOx-free o-AP solution for 2 min, although the biosensor suffers a loss of 30 % of the electrode response to glucose.

An interference test was also made for the different electrodes synthesized in [32] (Table 3.1). To this end the amperometric responses of POAP-GOx/PPy-Pt/GCE and POAP-GOx/Pt/GCE to the consecutive additions of glucose, UA, AA and AMP were analyzed. The current response for 5.5 mM glucose could be observed at both electrodes. However, the response of the POAP-GOx/Pt/GCE electrodes was much smaller than that of the POAP-GOx/PPy-Pt/GCE electrode. This difference was attributed to Ppy electroactivity. Also, for successive additions of 0.5 mM UA, 0.2 mM AA and 2.0 mM AMP to the glucose solution, the POAP-GOx/PPy-Pt/GCE electrode had nearly no response current from the interferents. The POAP-GOx/Pt/GCE electrode could also eliminate the influence of UA and AA. However, 2.0 mM AMP had significant influence.

Effect of the Temperature

Temperature is an important factor for the activity of the enzyme. The response of the POAP-GOx/PPy-Pt/GCE biosensor [32] was measured between 10 and 60 °C. The current response increased almost linearly with temperature from 10 to 40 °C, but decreased linearly from 40 to 60 °C. While the latter behavior was attributed to the deactivation of GOx, the former one was attributed to the increase in activity of the immobilized GOx. Thus, the activation energy (25.9 kJ mol^{-1}) of the immobilized GOx could be calculated on the basis of the Arrhenius equation. According to authors of [32], the PPy-Pt nanocomposite and POAP film offer a good environment for GOx, which makes the biosensor more stable at high temperature.

Stability of Glucose Biosensors

Table 3.2 Interferences of electroactive compounds to the glucose response for different biosensors based on poly(o-aminophenol). Magnitude of the interferent current (I_{G+I}) relative to the analytical signal (I_G) produced by the analyte (glucose)

Biosensor	I_{G+I}/I_G (AA)	I_{G+I}/I_G (UA)	I_{G+I}/I_G (AMP)	Ref.
Pt/PB/POAP/GOx	1.03	1.06	1.04	[28]
GC/BCNT/POAP-GOx	1.05	1.02	1.06	[29]
Au/POAP/CNT/GOx	1.05	1.06	1.08	[30]

The stability under storage conditions (phosphate buffer of *pH* 7 at low temperature) was analyzed for most of the glucose biosensors based on POAP.

After 7 days, an 8 % loss of the response signal was observed for every day of use in the GC/BCNT/POAP-GOx biosensor [29]. However, 80 % response current was retained after 20 days. The Au/POAP/CNT/GOx biosensor [30] showed that the 75 % response current was still retained after 30 days of use. The good stability of these biosensors was attributed to the enzyme entrapped in the POAP film that is stable in neutral medium.

The Pt/PB/POAP/GOx biosensor [28] showed only 6 % decrease of the original current response to glucose during the first 7 consecutive days of use. However, 75 % response current was still retained after 30 days (Fig. 3.5). This behavior was attributed to the high decrease in sensitivity of the PB film.

The POAP-GOx/PPy-Pt/GCE electrode [32], showed no significant decrease in current response in the first 7 days of use. However, a decrease of 11 % was observed after 30 days. A 76 % response current was retained after 60 days. This good stability was attributed, firstly, to GOx molecules entrapped in the POAP film that are stable and retain bioactivity, and secondly, to the PPy-Pt nanocomposite structure, which provides a biologically compatible matrix for immobilizing the GOx-POAP film.

The stability of the PGCE/POAP/GOx electrode was found to be better than that of the PDE/POAP/GOx electrode [31] (Table 3.1). The difference was attributed to a slow desorption and deactivation of the GOx entrapped in the micropores of the platinized platinum particle matrix, which are not as easy as on a smooth surface (platinum disc electrode).

Reproducibility and Sensitivity of the Biosensors

Fig. 3.5 Stability of the Pt/Prussian blue/poly (o-aminophenol)/glucose oxidase electrode stored in 1/15 M phosphate buffer solution (*pH* 7) at 4 °C. Stability determined by 5 mM glucose in 1/15 M phosphate buffer solution (*pH* 7). Applied potential, 0.6 V (SCE) [28]
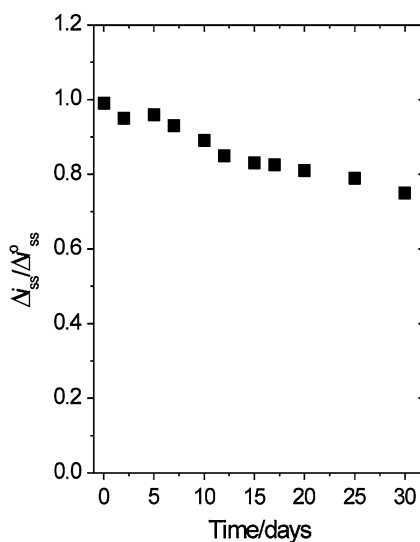
The reproducibility of the Pt/PB/POAP/GOx electrode was analyzed in [28]. It was estimated from the response to 1 mM glucose for five enzyme electrodes at a potential value of 0.6 V (SCE). The results revealed that the sensor exhibits satisfactory reproducibility with a mean change of the response current of 12.6 nA and a relative standard deviation of 4.32 %. With regard to the sensitivity (44 mA M^{-1}) of the Pt/PB/POAP/GOx electrode, it was nine times larger than that of the Pt/POAP/GOx electrode.

The GC/BCNT/POAP-GOx biosensor [29] showed good characteristics, such as high sensitivity (171.2 nA mM^{-1}), low detection limit (3.6 μM), wide linear range (up to 8 mM) and short response time (within 6 s).

The sensitivity reported for the Au/POAP/CNT/GOx biosensor [30] is 11.4 mA M^{-1} cm^{-2}, this is almost 2.5 times higher than that of the Au/POAP/GOx electrode. With regard to reproducibility, the results revealed that the sensor has satisfactory reproducibility, with a mean change of the response current of 3.6 nA and a relative standard deviation of 8.4 %.

The stability of the PGCE/POAP/GOx electrode [31] was evaluated by repetitive (200 times) measurements of its response to 1 mM glucose within a period of 10 h. The sensor sensitivity loss was only 14.3 % after the 200 measurements. With intermittent usage and storage at 4 °C in phosphate buffer for 10 months, the biosensor maintained 50 % of its original sensitivity and still displayed an excellent response to glucose.

The lower detection limit (0.45 μM) and high sensitivity (9.9 mA/Mcm^2) of the POAP-GOx/PPy-Pt/GCE (0.45 μM) sensor [32], as compared with those of POAP-GOx/Pt/GCE (0.90 μM and 5.5 mA/Mcm^2) and POAP-GOx/PPy/GCE (0.95 μM and 3.5 mA/Mcm^2), respectively, were attributed to the presence of a Ppy-Pt nanocomposite system.

Real Sample Analysis

Human plasma samples were assayed to demonstrate the practical use of the GC/BCNT/POAP-GOx biosensor [29]. A plasma sample (0.5 mL) was added to 5 mL PBS (*pH* 7.0), and the response was obtained at 0.6 V (SCE). The contents of glucose in blood could then be calculated from the calibration curve (Table 3.1). The results obtained agreed closely (relative error between 1 and 3 %) with those obtained from a biochemical analyzer (ASCA AG II Chemistry System, Landmark, USA).

3.2.2 Amperometric Hydrogen Peroxide Biosensors Based on POAP

Two interesting sensors based on POAP for the direct determination of hydrogen peroxide are reported in the literature [22, 34].

The immobilization of hemoglobin (Hb) in POAP films at iron-cobalt hexacyanoferrate (FeCoHCF) films to build the Hb/POAP/FeCoHCF/Au biosensor is

reported in [22]. The FeCoHCF film was firstly deposited on the gold electrode and then it was combined with a POAP film that entraps Hb. While the immobilized Hb in the Hb/POAP/FeCoHCF/Au film exhibits catalytic activity to H_2O_2 by the mediation of FeCoHCF, the POAP film reduces the interference from electroactive species.

The construction and characterization of a horseradish peroxidase (HRP)-ferrocene modified carbon paste biosensor, using an electrochemically generated POAP film (HRP-ferrocene/POAP), for the determination of hydrogen peroxide is reported in [34]. POAP in this biosensor was considered as a convenient means of immobilizing the enzyme and mediator on the electrode surface, while preventing electrode fouling.

3.2.2.1 Influential Factors in the Response Characteristic of the H_2O_2 Biosensors Based on POAP

Preparation of Films Employed in H_2O_2 Biosensors

A series of FeCoHCF films were electrodeposited on gold electrodes from solutions containing 6 mM $Fe(CN)_6^{-3}$ with different concentrations of Co(II) and Fe(III) to obtain the biosensor reported in [22]. The FeCoHCF film deposited from a solution with an iron molar ratio of 0.4 showed the largest response current to H_2O_2. Therefore, the optimized FeCoHCF film was combined with a nonconducting POAP film that entraps Hb to construct the biosensor Hb/POAP/FeCoHCF/Au electrode [22]. The electrochemical copolymerization of *o*-AP and Hb on the FeCoHCF/Au electrode was performed in a 5 mM *o*-AP and 0.04 mM Hb acetate buffer solution (*pH* 5.0) where the electrode was cycled between −0.2 and 0.8 V (vs. SCE) at a scan rate of 50 mV s^{-1}. All films used in [22] were grown for 15 cycles.

POAP films for the (HRP)-ferrocene modified carbon paste biosensor [34] were prepared by electropolymerization of a 5 mM *o*-AP solution where the electrode was cycled (40 cycles) between 0.0 and 0.8 V (vs. Ag/AgCl) at a scan rate of 50 mV s^{-1}. A fresh acetate buffer solution (0.1 M, *pH* 5) was employed as supporting electrolyte.

Effect of the Solution *pH*

With regard to the *pH* effect on the catalytic reduction current of the Hb/POAP/FeCoHCF/Au electrode reported in [22], the maximum response current was observed at *pH* 5.29. This was attributed to the entrapment of Hb in the POAP film deposited on the FeCoHCF/Au electrode, making Hb more active in weak acidic medium. Considering the high bioactivity of Hb at this *pH* and the stability of the Hb/POAP/FeCoHCF film, *pH* 5.29 was chosen as the *pH* value of the detection solution (Table 3.1).

Several experiments were carried out in [34] by using the (HRP-ferrocene/POAP) sensor coupled to a rotating disc electrode. Levich plots were obtained for

different H_2O_2 concentrations in a 0.1 M phosphate buffer solution at *pH* 8. The steady-state current was found to be directly proportional to the square root of the angular rotation speed according to the Levich equation (Eq. 3.1) at concentrations of hydrogen peroxide lower than 1×10^{-6} M:

$$i_L = 0.62\, n\, F\, A\, D_{H_2O_2}^{2/3}\, v^{-1/6}\, C_{H_2O_2}\, \omega^{1/2} \tag{3.1}$$

In Eq. (3.1), i_L is the mass-transfer limited current, n is the number of electrons transferred, A the electrode area, F the Faraday constant, $D_{H_2O_2}$ the diffusion coefficient of hydrogen peroxide, v the kinematic viscosity of the solution, $C_{H_2O_2}$ is the bulk concentration of hydrogen peroxide and ω is the electrode rotation rate. At concentrations of hydrogen peroxide higher than 1×10^{-6} M, a nonlinear behavior was observed. The responses of the rotating disc electrode prepared in [34] were very rapid. At 3000 rpm, 95 % of the steady-state current response could be reached in 2.3 s.

Effect of the Applied Potential

The relationship between the response current and applied potential in *pH* 5.29 buffer solution was also studied for the Hb/POAP/FeCoHCF/Au electrode [22].

The response current for this electrode gradually increased with the applied potential from 0.3 V to −0.25 V (vs. SCE) and then it decreased at a potential more negative than −0.25 V. Considering the possible interference effects and the operation stability of the electrode, −0.25 V was selected in [22] as operating potential.

The applied potential did not significantly influence the response of the HRP-ferrocene/POAP biosensor when changes in the range 0.0–100 mV (vs. Ag/AgCl) were considered. However, at a potential more negative than −100 mV, a rapid loss of activity was observed due to the irreversible reduction of the immobilized HRP (Fig. 3.6).

Effect of the Interferents

With regard to effects of electroactive interferents on the response current of the Hb/POAP/FeCoHCF/Au electrode, the influence of AA, UA and AP on the response current to H_2O_2 was analyzed in [22]. The observed response currents to AA, UA and AP at the Hb/POAP/Au electrode were very small. The good anti-interferent ability of the Hb/POAP/FeCoHCF/Au electrode was assigned to the low potential applied (−0.25 V) and the selective permeability of the POAP film. However, the effect of electroactive interferents on the response current is really not obvious due to the low applied potential. The low conductivity and small porous size of the POAP film did not allow a detailed investigation of the effect of electroactive interferents. However, the response time of the Hb/POAP/FeCoHCF/Au electrode is very fast (within 5 s) and this short response time, as compared

Fig. 3.6 Effect of operating
potential on the response of
the HRP-ferrocene/POAP
electrode (5 mM, 10 cycles,
50 mV s^{-1} to 10^{-4} M
injections of H$_2$O$_2$ [34])
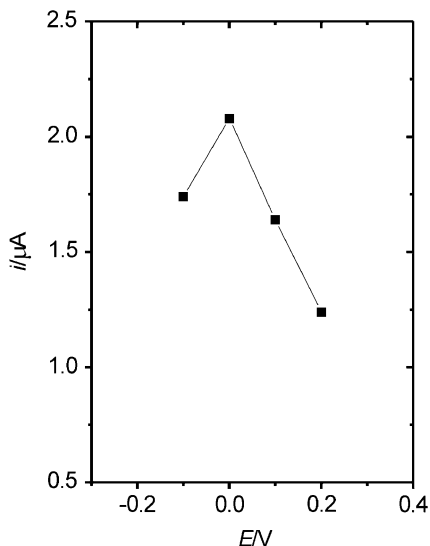
with those of other sensors, was attributed to the presence of the thin nonconducting POAP film.

Stability of Hydrogen Peroxide Biosensors

The stability of the HRP-ferrocene/POAP electrode stored at room temperature in acetate buffer (*pH* 5) was investigated in [34]. A 43 % decrease in response was observed after 7 days. However, the POAP-modified electrode was stable during at least a period of 6 successive days.

Reproducibility and Sensitivity of the Biosensors

The HRP-ferrocene/POAP sensor [34] shows a linear response in the concentration range 1×10^{-8} M to 2×10^{-6} M of H$_2$O$_2$, with a slope, intercept and correlation coefficient of 6.47×10^{-7} nA M^{-1}, 2.17 nA and 0.9995 ($n = 10$), respectively. A series of injections of 10^{-5} M H$_2$O$_2$ yielded a standard deviation of 0.8 %, which remained constant after 300 injections (50 injections per day during a period of six successive days).

Real Sample Analysis

Hydrogen peroxide may be used as a preservative in milk. However, the legal situation in the different countries has to be considered. Sufficient sterilization is obtained at 0.1 % hydrogen peroxide. The catalase present in the milk gradually destroys the H$_2$O$_2$. Hydrogen peroxide is also used for cleaning instruments and equipment used for cooling, mixing, transporting, bottling and packing milk. If the subsequent washing and drying is incomplete, the foodstuff is (illegally) contaminated with H$_2$O$_2$. In order to demonstrate the application of the HRP-ferrocene/POAP electrode [34] to real samples, the H$_2$O$_2$ concentration in a spiked milk sample containing 1.037 ± 0.003 mg mL^{-1} (for $n = 3$) of H$_2$O$_2$ was

measured. The H_2O_2 concentration in the spiked milk samples, determined by the four-point calibration curve prepared using standard H_2O_2 constructed prior to the measurement, was found to be 1.083 ± 0.054 mg mL^{-1} (for $n = 3$). A blank milk sample was tested in the same way and did not show any signal.

3.2.3 A Uric Acid Selective Biosensor Based on POAP

The detection, identification and quantification of uric acid (2,6,8-trihydroxipu-rine) in human physiological fluids is of great importance in the diagnosis and therapy of patients suffering from a range of disorders associated with altered purine metabolism, most notably gout and hyperuricemia. Other medical conditions, such as leukemia and pneumonia, have been associated with enhanced urate levels. POAP has been successfully used in the development of a uric acid (UA) biosensor [35]. The biosensor was obtained by immobilizing uricase and horseradish peroxidase (HRP) (7 % w/w uricase and 3 % w/w HRP) in carbon paste. Then, POAP was deposited on the working surface area of the electrode to obtain the CP/HRP-uricase/POAP biosensor. The response of the electrode is based on the enzymatic reduction of hydrogen peroxide in the presence of UA. Cyclic voltammetry and hydrodynamic studies were carried out in [35] order to ensure that current signals were due to enzymatically generated H_2O_2 and not due to direct electron transfer of UA at the working surface electrode. In this regard, cyclic voltammograms for both an unmodified carbon paste electrode (bare electrode) and a POAP-coated electrode were compared in solutions containing UA. POAP-coated electrodes yielded signals 50 % smaller in magnitude, as compared with the unmodified electrode. This was attributed to the imposition of an additional diffusion barrier in the presence of POAP. The ratio between the current at the POAP-coated electrode and that of the bare electrode was considered as a measure of the coating permeability. Hydrodynamic studies also indicated that the electrocatalytic reduction of H_2O_2 by HRP immobilized on the CP electrode takes place without electron-mediating substances, which suggests that peroxidase is by itself capable of performing electron-transfer to the electrode.

3.2.3.1 Influential Factors in the Response Characteristic of the Uric Acid Biosensor

Preparation of POAP Films

The effect of increasing the monomer (*o*-aminophenol) (*o*-AP) concentration during the electropolymerization process was explored in [35]. The most suitable monomer concentration for POAP coating was found to be 5×10^{-3} M, even though a 10 times lower concentration improved response times and showed more

rapid returns to base-line levels. In this regard, faster response times were recorded (24 s) for a polymer layer built in a 5×10^{-4} M concentration of *o*-AP.

Effect of the Solution pH

The behavior of the biosensor reported in [35] was studied within the *pH* range 5.0–9.0. Greater sensitivity was achieved at a *pH* value of 6.6. However, a *pH* value of 7.5 was selected in order to mimic the microenvironment of physiological fluids and to promote the long-term stability of the sensor.

Effect of the Applied Potential

Hydrodynamic voltammograms were recorded over the potential range −0.1 V–0.35 V (vs. Ag/AgCl). Then, steady-state currents were recorded and plotted as a function of the applied potential. At potential values more negative than – 0.2 V, a rapid loss of activity was observed due to irreversible reduction of HRP. As the degradation of POAP occurs at high positive potential values, an operating potential of 0.05 V was selected for amperometric measurements in [35].

Effect of the interferents

A range of naturally occurring substances in blood were examined in [35] for their potential interference effects. Ascorbic acid gave approximately 2 % and 15 % increase in signal intensity for mean (2.8×10^{-4} M) and upper (3.41×10^{-4} M) levels found in blood, respectively. The presence of bilirubin was found to have a detrimental effect on urate signals. A concentration of 1.7×10^{-4} M resulted in a decrease of 35 % in signal intensity. As bilirubin was considered too large to pass through the polymer layer, the effect was attributed to some form of interaction with uric acid at the working surface area of the electrode, resulting in a diminished current. The influence of allopurinol on uric acid amperometric signals was also examined. It is well-known that the oxidized form of the drug binds tightly to the reduced form of the enzyme. Repeated injections of UA (1×10^{-4} M) were carried out in the presence and absence of the drug. A reduction in current signal of 10.5 % was noted. Two possibilities were considered to explain this effect: the first one is that oxidation of allopurinol interferes with the oxidase catalytic mechanism, and the second one is an effect of blockage (or interaction) at the working electrode surface.

Stability of the Biosensor

The sensor response was found to be stable for 2 days while stored in the background electrolyte (0.1 M solution of phosphate buffer, *pH* 6.5) at room temperature (25 °C).

Analysis of Serum Samples

Serum samples containing different concentrations of UA were analyzed using the sensor described in [35]. Samples were diluted 1:10 with the supporting electrolyte solution and the *pH* adjusted at 7.5. Diluted samples were then directly injected into a flow system, and the concentration of UA was estimated from a calibration plot (Table 3.1). Results were in reasonable agreement with those determined by

UV spectrophotometry. Repeated exposure of the electrode to diluted serum had no adverse effect on the amperometric signal size.

3.2.4 A Lactate Amperometric Biosensor Based on Poly(o-phenylenediamine) and Poly(o-aminophenol) (PPD- POAP)

L-lactate is an important analyte in a number of different situations including clinical, food and bioprocesses analyses. A reagentless lactate amperometric biosensor, constructed by immobilizing pyruvic transaminase (GPT) and L-lactate dehydrogenase (LDH) together with its cofactor, nicotinamide adenine dinucleotide (NAD$^+$), in carbon paste using a poly(o-phenylenediamine) (PPD) film (CP/LDH-GPT-NAD$^+$/PPD) has been, described [36]. Interference by direct electrochemical oxidation of easily oxidizable substances, such as uric acid, L-ascorbic acid, L-cysteine, glutathione and paracetamol, was drastically reduced by covering the PPD-modified electrode with a second electrochemically synthesized non-conducting POAP film (CP/LDH-GPT-NAD$^+$/POAP-PPD). The response of both electrodes, (CP/LDH-GPT-NAD$^+$/PPD and CP/LDH-GPT-NAD$^+$/POAP-PPD) is based on the electrocatalytic oxidation, at low applied potentials, of the enzymatically produced NADH by the conducting PPD film. The bienzyme-double polymeric layer modified electrode, at an applied potential of 0.0 V (vs. Ag/AgCl), gives a linear response for lactate up to 8.5×10^{-5} M (I/nA $= 5.2 \times 10^5$ [Lactate]/M $+ 0.5$ $r = 0.9999$ $n = 17$) with a detection limit of 6×10^{-7} M (Table 3.1). The sensitivity to lactate of the POAP-PPD-modified electrode, and at an applied potential of 0.0 V (vs. Ag/AgCl), is about 50 % lower than that of the PDD-modified electrode at 0.15 V. In spite of this, the use of the POAP-PPD-modified electrode improved by 1–2 orders of magnitude the sensitivity and detection limit of lactate determination when compared with other lactate biosensors based on the use of LDH and immobilized mediators. The CP/LDH-GPT-NAD$^+$/POAP-PPD electrode was used for the determination of L–lactate in cider. A good correlation was found between the results obtained from the sensor and those from spectrophotometric methods.

3.3 POAP as an Electrochemical Gas Sensor

Nitric oxide (NO) has acquired considerable importance as biological analyte due to its role as a cell signaling molecule, involved in immunity regulation, defense mechanism and neurotransmission. Additionally, NO has a role in the action of nitrite as a food preserver. The development of a NO sensor based on hybrid films of POAP and the metal complex Ni sulfonated phtalocyanine is reported in [37].

POAP films were produced by cycling the base electrode (Pt or GC) between −0.25 and 0.7 V (SCE) at 50 mV s^{-1} in a 0.05 M *o*-aminophenol solution in 0.5 M HClO$_4$. To incorporate the metal complex, sulfonated nickel phtalocyanine was added to the solution at a 10 mM concentration. The polymerization in presence of the metal complex is faster than with *o*-aminophenol alone. This fact was attributed to a template effect of the sulfonic groups. After several cycles (> 50) a film of POAP-sulfonated nickel phtalocyanine (POAP/NiSuPh) was deposited on the electrode. The incorporation of the metal complex into the polymer film was tested by *ex-situ* reflection–absorption FTIR spectroscopy. The hybrid film, produced with the metal complex, revealed new bands at 1063 and 1030 cm^{-1}, with respect to those corresponding to POAP. These bands were assigned to stretching of the sulfonate group. The bands are retained after cycling in a solution without the complex, even at *pH* 7. The modified electrodes were tested for NO electrochemical oxidation. A peak at 0.95 V was observed on the cyclic voltammogram that corresponds to NO oxidation, and it increases with NO concentration. It was observed that both POAP and POAP/NiSuPh films present higher electrocatalytic activity for NO oxidation than the base substrate (GC). The oxidation current, in the electrode modified with the complex, is higher and the oxidation overpotential is lower, indicating that the Ni complex incorporated into the hybrid film could electrocatalyze NO oxidation. The peak current was measured to determine the concentration of NO in the solution. The peak current is linear with a concentration up to 200 μM (Fig. 3.7).

3.4 POAP as a Ferric Cation Sensor in Solution

It was reported that POAP films obtained on ITO electrodes by electropolymerization of *o*-aminophenol (0.1 M) in a 0.1 M H$_2$SO$_4$ aqueous solution can act as potentiometric Fe(III) ion sensors, after being soaked in a ferric cation solution [38].

POAP films freshly synthesized in [38] show IR spectra that are indicative of a 1,4-substituted structure. When these POAP films are soaked for 24 h in a 0.1 M H$_2$SO$_4$ aqueous solution containing 50 mM Fe$_2$(SO$_4$)$_3$, their XPS spectra show iron ion capture. After this cation capture process, the electrode potential of the POAP film was measured in various aqueous solutions containing Zn(II), Ni(II), Cu(II), Fe(II) and Fe(III) ions at different concentrations. The relationship between the electrode potential, E, and the logarithm of the concentration, C, in the different cations in solutions was recorded. The electrode showed no potential response to ion concentration for Zn(II), Ni(II), Cu(II) and Fe(II) ions. However, it showed a Nernstian potential response to Fe(III) ions with a slope −57 mV/log [Fe(III)] (Fig. 3.8). The response time was less than 10 s, and the response was observed until [Fe(III)] = 10^{-4} M. The response to Fe(III) ions in solution was considered indicative of the presence of Fe(II) in the POAP film. The response

Fig. 3.7 Relationship between the peak current and NO concentration during oxidation of NO on a poly (o-aminophenol)/Ni sulfonated phtalocyanine modified electrode. Electrode area 0.071 cm^2. Scan rate 0.010 V s^{-1} [37]
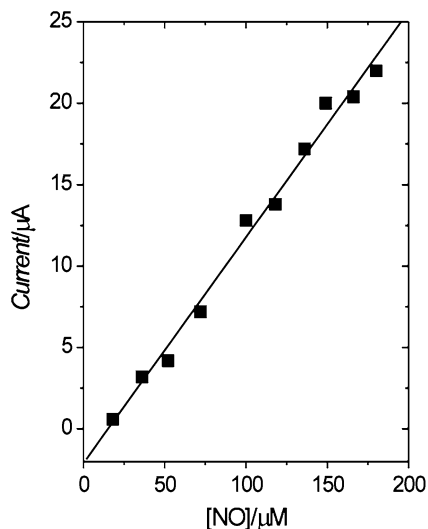
was attributed to the electron transfer between Fe(II) ions into the film and Fe(III) ions in solution, according to the Nernst equation:

$$E = E^o + 0.059 \log\left\{[Fe(III)]_{solution}/[Fe(II)]_{film}\right\} \qquad (3.2)$$

In Eq. (3.2), [Fe(II)]$_{film}$ denotes the concentration of Fe(II) ions in the POAP film. Even though authors of [38] indicate that POAP can function as a potentiometric Fe(III) sensor, they recognize that concentration sensitivity needs to be enhanced. It was demonstrated that this process of cation capture also leads to deactivation of POAP [39].

Fig. 3.8 Relationship between the electrode potential, E, and the logarithm of the concentration, log C. ($\bullet$) Fe(III); ($\blacktriangle$) Ni(II), ($\blacktriangledown$) Zn(II) [36]. POAP films soaked for 24 h in a 0.1 M H$_2$SO$_4$ aqueous solution containing 50 mM Fe$_2$(SO$_4$)$_3$ [38]
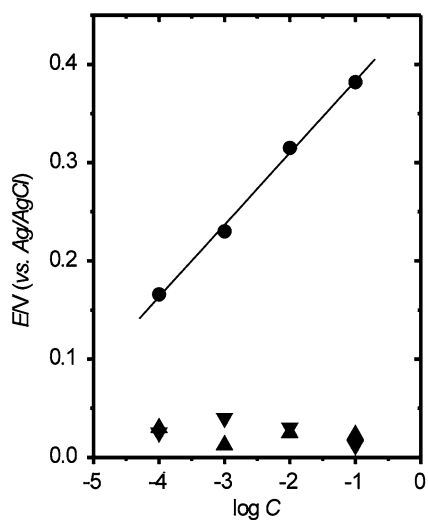
3.5 POAP as a Molecular Imprinting Material for Sensor Preparation

Molecular imprinting is a means of synthesizing some polymers with selectivity to some particular molecules (template molecules) developed in recent years. Molecularly imprinted polymers usually have some cavities with a given size and shape and arraying functional groups, so they lend some memorial function to the specific steric structures of template molecules, thus endowing them with good recognition ability. Traditionally, molecularly imprinted polymers prepared by routine methods, such as castings, *in situ* polymerization, spin coating, etc., are generally of a thickness over a micron and are poorly homogeneous, influencing the sensitivity and the final design of sensors to a certain degree. In this regard, an electrochemical sensor for nicotine based on the electropolymerization of a molecular imprinting polymer with *o*-aminophenol as monomer and nicotine as template was analyzed in [40]. Compared with nicotine imprinting membranes, the electropolymerization film of POAP had the following advantages: it was homogeneous, the thickness was of the order of the nanometer and its preparation was simple. In this regard, by employing cyclic voltammetry and weak acidity conditions, the sensor was prepared by electropolymerization of *o*-AP on a gold electrode in the presence of the template (nicotine). The determination limit was 2.0×10^{-7} molL^{-1}, and a linear relationship between current and concentration in the range 4.0×10^{-7} to 3.3×10^{-5} molL^{-1} was reported. The sensor was applied to the analysis of nicotine in tobacco samples with recovery rates from 99.0 to 102 %.

The preparation and properties of electrosynthesized POAP, as a molecular imprinting material, were also studied in [41] by the in situ Quartz Crystal Impedance method. 2,4-Dichlorophenoxyacetic acid was employed as template molecule. During the polymerization, the changes of frequency (Δf_o), resistance (ΔR_o) and capacitance (ΔC_o) of the equivalent circuit were analyzed on the basis of the Butterworth-Van Dyke model. The thickness shear mode acoustic sensor modified with this material exhibited molecular recognition ability to the template molecule. In the range 4.0×10^{-5} to 2.0×10^{-3} M, a linear relationship between the frequency shift ($-\Delta f_o$) and log C was found from the calibration curve. The determination limit was 1.0×10^{-5} M.

3.6 The Electrocatalytic Activity of Poly(*o*-aminophenol)

POAP has been employed to improve the activity of some electrocatalysts. Metallic nanoparticles dispersed into a POAP layer yield electrodes of high surface area and enhanced electrocatalytic activity in the oxidation of methanol. Also, it was demonstrated that some transition metal cations can increase their catalytic activity through their incorporation into the POAP matrix. In this regard, the

simultaneous presence of hydroxyl and amino groups on the POAP backbone renders the polymer more modifiable than other polymers because the lone pair electrons are available from nitrogen and oxygen atoms to coordinate with most transition metal cations. It is evident that in these different applications where POAP acts as a host material, thickness and morphology should play an important role. In some cases, POAP has been shown to exhibit catalytic activity. In the following paragraphs, the behavior of POAP in different electrocatalysts is treated together with some proposed mechanisms to explain its activity.

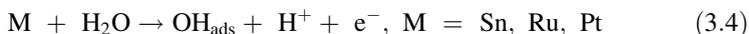### 3.6.1 Electrocatalytic Oxidation of Methanol with POAP Modified-Electrodes

The electro-oxidation of methanol has been the subject of numerous studies by several methods, because it is considered to be a liquid fuel of relatively high activity in fuel cell systems. The electro-oxidation of methanol in aqueous acid solutions using GC electrodes modified by a thin film of POAP containing dispersed platinum and platinum alloy microparticles was studied in [42]. Pt, Pt-Ru and Pt–Sn particles were incorporated into the polymer film by electrochemical deposition and the following electrodes were synthesized: GC/POAP/Pt, GC/POAP/Pt-Ru and GC/POAP/Pt–Sn. POAP films were synthesized by potentiodynamic methods, and a mean value of 0.52 ± 0.02 μm was employed for the polymer film thicknesses in the different electrodes. In all experiments the working electrode was submerged in open-circuit position into methanol solutions. Then, voltammograms were recorded by sweeping the potential from 0.0 V to 1.00 V (vs. SCE). Although the Pt loading for both electrodes (GC/Pt and GC/POAP/Pt) was similar, it was observed that the peak current for the oxidation of methanol (0.63 V vs. SCE) increased from 0.48 mA (GC/Pt electrode) to 1.73 mA (GC/POAP/Pt) (area of the GC electrodes: $0.07 \ cm^2$). This result was explained in terms of an enhancement of Pt microparticle efficiency towards the catalytic oxidation of methanol in the presence of POAP. Similar results were also obtained when Pt was replaced by Pt–Sn or Pt-Ru alloys. Chronoamperometric experiments indicated the existence of an increase in the real surface area of a GC/POAP/Pt electrode with respect to that of a GC/Pt electrode (the area of the GC/POAP/Pt electrode was 2.85 times larger than that of the GC/Pt electrode). Then, an augmentation of the real surface was invoked in [42] to explain the increase in reactivity of the electrocatalysts deposited in the presence of POAP. Thus, the role of the polymeric matrix is not directly connected with an increase of the intrinsic specific activity of electrocatalysts, but the polymer film only acts as a good and proper bed for deposition of electrocatalyst particles and increases the catalytic activity of active sites.

In respect to codeposits of Pt-Ru and Pt–Sn, the observed increase in the oxidation current of methanol (as compared with Pt alone) was considered in terms

of a bifunctional effect of the electrocatalyst toward the dissociative adsorption of methanol on Pt, mainly to CO adsorbed species that can be further oxidized into carbon dioxide due to the presence of Ru and Sn, which allows a sufficient coverage of HO species at low potentials. A mechanism was proposed, in which it is assumed that while the chemical properties of Pt and Ru surface atoms are similar to those of the respective monometallic surfaces, the formation of CO_{ads} species in a methanol dehydrogenation step is mainly facilitated by Pt sites:

$$CH_3OH_{ads} \rightarrow CO_{ads} + 4H^+ + 4\ e^- \tag{3.3}$$
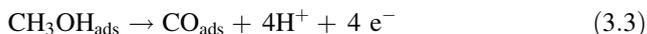
Then, the removal of CO_{ads} proceeds via adsorbed OH on both Pt and Ru sites formed by dissociative water adsorption:

$$M\ +\ H_2O \rightarrow OH_{ads} +\ H^+ + e^-,\ M\ =\ Sn,\ Ru,\ Pt \tag{3.4}$$

$$CO_{ads} +\ OH_{ads} \rightarrow CO_2 +\ H^+ +\ e^- \tag{3.5}$$

Since Ru and Sn have higher affinity than Pt towards oxygen-containing species, it was considered that sufficient amounts of OH_{ads}, to support reasonable CO oxidation rates, should be formed at low potentials on Ru and Sn sites rather than on Pt sites. Then, this effect leads to a higher activity for the overall methanol oxidation process on Pt-Ru and Pt–Sn compared with Pt alone. On the basis of the mechanism shown above, it is indicated that POAP can improve to some extent the adsorption of methanol on the catalytic sites, especially in the case of GC/POAP/Pt and GC/POAP/Pt–Sn electrodes due to the large surface area arising from Pt and Pt alloys particles in the polymer layer. Another noticeable feature observed in [42] was the fact that in the case of GC/POAP/Pt-Ru and GC/POAP/Pt–Sn electrodes, in contrast to the case of the corresponding polymer-free electrodes, the voltammetric curves recorded during positive and negative sweeps are close to each other (without hysteresis), which is an indication of a weak poisoning effect.

This result seems to indicate that the poisoning by adsorbed CO species decreases when the Pt alloys are highly dispersed into a POAP film. It was observed that the polymer thickness affects the electro-oxidation of methanol. Thus, for thickness greater than about 0.6 μm, the peak current is independent of the POAP thickness, whereas for lower values, the percent of anodic current decrease increases as the film thickness decreases (Fig. 3.9). The increase was attributed to a predominant effect of the electrode matrix nature over that of the polymeric film on the catalysis of methanol oxidation. That is, the effect of the deposited film on the enhancement of the catalytic current appears when the electrode surface is thoroughly covered by a POAP layer and methanol cannot reach the electrode matrix. Therefore, 200 cycles of potential scan yielding a 0.52 μm thickness for the POAP film were considered as an optimum value. In respect of electrode stability, the results indicated that by neglecting the weak decrease in peak current during the first 3 weeks, the responses were reproducible up to 60 days, which was indicative of the nearly long-term stability of POAP-modified electrodes.

Fig. 3.9 Plot of the anodic peak current decrease as a function of the polymer film thickness for: **a** glassy carbon/poly(o-aminophenol)/Pt electrode; **b** glassy carbon/poly(o-aminophenol)/Pt-Ru electrode; **c** glassy carbon/poly(o-aminophenol)/Pt–Sn electrode. Solution: 0.10 M $HClO_4$ + 0.10 M CH_4OH. Pt and Pt alloy loading 0.1 mg cm^{-2} [42]
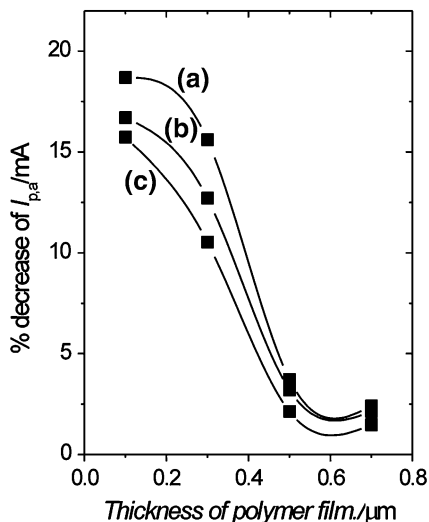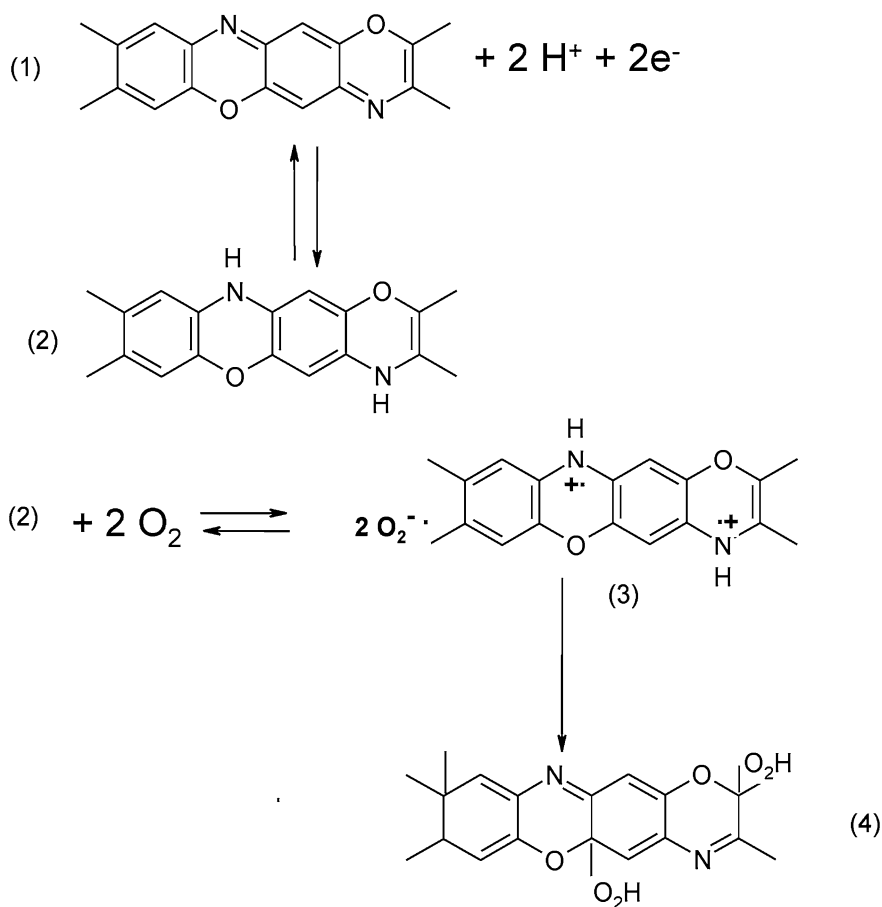

3.6.2 Electrocatalytic Oxygen Reduction with POAP-Modified Electrodes

The electrocatalysis of POAP-coated glassy carbon electrodes for O_2 reduction in acidic aqueous media (pH 1.0) was analyzed in [43] by employing Rotating Ring-Disk Electrode Voltammetry. POAP-coated GC electrodes were prepared by potential-sweep electrolysis at 50 mV s^{-1} in the potential range -0.4–1.0 V (SCE) in 0.2 mol dm^{-3} $NaSO_4$ aqueous solution (pH 1) containing 50 mmol dm^{-3} o-aminophenol under a nitrogen atmosphere. By comparing voltammetric responses of the POAP/GC-modified electrode with those of the bare GC electrode in O_2-saturated solutions, it was concluded that POAP exhibits a poor catalytic activity for O_2 reduction. In this regard, a reaction between POAP and O_2 was proposed in [43] (Fig. 3.10). On the basis of the proposed mechanism, the poor catalytic activity of POAP for oxygen reduction was attributed to different reasons. Firstly, no catalytic formation of H_2O_2 was detected by employing Rotating Ring-Disk Electrode Voltammetry. Secondly, as the reversible redox response of POAP remained substantially unchanged before and after the POAP film had been held in its reduced state for some time (e.g. 30 min) under O_2 atmosphere, it was suggested that the intermediate 3 in Fig. 3.10 was scarcely formed.

3.6.3 Electrocatalytic Activity of the POAP-Metal Cation Complex in Oxygen Reduction

Despite POAP itself showing a poor catalytic activity for oxygen reduction, POAP interaction with metal cations leads to a complex with catalytic activity for oxygen

reduction. In this regard, the interaction of POAP with silver cations was studied [33]. It was shown that the POAP-Ag(I) complex exhibits electrocatalytic activity in dissolved oxygen reduction. POAP was synthesized on GC and Pt from 0.05 M *o*-aminophenol in a mixture of 1 M H_2SO_4 and 0.5 M Na_2SO_4 by CV. The potential was scanned from -0.2 V to 0.8 V (vs. SCE) at 100 mVs^{-1} for different numbers of cycles (*N*). As the nature of interactions between Ag$^+$ and POAP was expected to vary according to the oxidation state of the polymer, the extent of the oxidation in POAP deposits of different thickness was also studied in [33]. It was observed that the diffusion of oxygen was impeded by the increase in POAP thickness. With regard to proper interaction of silver ions with POAP, it was found that they ranged from redox reactions, in which cations were reduced to the metallic form, to a partial charge transfer between the metal and the polymer

Fig. 3.10 Mechanism proposed in [43] to explain the poor electrocatalytic activity of POAP towards oxygen reduction

resulting in the formation of a metal-polymer complex. These two types of interaction predominate in thick films ($N = 120$) and thin films ($N = 1$), respectively. Films of moderate thickness ($N = 20$) exhibited intermediate behavior. In this regard, a morphologic study was also performed in [33], in which POAP and PANI morphologic characteristics were compared. The surface of POAP films ($N = 40$) was found to be continuous and smooth, in contrast with that richly textured surface of PANI, where fibrils or globules often stack up in layers. The POAP morphology underwent small changes upon AgNO$_3$ treatment. In this connection, the surface was apparently free from foreign matter. On the contrary, AgNO$_3$ treatment of a thick POAP film ($N = 150$) brought about remarkable changes in morphology. The surface was dominated by dendrites that grew out from fibrils. These dendrites were considered due to silver metal deposited on the POAP surface as a result of the silver-POAP interactions in thick films. However, POAP showed little increase in fused structures, typical of polymer degradation. This fact was considered as an indication of a good resistance of POAP to hydrolytic degradation. The Ag-POAP complex was also compared with that of Ag-PANI [44]. It was remarked that the Ag-POAP complex is expected to have an improved stability over that of Ag-PANI due to the cooperative action of the oxygen atom in the POAP chemical structure. Another difference with PANI is related to the fact that the redox reaction of silver is within the range of the POAP redox reaction, and then, changes of POAP conductivity were not significant during the redox reactions of the POAP-Ag$^+$ complex. This was remarkably different from the situation of the Ag-PANI complex, where the switching of PANI between the insulating state of leucoemeraldine and the conducting state of emeraldine has substantial influence on the voltammetric response of silver redox behavior. Also, it has been demonstrated that POAP is more resistant than PANI to electrochemical degradation and can capture four times much silver than PANI [33]. However, as the basicity of POAP is limited and also the silver cation is not a good acceptor, it was observed that silver can be released from the complex upon acidification of the nitrogen and oxygen atoms or upon application of a sufficient positive potential.

3.6.4 Electrocatalytic Detection of Nicotinamide Coenzymes by POAP

Although dehydrogenases dependent upon the nicotinamide adenine dinucleotide [(NAD(P)$^+$] cofactors are routinely used in a large number of solution phase enzymatic assays, they have been little used for the development of biosensors. A major problem in the dehydrogenase biosensor design is the regeneration of the oxidized coenzyme. Voltammetric and amperometric detection of NAD(P)H (dihydronicotinamide adenine dinucleotides) has been shown to be feasible at POAP-modified electrodes [45]. Voltammetric studies [45] demonstrate that

POAP can be used in the electrocatalytic detection of nicotinamide coenzymes. The electrocatalytic behavior of POAP results from a chemical interaction (reaction) between the active sites of the polymer and the adsorbed molecules (NADH or NADHP).

3.6.4.1 Influential Factors in the Response Characteristic of POAP in the Nicotinamide Coenzyme Detection

Effect of the POAP Thickness

POAP films were grown in [45] on carbon paste electrodes by potential cycling. The catalytic amperometric response of POAP-modified electrodes to NADH was evaluated as a function of the composition and *pH* of the electropolymerization solution, the monomer concentration and the number of potential scan cycles applied to the electrode during polymer film formation (thickness of the polymer).

It was found that the catalytic oxidation of NADH does not depend on the electrolyte used (NaCl, Na_2HPO_4, Na_2SO_4, 1-heptanesulphonic acid) in the film formation process nor on the film thickness. With regard to the solution *pH*, POAP-modified electrodes were prepared in background solutions of *pH* ranging from 1 to 9 at a monomer concentration of 5×10^{-4} M. POAP generated in this *pH* range always displayed catalytic activity, but the catalytic current was higher for the film prepared at *pH* 1 and 3 (Fig. 3.11) due to the higher conductivity of POAP at low *pH* values. Despite the higher electroactivity exhibited by POAP films prepared in solutions of low *pH*s, *pH* > 5 acetate buffer was preferred in [45] because a significant loss of enzymatic activity occurs when more acidic solutions are used.

Effects of pH and Applied Potential

The POAP-modified electrodes were used for cyclic voltammetry or amperometric measurements of NADH or NADPH in 0.1 M phosphate buffer of *pH* 7. Cyclic voltammetry shows that, the uncatalyzed oxidation of NADH at a bare carbon paste electrode in *pH* 7 phosphate buffer yields a single irreversible peak at *ca* 0.5 V (vs. Ag/Ag/Cl). The electrocatalytic activity of the POAP-modified carbon paste electrode for the oxidation of NADH was demonstrated by the appearance of an anodic current starting at potentials below 0.0 V and a pre-wave with a half-wave potential of 0.20 V. A second anodic process appears at a potential close to that corresponding to uncatalyzed NADH oxidation at a bare carbon paste electrode (0.5 V). An analogous cyclic voltammetric behavior for NADH was also observed for NADPH. The effect of the potential scan on the pre-wave limiting current and the uncatalyzed oxidation peak current of NADH was also examined for POAP-modified carbon paste electrodes. The peak current was found to be linearly related to the square root of the potential scan rate within the tested range 2–20 mV s^{-1}, indicating that this process is diffusion-controlled. Nevertheless, the pre-wave limiting current remains constant at different potential scan rates. An entirely analogous behavior was found for NADPH oxidation. It has been

Fig. 3.11 Amperometric currents developed by a POAP-modified electrode for 1.0×10^{-5} M NADH as a function of the electropolymerization pH medium. Applied potential 0.15 V (Ag/AgCl). Supporting electrolyte for the amperometric measurements: 0.1 M phosphate buffer pH 7 [45]
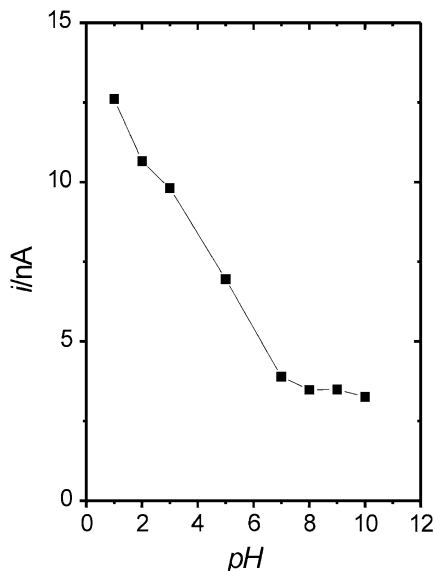
demonstrated that the POAP-modified carbon paste electrode lowers the oxidation overpotential of NADH and NADHP [45].

Hydrodynamic voltammograms for the unmodified and POAP-modified carbon paste electrodes have also been compared [45]. There was no appreciable oxidation of NADH or NADPH at the bare carbon paste electrode up to 0.3 V. For the POAP-modified carbon paste electrode a plateau was obtained for NADH oxidation at potentials between 150 and 300 mV, whereas the NADPH oxidation occurs at more positive potentials close to the uncatalyzed coenzyme oxidation. The amperometric response of POAP-modified electrodes to increasing concentrations of NADH and NADPH was also investigated using stationary working electrodes in magnetically stirred solutions.

Calibration plots were obtained in 0.1 M acetate buffer at pH 5.0 and 0.1 M phosphate buffer pH 7. With regard to the catalytic activity of POAP, a current value of about 0.16 nA for 1.0×10^{-7} M NADH at pH 7 was reported in [45]. The time required to obtain a steady-state response was less than 15 s. The detection limit was close to 1.0×10^{-9} M. Even though POAP-modified carbon paste electrodes are suitable for NADH detection in aqueous solutions, for NADPH detection a polymer such as poly(o-phenylenediamine) seems to be more appropiate.

3.7 Concluding Remarks

For many years different research groups, among them our group [10–14, 17, 18, 20, 21, 39], have studied the electrochemical properties of poly(o-aminophenol) in acidic media. The effects of different external variables, such as applied potential,

solution composition and *pH*, threshold potential for deactivation, etc., on the conduction properties of this polymer have been analyzed in detail. It has been observed that applied potentials slightly higher than 0.5 V (vs. SCE) and electrolyte media of relatively high *pH* strongly decrease POAP conductivity. These conditions, combined with the intrinsic low permeability of POAP towards species in solution, are negative factors, which should restrict the practical uses of POAP. However, the recent literature, describing numerous applications of POAP in the field of biosensors, has demonstrated that the isolating properties of POAP synthesized in neutral media are very useful in preventing the biosensor from fouling and eliminating the interference from electroactive species, which is essential in obtaining a selective response current. Also, even though it was demonstrated that the cation capture process by POAP decreases its conductivity [39], this property has usefully been employed to build sensors of ions in solution [38] and electrocatalysts for oxygen reduction [33]. Researchers within sensors and electrocatalysis fields are increasingly taking advantage of the isolating properties of poly (*o*-aminophenol), and showing the polymer to have considerable utility, when they were initially considered to have low practical value.

References

 1. Inzelt, G., Pineri, M., Schulttze, J.W., Vorotyntsev, M.A.: Electron and proton conducting polymers: recent developments and prospects. Electrochim. Acta **45**, 2403–2421 (2000)
 2. Barbero, C., Silber, J.J., Sereno, L.: Formation of a novel electroactive film by electropolymerization of orthoaminophenol. Study of its chemical structure and formation mechanism. Electropolymerization of analogous compounds. J. Electroanal. Chem. **263**, 333–352 (1989)
 3. Kunimura, S., Ohsaka, T., Oyama, N.: Preparation of thin polymeric films on electrode surfaces by electropolymerization of o-aminophenol. Macromolecules **21**, 894–900 (1988)
 4. Barbero, C., Zerbino, J., Sereno, L., Posadas, D.: Optical properties of electropolymerized orthoaminophenol. Electrochim. Acta **32**, 693–697 (1987)
 5. Ohsaka, T., Kunimura, S., Oyama, N.: Electrode kinetics of poly(o-aminophenol) film prepared by electro-oxidative polymerization of o-aminophenol and its electrochromic properties. Electrochim. Acta **33**, 639–645 (1988)
 6. Guenbourg, A., Kacemi, A., Benbachir, A., Aries, L.: Electropolymerization of 2-aminophenol. Electrochemical and spectroscopic studies. Prog. Org. Coat. **38**, 121–127 (2000)
 7. Ortega, J.M.: Studies of Poly(o-Aminophenol) by Quartz Crystal Impedance Measurements. Synth. Met. **97**, 81–84 (1988)
 8. Zhang, A.Q., Cui, C.Q., Chen, Y.Z., Lee, J.Y.: Synthesis and electrochromic properties of poly-*o*-aminophenol. J. Electroanal. Chem. **373**, 115–121 (1994)
 9. Barbero, C., Silber, J.J., Sereno, L.: Electrochemical properties of poly-*ortho*-aminophenol modified electrodes in aqueous acid solutions. J. Electroanal. Chem. **291**, 81–101 (1990)
10. Barbero, C., Tucceri, R.I., Posadas, D., Silber, J.J., Sereno, L.: Impedance characteristics of poly(o-aminophenol) electrodes. Electrochim. Acta **40**, 1037–1040 (1995)
11. Tucceri, R.I.: Surface resistance measurements on thin gold film electrodes coated with poly(o-aminophenol) films. J. Electroanal. Chem. **505**, 72–84 (2001)
12. Tucceri, R.I.: Specularity change of a thin gold film surface coated with poly(*o*-aminophenol) during the polymer redox conversion. The pH affect on the redox sites distribution at the metal‖polymer interface. J. Electroanal. Chem. **543**, 61–71 (2003)

13. Tucceri, R.: A review about the surface resistance technique in electrochemistry. Surf. Sci. Rep. **56**, 85–157 (2004)
14. Tucceri, R.I.: The change of the electron scattering at the gold film/poly(o-aminophenol) film interface after partial degradation of the polymer film. Its relation with the electron transport within the polymer film. J. Electroanal. Chem. **562**, 173 (2004)
15. Komura, T., Ito, Y., Yamaguti, T., Takahasi, K.: Charge-transport processes at poly-o-aminophenol film electrodes: electron hopping accompanied by proton exchange. Electrochim. Acta **43**, 723–731 (1998)
16. Levin, O., Kondratiev, V., Malev, V.: Charge transfer processes at poly-o-phenylenediamine and poly-o-aminophenol films. Electrochim. Acta **50**, 1573–1585 (2005)
17. Rodríguez Nieto, F.J., Posadas, D., Tucceri, R.: Effect of the of the bathing Electrolyte Concentration on the Charge Transport Process at Poly(o-aminophenol) Modified Electrodes. An ac Impedance study. J. Electroanal. Chem. **434**, 83–91 (1997)
18. Rodríguez Nieto, F.J., Tucceri, R.: The pH Effect on the Charge Transport at Redox Polymer-Modified Electrodes. An ac Impedance Study applied to Poly (o-aminophenol) Film Electrodes. J. Electroanal. Chem. **416**, 1–24 (1996)
19. Ortega, J.M.: Conducting potential range of poly(o-aminophenol). Thin Solid Films **371**, 28–35 (2000)
20. Bonfranceschi, A., Pérez Córdoba, A., Keunchkarian, S., Zapata, S., Tucceri, R.: Transport across poly(o-aminophenol) modified electrodes in contact with media containing redox active couples. A study using rotating disc electrode voltammetry. J. Electroanal. Chem. **477**, 1–13 (1999)
21. Tucceri, R.: The effect of high positive potentials on the different charge transport and charge transfer parameters of poly(o-aminophenol) modified electrodes, A study using cyclic voltammetry, rotating disc electrode voltammetry and ac impedance measurements. J. New Mat. Electrochem. Systems **8**, 305–315 (2005)
22. Tao, W., Pan, D., Liu, Y., Nie, L., Yao, S.: An amperometric hydrogen peroxide sensor. Anal. Biochem. **338**, 332–340 (2005)
23. Guerrieri, A., Ciriello, R., Centonze, D.: Permselective and enzyme-entrapping behaviors of an electropolymerized, non-conducting, poly(*o*-aminophenol) thin film-modified electrode. A critical study. Biosens. Bioelectron. **24**, 1550–1556 (2009)
24. Koopal, C.G.J., Nolte, R.J.M.: An amperometric biosensor based on polypyrrole. Bioelectrochem. Bioenerg. **33**, 45–53 (1994)
25. Cosnier, S., Gunther, H.: A polypyrrole [Rh(III)(C$_5$Me$_5$)(bpy)Cl]$^+$ modified electrode for the reduction of NAD$^+$ cofactor. J. Electroanal. Chem. **315**, 307–315 (1991)
26. Foulds, N.C., Lowe, C.R.: Immobilization of glucose oxidase in ferrocene-modified pyrrole polymers. Anal. Chem. **60**, 2473–2478 (1988)
27. Lu, S., Li, C., Zhang, D., Zhang, Y., Mo, Z., Cai, Q., Zhu, A.: Electron transfer on an electrode of glucose oxidase immobilized in polyaniline. J. Electroanal. Chem. **364**, 31–36 (1994)
28. Pan, D., Chen, J., Nie, L., Tao, W., Yao, S.: Amperometric glucose biosensor based on immobilization of glucose oxidase in electropolymrized *o*-aminophenol film at Prussian blue-modified platinum electrode. Electrochim. Acta **49**, 795–801 (2004)
29. Chen, X., Chen, J., Deng, C., Xiao, C., Yang, Y., Nie, Z., Yao, S.: Amperometric glucose biosensor based on boron-doped carbon nanotubes modified electrode. Talanta **76**, 763–767 (2008)
30. Pan, D., Chen, J., Yao, S., Tao, W., Nie, L.: An amperometric glucose biosensor based on glucose oxidase immobilized in electropolymerized poly(*o*-aminophenol) abd carbon nanotubes composite film on a gold electrode, Analytical Sciences. Jpn Soc. Anal. Chem. **21**, 367–371 (2005)
31. Zhang, Z., Liu, H., Deng, J.: A glucose biosensor based on immobilization of glucose oxidase in electropolymerized *o*-aminophenol film on platinized glassy carbon electrode. Anal. Chem. **68**, 1632–1638 (1996)
32. Li, J., Lin, X.: Glucose biosensor based on immobilization of glucose oxidase in poly(*o*-aminophenol) film on polypyrrole-Pt nanocomposite modified glassy carbon electrode. Biosens. Bioelectron. **22**, 2898–2905 (2007)

33. Zhang, A.Q., Cui, C.Q., Lee, J.Y.: Metal-polymer interaction in the Ag$^+$/poly-*o*-aminophenol system. Electroanal. Chem. **413**, 143–151 (1996)

34. Valdés García, M.A., Tuñón Blanco, P., Ivaska, A.: A poly(*o*-aminophenol) modified electrode as an amperometric hydrogen peroxide biosensor. Electrochim. Acta **23**, 3533–3539 (1998)

35. Miland, E., Miranda Ordieres, A.J., Tuñón Blanco, P., Smyth, M.R., Fágáin, C.O.: Poly(*o*-aminophenol)-modified bienzyme carbon paste electrode for the detection of uric acid. Talanta **43**, 785 (1996)

36. Lobo Castañón, J., Miranda Ordieres, A.J., Tuñón Blanco, P.: A bienzyme-poly(*o*-phenylenediamine)-modified carbon paste electrode for the amperometric detection of L-lactate. Anal. Chim. Acta **346**, 165–174 (1997)

37. Miras, M.C., Badano, A., Bruno, M.M., Barbero, C.: Nitric oxide electrochemical sensors based on hybrid films of conducting polymers and metal phtalocyanines. Portugaliae Electrochimica Acta **21**, 235–243 (2003)

38. Yano, J., Kawakami, H., Yamasaki, S., Kanno, Y.: Cation capture ability and the potential response of a poly(*o*-aminophenol) film electrode to dissolved ferric ions. J. Electrochem. Soc. **148**, E61–E65 (2001)

39. Tucceri, R.: Redox mediation and permeation process a deactivated poly(*o*-aminophenol) films. A study applying rotating disc electrode voltammetry and electrochemical impedance spectroscopy. J. Electroanal. Chem. **633**, 198–206 (2009)

40. Zhaoyang, W., Xiaolei, Z., Yunhui, Y., Guoli, S., Ruqin, Y.: A sensitive nicotine sensor ased on molecularly imprinted electropolymer of o-aminophenol. Front. Chem. China **2**, 183–187 (2006)

41. Peng, H., Yin, F., Zhou, A., Yao, S.: Characterization of electrosynthesized poly(*o*-aminophenol) as a molecular imprinting material for sensor preparation by means of quartz crystal impedance analysis. Anal. Lett. **35**, 435–450 (2002)

42. Golabi, S.M., Nozad, A.: Electrocatalytic oxidation of methanol at lower potentials on glassy carbon electrode modified by platinum and platinum alloys incorporated in poly(*o*-aminophenol) film. Electroanalysis **15**, 278–286 (2003)

43. T. Ohsaka, T. Watanabe, F. Kitamura, N. Oyama, K. Tokuda, Electrocatalysis of O_2 reduction at poly(*o*-phenylenediamine) and poly(*o*-aminophenol)-coated glassy carbon electrodes. J. Chem. Soc. Chem. Commun. 1072–1073 (1991)

44. Zhang, A.Q., Chen, Y.Z., Tian, Z.W.: Metal-polymer interaction in the Ag$^+$/polyaniline system. Acta Phys. Chem. China **9**, 523 (1993)

45. Lobo, M.J., Miranda, A.J., López-Fonseca, J.M., Tuñón, P.: Electrocatalytic detection of nicotinamide coenzymes by poly(*o*-aminophenol) and poly(*o*-phenylenediamine)-modified carbon paste electrode. Anal. Chim. Acta **325**, 33–42 (1996)